Multi-phase modelling of multi-species ionic migration in concrete

by

Qingfeng Liu, ***BEng, MSC***

Doctor of Philosophy

School of Marine Science and Engineering

University of Plymouth

December 2013

ABSTRACT

Chloride-induced corrosion of reinforcing steel in concrete is a worldwide problem. In order to predict how chlorides penetrate in concrete and how other ionic species in concrete pore solution affect the penetration of chlorides, this thesis presents a numerical study on multi-phase modelling of ionic transport in concrete dominated by migration process.

There are many advantages in rapid chloride migration test (RCM) method and numerical approach. However, most of models in the literature predicting chloride diffusivity in concrete are diffusion models, which not consider the action of externally applied electric field. In view of this, the specific aim of this thesis is to develop a rational numerical migration model to simulate chloride migration tests. By using this model, the diffusion coefficient of chlorides in concrete will be efficiently predicted. Furthermore, other mechanisms of ionic transportation in composite materials can be scientifically investigated in the meantime.

In most existing work, researchers tend to use the assumption of electro-neutrality condition, which ensures that no external charge can be imported (Bockris and Reddy, 1998), to determine the electrostatic potential within concrete as well as considering a 1-D problem with only one phase structure and single species (i.e. the chlorides) for predicting the ionic migration. In contrast, this thesis presents a number of sets of multi-phase migration models in more than one dimension and uses the Poisson's equation for controlling the multi-species interactions. By solving both mass conservation and Poisson's equations, the distribution profiles of each ionic species and electrostatic potential

at any required time are successfully obtained. Some significant factors, i.e. the influence of dimensions, aggregates, interfacial transition zones (ITZs), cracks and binding effect have also been discussed in detail. The results reveal a series of important features which may not be seen from existing numerical models.

For quantitative study, this thesis also provides the prediction method of chloride diffusivity not only by the traditional stationary diffusion models but also by the migration models presented in the thesis. The obtained results are compared with three proven analytical models, i.e., Maxwell's model (Dormieux and Lemarchand, 2000), Bruggeman's equation (Bruggeman's, 1935) and the lower bound of the effective diffusion coefficient proposed by Li et al. (2012) as well as validated against experimental data sets of an accelerated chloride migration test (ACMT) brought by Yang and Su (2002).

KEYWORDS: Corrosion; chloride; migration; diffusion; concrete; cement; ionic transport; multi-phase; 2-D modelling; 3-D modelling; multi-species; ionic interaction; binding effect; aggregates; ITZs; cracks; chloride diffusivity prediction;

ACKNOWLEDGEMENT

First and foremost, I want to express my highest gratitude to my supervisor, Prof Long-Yuan Li, who directed me into this challenging and fascinating academic field as well as provided me such an excellent research environment. As an admirable scholar, his innovation, dedication, patience and consideration are the qualities that impressed me greatly throughout my PhD career. Without his consistent guidance and support, this thesis would never been completed.

Massive thanks go to my second supervisor in Plymouth, Dave Easterbrook, and my co-supervisor in Birmingham, Dr Jian Yang, for their supervision, supports as well as helpful comments for my published papers within their valuable time.

I would also like to appreciate Dr Jin Xia, a one-year visit scholar in University of Birmingham. His selfless assistance and valuable suggestions helped me overcome many academic difficulties of my research.

I would like to acknowledge the financial support provided by School of Civil Engineering, University of Birmingham for my 1st year, School of Marine Science and Engineering, University of Plymouth for my 2nd and 3rd years, and China Scholarship Council for my UK PhD scholarship. Thanks also to European Union Research Council for the research grant (FP7-PEOPLE-2011-IRSES-294955) from which I gain valuable experiences in visiting the collaborated universities.

Of course, thanks to my PhD colleagues and dear friends at the Birmingham and Plymouth two universities. Dr Chong Ren, Ms Congxiao Zhao, Ms Minxi Bao, Dr Qiang Liu and Dr Xudong Chen, who helped me a lot with my life and study during my beginning

period in the UK. Their friendship made my wonderful memories of Birmingham. After transferring to Plymouth, Ms Shanshan Cheng, Ms Xiaoqing Liu, Dr Daniel Roper and Mr Bing Li, who made me feel quite warm and comfortable in this southern coastal city. It is lucky to work and share spare time with them. In addition, special thanks to Daniel and Ms Yufei Sun for helping and encouraging me to write formal English.

As always, immense appreciation attributes to Ms Yun Lin, who I loved. In the past seven years, Yun has been sharing, supporting and understanding everything of me without reservation. I cannot imagine spending a moment of my life without her. Finally and most importantly, I would like to give my best honour to my ever-supportive parents, Mr Haigang Liu and Ms Qingping Zhao. Never enough thanks to them for bringing me to this colourful world and teaching me right from wrong. It is to them that this thesis is dedicated.

AUTHOR'S DECLARATION

At no time during the registration for the degree of Doctor of Philosophy has the author been registered for any other University award without prior agreement of the Graduate Committee.

Work submitted for this research degree at the University of Plymouth has not formed part of any other degree either at University of Plymouth or at another establishment.

This PhD study was financed with the aid of School of Civil Engineering, University of Birmingham for the 1st year, School of Marine Science and Engineering, University of Plymouth for the 2nd and 3rd years, China Scholarship Council for the UK PhD scholarship and European Union Research Council for the research grant (FP7-PEOPLE-2011-IRSES-294955).

External Contacts: henrylqf@163.com

Word count of main body of thesis: 38790 words

Signed: _____

Date: _____

CONTENTS

LIST OF FIGURES

LIST OF TABLES

NOMENCLATURE

A area

A_a the area fraction of aggregate

A_i the area fraction of ITZ

A_D the area fraction of damage zone

C concentration

C_1 the concentration of chloride at upstream boundary

C_A the volume fraction of aggregates

C_b the concentration of the bound ions adsorbed by solid cement matrix

C_{Cl} the concentration of chloride

C_d the chloride concentration at x_d ,

C_I the volume fraction of ITZ

C_f the concentration of free ions existing in concrete pore solution

C_k the concentration of the *k-th* ionic species

C_K the concentration of potassium

C_{Na} the concentration of sodium

C_{OH} the concentration of hydroxide

C_P the volume fraction of cement paste

C_t total concentration contained in concrete pore solution

D diffusion coefficient

d the distance between two electrodes of the electric field

D_0 the diffusion coefficient in matrix (usually the aqueous solution)

D_A the diffusion coefficient of aggregates

D_a the apparent diffusion coefficient

D_B the diffusion coefficient of bulk cement matrix

D_c the average chloride diffusion coefficient in concrete

D_{cem} the diffusion coefficient of cement paste

D_{D} the diffusion coefficient of damage zone

D_{Cl} the diffusion coefficient of chloride

D_{eff} the effective diffusion coefficient

D_e the biofilm effective diffusion coefficient

D_{ea} the equivalent diffusion coefficient of aggregat

D_{ITZ} the diffusion coefficient of ITZ

D_k the diffusion coefficient of the *k-th* ionic species

D_P the diffusion coefficient of cement paste matrix

E_d the linear electric field

erf^{-1} the inverse of error function

F Faraday's constant

$\overline{f}$ the frictional coefficient

F_e the electrical force per mole of ions

H the Heaviside function

I current density

J flux

J_c the average flux of the liquid phase of concrete

J_{K} the flux of potassium

J_k the flux of the *k-th* ionic species

J_l the flux of chloride at downstream boundary

J_{Na} the flux of sodium

J_{OH} the flux of hydroxide

J_t total flux

J_x the flux of inflow

$J_{x+\Delta x}$ the flux of outflow

K the conductivity of medium

$k(s)$ the function of pore structure and saturation of solution

k_B the Boltzmann constant

L the length of concrete specimen at x-axis

m mass

N number

N_A Avogadro's number

p pressure

P_e the Peclet number

Q the Darcy flux

q the ratio between diffusion coefficient of ITZ and cement paste

R the universal gas constant

R_r resistance

s the saturation

S_{Cl} the concentrations of bound chlorides

T the absolute temperature

t time

t_d the time of test duration

U the externally applied DC voltage

u the advective velocity

u_k the advective velocity of the *k-th* ionic species

x the distance at x-axis

x_d the penetration depth of chloride ions at a test duration t_d ,

y the distance at y-axis

z net charge

z_k the net charge of the *k-th* ionic species

β the tortuosity

γ_k the chemical activity coefficient of the *k*-th species

η the viscosity of fluid

ω_e the volume fraction of vaporizable water

ρ resistivity

σ conductivity

λ defined parameter

Φ electrical potential

$(1-\phi_c)$ the volume fraction of aggregate phase in meso-scale model.

ϕ porosity

$\phi(x)$ the capillary porosity volume fraction at a distance x from an aggregate surface

ϕ_{cap} the porosity of capillary

ϕ_{ITZ} the porosity of ITZ

ε the porosity of two-phase concrete

ε_o the permittivity of a vacuum

ε_r the relative permittivity of water at temperature of 298K

∇ the Laplace operator

μ the ratio of major and minor axes of the elliptical aggregate particles.

w the content of the water

1 CHAPTER ONE – INTRODUCTION

The first chapter of this thesis presents an introduction to the problem of chloride-induced corrosion of steel in reinforced concrete structures and a brief survey of the research status of the study of chloride transport in concrete. Additionally, the objectives of this study and the structure of the thesis are described.

1.1 The problem: chloride-induced corrosion of steel in reinforced concrete structures

Concrete is the most widely used man-made material in modern construction industry. It is frequently applied in architectural structures, foundations, roads, pavements, pipe, bridges/overpasses, etc. However, the service life of concrete has been seriously shortened due to the durability problems. It is widely known that a key source of durability problems is the ingress of ions; especially the penetration of chloride ions into concrete which will seriously corrode the reinforcing steel within. Thus, the investigation of transport of ionic species in concrete is very important and has received great attention in past decades. In the literature, the primary concern is predicting the diffusion coefficient of chlorides in concrete.

In the past, traditional concrete is produced by solidifying and hardening the mixture containing Portland cement, water and aggregates (typically using sand stones or granular materials). After the chemical process known as hydration, the water reacts with the cement, which bonds the other components together, eventually creating a robust stone-like material. Recently, high-performance concrete (HPC) has emerged as a relatively new term used to describe concrete that have higher durability, workability, volume stability, corrosion resistance, thermal resistance or lifetime. Configuration characteristic of HPC is generally with low water-binder ratio, high-quality raw materials and addition of efficient admixtures. Furthermore, due to the new regulation on the limitation of CO_2 emission, cement industry also need to use additives to reduce the cement content in concrete. Different types of concrete are produced by using different additives. Most commonly used additives include fly ash and blast-furnace slag (a non-metallic co-

product produced in the manufacturing of iron). Numerical speaking, this kind of additives will form new phases in concrete models.

It is apparent that the properties of concrete including chloride diffusivity will be different when using different additives. However, unfortunately most existing experimental data for concrete properties were obtained from traditional concrete.

To deal with this, from the mechanics point of view, if the properties of each individual material involved in the concrete are known then the properties of the concrete mixture should be predictable. This means one can treat the concrete as a composite material with different phases for simulating the influence of different additives, which give the possibility of prediction chloride diffusivity within the entire concrete.

1.2 Brief research status of the study of chloride transport in concrete

There are three main categories of studies aiming to characterise the transport behaviour of chlorides in cement and/or concrete materials: analytical, experimental and numerical studies.

In the analytical study, there are a number of publications which have focussed on clarification of the diffusion coefficient on the basis of different scales. At the macroscopic level, the analytical method brings some empirical models. It was revealed from these models that the diffusion coefficient tends to have a connection with the water to cement ratio (Atkinson and Nickerson, 1984; Hobbs, 1999). In the work of Van Brakel and Heetjes (1974), Garboczi and Bentz (1992; 1997) , Zhang and Bishop (1993), Dormieux and Lemarchand (2000), Xu et al. (1997), Li and Xia (2011), Jiang et al. (2012) the relationship between diffusion coefficient and the conception of porosity and tortuosity was discussed at a microscopic level. The mesoscopic models consider the components of the two or three phases (aggregate and cement matrix; aggregate, bulk cement paste and interfacial transition zone) and their corresponding diffusive properties respectively in these different phases (Hobbs, 1997; 1999; Xi and Bazant, 1999; Caré and Hervé, 2002; Yang and Su, 2002; Oh et al., 2004; Zheng and Zhou, 2007; Zheng et al., 2009; 2012; Li et al., 2012; Dehghanpoor Abyaneh et al., 2013). However, all of the models mentioned above focus only on the ionic transport of a single-species, i.e. the chloride ions.

Great efforts have been made to assess ionic transport by using experimental techniques. For ionic diffusion, there are two common test methods which are often used for measuring the chlorides' penetration in concrete. One is the salt ponding test (AASHTO

T259, 1980; ASTM C1543, 2002) and the other is the bulk diffusion test (NordTest NTBuild 443, 1995). However, these two diffusion tests are very time-consuming, especially for high-performance concrete, of which the test duration may last 90 days or even longer in order to get a sufficient chloride profile. Hence, recent research tends to adopt alternative experiments based on electro-migration of ions, which include the rapid chloride permeability test and the rapid migration test.

The Coulomb Test, also called rapid chloride permeability test (RCPT), undertaken by gauging the electrical conductivity or resistance of concrete directly or indirectly, was initially presented by Whiting (1981) and then adopted as AASHTO T277 (1983) and ASTM C1202 (1994). However, during the last two decades, a number of studies (Andrade, 1993; Feldman et al., 1994; Pfeifer et al., 1994; Scanlon and Sherman, 1996; Shi et al., 1998; Shane et al., 1999; Hooton et al., 2000; Shi, 2004) have raised criticisms of the RCPT test method based on a variety of aspects. The main criticism of this method is that the results obtained from electrical conductivity or resistance measurement cannot exactly represent the permeability, since the permeability of concrete attributes to its pore structure, whereas the electrical conductivity or resistance depends on not only the pore structure but also the chemistry of the pore solution. This deviation will be even higher when acting on HPC made with fly ash, siliceous dust and other super-plasticizer admixture. In view of the drawbacks of Coulomb Test, two alternative test methods were developed based on accelerated electrical field: steady and non-steady state migration tests. The latter also called rapid chloride migration test (RCM) is the more recent. Non-steady state migration test was initially developed by Tang and Nilsson (1992) and adopted by Nordtest and AASHTO as NT Build 492 (1999) and provisional Standard TP64 (2003). The test is very similar with the rapid chloride permeability test. However,

it allows direct measurement by the depth of chloride penetration instead of using the total passed charge to estimate the permeability. The calculation of chloride diffusion coefficient in the rapid migration test requires the concentration of chlorides at the depth they penetrated, which is often difficult to obtain. In current practice it usually uses the surface chloride concentration, which means that the penetration of chlorides in concrete exactly follows the 1-D migration pattern.

Nevertheless, the experimental data in the literature were mostly obtained by means of taking traditional concrete as a specimen while very few were for the new types of concrete. Additionally, similar to analytical approach, the migration tests described above are mainly used to investigate the transport of chloride ions alone, the transport of other ions and their effect on the chloride transport are not addressed.

Since the analytical and experimental techniques usually take simple cases and there are difficulties in reporting interactions between different ionic species and the electrostatic coupling of ions in a multi-component electrolyte solution, researchers began to use numerical methods to investigate the transport behaviour of multi-species in concrete. Methodologically speaking, these works can be divided into four categories. Firstly, a series of studies (Samson et al., 1999; Lorente et al., 2003; Khitab et al., 2005; Lizarazo-Marriaga and Claisse, 2009a; 2009b; Elakneswaran et al., 2010; Yaya et al., 2011) established numerical models to simulate the penetration process through a saturated cement paste under the hypothesis of zero current and electro-neutrality condition. Secondly, there were also some works other than the above, which added the effect of externally applied current density as well as considering the interactions between ionic species during the transport of ionic species in cement-based porous materials (Li and Page, 1997; 2000; Truc et al., 2000a; 2000b; Wang et al., 2000; Frizon et al., 2003;

Toumi et al., 2005; Kubo et al., 2006; Ouyang et al., 2009; Liu and Shi, 2012; Ukrainczyk et al., 2013). Also, in these studies, the electrostatic potential throughout the electrochemical process was still controlled by assuming the electro-neutrality condition. Similarly, Walton (1990), Sa'id-Shawqi et al. (1998), Zelinsky and Pirogov (2006), Narsillo et al. (2007), Krabbenhoft and Krabbenhoft (2008), Friemann et al. (2008) utilised externally applied voltage instead of the external current density as adopted in the second category. Here, it should be pointed out that, the electro-neutrality condition, which is employed in the work mentioned above to govern the electrostatic potential at any point in an electrolyte solution, is not a constitutive law but only a mathematical approximation in the electrochemistry field and may cause numerical inaccuracy. The real constitutive law for governing the electrostatic potential is the Poisson's equation (will be showed in the next chapter). However, some numerical difficulty exists in solving the Poisson's equation because of the large and small numbers involved in the equation. More recently, Johannesson et al. (2006; 2009; 2010a; 2010b) conducted a series of studies exploring the ionic diffusion in a multi-component solution by using the Poisson's equation instead of the electro-neutrality condition. However, his studies did not involve external voltage. Hence, the transport of ions in those cases is actually still dominated by diffusion, whereas the migration occurred only because of the imbalance diffusion between different ionic species.

1.3 Objectives of this study

Due to the advantages of both rapid chloride migration test (RCM) method and numerical approach, the aim of this thesis is to develop a rational numerical model to simulate non-steady state migration tests. By using this model, the diffusion coefficient of chlo-

rides in concrete will be efficiently predicted. Furthermore, other mechanisms of ionic transportation in composite materials can be scientifically investigated. More specifically, the individual objectives are orderly listed as follows:

1) To simulate multi-species ionic transport in concrete with ionic interactions under externally applied electric field and to obtain the distribution profiles of ionic concentration and electrostatic potential.

2) To adopt the real constitutive law of electrochemistry, Poisson's equation, instead of the more popular but questionable mathematic approximation, electroneutrality condition, to determine the electrostatic potential. Then to demonstrate the significance of using Poisson's equation by comparing the electrostatic potential gradient, concentrations, fluxes and current density distribution profiles of two categories of results.

3) To apply the governing of Poisson's equation and mass conservation equations, to develop a 2-D concrete model with aggregates and mortar/cement two phases instead of one-phase models. To study the influence of a second movement dimension, the aggregate morphology and the inclusion volume fraction on the chloride migration.

4) To implement a more accurate 2-D two phase model, to examine the influence of various forms of ionic binding between solid and liquid phases. Meanwhile, to explore whether the binding effect of one species also has impact on the penetrations of other ionic species.

5) To present a 2-D three phase model which can separately take the extremely thin structure in concrete, the ITZ phase, into account during the simulated migration

test. By examining the influence of ITZ, to demonstrate two opposing effects on ionic migration caused by aggregate particles.

6) To establish a group of 2-D cracked concrete models to examine the effect of geometric properties of cracks on the transport of chlorides.

7) To predict the chloride diffusion coefficient of concrete by the traditional stationary diffusion models (both in 2-D and 3-D models). To compare the results with three proven analytical models and to validate against experimental data of an accelerated chloride migration test (ACMT).

8) To predict the chloride diffusion coefficient of concrete by more improved migration models presented in Chapter 3-5. To compare the results with three proven analytical models and to validate against experimental data of an accelerated chloride migration test (ACMT). Also, to present a quantitative study about the influences of a series of significant factors (i.e. the external electrical field, ITZ phase, binding effect, etc.) on chloride migration.

1.4 Structure of the thesis

Chapter One presents an introduction to the problem of chloride-induced concrete and a brief research status of studying chloride transport in concrete. Additionally, the objectives of this study are highlighted in this chapter.

Chapter Two outlines the research background relevant to this study: scale definitions, theoretical basis, methodology discussions and literature review. Based on this review, the knowledge gap of existing work are summarised and the innovations of the present study are described.

Chapter Three presents a series of 1-D numerical models with a single phase to simulate the chloride migration test in a saturated cement paste specimen. This simple numerical model highlights several fundamental issues, including: the behaviours of multi-species transport, effects of non-linear potential, and the influence of initial ionic concentrations on the transport of individual ionic species. By comparing the electrostatic potential gradient, concentrations, fluxes and current density distribution profiles of two categories of results, the significance of using Poisson's equation is demonstrated in this chapter.

Chapter Four develops a series of 2-D models with two-phase composite to investigate the influence of movement dimension. Also, by exploring models with different shapes and volume fractions of aggregates, some important interaction transport features between ionic species have been found, which have not been seen before in the 1-D model of single phase. The influence of various forms of ionic binding between solid and liquid phases is also examined in this chapter.

Chapter Five includes two parts. In the first part, a series of 2-D concrete models with three-phased composite considering the ITZ phase are developed in order to simulate the chloride migration test and explore the impacts of ITZs on migration rate. Some important factors such as the thicknesses of ITZ, diffusion coefficients in ITZ phase and the volume fractions of aggregates are discussed in detail. In the second part, a group of 2-D cracked concrete models are proposed to examine the effect of cracks on the transport of chlorides. The investigation of the influence of geometric properties of cracks on the transport of chlorides is also detailed in this chapter.

Chapter Six presents the findings of a quantitative study to check the validity of models featured in the preceding chapters. The diffusion coefficient of chloride in concrete is evaluated during both diffusion and migration processes. The normalized concrete diffusion coefficients are firstly calculated by using the traditional stationary diffusion models in both 2-D and 3-D, then also calculated by using the migration models which have been proposed in preceding chapters. All of the obtained results are compared with three proven analytical models, i.e., Maxwell's model (Dormieux and Lemarchand, 2000), Bruggeman's equation (Bruggeman's, 1935) and the lower bound of the effective diffusion coefficient proposed by Li et al. (2012) as well as validated against experimental data sets of an accelerated chloride migration test (ACMT) brought by Yang and Su (2002).

The last chapter summarized the main contributions of the thesis. Findings and the limitations of presented models are listed, and several suggestions are given for possible further studies.

2 CHAPTER TWO – RESEARCH BACKGROUND

The second chapter of this thesis outlines the research background relevant to this study: scale definitions, theoretical basis, methodology discussions and literature review. Based on this review, the knowledge gap of existing work are summarised and the innovations of the present study are described.

2.1 Schematic structure of concrete at different scale definition

In concrete research field, the first concept should be given is scale. Since concrete, mortar and other cement based materials exhibit distinct behaviours of phase distribution under different scales, before summarising the methodology of analytical and numerical methods used to investigate structural properties of concrete, some definitions on the scales need to be clarified. Among most of the articles cited, there are three categories of scales being considered by researchers (Caré S. and Hervé E., 2004).

The first category is the macroscopic scale sketched in Fig.2.1 (a), which has the order of magnitude of 10^{-2} m. At this size, the objects being studied are usually global concrete specimens and the determination of various properties is relatively convenient but less accurate.

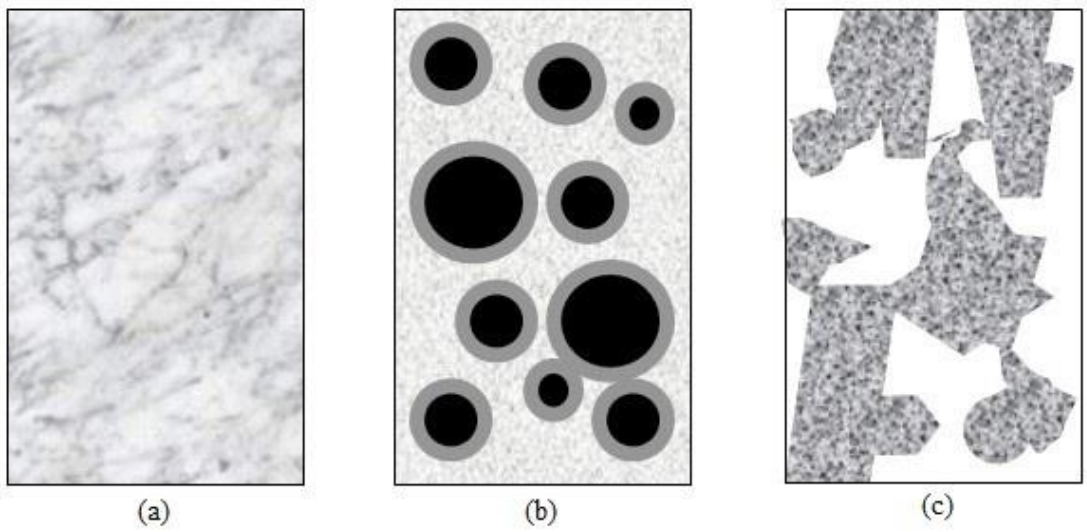

Figure 2.1. Three types of scales: (a) macroscopic, (b) mesoscopic and (c) microscopic (Caré S. and Hervé E., 2004).

The second category is called the mesoscopic scale ($10^{-6} - 10^{-3}$ m), which is adopted in the majority of studies cited herein and also in the present thesis. At this scale, the properties of concrete are controlled by the features of the aggregates and cement paste.

More precisely, concrete here is viewed as a heterogeneous three-phase composite material. According to the Fig.2.1 (b), the first phase represents the aggregates, which include not only the rigid material (siliceous aggregates) but also the porous material (calcareous aggregates). The aggregates are usually treated as an impermeable material. The second phase is the bulk cement phase, which is also called "matrix". The matrix is a porous medium filled with water, through which ionic transport can take place. The final phase is the interfacial transition zone (ITZ), which is an interface between the aggregate and cement paste phases and compounded by anhydrous and hydrated cement with certain porosity and volume fractions gradients. Unlike the bulk cement paste, ITZ, at the micro level, suffers an extra constraint due to the influence of aggregate surface (Garboczi and Bentz, 1997). ITZ can be ignored due to its small volume ratio in some of properties.

The third scale considered is the microscopic (order of magnitude: 10^{-9} m), showed in Fig.2.1(c). Compared to the mesoscopic scale, microscopic scale normally emphasizes the characteristic of the pore structure of the bulk cement paste phase. Among the studies of microscopic scale, the two major parameters used in describing the pores are porosity and tortuosity, which offer a convenient and qualitative approach to simulate the pore solution of mortar by using one phase model. Specifically, as it is illustrated in Fig.2.2, the bulk cement paste phase itself also can be divided into two parts; one is solid phase consisting of various hydration products, and the other is the capillary and gel pore phase, where the transport can take place. More precisely, the pore network structure possesses three kinds of characteristic: constrictivity, tortuosity, and conenetivity, as illustrated in Fig.2.3 (all white parts stand for pores and the remaining is solid phase).

The specific differences between these three scales on the structural properties of concrete research will be addressed in detail, later in the analytical method part (Section 2.3.1).

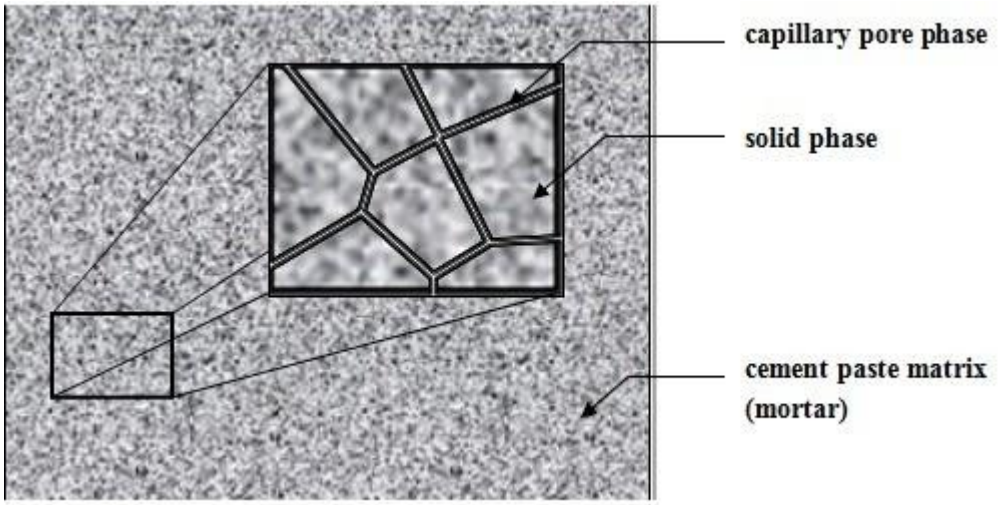

Figure 2.2. Microscope structure of bulk cement paste.

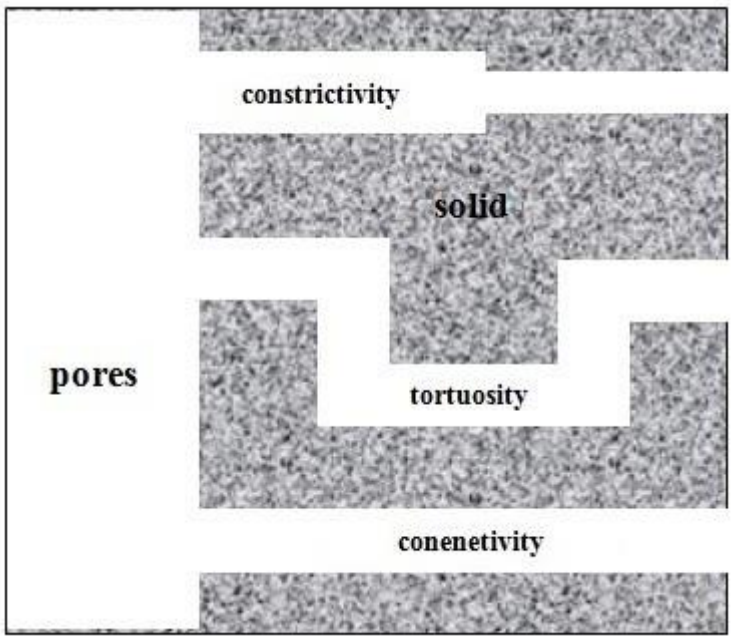

Figure 2.3. Schematic of constrictivity, connectivity and tortuosity of a pore network.

2.2 Theoretical basis

This section aims to explain the purpose of classifying the ionic transport behaviours, binding effect isotherms, and the classical equations in electrochemistry.

2.2.1 *Mechanisms of ionic ingress in concrete*

The durability problem of concrete regarded in this work is the penetration of ions. It is widely known the ingression of ions; especially the chloride ions in concrete will seriously corrode the reinforcing steel within. Hence the ionic transport behaviours in electrolyte solution should be clarified in the first place. Generally speaking, the mechanisms of ionic transport in a porous material can be classified into three basic categories: diffusion, convection and migration.

For consistency of description, the transport behaviours are expressed as a flux J (the moles of an ionic specie crossing per second per unit area of a plane normal to the flow direction) in the following sections.

2.2.1.1 *Diffusion*

Diffusion, describes the movement of ions through random motion from regions of higher concentration to regions of lower concentration, has been treated as a major driver of ionic transport in this study. The steady-state diffusion can be obtained easily from Fick's first law

$$J = -D\nabla C \tag{2.1}$$

where J, D, C are the flux, diffusion coefficient and concentration respectively of the diffusing material. It shows that diffusion flux of ions is proportional to the concentration gradient.

2.2.1.2 *Convection*

Convection of ions is caused by the bulk flow of the solution where ions are dissolved. Usually the convection term can be expressed as follows,

$$J = C \cdot u \tag{2.2}$$

where u stands for the advective velocity.

Specifically, the convection taken place in concrete or cementitious materials is normally aroused by pressure gradient, capillary adsorption and electro-osmosis flow.

a) Pressure flow

The driven pressure flow is the most common occurrence in the convection of pore solution within concrete. The essence of this phenomenon is that, the liquid experiences directional flow when subjected to pressure gradient. The pressure flow process can be described by Darcy's Law,

$$Q = -\frac{k}{\eta}\nabla p \tag{2.3}$$

where Q is Darcy flux (discharge per unit area, with units of length per time, m/s), k is the conductivity of medium, η is the viscosity of fluid, ∇p is the pressure gradient.

b) Capillary adsorption

In the presence of surface tension of fluid, the bulk fluid flow will occur to maintain the pressure equilibrium on both sides of liquid level in capillary. This behaviour is frequently found at the corroded concrete bridge pier above waterline. During the calculation, the capillary adsorption is equivalent to the pressure flow; therefore the flux of capillary adsorption can also be expressed in the form of Darcy's Law,

$$Q = -\frac{k(s)}{\eta}\nabla p \tag{2.4}$$

where *s* is the saturation. Because the capillary adsorption generally takes place at the unsaturated porous medium, the conductivity *k* here is a function of pore structure and saturation of solution.

c) Electro-osmosis flow

Maintenance of the chemical equilibrium between an electrolyte solution and a solid surface leads to the interface acquiring a net fixed electrical charge. As a result the hydrate of CaO, SiO_2, Al_2O_3, which contained in the cementing material, typically forms a layer of mobile ions, known as an electrical double layer or Debye layer in the region near the interface. When the fluid is subjected to an external electric field, the Coulomb force induces the net charge in the electrical double layer to move as well as drives the pore solution nearby as a resulting convection (Zhang and Gjorv, 1996). This kind of convection is termed electro-osmotic flow.

In terms of relationships between diffusion and convection, in most cases, diffusion and convection of ions occur simultaneously. A concept to govern them is the Peclet number, produced by the ratio of the diffusion time L^2/D to the convection time L/u, i.e;

$$P_e = \frac{u \cdot L}{D} \tag{2.5}$$

It is obvious to see that, if the effect of diffusion and convection in ionic transport are well-matched, the Peclet number will be approximate unity; while if the diffusion is the dominated transport, the Peclet number will be less than 1.

2.2.1.3 *Migration*

Migration is another major cause of ionic transport in concrete materials. When charged ions in a dilute solution are subjected to an electric field, their transport will be influenced by the electrical potential gradients.

The migration velocity equals to the electrical force per mole of ions divided by the frictional coefficient multiplied by Avogadro's number $F_e/(\overline{f}N_A)$. The electrical force acting on a mole of ions is comprised of the electrical potential gradient ($\nabla\Phi$), the net charge of the *k-th* ionic species z_k, and Faraday's constant F= 96487 C/mol. The flux caused by the electric field can be express as (Truskey et al., 2004),

$$J_k^{*e} = -\frac{C_k z_k F}{\overline{f}N_A}\nabla\Phi \tag{2.6}$$

where C_k is the concentration of the *k-th* ionic species. The flux and the potential gradient are in the same direction for anions and opposite for cations.

According to Stockes-Einstein equation (Truskey et al., 2004), the frictional coefficient and the diffusion coefficient have the relation of $\overline{f} = k_B T / D$. By using the universal gas constant $R = 8.314\text{J}\cdot\text{mol}^{-1}\cdot\text{K}^{-1}$ and the absolute temperature *T*=298K (273+25K) to substitute the Boltzmann constant k_B as well as to calculate $\overline{f}$, the Eq. (2.6) yields

$$J_k^{*e} = -\frac{DC_k z_k F}{RT}\nabla\Phi \tag{2.7}$$

2.2.2 *Binding effect*

A kind of binding effect, also called adsorption effect, experiences both physically and chemically at the pore surfaces. Since a portion of the free ions in pore solution are believed to be adsorbed by the cementing material of concrete. Thus, the total concentra-

tion of an ionic specie contained in concrete can be generally divided into two forms – free ions existing in concrete pore solution and the bound ions adsorbed by solid cement matrix. Since it can be assumed that the bound ions do not participate in the ionic transport process yet will certainly influence the concentration distributions within concrete, it is necessary to pay special attention to the binding effect.

The physical adsorption depends on the Van der Waals force and is very unstable, the bound ions adsorbed by the amorphous calcium silicate hydrates are likely be rereleased when subjected to exogamic force. Correspondingly, the chemical adsorption combined by chemical bond is significantly more stable. Taking the chloride ions as a typical example, they react with calcium and aluminates within cement to product Fieldel's salt ($3CaO \cdot Al_2O_3 \cdot CaCl_2 \cdot 10H_2O$) for chemistry reasons (Sahu et al., 2002):

$$3CaO \cdot Al_2O_3 \cdot 6H_2O + Ca^{2+} + 2Cl^- + 4H_2O \longrightarrow 3CaO \cdot Al_2O_3 \cdot CaCl_2 \cdot 10H_2O \quad (2.8)$$

As concrete mixtures have higher chloride binding capacities, they have increased capability to hinder the ingression of chloride ions. Generally, the mineral admixtures (i.e. fly ash, furnace slag) raise chloride binding capacity whereas the silica fume reduces it.

Nevertheless, it should be mentioned that the chemical binding process is not irreversible. There are two primary mechanisms for binding reversal. The first is that due to the equilibrium between free and bound concentrations, for which the bound ions will be released as the concentration in the electrolyte becomes lower (Wang et al., 2001). The second is that Fieldel's salt will be destroyed when subjected to the carbonation process and sulphates erosion, which also results in the chloride desorption (Yuan et al., 2009). Martin et al. (2000) suggested that the influence generated by binding effect during the ionic diffusion process can be described by the following equation,

$$\frac{\partial C_t}{\partial t} = \frac{\partial}{\partial x}(D\omega_e \frac{\partial C_f}{\partial x}) \tag{2.9}$$

where C_t is the total concentration of an ionic specie contained in concrete pore solution, C_f is the free ions existing in concrete pore solution, *D* here is the diffusion coefficient of free chlorides in pore solution, ω_e is volume fraction of vaporizable water.

Let $C_t = C_b + \omega_e C_f$, Eq. (2.9) can be modified as the form of Fick's Second Law (Eq. (2.10)) ,

$$\frac{\partial C_f}{\partial t} = \frac{D}{1+\frac{1}{\omega_e}\frac{\partial C_b}{\partial C_f}} \frac{\partial^2 C_f}{\partial x^2} \tag{2.10}$$

where C_b is the bound ions adsorbed by solid cement matrix.

Thus, the term $D_a = \frac{D}{1+\frac{1}{\omega_e}\frac{\partial C_b}{\partial C_f}}$ is defined as apparent diffusion coefficient by Nilsson et al. (1994).

$\frac{\partial C_b}{\partial C_f}$ represents the gradient of the concentration ratio between the bound and free ions, which indicates the binding capacity of concrete. Different kinds of concrete have different corresponding binding capacity. Generally, there are four categories of isotherm in defining the relationship between free and bound ions over a range of concentrations at a given temperature:

2.2.2.1 *No binding*

$$C_b = 0 \tag{2.11}$$

$$D_a = D \tag{2.12}$$

2.2.2.2 *Linear sorption isotherm*

$$C_b = \alpha C_f \tag{2.13}$$

$$D_a = \frac{D}{1+\frac{\alpha}{\omega_e}} \tag{2.14}$$

where α is an experimentally determined constant. Due to the simple expression, linear sorption isotherm is the most widely used in previous numerical studies. However, Nilsson et al. (1994) pointed out that linear isotherm may underestimate the binding capacity of concrete at lower ionic concentrations and overestimate that at higher ionic concentrations.

2.2.2.3 *Langmuir isotherm*

Langmuir isotherm is a more accurate expression than linear sorption isotherm and has been frequently adopted in literature (Sergi et al., 1992; Delagrave et al., 1997; Li and Page, 2000; Wang et al., 2001). The expression of Langmuir isotherm is as below,

$$C_b = \frac{\alpha C_f}{1+\beta C_f} \tag{2.15}$$

$$D_a = \frac{D}{1+\frac{\alpha}{\omega_e (1+\beta C_f)^2}} \tag{2.16}$$

where α and β are experimentally determined constants. From the examples of schematic of isotherms shown in Fig. 2.4, it can be found that the curve of Langmuir isotherm becomes horizontal at high concentration value of ions, which implicates that

the binding capacity of concrete has upper limit. Tang and Nilsson (1993) indicated that Langmuir isotherm is only valid when the concentration of chloride ions is lower than 0.05 mol/L in pore solution. However, later in the experiment of Li and Page (1998), it was proved that Langmuir isotherm still work well even if concentration of chloride ions is higher. It also should be noticed that, the assumption made in Langmuir isotherm that the binding capacity has a limitation is theoretically reasonable.

2.2.2.4 *Freundlich isotherm*

Due to the drawbacks of Langmuir isotherm, researchers tend to use Freundlich isotherm in simulating the ionic binding behaviour for high concentration pore solution (Truc, 2000; Spiesz et al., 2012). Mathematically, Freundlich isotherm is expressed as follows,

$$C_b = \alpha C_f^{\beta} \tag{2.17}$$

$$D_a = \frac{D}{1+\frac{\alpha\beta C_f^{\beta-1}}{\omega_e}} \tag{2.18}$$

It can be seen from Fig. 2.4 that, Langmuir isotherm allows the concrete to continue binding free ions even at high concentration, which was confirmed by Tang and Nilsson's experiments (1993). Tang and Nilsson also concluded that, when the concentration of ions in pore solution is higher than 0.01 mol/L , Freundlich isotherm has the best fit to the experimental data.

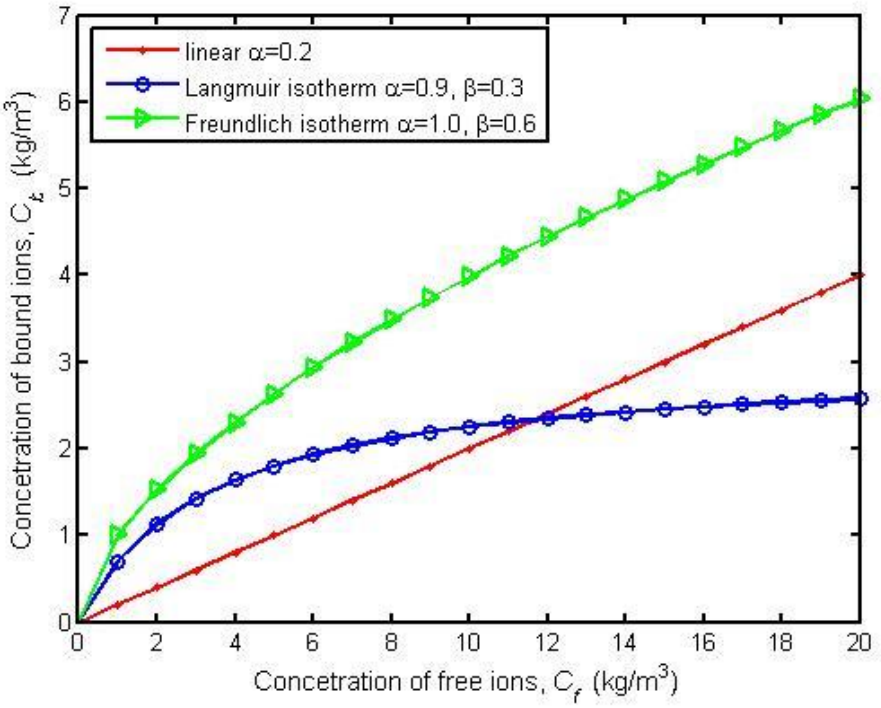

Figure 2.4. A comparison between linear, Langmuir, and Freundlich isotherms.

2.2.3 *Classic equations employed in electrochemistry*

In order to describe the ionic ingress in concrete as well as explain the relationship between the flux and the concentration of ionic species, three kinds of equation have been employed in literature, namely, Fick's laws, Nernst-Planck equation, and Nernst-Einstein equation.

2.2.3.1 *Fick's laws*

As it was mentioned above when the diffusion behaviour dominates the ionic movement process, the relationship between the flux J_k and the concentration C_k in a solution follows the Fick's first law, i.e.,

$$J_k = -D_k \nabla C_k \tag{2.19}$$

Fick's first law can empirically fit the steady state conditions of diffusion. However, when diffusion occurs in time-dependent circumstances, Fick's second law needs to be used to describe the non-steady state conditions. Suppose that ions are diffusing along parallel pipes with a volume $A\Delta x$ (a unit area A and length Δx). Let J_x and $J_{x+\Delta x}$ are the fluxes of inflow and outflow respectively, the accumulated mass within the reference volume in the time period Δt can be obtained,

$$\Delta m = (J_x A - J_{x+\Delta x} A)\Delta t \tag{2.20}$$

Dividing both sides of Eq. (2.20) by $\Delta x A \cdot \Delta t$, it yields

$$\frac{\Delta m}{\Delta x A \cdot \Delta t} = \frac{J_x - J_{x+\Delta x}}{\Delta x} \tag{2.21}$$

Obviously, the left hand side of Eq. (2.21) is the concentration change per unit time, and the right hand side is the flux gradient, that is,

$$\frac{\partial C}{\partial t} = -\nabla J \tag{2.22}$$

Substituting J with Fick's first law (Eq. (2.19)), Eq. (2.22).can be transformed into the expression of Fick's second law,

$$\frac{\partial C_k}{\partial t} = -D_k \nabla^2 C_k \tag{2.23}$$

2.2.3.2 *Nernst-Planck equation*

Fick's laws are unable to describe the ionic transport other than the diffusion process. When a transport process includes concentration gradient, electrical field, pressure flow and chemical activity, the flux of ionic species can be expressed by Nernst-Planck equation (Yang et al., 2002) as follows,

$$J_k = -D_k \nabla C_k - \frac{z_k F}{RT} D_k C_k \nabla \Phi - C_k u_k - \frac{C_k}{\gamma_k} \nabla \gamma_k \tag{2.24}$$

where γ_k is the chemical activity coefficient of the *k*-th species. For an ideal diluted solution, this chemical activity term can be ignored. Also, if the pore solution is fully saturated and there is no pressure differences, the convection term ($C_k u_k$) will vanish (Andrade, 1993). Hence, the Nernst-Planck equation can be simplified to a diffusion-migration form, as is adopted in the majority of the literature, that is,

$$J_k = -D_k \nabla C_k - \frac{z_k F}{RT} D_k C_k \nabla \Phi \tag{2.25}$$

Similarly to Fick's laws, for time-dependent conditions, Eq. (2.25) can be transformed into non-steady state form by using the mass conservation of individual ionic species as follows,

$$\frac{\partial C_k}{\partial t} = D_k \nabla^2 C_k + \frac{z_k D_k F}{RT} \nabla (C_k \nabla \Phi) \tag{2.26}$$

Sometimes, Eq. (2.25) is also called simplified Nernst-Planck equation in literatures.

2.2.3.3 *Nernst-Einstein equation*

Unlike Fick's laws and Nernst-Planck equation, which consider only the liquid phase in concrete, Nernst-Einstein equation (Lu, 1997) is applied to concrete and use the diffusivity and conductivity of ionic species in concrete.

Note that the total current carried by ionic transport can be expressed in terms of flux as follows,

$$I = zFJA \tag{2.27}$$

With the use of Ohm's Law, if the electric field (E_d) is linear, E_d can be redefined by the resistance R_r ,

$$E_d = \frac{\Phi}{d} = \frac{IR_r}{d} = \frac{zFJAR_r}{d} \tag{2.28}$$

where d is the distance between two electrodes of the electric field.

Meanwhile, the resistance R_r can be related with the resistivity (ρ) and conductivity (σ) as follows,

$$R_r = \frac{\rho d}{A} = \frac{d}{\sigma A} \tag{2.29}$$

Substituting Eq. (2.29) into (2.28), it yields,

$$E_d = \frac{zFJ}{\sigma} \tag{2.30}$$

According to the migration flux given in the Nernst-Planck equation, we have,

$$J_k = -\frac{D_k C_k z_k F}{RT} \nabla \Phi = -\frac{D_k C_k z_k F}{RT} E_d \tag{2.31}$$

Substitute Eq. (2.30) into Eq. (2.31), the following proportion relationship between the diffusivity and conductivity can be obtained,

$$D_k = \frac{RT\sigma_k}{z_k^2 F^2 C_k} \tag{2.32}$$

Eq. (2.32) is frequently utilised in the analytical method and Resistivity Techniques with the aim of measuring the diffusion coefficient of ions.

Fick’s Laws, Nernst-Planck equation, and Nernst-Einstein equation are the most often used approaches in the field of electrochemistry in relation to ionic transport in electrolyte in porous media.

2.3 Methodology

This section discusses different methodologies and offers a review of literature in relation to ionic transport in concrete. The review was carried out in terms of the methods used, namely, analytical, numerical, and experimental methods.

2.3.1 *Analytical method*

There is a large body of analytical approaches aiming to predict the diffusion coefficient on the basis of different scales.

2.3.1.1 *Macroscopic analysis*

At macroscopic scale, analytical method brings some empirical models. It is revealed from the existing data that the diffusion coefficient tends to have a connection with the water to cement ratio. Atkinson and Nickerson (1984) indicated that this relationship is approximately exponential in cement paste. However, Hobbs (1999) found the relationship between diffusion coefficient and water to cement ratio was weaker in concrete than in cement pastes, which shows that the influence made by aggregates cannot be negligible.

2.3.1.2 *Microscopic analysis*

Referring to section 2.1, there are two significant parameters of pore system in micro-scale situation: porosity ϕ and tortuosity β. According to Maxwell's model, β equals to $2/(3-\phi)$.

Zhang and Bishop (1993) evaluated the influence of porosity and tortuosity on the effective diffusivity in biofilms. They found that with porosities of 0.84-0.93 in the top layer and 0.58-0.67 in the bottom layer, tortuosity increases approximately from 1.15 in the

top layer to 1.6 in the bottom layer, while the ratio of biofilm effective diffusivity to the bulk solution diffusivity (D_e / D_b) decrease from 68-81% in the top layer to 38-45% in the bottom layer, when a cylindrical model as used.

Based on the concepts of porosity and tortuosity, the effective diffusion coefficient of an ionic species in porous media is given by $D_{eff} = D_0 \phi \beta$; see, for example, the work of Dormieux and Lemarchand (2000), Garboczi (1990), Van Brakel and Heetjes (1974) , where D_0 is the diffusion coefficient of the same ions in aqueous solution.

Garboczi and Bentz (1992) found the relative diffusivity, as a function of porosity and distance from the aggregate can be estimated as,

$$\frac{D}{D_0}(x) = 0.001 + 0.07\phi^2(x) + 1.8 \cdot H(\phi(x) - \phi_{cri}) \cdot (\phi(x) - \phi_{cri})^2) \qquad (2.33)$$

where D is the diffusivity of ions in the material of interest and D_0 is the diffusivity in bulk water, $\phi(x)$ is the capillary porosity volume fraction at a distance x from an aggregate surface and ϕ_{cri} =0.18 is the critical porosity, below which the capillary pore space will be disconnected. H is the Heaviside function (i.e., if $x>0$, $H(x)$=1, other wise $H(x)$=0).

Xu et al. (1997) employed the multi-scale percolation system concept to resolve the diffusion coefficient. The model was made of several elementary networks having mesh size proportional to the diameter of the real pores.

Garboczi and Bentz (1997) presented methods for use of a multi-phase microscope analytical model to solve some problems which previously required supercomputer-magnitude simulations, such as determination of the total volume of interfacial zones for

a given aggregate distribution and/or calculation of the effect of aggregates and ITZ on the overall diffusivity of the concrete.

Li and Xia (2011) proposed the upper and lower bounds of the effective diffusion coefficient of chlorides in concrete, which are expressed as $D_{eff}^{\max} = D_{cem}\phi$ and $D_{eff}^{\min} = D_{cem}\phi(1+\phi)/(3-\phi)$, were obtained by using 2-D series and parallel models.

Jiang et al. (2012) addressed further questions relating to the diffusion coefficient of ITZ with regard to the porosity distribution. The model considers the influence of water-to-cement ratio, the thickness of ITZ and the degree of hydration on the porosity distribution of ITZ. In their study, the relative diffusivity of bulk paste and ITZ proposed by Garboczi and Bentz (1992) was adopted and the diffusion coefficient of chloride ions in ITZ was given by,

$$D_{ITZ} = D_0(0.001 + 0.07\phi_{ITZ}^2 + 1.8 \cdot H(\phi_{ITZ} - \phi_{cri}) \cdot (\phi_{ITZ} - \phi_{cri})^2) \quad (2.34)$$

where D_0 is the corresponding diffusion coefficient in a bulk water at room temperature and ϕ_{ITZ} is the porosity of ITZ.

2.3.1.3 *Mesoscopic analysis*

In mesoscopic scale, analytical models consider the components of the two or three phases (aggregate and cement matrix; aggregate, bulk cement paste and ITZ) and their corresponding diffusive properties in these different phases.

Hobbs (1997) determined the lower and upper bounds of the effective diffusion coefficient in two-phase analytical model. By expressing the volume fraction and diffusion coefficient of the aggregates as C_A and D_A, respectively, as well as volume fraction

and diffusion coefficient of the cement paste as $(1-C_A)$ and D_P, respectively, the estimation of the bounds is,

$$\begin{cases} D_{eff}^{\min} = \dfrac{1}{C_A / D_A + (1-C_A)/D_P} \\ D_{eff}^{\max} = (1-C_A)D_P + C_A D_A \end{cases} \tag{2.35}$$

If it is assumed that the diffusion only takes place in the cement phase due to its much higher diffusivity, i.e., the diffusion coefficient of aggregates vanishes ($D_A = 0$), Eq.(2.35) can be simplified as,

$$\begin{cases} D_{eff}^{\min} = 0 \\ D_{eff}^{\max} = (1-C_A)D_P \end{cases} \tag{2.36}$$

Later, Hobbs (1999) proposed the specific relationship between D_{eff}, D_A and D_P as follows,

$$D_{eff} = D_P \frac{(D_A - D_P)C_A + (D_A + D_p)}{(D_P + D_A) + (D_P - D_A)C_A} \tag{2.37}$$

Xi and Bazant (1999) developed a more accurate two-phase analytical model, in which the effective diffusion coefficient is expressed by

$$D_{eff} = D_P \frac{2D_P(1-C_A) + D_A(1+2C_A)}{D_P(2+C_A) + D_A(1-C_A)} \tag{2.38}$$

Similarly, Eq. (2.38) can be simplified as $D_{eff} = D_P \dfrac{2(1-C_A)}{(2+C_A)}$ if the aggregates are treated as impermeable.

Carré and Hervé (2002) brought a three-phase analytical model for evaluating the effective diffusion coefficient of ions in mortar, which took into account the characteristic of

ITZ. The model assumed that each phase obeys the Fick's first law of ionic diffusion with no source or sink of ions. Under the Fick's law, the effective diffusion coefficient is presented as,

$$D_{eff} = D_B \frac{N}{D} \tag{2.39}$$

in which,

$$N = 6D_B D_I (1-C_A)(C_A + C_I) + C_I(1+2C_A+2C_I)(D_I - D_B)\times \\ (2D_I + D_A) + 3D_A[C_I D_B + C_A D_I (1+2C_A+2C_I)]$$

$$D = 3D_B D_I (2+C_A)(C_A + C_I) + C_I(1-C_A-C_I)(D_I - D_B)\times \\ (2D_I + D_A) + 3D_A[C_I D_B + C_A D_I (1-C_A-C_I)]$$

where C_I is the volume fraction of ITZ, D_I is the diffusion coefficient of ITZ and D_B is the diffusion coefficient of bulk cement matrix. Also, if aggregates are assumed to be impermeable ($D_A = 0$), Eq. (2.39) is simplified as,

$$D_{eff} = D_B \frac{6D_B(1-C_A)(C_A + C_I) + 2C_I(D_I - D_B)(1+2C_A+2C_I)}{3D_B(2+C_A)(C_A + C_I) + 2C_I(1-C_A-C_I)(D_I - D_B)} \tag{2.40}$$

Yang and Su (2002) considered not only the ITZ phase but also the migration of ions. The diffusion coefficient was replaced by the "migration coefficient", which was used to describe the diffusion coefficient during the accelerated chloride migration test (ACMT). Based on the experiment results they concluded an empirical formula to calculate the chloride migration coefficient as follows,

$$D_{\mathrm{cl}} = D_0(1-V_{\mathrm{f}})^{3/2} + D_0(\alpha - 1)(\beta V_{\mathrm{f}}) \tag{2.41}$$

where D_0 is the migration coefficient of ions in the matrix, V_f is the aggregate volume fraction. αD_0 is the migration coefficient of ions in ITZ , and βV_f is the volume fraction of ITZ. Note that this model assumes that the migration coefficient of the ITZ is constant and the chloride flow in the ITZ is locally parallel to the aggregate surface.

Caré (2003) developed a similar empirical formula, in which the chloride diffusion coefficient was expressed as a function of the volume fraction of aggregate and ITZ phase. From the diffusion test result, the effective diffusion coefficient can be estimated as,

$$D_{eff} = D_p[0.11C_I + (1-C_A)]\frac{2}{2+C_A} \tag{2.42}$$

Oh et al. (2004) combined both mesoscopic and microscopic scale in their analytical model to predict the diffusivity of concrete. In their study, the concrete was divided into three phases (aggregates, ITZ, and bulk cement paste) at mesoscopic level, then the bulk cement paste phase itself was treated as a two-phase porous media consisting of solid phase and capillary pore phase. The effective diffusivities of porous media was derived from general effective media (GEM) equation (McLachlan et al., 1990), and that of three-phase mesoscopic concrete was expressed by utilising the composite spheres assemblage (CSA) model (Hashin, 2001). With the help of Nernst–Einstein relation (Eq. (2.25)), the effective diffusivity of concrete or mortar can be written as,

$$D_{eff} = D_0 \cdot \Delta_\phi \cdot \Delta_a \tag{2.43}$$

where

$$\Delta_\phi = \left[\begin{array}{l} 0.5\{(D_s/D_0)^{1/n} + 1.22\phi_{cap}[1-(D_s/D_0)^{1/n}] - 0.22\} + \\ \sqrt{0.25\{(D_s/D_0)^{1/n} + 1.22\phi_{cap}[1-(D_s/D_0)^{1/n}] - 0.22\}^2 + 0.22(D_s/D_0)^{1/n}} \end{array}\right]^n$$

$$\Delta_a = 1 + \frac{V_a}{\frac{1}{2(D_i / D_p)t - 1} + \frac{1 - V_a}{3}}$$

Thus, the concrete diffusivity is determined by two main variables, i.e., the capillary porosity ϕ_{cap} and the aggregate volume fraction V_a.

Zheng and Zhou (2007) established a similar model with Caré and Hervé's (2002). Based on the three-phase composite circle model, the chloride diffusion coefficient of concrete can be determined as follows

$$D_c = D_m - \frac{2[2A_a + (1-q)A_i]D_m}{1 + q + (1-q)A_a(A_a + A_i)^{-1} + 2A_a + (1-q)A_i} \tag{2.44}$$

where D_m is the diffusion coefficient of cement paste, q is the ratio between diffusion coefficient of ITZ and cement paste, A_a and A_i are the volume fraction of aggregate and ITZ, respectively. Later, Zheng et al. (2009) further investigated the influence of ITZ on the steady-state chloride diffusion in mortars and concretes.

More recently, Zheng et al. (2012) represented another analytical model which contains the diffusivity of aggregate and aggregate shape effect. For the elliptical shaped aggregate, equivalent diffusion coefficient of aggregate is,

$$D_{ea} = D_{itz} - \frac{(1+\mu)^2 f_{agg}(f_{itz} + 2f_{agg})}{2[f_{itz} + (1+\mu)f_{agg}][\mu f_{itz} + (1+\mu)f_{agg}]} D_{itz} \tag{2.45}$$

where μ is the ratio of major and minor axes of the elliptical aggregate particles.

However, it should be mentioned here that, all of the analytical models presented above are for the steady state conditions, regardless of diffusion or migration process.

2.3.2 *Experimental method*

For the sake of protecting the reinforced steel within concrete from corrosion induced by chloride ions and improving the understanding of the ionic transport in concrete, great efforts have been made on the assessment of ionic transport by using experimental techniques. In this section, the experimental methods used in investigating the chloride penetration in cement related materials are reviewed.

2.3.2.1 *Diffusion tests*

Diffusion test is a traditional way for measuring the chloride penetration in concrete based on Fick's Laws. In early years, two standard test methods have been designed. One is the salt ponding test and the other is the bulk diffusion test.

a) Salt Ponding Tests

Salt Ponding Test, standardised by American Association of States Highway and Transportation Officials and American Society of Testing and Materials as T259 (AASHTO T259, 1980) and C1543 (ASTM C1543, 2002) was developed to investigate the penetration mechanism of chloride ions into concrete bridge decks. The schematic of Salt Ponding Test is shown in Fig. 2.5. Generally speaking, the chlorides in the upstream cell will diffuse into the downstream chloride-free cell if the time is sufficient (normally in 90 days). The test specimen consists of a concrete slab with a dike located around the top perimeter to store the ponding solution (Fig.2.6).

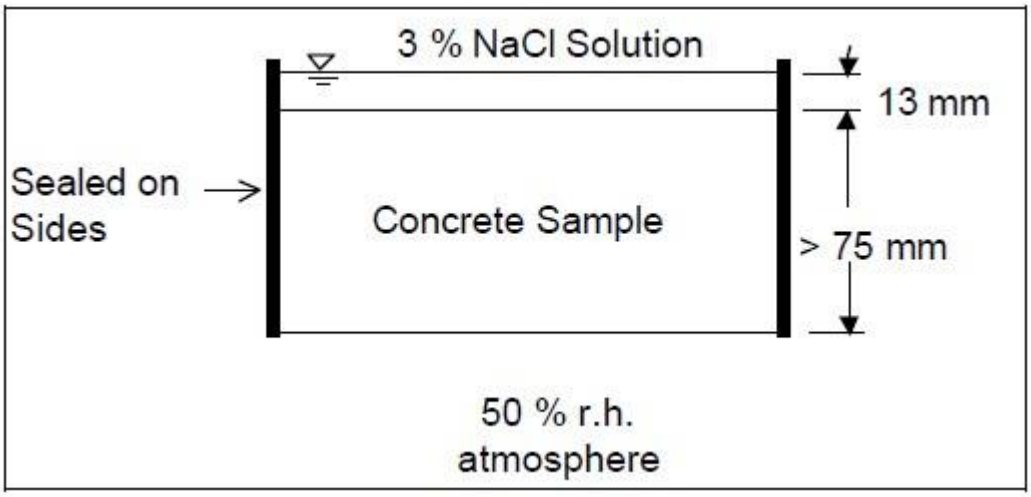

Figure 2.5. Schematic of Salt Bonding Test (AASHTO T 259, 1980) set up.

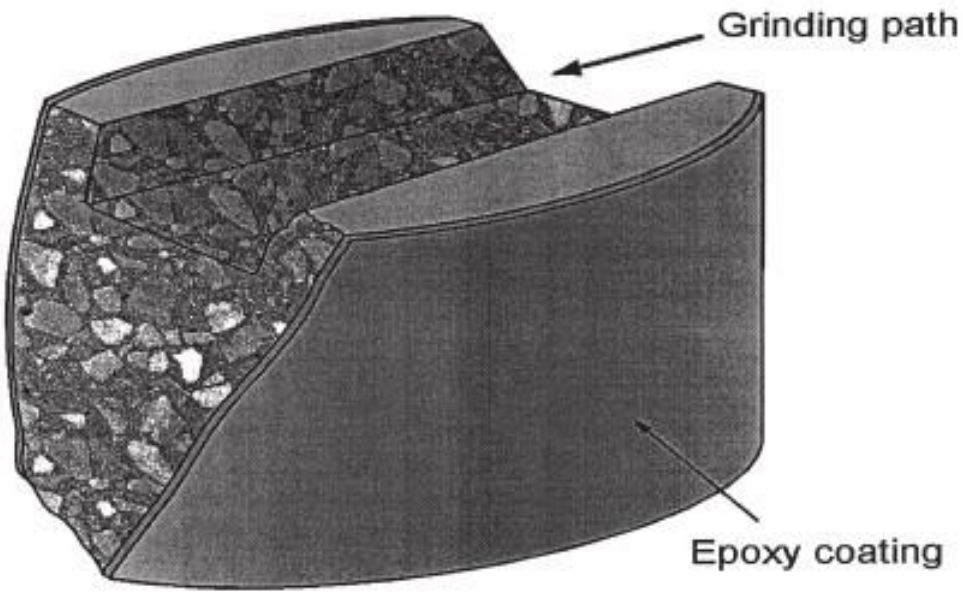

Figure 2.6. Schematic of profile ground specimen (Patrick et al., 1999).

b) Bulk Diffusion Test

An alternative test method, Bulk Diffusion Test, was developed to measure chloride diffusivity during a diffusion progress. In terms of initial moisture condition of the sample, the specimen to be tested in a Bulk Diffusion Test is saturated with limewater instead of being dried for 28 days in Salt Ponding Test, which can prevent any initial sorption ef-

fects when the chloride solution is introduced. Besides, the Bulk Diffusion Test makes the uncovered face expose to a 2.8 mol/L NaCl solution, unlike Salt Ponding Test leaving one face exposed to air. All these modifications can certainly improve the test accuracy and reduce the test duration.

The Bulk Diffusion method was adopted by Nordic standard as NordTest NTBuild 443 (1995). Fig.2.7 shows a schematic diagram of the test.

Note that both Salt Ponding and Bulk Diffusion Tests are time-consuming, especially the Salt Ponding Test when applied for high-performance concrete (HPC), of which the test duration maybe last 150 days or even longer to get a sufficient chloride profile.

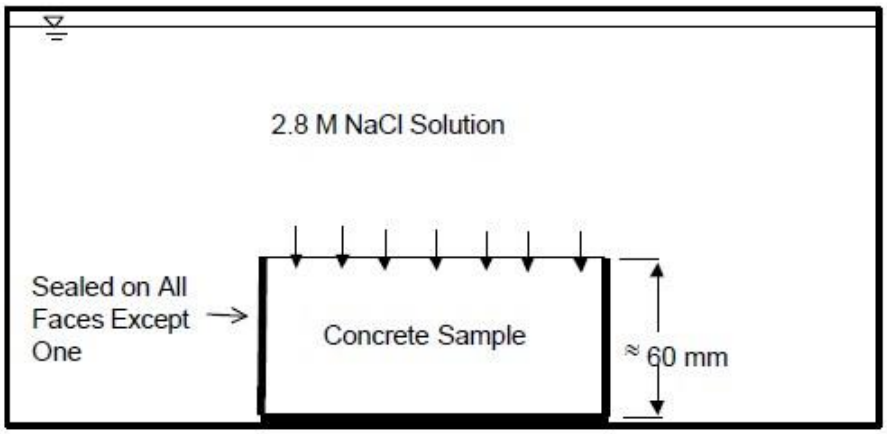

Figure 2.7. Schematic of Bulk Diffusion Test (NordTest NTBuild 443, 1980) set up.

2.3.2.2 *Migration tests*

Due to the long duration of diffusion tests, people tend to adopt experiments based on migration, which contain the Coulomb test, steady state migration test, Resistivity Techniques, and non-steady state migration test to obtain more information about chloride penetration.

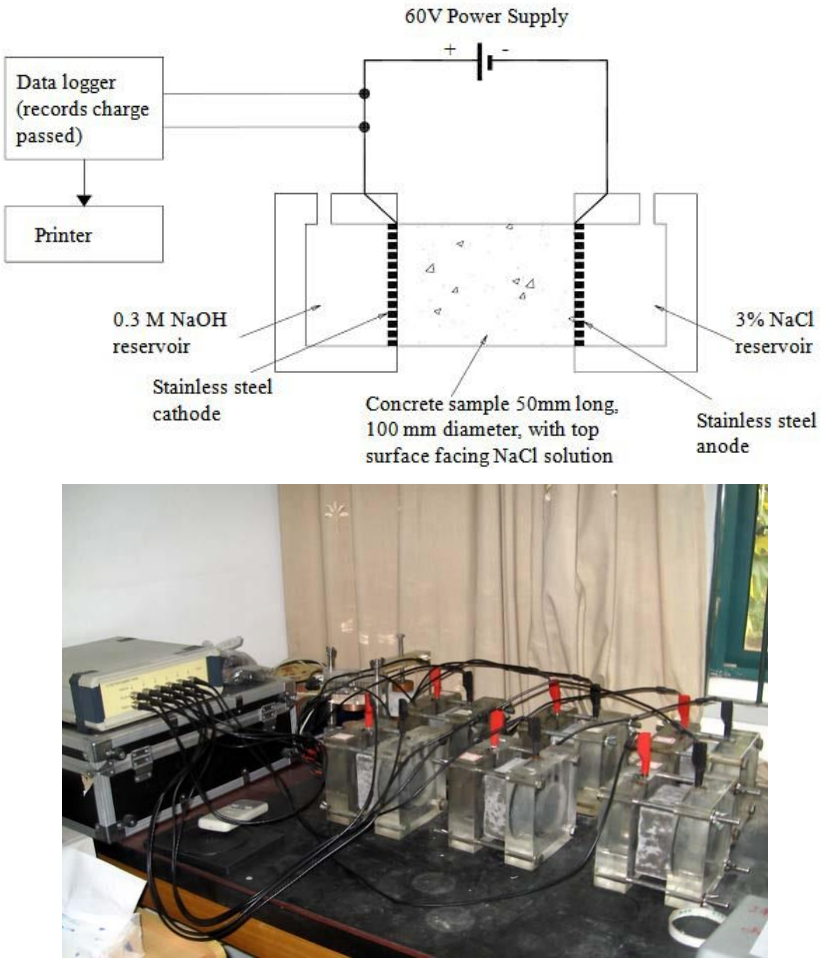

Figure 2.8. Rapid chloride permeability test (AASHTO T277, 1983) set up: schematic (above) and actual (below).

a) Coulomb Test

Coulomb test, initially developed by Whiting in 1981 (Whiting, 1981) and then adopted as AASHTO T 277 (1983) and ASTM C1202 (1994), was the first famous approach replacing diffusion tests to measure chloride diffusivity. As is illustrated in Fig. 2.8, a water-saturated, 50mm thick, 100mm diameter concrete cylinder is located between two compartments; one has a 3.0% NaCl solution and the other has a 0.3 mol/L NaOH solution. Externally, there is a 60V DC voltage applied between the two compartment solutions. After a 6-hour migration test, the total charge passed (coulombs) is measured and this is used to rate chloride ions penetrability. This test method is also known as the

Rapid Chloride Permeability Test (RCPT) though this name is inaccurate as it is actually not the permeability that is being measured but coulomb charge movement.

However, during the last two decades, a number of studies (Andrade, 1993; Feldman et al., 1994; Pfeifer et al., 1994; Scanlon and Sherman, 1996; Shi et al., 1998; Shane et al., 1999; Hooton et al., 2000; Shi, 2004) have raised criticisms of the RCPT test method based on a variety of reasons. In general, their opinions can be summarised as this: factors which normally have much to do with electrical conductivity or resistance of concrete make insufficient influence on the transport of chloride. More specifically, the results obtained from charge passed in the test cannot exactly represent the permeability especially when the chemistry of pore solution was taken into account. Andrade (1993) employed a migration test and indicated that the function between measured charge through the concrete and the moving ions is more suitable for hydroxyls than chlorides. A comparison made by Pfeifer et al. (1994) also showed that 6 to 15 times coulomb value growth only arouse 1 to 2 times increase of actual chloride ingression in the corresponding 90-day ponding test. Shane et al. (1999) confirmed that the deviation between permeability and electrical conductivity or resistance will be even higher when acting on concrete made with silica fume, fly ash, and other super-plasticizer admixture. Another research proposed by Shi (2004) concluded that an increase of volume fraction can decrease the electrical conductivity of concrete due to the dilution effect of conductive ions in pore solution and the adsorption of alkalis on the surface of aggregates. Briefly speaking, unstable scientific bases and rough testing method make the measured diffusion coefficient of chloride quite unreliable.

Nonetheless, even though Coulomb Test experiences a series of deficiencies, it has been treated as a classical technique for bringing accelerated electrical field in chloride in-

gression measurement. Since it was adopted as a standard test method, during last 30 years or so, it has gathered a great quantity of experimental data, which is often referenced in literature. Additionally, the apparatus set up of RCPT provided a valuable groundwork for developing other migration test methods such as steady and non-steady state migration tests.

b) Steady state migration tests

In view of the drawbacks of Coulomb Test, an alternative test method was developed based on accelerated electrical field – steady state migration test. The theoretical background of this test method is attributed to the Nernst-Planck equation (Eq. (2.25)). When the transport process reaches a steady state, the diffusion term in Eq. (2.25) can be removed, which leads,

$$J_k = -\frac{z_k F}{RT} D_k C_k \nabla \Phi \tag{2.46}$$

If the potential gradient in Eq. (2.46) is assumed to be a constant, i.e., $\nabla \Phi = \frac{U}{L}$ where U is the externally applied DC voltage, then from Eq. (2.46) one can obtain the diffusion coefficient as follows,

$$D_{\mathrm{Cl}} = \frac{RTL}{FU} \times \frac{J_l}{C_1} \tag{2.47}$$

where J_l is the flux of chloride at downstream boundary and C_1 is the concentration of chloride at upstream boundary. Note that because of the steady state, the flux of chloride is approximately a constant. By gauging the flux of chlorides at downstream boundary, the chloride diffusion coefficient can be obtained. In some literatures, D_{Cl} calcu-

lated from Eq. (2.47) is also named as migration coefficient due to the dominant role of migration flux in the steady state migration test.

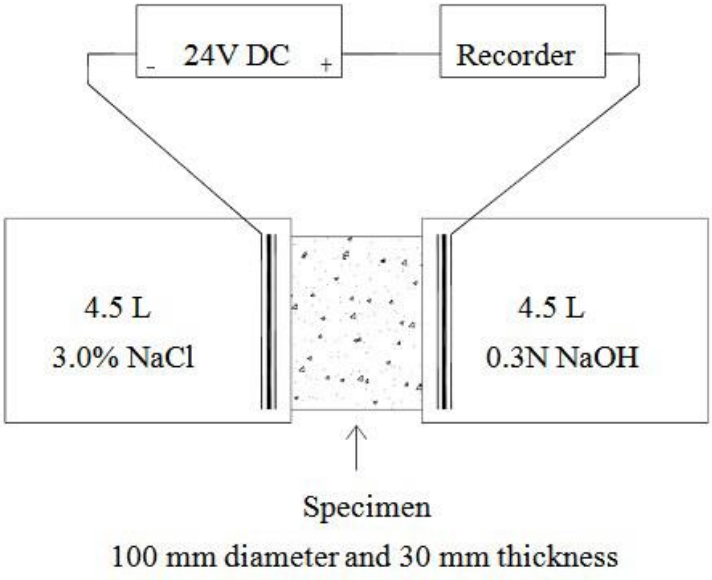

Figure 2.9. Schematic of steady state migration test (NordTest NTBuild 335, 1997) set up.

This method was carried out in the early 1980's and revised in 1990's. In 1997, it was recommended by Nordic standard as NordTest NTBuild 335 (1997). The equipment set is very similar to Coulomb Test and is shown in Fig. 2.9.

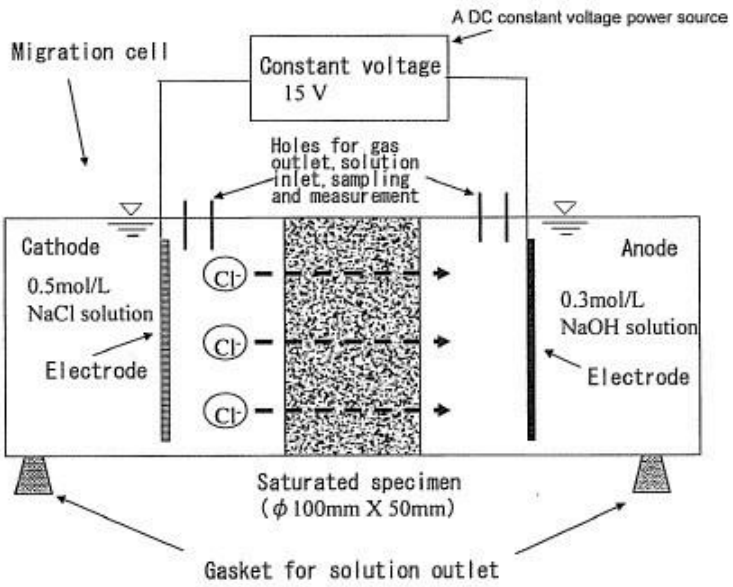

Figure 2.10. Schematic of steady state migration test (JSCE-G571, 2003) set up.

Another standard steady state migration test was adopted by the Japan Society of Civil Engineers as JSCE-G571 (2003), the purpose of which was the calculation of the effective diffusion coefficient of chloride ions in concrete from migration, which is depicted in Fig. 2.10 Distinctly from RCPT and NTBuild 335, the volume of two cells is not strictly specified in JSCE-G571.

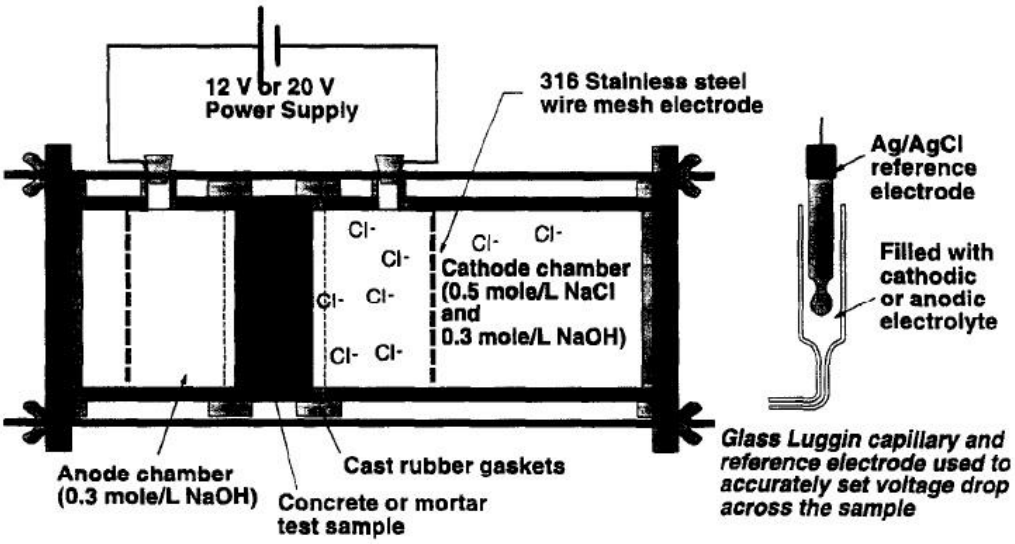

Figure 2.11. Schematic of steady state migration test (Mcgrath and Hooton, 1996) set up.

Mcgrath and Hooton (1996) built another apparatus based on the steady state migration test method. As it is demonstrated in Fig. 2.11, the sizes of upstream and downstream cells are unsymmetrical there. In the cathode chamber, there are not only NaCl but also 0.3 mol/L NaOH solution. An Ag/AgCl reference electrode assembly was placed in the gap between the specimen face and the stainless steel electrodes to adjust the desired driving potential for the test set up.

Delagrave et al. (1996) ran a 3-week steady state migration test to determine the migration coefficient of chloride ions in several different concrete mixes. In their experiments, the solutions in two cells are the same as those in Mcgrath and Hooton's work. But differently, the compartments of two cells were equipped with an agitating facility for bet-

ter maintaining the homogeneity of the solutions, and ruthenium-coated titanium electrodes were used.

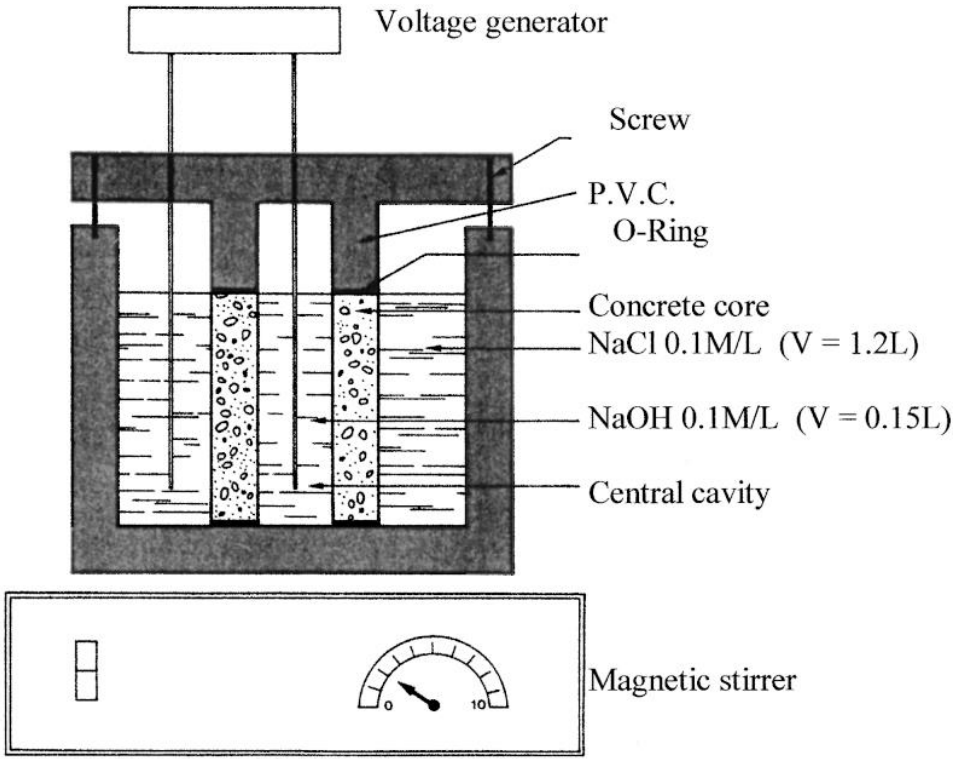

Figure 2.12. Schematic of 'concrete cube' migration test (Prince et al., 1999) set up.

Prince et al. (1999) presented a novel 'concrete cube' migration test, which permits continuous determination of the main physical parameters during a concrete migration test. The schematic diagram of test arrangement is described in Fig. 2.12. The diffusion cell is a cylindrical PVC tank covered with a lid. The test tube is a cylindrical core of concrete as a concrete sample with 100 mm diameter and 100 mm height, in which a secondary drilling produced a central cavity of 40 mm diameter. This tube is fixed firmly in the cell by the intermediary of a hollow PVC roll and divides two compartments filled with NaCl and NaOH solutions. A stainless steel electrode is inserted in the external chamber as a cathode, while a carbon electrode is inserted in the internal chamber as an anode. The power is supplied across these two electrodes with values limited to 30V and run

over several days. During the treatment time, the amount of chloride migrated through the concrete, the conductivity, and the pH are monitored.

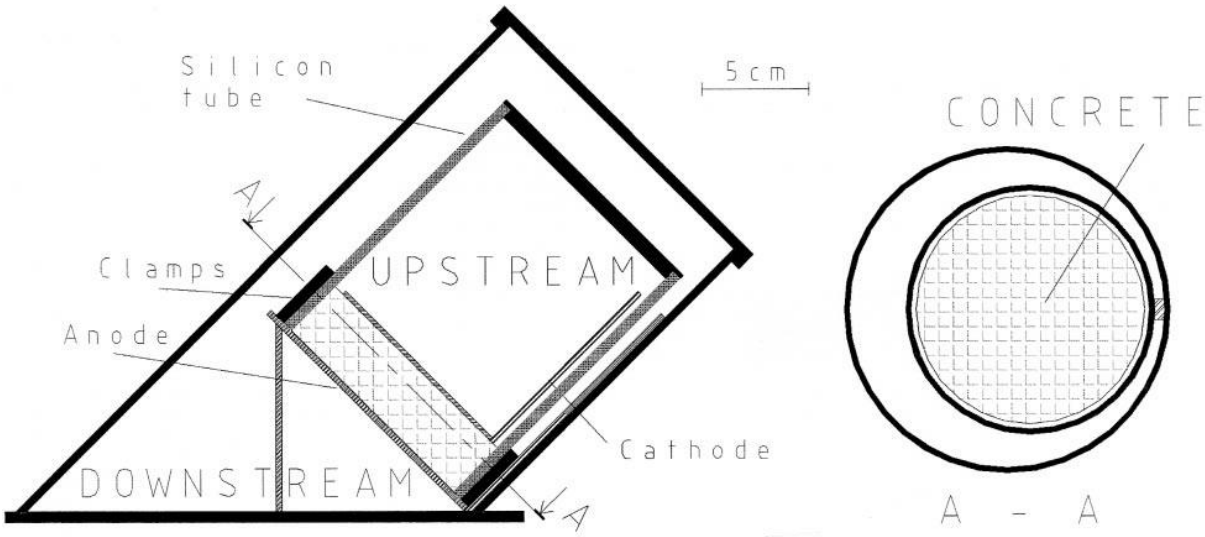

Figure 2.13. Schematic of LMDC (Truc et al., 2000) set up.

Figure 2.13 shows an additional steady state migration test proposed by Truc et al. (2000). This test is called LMDC (Laboratoire Matériaux et Durabilité des Constructions) and allows the determination of the effective diffusion coefficient by measuring the drop in chloride concentration in the cathode chamber. The upstream cell contains 0.5 L of chloride salts (NaCl, NaOH and KOH) and the downstream cell contains 2.5 L of a hydroxide solution (NaOH and KOH). A 12V DC voltage is applied across the cylinder concrete specimen and the solution in chamber is renewed frequently during the test.

With the aim of eliminating the Joule effect caused by high current density, Yang et al. (2002) modified the device of Coulomb Test (ASTM C1202, 1994) by enlarging the capacities of two cells from 0.25L to 4.5L (shown in Fig. 2.14). This accelerated chloride migration test abbreviated to ACMT was adopted in a series of studies thereafter (Yang and Su, 2002; Yang, 2003; Yang and Cho, 2003; Yang and Wang, 2004; Yang, 2005;

Yang and Cho, 2005; Yang, 2006; Yang et al., 2007) to explore different parameters and features during the migration of ions, such as the diffusion/migration coefficient, charge passed, ITZs, pore structure effect, etc. The durations of the test used in most studies are more than 3 weeks.

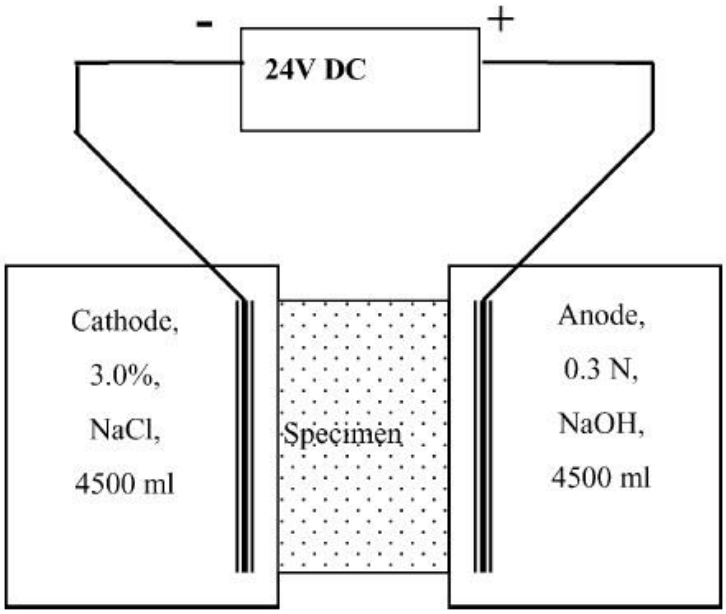

Figure 2.14. Schematic of ACMT (Yang and Su, 2002) set up.

In summary, though the steady state migration tests achieve more stable scientific bases than the Coulomb Test, it still has some disadvantages. The fatal one is that it takes a very long time (normally more than 2 weeks) from power on to reaching steady state especially for the large thickness specimen. If one increases the external voltage to speed up the process, it will lead to polarization phenomenon and Joule Heat, just like Coulomb Test does. Additionally, when it reaches steady state, it is still difficult to monitor the concentration changes in downstream cells.

c) Resistivity Techniques

Resistivity Technique is a special case of steady state migration test. If a vacuum equipped concrete specimen saturated in a highly conductive chloride solution, it will

reach steady state migration instantly. By then the pore water conductivity of the concrete sample equals to that of solution. This conductivity can be easily obtained by ordinary ways just like measuring electric circuit. With the help of Nernst-Einstein equation, the chloride diffusion coefficient can be calculated if the conductivities are known.

Streicher and Alexander (1995) carried out a rapid chloride conduction test based on above idea. As it is shown in Fig. 2.15, except for the use of the two traditional cells both containing 5 mol/L NaCl solution, two $Cu/CuSO_4$ half cells are placed to measure the potential difference across the concrete specimen. All the cylinder concrete samples will firstly be dried in an oven at 323K for 7 days to remove moisture from the capillary pores. After that, they will be vacuum saturated in a 5 mol/L NaCl solution for 5 hours and left to soak for 18 hours. A 10V voltage is applied between two electrodes to accelerate the procedure of becoming steady state.

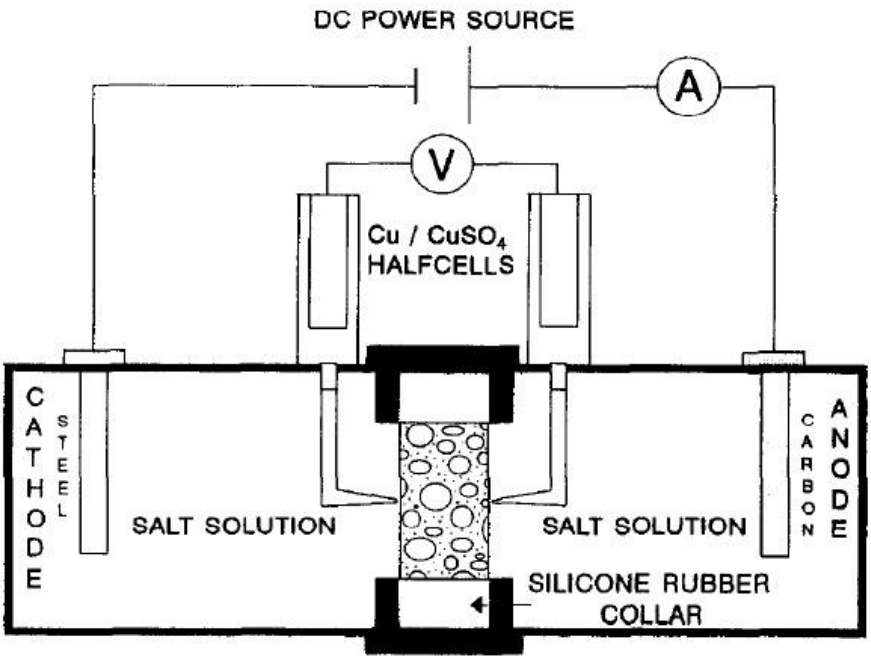

Figure 2.15. Schematic of Resistivity Technique (Streicher and Alexander, 1995) set up

Streicher and Alexander's test method was shortly confirmed by Lu (1997). He also indicated that the problem of temperature can be eliminated when a low voltage is applied and the binding effect can be ignored when the concrete was saturated with salt solution.

Otsuki et al. (1999) modified the Coulomb Test (ASTM C1202, 1994) for another resistivity test. The cylinder specimen in the classical Coulomb Test is replaced by a 30 mm thick concrete disk as shown in Fig. 2.16. The concrete disk was adhered to a rubber attachment using epoxy resin. Besides, a saturated $Ca(OH)_2$ solution is added to the anode and a 5% NaCl solution is added to the cathode. Finally, an electrical potential difference was externally applied to the two titanium electrodes under monitoring. When it reaches the specific electric current density, one can employs Nernst-Einstein equation to calculate chloride diffusivity within the sample.

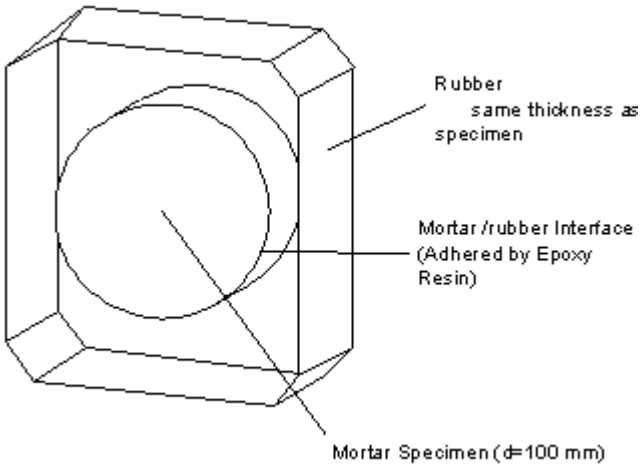

Figure 2.16. Schematic of disk-type specimen (Otsuki et al., 1999).

Generally speaking, Resistivity Techniques can significantly reduce the treatment time relative to the normal steady state migration tests as well as the influence caused by other ion species within pore solution. However, resistivity techniques are still based on electrical measurements and have accuracy problems just like the Coulomb Test (RCPT). Moreover, theoretically, the high concentrations of ions may affect the valida-

tion of classical equations such as Nernst-Planck equation and Nernst-Einstein equation. It also should be noted here that, the operation of vacuum saturating will cause an irreversible damage on the inherent structure of the concrete.

d) Non-steady state migration tests

In consideration of the criticisms about Coulomb Test (RCPT) and long treatment duration of the steady state migration tests, researchers developed the non-steady state migration test.

Initially, Tang and Nilsson (1992) proposed a migration test scheme named CTH (Chalmers Tekniska Högskola) and provided a mathematical theory for calculating the diffusion coefficient of chloride ions, which is expressed as follows,

$$D_{\mathrm{Cl}} = \frac{RTL}{FU} \times \frac{x_d - 2\sqrt{\frac{RTLx_d}{FU}}\,\mathrm{erf}^{-1}(1-\frac{2C_d}{C_1})}{t_d} \tag{2.48}$$

where x_d is the penetration depth of chloride ions at a test duration t_d, C_d is the chloride concentration at x_d, erf^{-1} is the inverse of error function. Other parameters are accordant with Eq. (2.47).

The essence of CTH apparatus is almost the same as Coulomb Test and can also be taken as steady state migration test; however it allows direct measurement by the depth of chloride penetration instead of using the total passed charge to estimate the permeability or calculating the chloride flux at downstream boundary. After completion of the 18-hour test, the specimen is split in half. An exposed surface misted with a silver nitrate solution changes colour to off-white because of the chemical reaction between silver and chloride ions, therefore indicating penetration depth (Fig. 2.17). The results are ex-

pressed in $\text{mm}/(\text{V}\cdot\text{hr})$ by dividing the average chloride penetration depth by the product of the applied voltage and the duration of the test (as shown in Eq. (2.48)).

Figure 2.17. Split specimen and penetration depth displayed (Tang and Nilsson, 1992).

Later, the above method was adopted by Nordtest and AASHTO as NT Build 492 (1999) and AASHTO provisional Standard TP64 (2003), called as the rapid chloride migration test (RCM) or the rapid migration test (RMT). As it is depicted in Fig. 2.18, the concrete specimen employed in NT Build 492 is a series of cylinder samples with 100mm diameter and 50mm thickness. The pre-treatment of the samples before the test is very similar with that in RCPT standard; however, the fluid used for soaking the samples is a saturated Ca(OH)_2 solution. Then, the concrete sample is tilted into a $370\times270\times280\text{mm}$ plastic box. The solutions contained in the cathode and anode cells are a 10% NaCl and a 0.3 mol/L NaOH, respectively. The voltage and the time used in the test depend on the electrical properties of the concrete sample which is shown in Fig. 2.19. Firstly, an initial current I_0 is obtained from an initial voltage of 30 V. With this current, the voltage to be applied in the test, *U*, is found from the standard. Finally, once

the voltage *U* is applied, the test duration in hours is obtained from the standard using the possible new initial current.

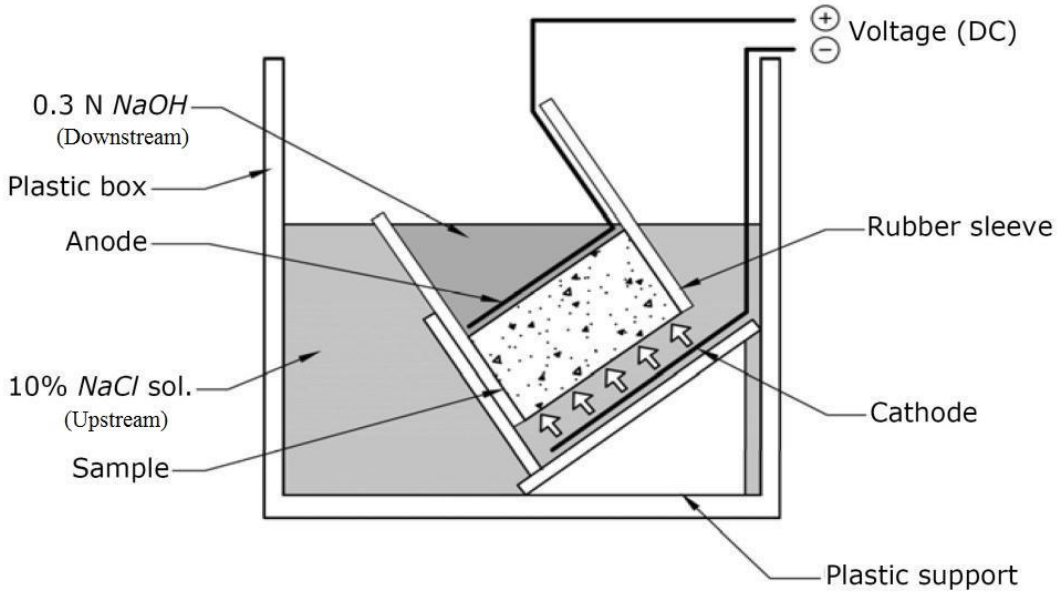

Figure 2.18. Schematic of steady state migration test (NT Build 492, 1999) set up.

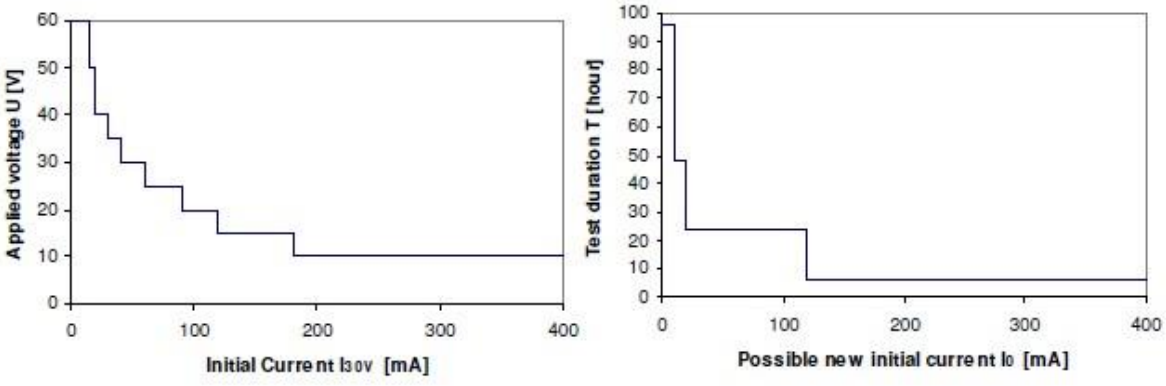

Figure 2.19.Determination of the voltage and time (NT Build 492, 1999).

Castellote et al. (2000) created another non-steady state migration test using an apparatus similar to the Salt Ponding Test (Fig. 2.20). The cathode stainless steel mesh is placed on the top of the specimen with a 0.5 mol/L NaCl Solution. A steel plate and a damp sponge acting as an anode are placed on the bottom of the specimen.

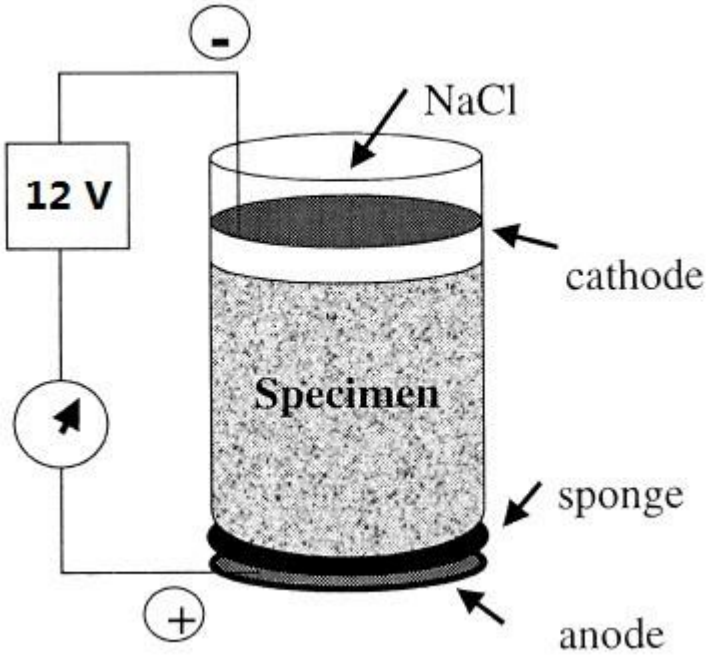

Figure 2.20. Schematic of non-steady state migration test (Castellote et al., 2000) set up.

The non-steady state migration tests (RCM) support a number of important advantages, i.e. simple test procedure, short testing duration and a good repeatability of results; therefore this method is widely used in recent years and has been suggested to substitute for the traditional Coulomb Test (RCPT).

To sum up, the experimental data in the literature were mostly obtained by means of taking traditional concrete as a specimen while very few were for the new types of concrete. Additionally, similar to analytical approach, the migration tests described above are mainly used to investigate the transport of chloride ions alone, the transport of other ions and their effect on the chloride transport are not addressed.

2.3.3 *Numerical method*

Owing to a series of important advantages against experimental techniques, i.e. the convenience of preparation, ease in governing parameters, shorter calculating duration and

better view of results, numerical methods have become a favoured method used to explore the mechanism of ionic transportation in composite materials.

2.3.3.1 *Ionic transport of single-species*

Similar to the analytical and experimental methods, this category of study focuses on only one specie (chloride for the most part) during the ionic transport process, neglecting the ion-ion interactions from microscopic point of view. Since this kind of issue is not the main concern of this thesis, only recent work is listed here.

a) Solving the single-species transport by using Fick's Law

The aim of studies under this category is usually to investigate chloride diffusion behaviour in more complex concrete models.

Zeng (2007) established a 2-D hetero-structure model and used FEM to simulate the chloride diffusion behaviour in a heterogeneous concrete composed of two phases (aggregates and cement paste matrix) with distinct chloride diffusivities. It was found that in a heterogeneous concrete, the chloride diffusion is quite different from that in the homogeneous medium. Another conclusion is that, the chloride binding effect and time-reducing effect of diffusion coefficient in cement paste may remarkably slow down the chloride diffusion in concretes.

Zheng and Zhou (2008) proposed a three-phase composite sphere model to represent the heterogeneous nature of concrete and derived a closed form expression for chloride diffusion in concrete. Later, Zheng et al. (2009) further investigated the influence of ITZ on the steady-state chloride diffusion in mortars and concretes. More recently, Zheng et al. (2012) presented a 2-D lattice model which contains the diffusivity of aggregate and ag-

gregate shape effect. They obtained an expression which includes the ratio of major and minor axes of the elliptical aggregate particles.

To describe the effect of recycled aggregate (RA) on the chloride diffusion in recycled aggregate concrete (RAC), Xiao et al. (2012) proposed a five-phase mesoscope sphere model to simulate recycled aggregate concrete (RAC). The five-phase composite sphere contains the old and new interfacial transition zones (ITZs) as inter phases, and the new mortar, old attached mortar and original aggregate, which is illustrated in Fig. 2.21. The work also used Fick's second law and finite element methods.

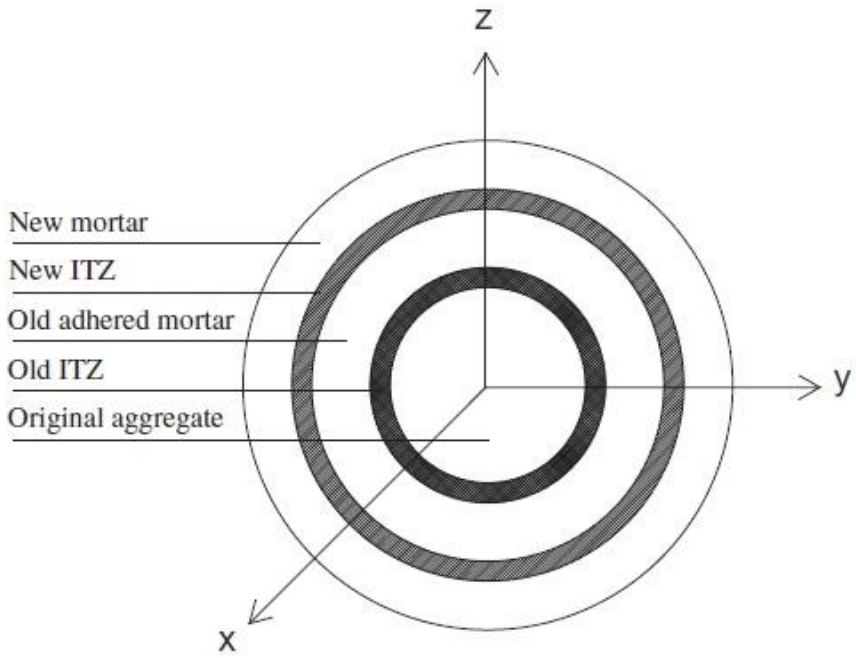

Figure 2.21. Five-phase composite sphere model. (Xiao et al., 2012).

Li et al. (2012) used two-phase models in both two and three dimension to predict effective diffusion coefficient of chlorides in concrete. They found that the shape of aggregate has a small influence during the diffusion process and also gave a lower bounds of the effective diffusion coefficient of chlorides in concrete as a function of porosity.

More recently, Dehghanpoor Abyaneh et al. (2013) represented a 3-D numerical model with three phases to investigate the diffusion coefficient of chlorides in concrete. The effects of the shape and orientation of ellipse particles on diffusivity was found in this 3-D model.

b) Solving the single-species transport by Nernst-Planck equation

Adopting the Nernst-Planck equation allows one to simulate the electro-migration process such as the processes occurred in the Rapid Chloride Permeability Test and Rapid Chloride Migration test.

Claisse et al. (2010) developed a computer model to simulate the Rapid Chloride Permeability Test (ASTM C1202). This study models the changes of the voltage distribution to hold the charge neutrality and enables the model to predict current-time transients similar to those recorded in experiments. Then, the basic parameters such as diffusion coefficients for tested samples by optimising to the observed data can be obtained.

Spiesz et al. (2012) set up a new theoretical model for calculating effective chloride diffusion coefficient and concentration profiles for the Rapid Chloride Migration test (NT Build 492). This model accounts for the chloride Freundlich isotherm binding and non-equilibrium conditions between the concentrations of free and bound ions in concrete. The results show that this model can offer a better accuracy while the D_{RCM} calculated in the traditional way is overestimate.

2.3.3.2 *Ionic transport of multi-species*

Due to the limitation of single-species transport, extendedly, more work has to do in exploring the interactions between different ionic species in the pore electrolyte solution

on the ionic transport, particularly the diffusion and migration of chloride ions. For coupling the movements run by different ions together, one needs to determine the electrostatic potential in the first place. There are two fundamental kinds of approach in literature for governing the potential in bulk solution matrix.

The first approach is called electro-neutrality condition, which ensures that no external charge can be imported (Bockris and Reddy, 1998) and determines the electrostatic potential of each point of the electrolyte solution:

$$\sum_{k=1}^{N} z_k C_k = 0 \tag{2.49}$$

where C_k is the concentration of the *k-th* ionic species in the pore solution.

However, it should be noted that, electro-neutrality condition, which is employed in the above studies to govern the electrostatic potential in solution, is not a constitutive law but only a mathematical assumption and may cause problems. The real constitutive law for governing the electrostatic potential is the Poisson's equation.

$$\nabla^2 \Phi = -\frac{F}{\varepsilon_0 \varepsilon_r} \sum_{k=1}^{N} z_k C_k \tag{2.50}$$

where Φ is the electrostatic potential, F = 9.648×10^{-4} C·mol^{-1} is the Faraday constant, ε_o=8.854×10^{-12} C·V^{-1}·m^{-1} is the permittivity of a vacuum, and ε_r=78.3 is the relative permittivity of water at temperature of 298K.

It is obvious from Eq. (2.50) that, if the electro-neutrality holds then Eq. (2.50) can be simplified as $\nabla^2 \Phi = 0$. This implies that if the problem is one-dimensional then the electric field would be a constant. Numerical examination of Eq. (2.50) shows that, the

constant factor in the right-hand-side of Eq. (2.50), $\frac{F}{\varepsilon_0 \varepsilon_r}$, is a very large number with the order-of-magnitude of 10^{14}. In order that the left-hand-side of Eq. (2.50) be finite, the concentration terms in the right-hand-side of Eq. (2.50) must be very small, i.e. $\sum_{k=1}^{N} z_k C_k \approx 0$. This indicates that the electro-neutrality is not a physical condition but only a numerical approximation. It should be pointed out here that, $\sum_{k=1}^{N} z_k C_k = 0$ and $\sum_{k=1}^{N} z_k C_k \approx 0$ are qualitatively different, although from a numerical point of view these two may be very close. The former implies $\nabla^2 \Phi = 0$ while the latter is not.

However, numerically, directly solving the Poisson's equation is a difficult job in the early years since it involves calculations of large and small numbers.

a) Solving the multi-species transport by Fick's Laws

Under this category, studies look into the diffusion behaviour as the dominant form in the ionic transport process by coupling Fick's Laws and electro-neutrality condition (Eq. (2.49)) to model the multi-species diffusion in electrolyte solutions.

Snyder and Marchand (2001) investigated the effects of ionic species and their initial concentrations on the apparent diffusion coefficient of chlorides in cementitious materials. The results showed that concentration made a relatively slight influence while the speciation impacted markedly during the short-time period.

Taking into consideration of dissolved calcium ions, Sugiyama et al. (2003) proposed a simultaneous ionic transport model (SiTraM) for chloride penetration into a cement-based material on the basis of the generalized form of Fick's first law and corresponding

chemical reactions. The calculated concentration profiles of calcium within solid phase and chloride confirmed the presence of Friedel's salt generated by the binding of chloride ions. In 2008, they (Sugiyama et al., 2008) again applied this SiTraM method to simulate the profiles of chloride and calcium to pore structures. Meanwhile, effects of other parameters like w/c ratio, temperature, time and depth were discussed on ionic transport.

b) Solving the multi-species transport by Nernst-Planck equation

Obviously, Fick's laws are insufficient for studying the mechanisms of actual ionic transport since plenty of cases or experiments involve externally applied electrical field to accelerate the diffusion procedure. In order to find the concentration/flux profiles and other transport properties of ions during the diffusion-migration process, a great significant body of work has been conducted in the last few decades using the Nernst-Planck equation. Methodologically speaking, these works can be divided into four categories as described below in detail.

i) Integration of zero current method with the use of electro-neutrality condition

In electrolyte solution, if there is no charge at any point, a zero current condition can be adopted. As the current density into any point equals the one out of it, the conservation equation of current density is given as follows:

$$I = F\sum_{k=1}^{N} z_k J_k = 0 \tag{2.51}$$

where I is the current density, z_k and J_k are the charge number and the flux of the *k-th* ionic species in the cement paste and N is the total number of the species involved in the pore solution.

A series of studies investigated the diffusion of chloride ions in the cement pore electrolyte solution under the above-mentioned hypothesis of zero current and electroneutrality condition.

In order to explain the interactions between multi-species, Lorente et al. (2003) developed and proved a new approach based on the Nernst-Planck equation instead of the Fick's laws to describe ionic transfer in cement-based porous media.

Similarly, Khitab et al. (2005) built another numerical model, a new version of Msdiff (Multi-Species Diffusion), to simulate the process of chloride ingression through the saturated cement paste. In the work, they accounted for the interactions of ions and solid phase in concrete and also employed the Nernst–Planck/current law equations. This study pointed that the chloride diffusion coefficient should be evolved with time since the constant one caused an over-estimation on the predictions.

Since the properties of Electrical Double Layer (EDL) generated at solid/liquid interface plays a significant role in the transportation of ions through cementitious systems. Elakneswaran et al. (2010) presented an integrated thermodynamic model including the surface complex, the phase-equilibrium model, and the multi-component diffusion mode to describe the interaction between cement hydrates and electrolyte solution during the ionic penetration process. Thereinto, thermodynamic equilibrium of solid/solution and the interaction of different ionic species were managed by the phase-equilibrium model and surface complexation model respectively. The simulated results revealed that the rate of ingression of ions through the pore solution of cement paste was distinctly affected by the physical adsorption ions on cement hydrate surfaces, the size of pores, and the surface site density of calcium silicate hydrate.

Based on the finite element method, Yaya et al. (2011) applied Nernst–Planck equation, electro-neutrality condition and zero current method to investigate the initiation stage of localized corrosion in AISI 316L stainless steel (AISI 316L SS) and commercially pure titanium (cpTi). They concluded that both these two alloy systems are highly resistant to the initiation of crevice corrosion in 0.9% NaCl solution. A comparative analysis showed that the cpTi is more corrosion-resistant than the AISI 316L SS.

Samson et al. (1999) proposed a slightly different model relative to above researches. This method also combined the electro-neutrality condition and zero current method, but adopted an extended Nernst–Planck equation with a chemical activity term ($\frac{C_k}{\gamma_k}\nabla\gamma_k$) instead of the more commonly used diffusion-migration form of Nernst–Planck equation, so that it can be taken for clarifying more complex problems. As a result, they found the effect of chemical activity on the concentration profiles is only a slight error, thus one could be tempted to ignore chemical activity and just use the diffusion-migration form of Nernst–Planck equation. However, the total membrane potential becomes about two times larger when adding the chemical activity term, so the effect of chemical activity coefficients cannot be neglected from the potential point of view.

Lizarazo-Marriaga and Claisse (2009a; 2009b) proposed a special concept, membrane potential (produced by the differences in mobility of the species), to solve the multi-species diffusion-migration problem. Their computer models also use the hypothesis of charge neutrality of the different ionic species.

ii) Integration of externally applied current density with the use of electro-neutrality condition

There were also studies other than those cited above which added the factor of externally applied current density as well as considering the interactions between ionic species during the transport of ionic species in cement-based materials. Besides, in these studies, the electrostatic potential throughout the electrochemical process was still controlled by assuming the electro-neutrality condition.

Li and Page (1997) proposed a mathematical model based on a semi-empirical expression of activity coefficients of ions for simulating the transport of different ionic species in concrete. They found that the influence of activity coefficients of ionic diffusion and migration on the transportation became increasingly considerable along with the rise of externally applied current density. At the year of 2000, they established a finite element model of the previous Yu and Page's work (1996), which took into account the influence of factors including externally applied current density, treatment period, diffusion coefficients, ionic binding, boundary conditions and medium porosity on the ionic mass transport behaviour. The simulated results exhibited that the amount of chloride removed increased with the externally applied current density, chloride diffusion coefficient and time. Chloride binding also played a significant role during the process.

It is widely accepted that the effective diffusion coefficient is one of the most important parameter in the ionic transport research. The LMDC test method, which is a recent technique in order to obtain the effective diffusion coefficient efficiently, gets distinct result from experimental conditions. To explain this discrepancy, Truc et al. (2000a) developed a new numerical approach and an MsDiff code based on Matlab. This theory allows for simulating the removal of chloride from concrete under an electrical field. They not only computed profiles of ionic concentration, flux, and the potential, but also studied the effect of pore solution composition, chloride binding and the non-ideality of so-

lutions. A procedure explaining how to cope the effective diffusion coefficient with the LMDC test method accurately is also proposed in this article. Meanwhile, Truc et al. (2000b) indicated that the membrane potential and the pore solution composition, which have usually been neglected in previous work, influenced chloride transport substantially by using numerical model based on the Nernst-Planck system of equations as well as a detailed comparison between the simulations and experiments. This work proved that employing Fick's first law to calculate the effective diffusion coefficient would overestimate the rate of chloride transport or/and removal.

Most of the electrochemical chloride removal (ECR) research discussed above was only treated as 1-D problems. Considering on this point, Wang et al. (2000) set up a 2-D numerical model yielding a non-linear convection-diffusion equations based on Galerkin finite methods to predict the transport of ions within porous media. A number of factors, electrostatic coupling of charged ions, treatment time, position of anode, VIZ, ionic binding, porosity and tortuosity of pore material, enrolled in this model as well. The profiles highlighted the significance of influence of position of anode on chloride removal, as well as exhibited that electrochemical process could also increase the concentration of hydroxyl ions next to the steel when decreased the chloride concentration.

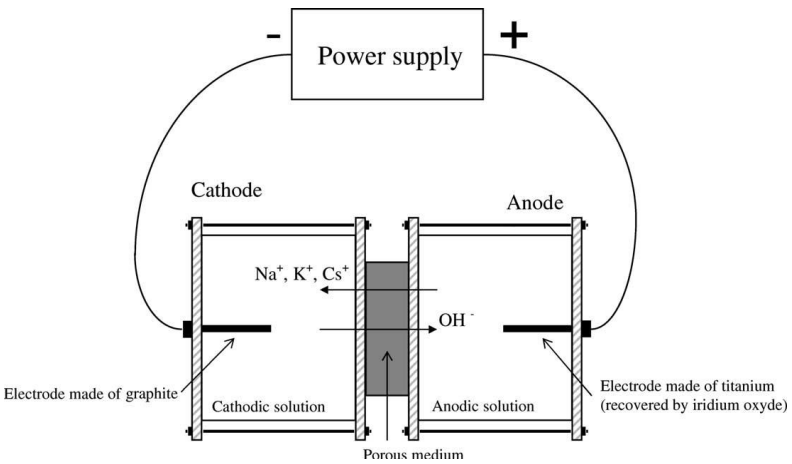

Figure 2.22. Decontamination cell (Frizon et al., 2003).

For the purpose of nuclear decontamination, Frizon et al. (2003) built a mass transfer model on the basis of Nernst-Planck equation, the current density conservation and the mass balance equation to simulate a laboratory experiment of cesium decontamination in cementitious materials under an external applied electrical field. A sketch of set-up of this experiment is shown by Fig. 2.22. The computing results led to a conclusion that, though the liquid junction potential was far less than the external electrical field applied, it should be taken into account for the accurate prediction. Further attentions should be paid to the sensitivity analysis on the initial cesium concentration, the hypothesis of irreversible cesium binding/reversible cesium sorption must be treated as two extreme conditions.

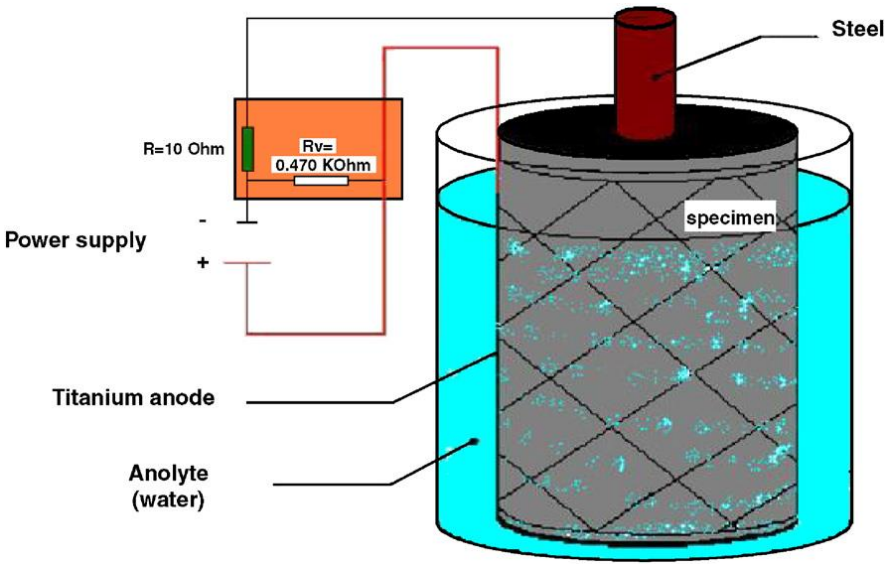

Figure 2.23. Electrochemical chloride extraction setup (Toumi et al. 2005).

Toumi et al. (2005) developed a numerical model based on the Nernst-Planck equations to simulate an experiment of Electrochemical Chloride Extraction (ECE) briefly illustrated in Fig. 2.23. With the purpose of to reduce binding between chloride and matrix as well as to restrict the number of species considered in the computation, they combined cylindrical brick with concrete specimens to produce this desalination programme.

By comparison of numerical and experimental results, it was validated that ECE method can substantially prevent the chloride ions from reaching central steel while increase the positive species amount. They also found binding isotherm affected significantly in the estimation.

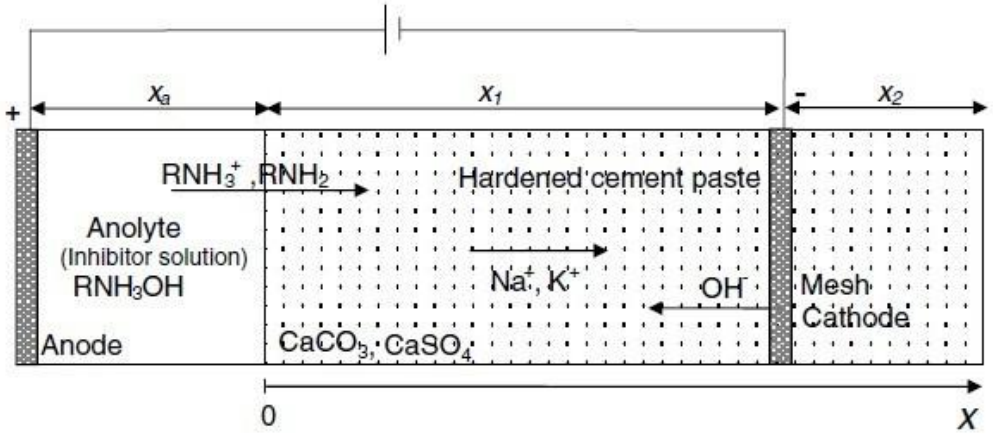

Figure 2.24. Physical system of transport in hardened cement (Kubo et al., 2006).

In order to simulate the previous experiment of ionic transport in carbonated hardened cement paste employing constant current density with the use of organic base corrosion inhibitors (ethanolamine and guanidine), which is shown in Fig. 2.24, Kubo et al. (2006) proposed a mathematical model solving Nernst-Planck equations to predict the concentration profiles of injected inhibitors and other major ionic species in pore solution phase. The interactions of various ions in solution, acid/base dissociation balance and the solubility products of dicalcium were also examined in this work.

Ouyang et al. (2009) presented a mathematical model coupling Nernst-Planck equation and externally applied current density to simulate the process of ECR treatment of marine cast iron artifacts. Based on linear sorption isotherm, the release of binding chloride ions were also taken into account in this model. The result profiles clearly indicate that increasing treatment time, current density, chloride diffusion coefficient by a constant

factor, together with the rate constant of release of binding chloride ion all results in an increase of the chloride removal.

iii) Integration of externally applied voltage with the use of electro-neutrality condition

Similar researches with externally applied voltage instead of the current density on the transport of ionic species in the pore solution of cement paste have been done.

The earlier model included Nernst–Planck equation, electro-neutrality condition and externally applied voltage can be traced back to Walton's work (1990). The governing equations system was developed for modelling the localized corrosion of iron. In the bulk solution, the Laplace's equation ($\nabla^2 \Phi = 0$) was utilised for potential. According to the statements in Section 2.3.3.2, this equation agrees with the electro-neutrality condition ($\sum_{k=1}^{N} z_k C_k = 0$). This model was confirmed by the comparison between experimental and theoretical results and evidenced that large potential drops can occur in some localized corrosion systems even in the absence of cavity blockage by build-up of corrosion products.

Sa'id-Shawqi et al. (1998) continued to apply the above model to the problem of electrochemical chloride removal (ECR) and obtained the chloride profiles of both removed ones (at anode) and the remaining ones in concrete.

Zelinsky and Pirogov (2006) set up a simple kinetic model utilised Nernst–Planck equation and electro-neutrality condition to simulate the corrosion in the $Cu/CuSO_4 + H_2SO_4$ system based on a two-stage charge transfer mechanism. Consequently, the homogeneous dissociation reactions of cupric sulphate and sulphuric acid,

as well as diffusion and migration of the dissolved ions were both solved in this numerical study.

Narsillo et al. (2007) proposed an accurate numerical multi-ion transport model coupled with the Nernst–Planck equation and electro-neutrality condition for simulating the electro-migration test and some of factors which can contribute to the discrepancies of the results: temperature, intensity of applied electric field, concentration of testing solution, electrode types and chemical activity. One of the major conclusions is that, relative to diffusion induced by concentration gradients and ionic interactions, the migration due to the external voltage different dominated the removal process. They also found that the differences of initial chloride concentration caused growing non-linearity in electrical potential and simultaneously impacted the prediction in non-steady-state conditions.

Krabbenhoft and Krabbenhoft (2008) compared the variation between the conventional single-species model (SSM) and the more complete Poisson–Nernst–Planck (PNP) model and derived a simple closed-form expression of effective chloride diffusivity. As the computed results showed, the difference of these two models could amount to 50 to 100%. They also indicated that SSM model would be reasonable by proper experiment set-up, such as adjusting the ratio of sodium chloride and sodium hydroxide.

With the aim of investigating the limitation of a purely geometrical approach in describing the transport of ionic species in cementitious materials, Friemann et al. (2008) implemented a comparison between the measured currents obtained from migration tests on cement mortars with different w/c ratios and the simulated ones given by a multi-species model. They concluded that a simulated current evolution got a higher rate than

the measured results regardless isotherms existed or not, which derived that a purely geometrical approach alone was insufficient to represent the ionic transport problem.

iv) Poisson's equation

As it was mentioned in Section 2.3.3.2 that the hypothesis of electro-neutrality condition may cause invalidations, more recently, studies were carried for exploring the ionic diffusion in multi-phase materials by using the Poisson's equation instead of electro-neutrality condition. Among these works, there is no external voltage setting throughout the electrolyte solution; hence, the transport of ions is still dominated by the diffusion and the migration is occurred only because the imbalance diffusion of various ionic species.

Johannesson et al. (2006) attempted to use a numerical model based on the Nernst-Plank equations for the purpose of quantitative understanding of the basic mechanisms of multi-species ionic diffusion process and the accurate agreement with the experimental results. The chemical interaction between different types of ions in solid/liquid phase in this model is assumed to be determined by simple ion exchange processes. When the comparing with the measured electron probe micro analysis data, one of their main conclusions was that, to establish an accurate multi-species model, it was insufficient to only consider standard solubility calculations.

The work of Samson and Marchand (2007) explored the effect of temperature on ionic transport in cementitious materials. This model including the Extend Nernst-Planck equation and Poisson's equation paying attention to not only the multi-species ionic transport and temperature field, but also some other transport properties (i.e. porosity, tortuosity, and unsaturated water content field) and chemical reactions (i.e. the for-

mation of Friedel's salt). As a consequence, they states that considering only an average constant temperature can lead to inaccurate estimations due to the nonlinear nature of the temperature effects.

Johannesson et al. (2009) proposed a numerical model employing finite element techniques to investigate a coupled non-linear problem, involving the ionic diffusion and moisture transport in the pore solution of porous material. The technique processed a linearization procedure on the non-linear systems and coupled set of Nernst-Planck equations to produce an iterative scheme and adopted Petrov-Galerkin method to solve convective terms directly. Calculations showed that, the two non-standard terms in the Nernst-Planck equations led a significant influence on the test simulation. They also verified that the application of implicit time integration approach as well as an evolutionary Newton-Raphson iteration scheme could be qualified to the mentioned problems. In term of chemical reactions among the ionic species, it was not taken into account in this model in order to of make it suitable to be implemented into existing computer codes for chemical equilibrium.

In view of the constituent forms of the quasi-static versions of Maxwell's equations and mass conservation, Johannesson (2010a) used a simplified version of hybrid mixture theory (HMT) to generalise the Poisson-Nernst-Planck (PNP) equations including a set of diffusion equations of charged species for cases where the deformation and stresses of the porous materials can be neglected. Similar with the previous work, the finite element method was used to product the coupled non-linear matrix system. Then, Johannesson (2010b) developed another numerical technique under the zero current condition and based on the FEM for calculating a set of Nernst-Planck diffusion equations of multi-species ionic transport in saturated uncharged porous materials. On the part of the

equilibrium of each time step, the author employed a one-step truly implicit time stepping scheme as well as an implementation of a modified Newton-Raphson iteration scheme. This method was studied numerically together with the more general Gauss' law method. By comparing the results of two distinct physical based approaches, it concluded that the zero current based method had the benefit of calculation speed since one less state variable while it was not valid for microscopic configurations existing charge separation.

2.4 Knowledge gap and innovations

There have been substantial work and publications done for the exploration of chloride transport in concrete. Regarding the most concerned problem, the multi-species transport in concrete, due to its short research history, some issues need further investigation, especially in the following aspects:

1) Most simulations model for ionic migration used electro-neutrality condition to determine the electrostatic potential of each point in solution instead of the real constitutive law of electrochemistry, Poisson's equation, due to its difficulty in calculating the large and small terms. Though electro-neutrality condition can be tenable in some cases, it is only a mathematic approximation and the validity of result is questionable.

2) The existing numerical concrete models subjected to external electric field for predicting the ionic migration were one-phase, only having the liquid section of cement phase. The influence of aggregate phase and ITZ phase on chloride migration has never been addressed in the literature. Apparently, it is defective for precise simulation of the ionic removal without considering the aggregate inclusions and ITZs in concrete simulation.

3) No research has been done to consider the chloride transport under externally applied electric field in more than 1-D model. How the motion in the second and third dimension will affect the result has not been reported in literature.

4) Most of publications exploring chloride penetration in concrete only taken the single-component transport (i.e. the chlorides) into account. The transport of other ionic species and their effect on the chloride transport were seldom inves-

tigated, especially for the literature which utilise analytical and experimental approach.

5) Multi-phase numerical concrete models which were carried out for predicting the chloride diffusivity in recent years only considered the diffusion process of ions and mostly of focused on a stationary problem. It is evident from the Fick's laws and Nernst-Planck equations that, the migration results in a much more complex transport behaviour than the diffusion process. Also, similar to analytical and experimental approaches, these numerical diffusion models only take a single-species of ions (i.e. the chlorides) into account during the transport, neglecting the effects of ionic interactions.

In this thesis, a series of multi-phase meso-scale models with 2-D and/or 3-D will be established to address the above problems.

2.5 Summary

This chapter outlines the research background relevant to the study of chloride transport in concrete. The most important points are highlighted as follows:

1) The concrete researches are mainly based on three categories of scales: macroscopic, mesoscopic and microscopic. The focus of studies will be different when consider different scales.

2) The theoretical basis: three behaviours of ionic transport mechanism, three forms of binding effect and three sets of classic equation employed in electrochemistry have been demonstrated and discussed.

3) The methods of exploring chloride transport in concrete are classified. The existing literatures which utilised analytical, experimental and numerical approaches are respectively reviewed.

4) The knowledge gap of the research background is summarised and the innovations of the present study are also described.

3 CHAPTER THREE – 1-D ONE PHASE MIGRATION MODEL

The third chapter of this thesis presents a series of 1-D models with a single phase to simulate the chloride migration test in a cement paste specimen. This simple numerical model highlights several fundamental issues, including: the behaviours of multi-species transport, effects of non-linear potential, and the influence of initial ionic concentrations on the transport of individual ionic species.

3.1 Introduction

Due to the long duration of diffusion tests, it appears to be favourable to adopt migration tests for the investigation of chloride penetration in cement and concrete materials. As the transport of ions manifests as a one-way flow between two electrodes when subjected to a large externally applied electric field, it is reasonable to take the simulation as a 1-D, one phase problem, which is more effective to examine the transport behaviour of ionic species.

As mentioned in Section 2.3.3.2, in most of the existing literature the electrostatic potential is determined based on the assumption of electro-neutrality (Eq. (2.49)). This assumption is questionable during the eletro-migration process. Numerically, it was difficult to solve the real constitutive law, Poisson's equation (Eq. (2.50)), directly in the early years since the calculations involve large and small numbers. More recently, Johannesson et al. (2006, 2009, 2010a, 2010b) adopted Poisson's equation to investigate the multi-species transport problem, however their work did not involve the influence of externally applied electrical field. Additionally, a significant cohort of numerical studies of the multi-species transport has been lacking detailed concentration distribution profiles, which makes the examination of validity of electro-neutrality condition during the electro-migration even more difficult.

In this chapter, a 1-D numerical study on the multi-species transport in a porous medium under an externally applied electrical voltage is proposed to simulate migration tests. The transport process is performed by solving mass conservation equations for each individual species of ions under electrostatic ionic coupling. In order to determine the electrostatic potential to describe the interactions between ionic species in the multi-

species ionic system, electro-neutrality condition and Poisson's equation are used. By comparing the electrostatic potential gradient, concentrations, fluxes and current density distribution profiles of two categories of results, the significance of using Poisson's equation is demonstrated.

In the meantime, from the results of using Poisson's equation, a remarkable behaviour driven by different initial concentrations of ions is highlighted. This is usually ignored in the reports of migration tests.

3.2 Basic equations

As this Chapter adopts the 1-D model with one phase, we assume that the specimen tested in the migration test is a cementitious material (i.e. cement paste) with saturated pore medium and there are no chemical reactions between ionic species occurring in the material. By employing the conception of porosity to describe the pore structure, the following mass conservation for each individual ionic species involved in the cementitious solution can be obtained,

$$\frac{\partial(\phi C_k)}{\partial t} = -\nabla J_k \qquad k = 1, \ldots, \mathrm{N} \tag{3.1}$$

where ϕ is the porosity of the cement paste, C_k is the concentration of the k-th ionic species, t is the time, J_k is the flux of the k-th ionic species, and N is the total number of the ionic species contained in the concrete. It should be mentioned that the mass conservation here is established in the unit volume of the cement paste rather than that of the electrolyte solution. Likewise, the flux here is defined as the mole number of ionic species passed through the unit area of the cement paste rather than that of the electrolyte solution in unit time, which contradicts the definition of the ionic concentration described as the mole number in the unit volume of the electrolyte but not of the cement paste. To cope with this contradiction, in Eq. (3.1), the total mass of the ionic species in the unit volume of the cement paste is ϕC_k rather than C_k.

Since diffusion and migration are treated as the major reason for ionic transport in this study, diffusion-migration form (Eq. (2.25)) of Nernst-Planck equation is adopted. As the ions are transport in the cement paste, Nernst-Planck equation can be modified as follows,

$$J_k = -D_k^{eff}\nabla C_k - D_k^{eff} C_k \frac{z_k F}{RT}\nabla \Phi \qquad k = 1, \ldots, N \tag{3.2}$$

where D_k^{eff} and z_k are the effective diffusion coefficient in the cement paste and the charge number of the *k*-th ionic species, respectively, $F = 9.648 \times 10^{-4}$ C mol^{-1} is the Faraday constant, $R = 8.314$ J mol^{-1} K^{-1} is the ideal gas constant, $T = 298$ K is the absolute temperature, Φ is the electrostatic potential. Substituting Eq. (3.2) into (3.1), yields,

$$\frac{\partial(\phi C_k)}{\partial t} = \nabla(D_k^{eff}\nabla C_k) + \frac{z_k D_k^{eff} F}{RT}\nabla\left(C_k \nabla \Phi\right) \qquad k = 1, \ldots, N \tag{3.3}$$

Meanwhile, the effective diffusion coefficient of ions in the cement past (D_k^{eff}) can be related with that in the electrolyte solution (D_k) and the porosity (ϕ) as follows,

$$D_k^{eff} = \phi D_k \qquad k = 1, \ldots, N \tag{3.4}$$

Substituting Eq. (3.4) into (3.3), it yields,

$$\frac{\partial C_k}{\partial t} = \nabla(D_k \nabla C_k) + \frac{z_k D_k F}{RT}\nabla\left(C_k \nabla \Phi\right) \qquad k = 1, \ldots, N \tag{3.5}$$

As it was mentioned in Section 2.3.3, the electrostatic potential at any point can be determined by using the electro-neutrality condition

$$\sum_{k=1}^{N} z_k C_k = 0 \tag{3.6}$$

or Poisson's equation,

$$\nabla^2 \Phi = -\frac{F}{\varepsilon_0 \varepsilon_r}\sum_{k=1}^{N}(z_k C_k) \tag{3.7}$$

It is obvious that, if the electro-neutrality holds, the electrostatic potential can be described by Laplace Equation as follows,

$$\nabla^2 \Phi = 0 \tag{3.8}$$

This implies that if the electro-neutrality is employed in 1-D models, the electrostatic potential within the cement paste would be a linear function of the space coordinate. In the following section, the Laplace Equation (Eq. (3.8)) on behalf of electro-neutrality condition or the Poisson's equation (Eq. (3.7)) is used respectively with Eq. (3.5) to govern the concentrations C_k and electrostatic potential Φ during the migration tests.

3.3 The simulation of migration tests by using electro-neutrality condition

As mentioned in the preceding section, the governing Eqs. (3.5) and (3.8) can be used to describe the ionic transport of migration tests with the assumption of electro-neutrality condition when the initial and boundary conditions are properly defined.

3.3.1 *Numerical simulation*

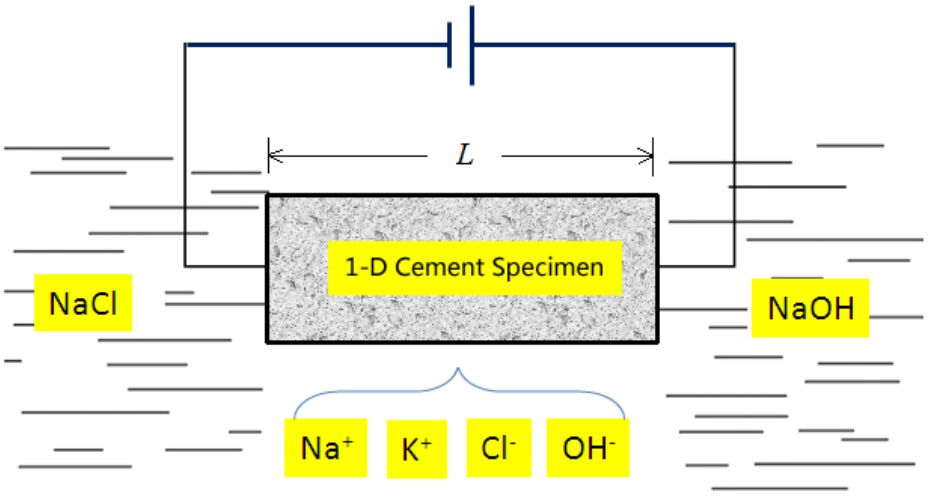

Figure 3.1. Schematic representation of a migration test (section of a 1-D concrete specimen).

As shown in Fig. 3.1, a 1-D numerical model is used to simulate an eight-hour migration test, in which a $L = 50\,\text{mm}$ slender 1-D compartment of cement paste specimen is located between two compartments, one of which has a 0.52 mole/L NaCl solution, the other of which has a 0.30 mole/L NaOH solution (both of sodium solutions are treated as individual ions in the simulation). Externally, there is a 24V DC potential difference applied between two electrodes inserted into the two compartment solutions. The cement paste is saturated with a solution of four ionic species (K, Na, Cl and OH) at the initial time. Other ionic species (such as calcium and sulphate) may also exist in the concrete. However, due to their concentrations that are much lower than the four ionic

species, only K, Na, Cl and OH are considered in the present simulations. The porosity of the cement paste specimen is assumed to be $\phi = 0.11$. Since the volume of either compartment is much greater than the pore volume of the specimen, it is reasonable to assume that the concentration of each ionic species in the two compartments remains constant during the migration test. The diffusion coefficients of individual ionic species, and the initial and boundary conditions of five variables used in the model are given in Table 3.1, in which the diffusion coefficients of ionic species within pore solution are given by Xia and Li (2013).

Table 3.1. Boundary conditions, initial conditions and diffusion coefficients

Field variables		Potassium (mole/m^3)	Sodium (mole/m^3)	Chloride (mole/m^3)	Hydroxide (mole/m^3)	Electrostatic potential (V)
Boundary conditions	x = 0	0	520	520	0	= 0
	x = L	0	300	0	300	= 24
Initial conditions		200	100	0	300	0
Charge number		1	1	-1	-1	N/A
Diffusion coefficient, $\times 10^{-10}$ m^2/s		1.957	1.334	2.032	5.260	N/A

3.3.2 *Finite element meshing*

Referring to Section 2.2.1, the accuracy of the numerical solution of the convection-diffusion equation governed by Eqs. (3.5) and (3.8) is highly dependent upon the element sizes used. Mathematically, to achieve a reasonably accurate numerical solution, one has to make the Peclet number (Eq. (2.5)) less than one. Hence, the larger the convection velocity, the smaller the element size required. In the present problem, the convection velocity is the migration velocity of ionic species. When there is an external electric field, the transport of ions in the electrolyte is usually dominated by the migration, which means that the element size must match with the electrostatic potential gradient. Otherwise, the numerical solution obtained might not be convergent. In this case,

the electrostatic potential gradient is linear and equals $\Delta\Phi / L = 480\ \text{V/m}$. Thus, the use of 2000 1-D equal size elements would be sufficient.

3.3.3 *Simulation results*

Figs. 3.2-3.6 show the distribution profiles of five field variables (the electrostatic potential and the concentrations of four ionic species) in cementitious solution obtained at four different times, in which the horizontal coordinate represents the position of the variable in 1-D cement paste model and the vertical coordinate is the value of the variable (electrostatic potential or concentration). Each curve of individual variable represents one instantaneous moment from the first hour to the fourth hour.

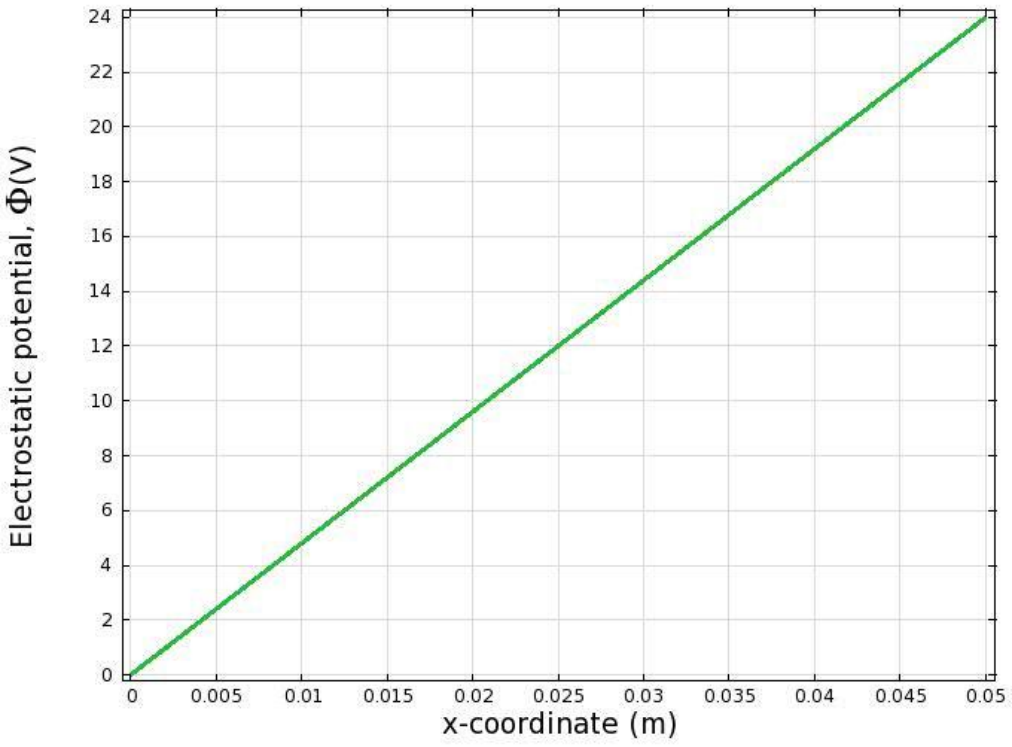

Figure 3.2. Electrostatic potential distribution profile.

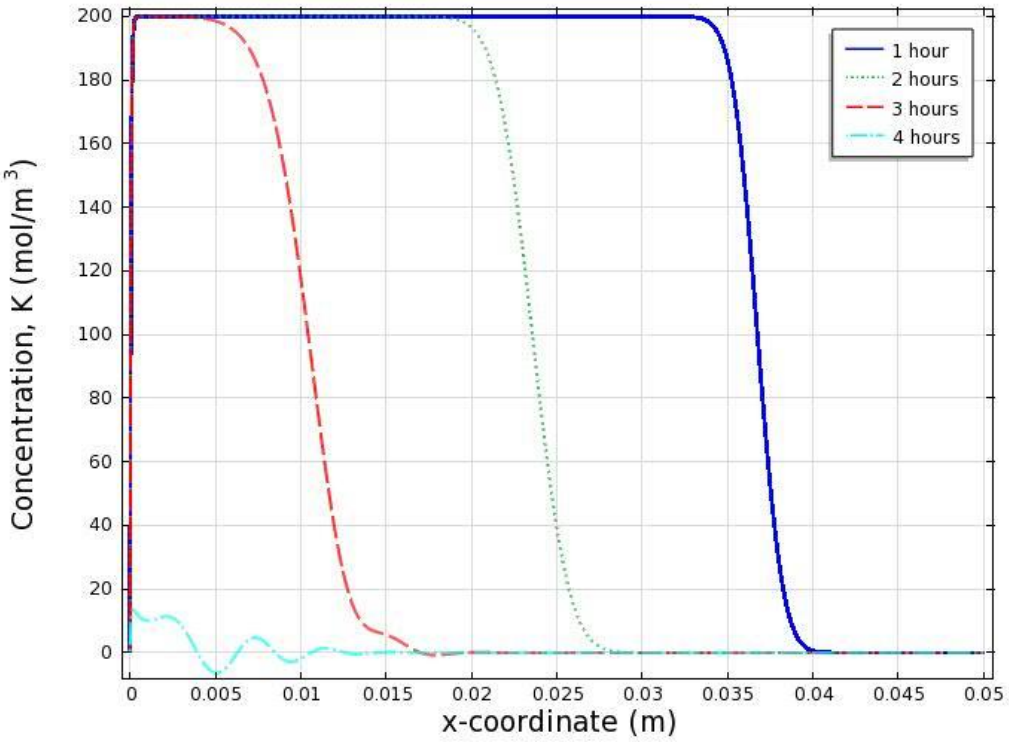

Figure 3.3. 4-hour concentration distribution profiles of potassium ions.

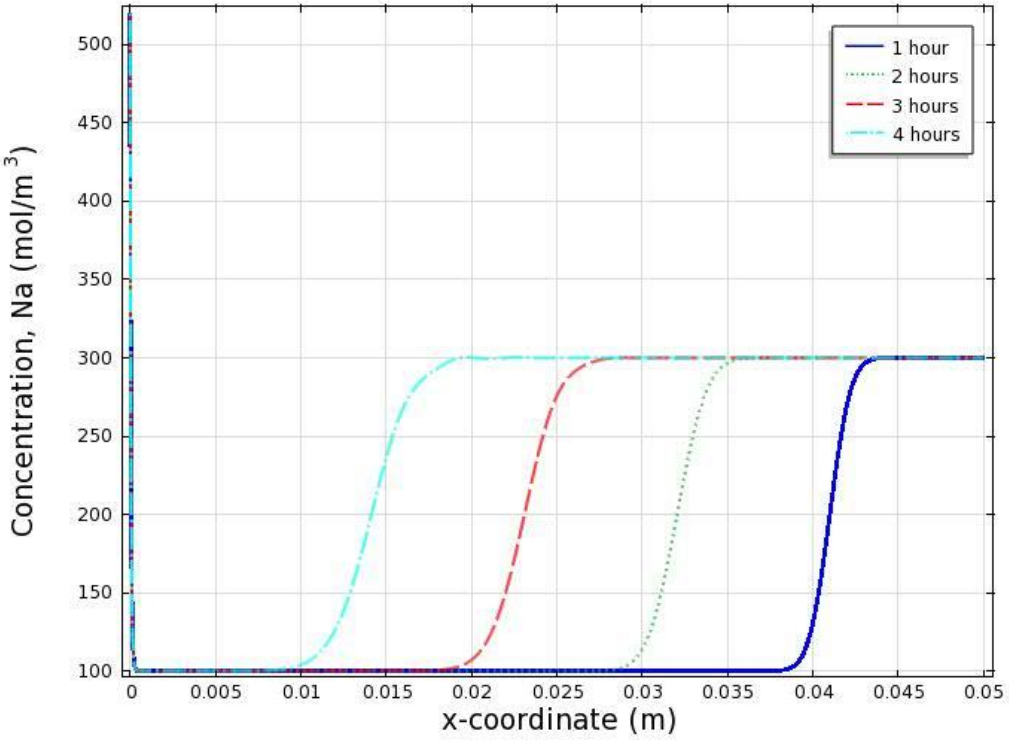

Figure 3.4. 4-hour concentration distribution profiles of sodium ions.

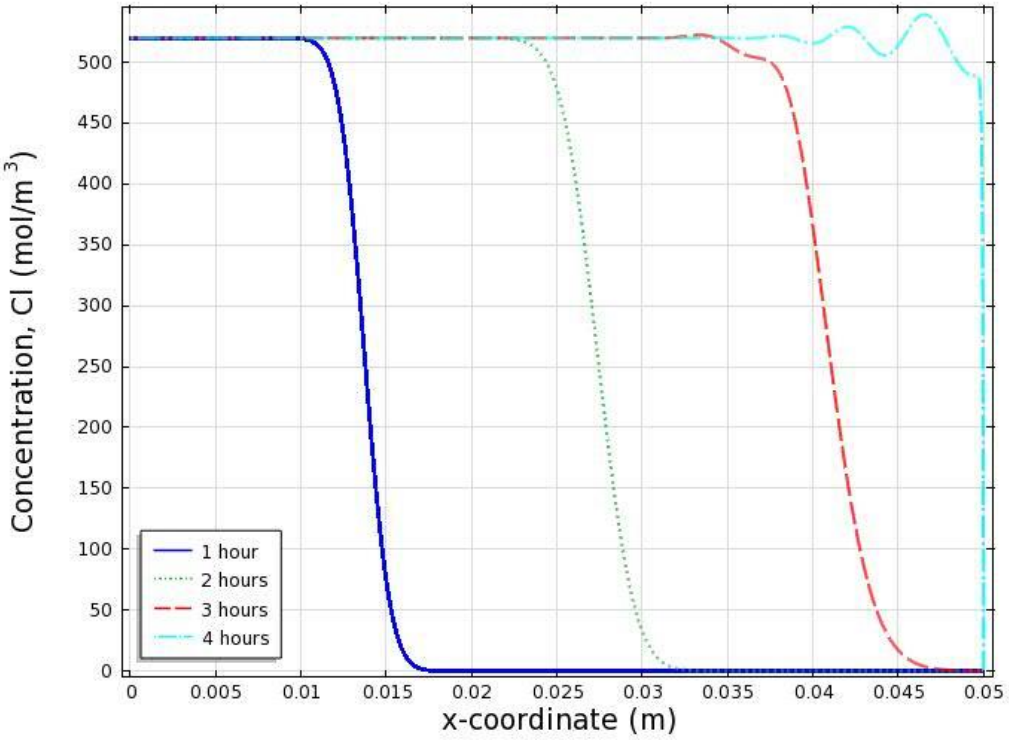

Figure 3.5. 4-hour concentration distribution profiles of chloride ions.

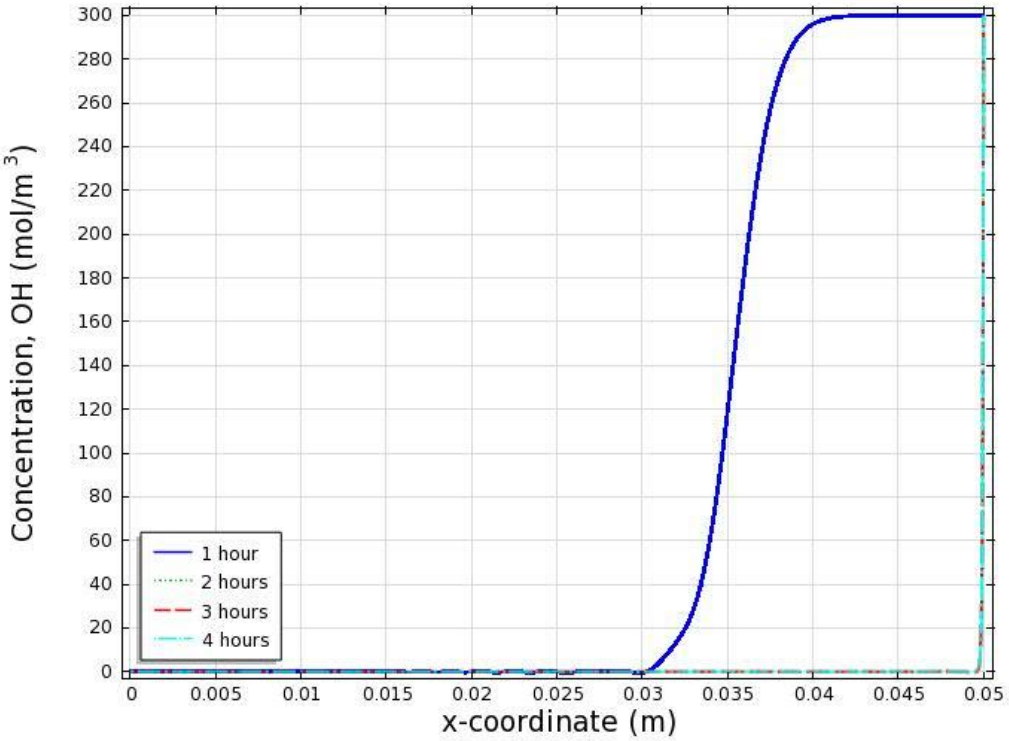

Figure 3.6. 4-hour concentration distribution profiles of hydroxide ions.

As implied in Eqs. (3.7) and (3.8), if the electro-neutrality condition holds, the electric field within the model would be constant, which is in agreement with Fig. 3.2: i.e. elec-

trostatic potential increases from $\Phi = 0$ at the cathode to $\Phi = 24$ V at the anode and the increase is perfectly linear.

It can be seen from Figs. 3.3-3.6 that, during the electro-migration process the positively charged ions (both potassium and sodium) move towards the cathode, while the negatively charged ions (both chloride and hydroxide) move towards the anode. The travel speeds of individual ionic species, however, are different. Due to the influence of linear electrostatic potential, the concentration distribution curves are very smooth in this 1-D model. Note that the isolation of the curve of t = 4 hours in Figs. 3.3 is due to boundary effect when the wave reaches to edge. Figs. 3.3-3.6 show that under the action of externally applied electric field, the transport of ionic species is dominated by migration, which is characterised by the waves of parallelogram shapes. Diffusion behaviour only experiences near the two electrodes and the region where migration wave front reaches.

Careful examination of Figs. 3.3-3.6 indicates that the wave speeds of four ionic species differ significantly but proportionally match the value of diffusion coefficient listed in Table 1. Hydroxide has the largest diffusion coefficient and its migration wave front moves fastest, while the ionic species with the smallest diffusion coefficient, sodium, has the slowest wave speed. Potassium and chloride have very close diffusion coefficient values, so that their wave speeds are also very close. This phenomenon implies that under the constant externally applied electric field, the migration velocity of each ionic species is constant and entirely depends on its diffusion coefficient, which means that the ionic electro-coupling cannot be achieved if the electric field is indeed constant. In other words, assumption of linear electrostatic potential leads the calculation of individual ionic species transport to be independent, which makes the ionic transport act

like a one-component system. Therefore, Eq. (2.47) employed in the steady state migration tests is questionable.

Figs. 3.7-3.9 illustrate the distribution profiles of the total fluxes, diffusion fluxes and migration fluxes of the four ionic species passing through in the cement paste respectively. It is easy to see that except the region near the cathode for positively charged ions and the anode for negatively charged ions the diffusion flux shown in Fig. 3.3 is small relative to the other two categories of flux shown in Figs. 3.8-3.9. Also, the values of the total fluxes and migration fluxes profiles are very similar. This again demonstrates that the influence of a high externally applied voltage causes the ionic transport in the model to be dominated by migration behaviour. Additionally, by comparison between concentrations and fluxes, all flux waves in Figs 3.7-3.9 begin/occur at the exact location that the migration waves occur in Fig.3.3-3.6.

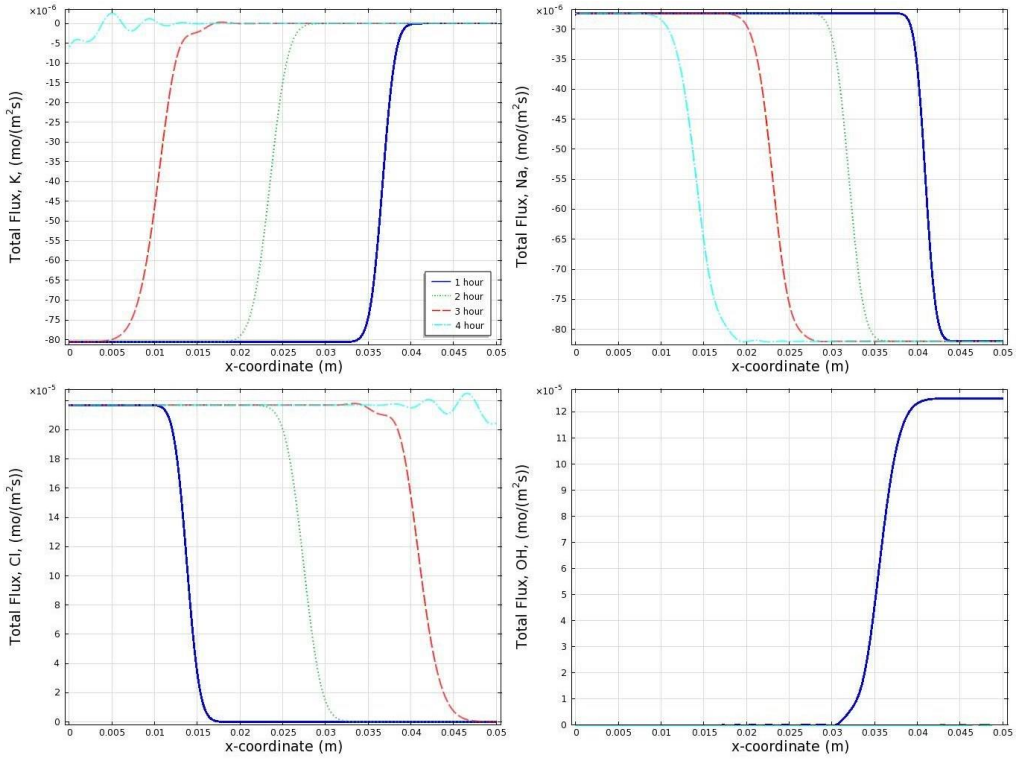

Figure 3.7. Distribution profiles of total fluxes of four ionic species

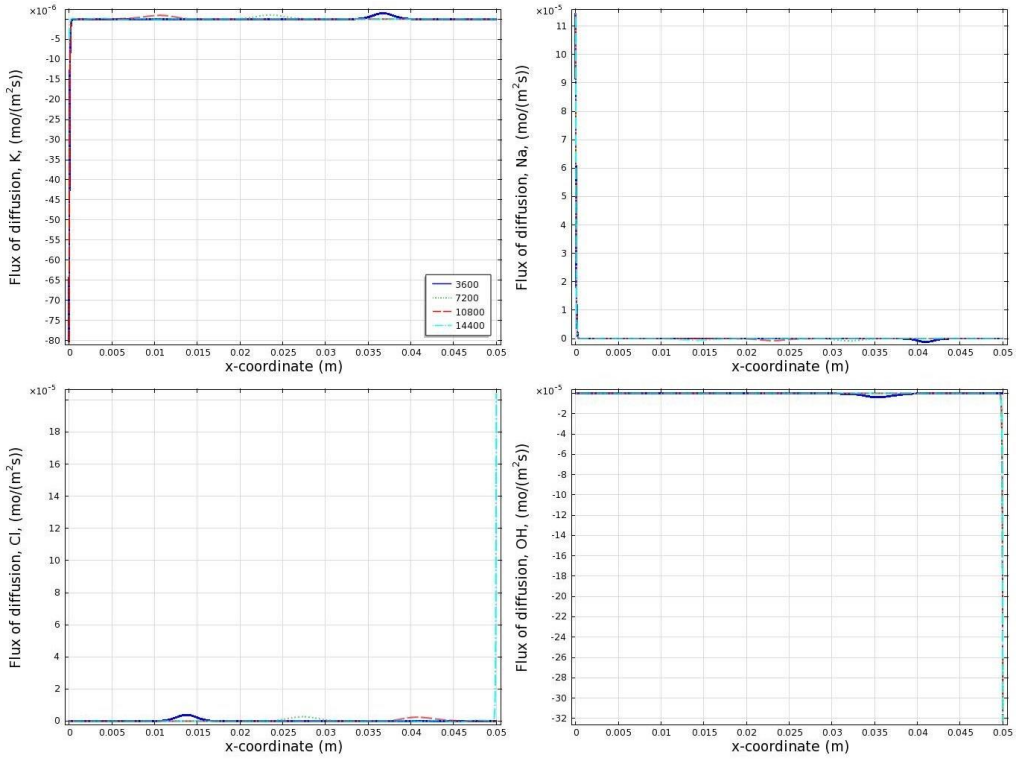

Figure 3.8. Distribution profiles of diffusion fluxes of four ionic species.

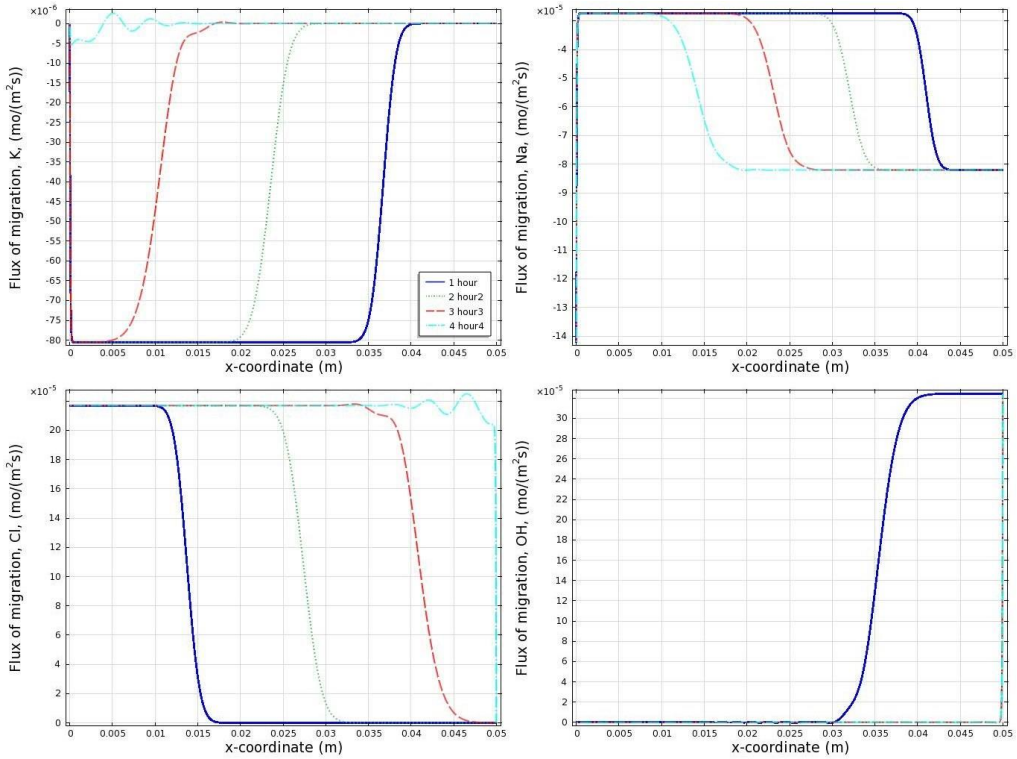

Figure 3.9. Distribution profiles of migration fluxes of four ionic species.

Fig. 3.10 plots the current density carried by four ionic species passing through in the cement paste model using the following equation,

$$I = F\sum_{k=1}^{N} z_k J_k \tag{3.9}$$

where I is the current density. The current density seems to be fluctuant throughout the model at all times. This indicates that the current density is not regionally constant when there is a constant electrical field, which will be proved to be incorrect in the next section. The average of current density along the x-coordinate is 24.18, 17.94, 25.56 and 27.42 A/m^2 at 1, 2, 3 and 4 hours, respectively, which seems very random.

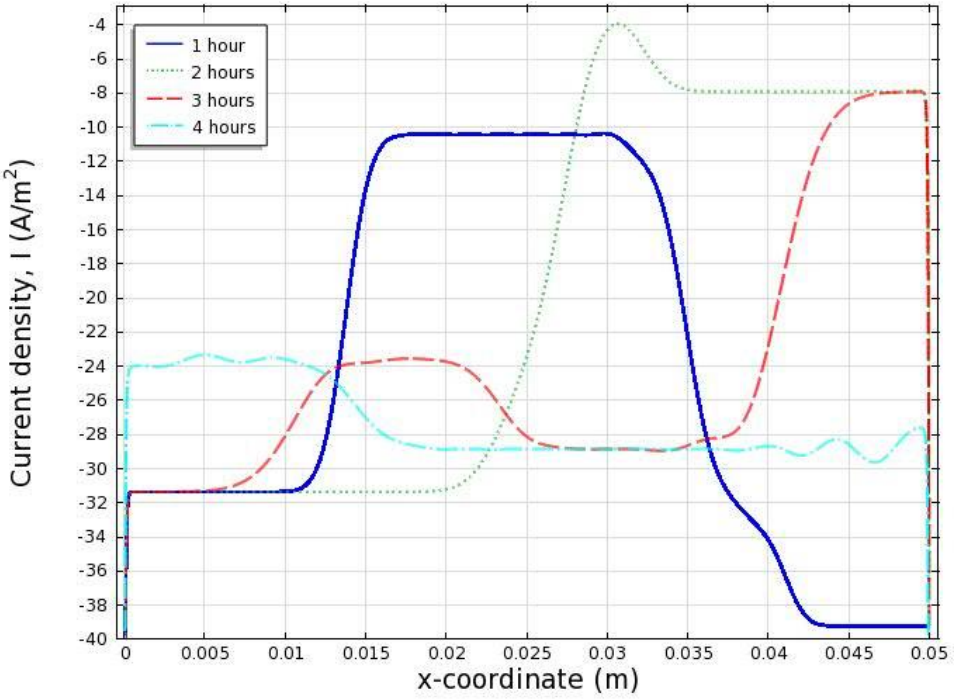

Figure 3.10. Current density distribution profiles.

3.4 The simulation of migration tests by using Poisson's equation

The Poisson's equation is the rigorous law relating the space-variation in the electric to the charge distribution. In this section, a numerical investigation which employs Poisson's equation rather than electro-neutrality assumption to control the ionic transport in migration tests is conducted, from which a series of simulation results are obtained.

3.4.1 *Numerical simulation*

The simulation is similar to that described in Section 3.3. The only distinction is the use of Poisson's equation instead of the use of Laplace equation in controlling the electrical coupling of ionic species in a multi-component solution within a saturated cement paste specimen. In addition, to investigate the influence of initial concentrations of ions, the initial conditions of ions are divided into three cases, which are given in Table 3.2.

Table 3.2. Boundary conditions, initial conditions and diffusion coefficients.

Field variables		Potassium (mole/m^3)	Sodium (mole/m^3)	Chloride (mole/m^3)	Hydroxide (mole/m^3)	Electrostatic potential (V)
Boundary conditions	$x = 0$	0	520	520	0	$\Phi = 0$
	$x = L$	0	300	0	300	$\Phi = 24$
Initial conditions	Case 1	200	100	0	300	0
	Case 2	110	55	0	165	0
	Case 3	20	10	0	30	0
Charge number		1	1	-1	-1	N/A
Diffusion coefficient, $\times 10^{-10}$ m^2/s		1.957	1.334	2.032	5.260	N/A

3.4.2 *Simulation results*

Similar to Section 3.3.3, Figs. 3.11-3.16 show the distribution profiles of variables obtained at four different times in Case 1. It can be seen from Fig. 3.11 that, when the transport process is controlled by Poisson's equation, electrostatic potential increases from $\Phi = 0$ at the cathode to $\Phi = 24$ V at the anode but not completely linear. It is inter-

esting to notice from the electrostatic potential plot shown in Fig. 3.11 that, the electrostatic potential curve varies from a convex shape at the first hour to a concave shape at the later hours. This means that, initially the higher migration speed of ionic species is in the region near the cathode, but with the increase of time the higher migration speed gradually shifts to the region near the anode. This implies that migration speed will not be constant but varies not only in time but also regionally.

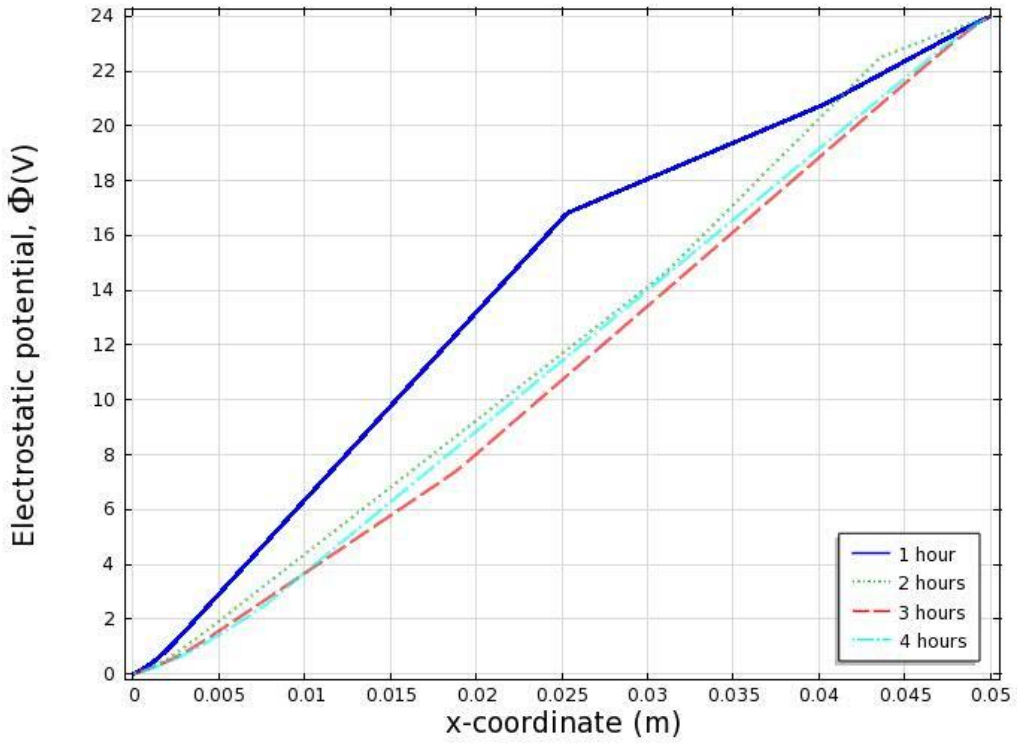

Figure 3.11. Electrostatic potential distribution profiles.

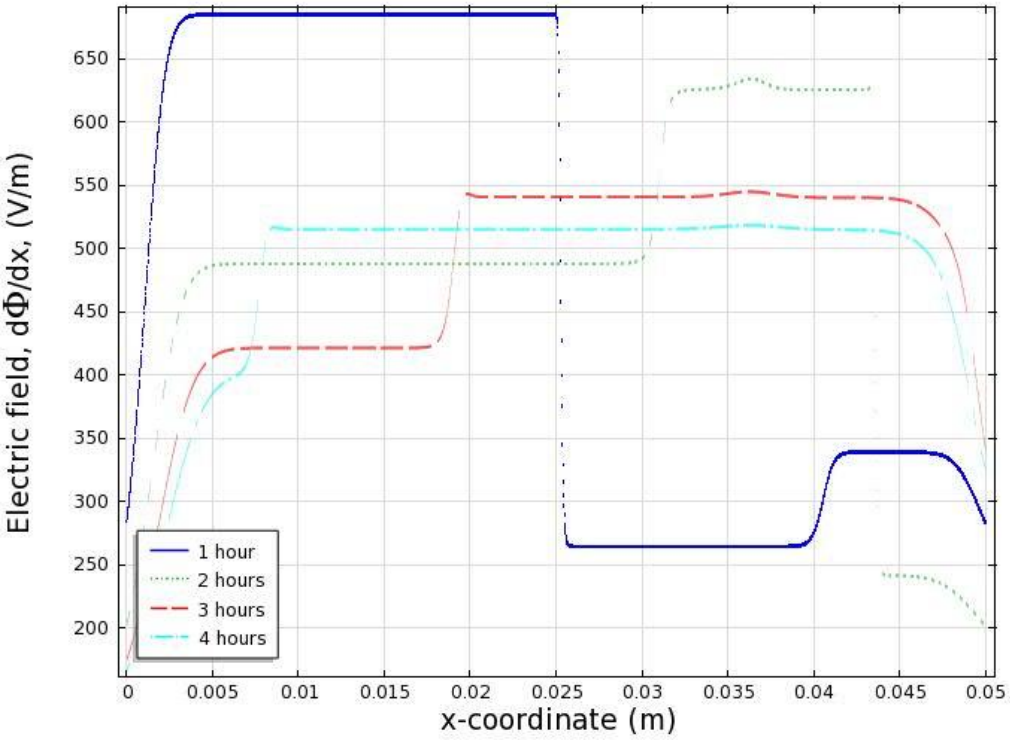

Figure 3.12. Electrostatic potential gradient distribution profiles.

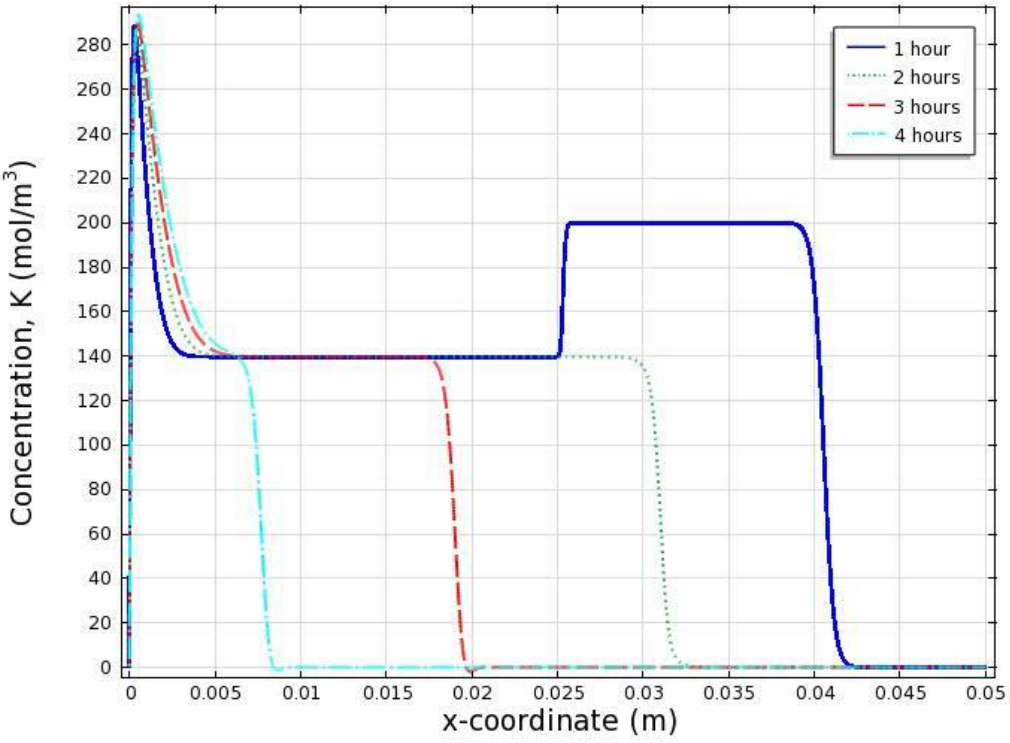

Figure 3.13. 4-hour concentration distribution profiles of potassium ions.

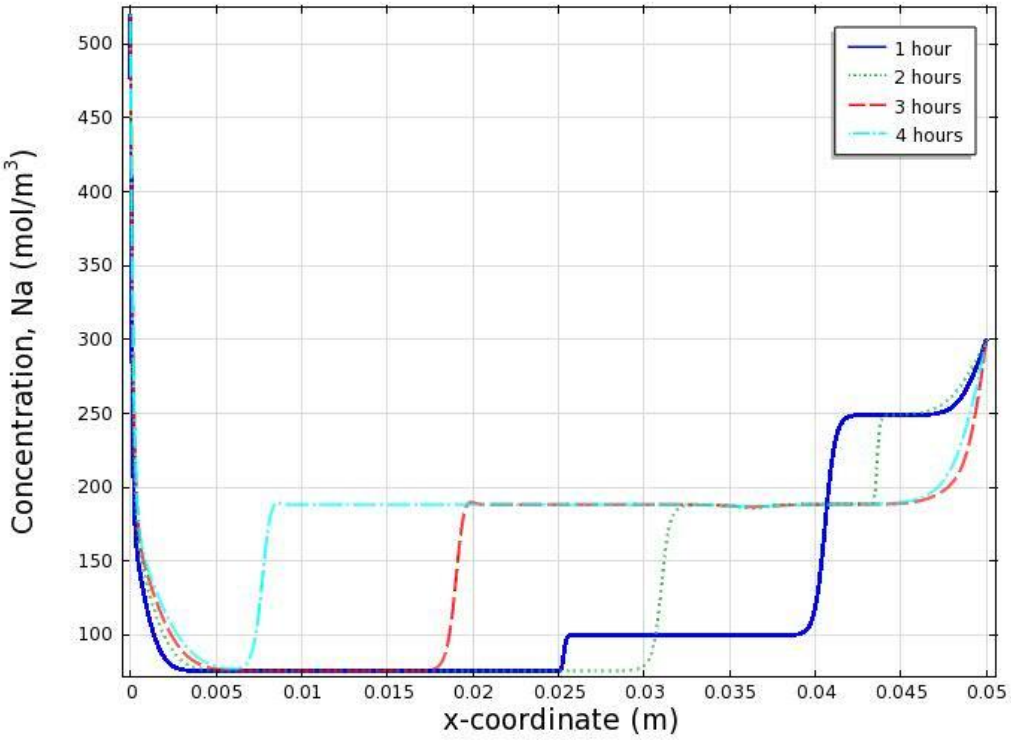

Figure 3.14. 4-hour concentration distribution profiles of sodium ions.

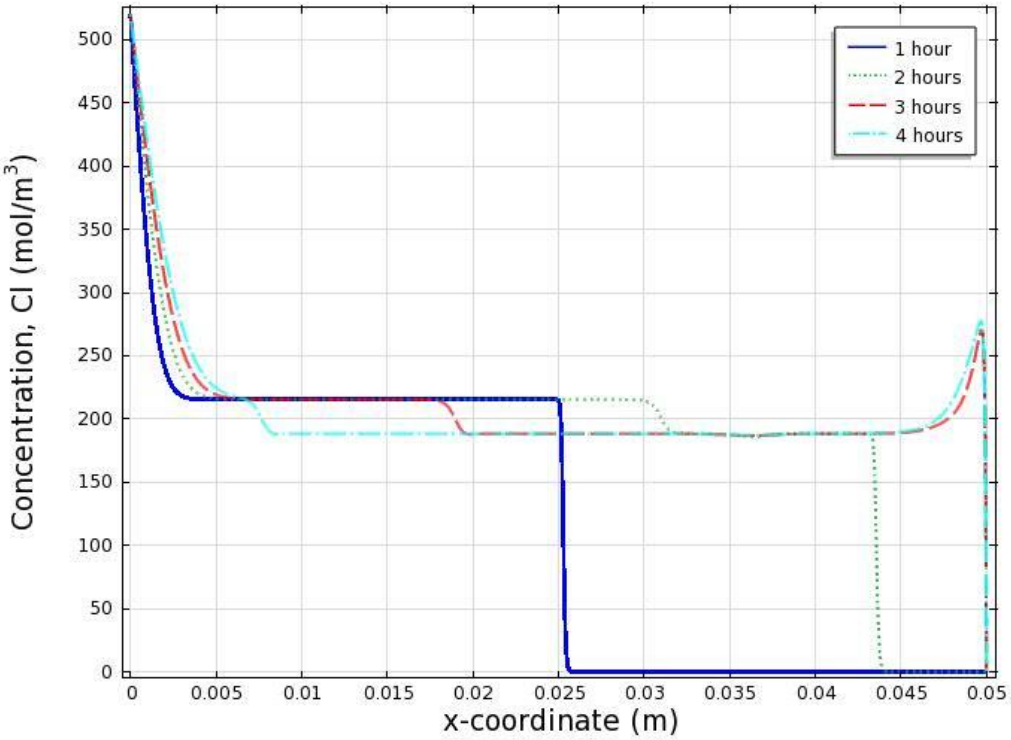

Figure 3.15. 4-hour concentration distribution profiles of chloride ions.

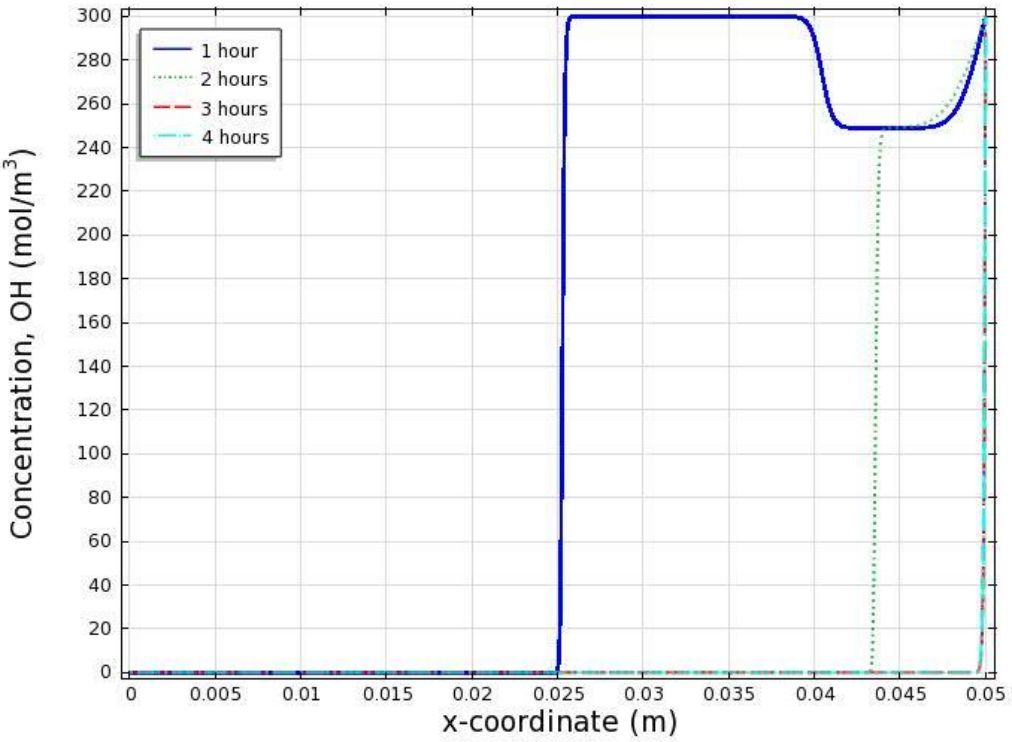

Figure 3.16. 4-hour concentration distribution profiles of hydroxide ions.

For a further investigation, Fig. 3.12 provides a good view on the examination of the electrostatic potential gradient. It is observed that the electric field jumps from one region to another, except near the boundaries where it varies smoothly. From the four different time frame plots, it can be noticed that the regional difference of electric field becomes gentler as the time passes. The detailed feature of the electrostatic potential gradient again demonstrates the difficulty of using a single migration velocity to represent the actual transport of chloride ions in the specimen, although it has been widely adopted in the reported migration tests.

Under such a nonlinear electrostatic potential gradient, the transport behaviour found from Figs. 3.13-3.16 is totally different from that of Figs. 3.3-3.6. Generally speaking, ionic species no longer travels as steadily as they do in the model controlled by the linear electrostatic potential gradient. The more frequency of concentration drop indicates that the diffusion behaviour plays a more important role. The transport evolutions of po-

tassium, sodium and chloride ions all have a very clear diffusion layer near the cathode. Nevertheless, although the diffusion becomes more important, the ionic transport is still dominated by migration, which is characterised by the waves of parallelogram shape. It is also observed that, as time goes on, the amount of sodium and chloride ions rises, whereas that of potassium and hydroxyl ions reduces in the concrete specimen. Due to the difference in diffusion coefficient values of four ionic species, the rates of the increase of sodium and chloride ions in the specimen are lower than those of the decrease of potassium and hydroxide, which makes the total amount of ions in the cement paste specimen reduce with time.

More interesting features are found from the wave speeds of four ionic species. As it was described in Section 3.3.3, under the constant externally applied electric field, the migration velocity of each ionic species depends on its diffusion coefficient. However, in the present model, the ionic electro-coupling phenomenon occurs. Here, the wave speeds of positively (or negatively) charged ions are almost the same but are significantly different from those of their opposite charged ions. This again highlights that the electrostatic potential gradient and the migration velocity of ionic species in the pore solution are not constants but dependent on both time and position.

The total fluxes, diffusion fluxes and migration fluxes of the four ionic species distributing in the model are plotted in Figs. 3.17-3.19. The value of the fluxes is also no longer constant and varies with the space and time. More specifically, the variation of fluxes is more notable during the first two hours. This indicates the interactions between ionic species are stronger in the beginning of the electrochemical process. Similar to the result

of electro-neutrality, the influence of an externally applied voltage means that the ionic transport process is controlled by migration.

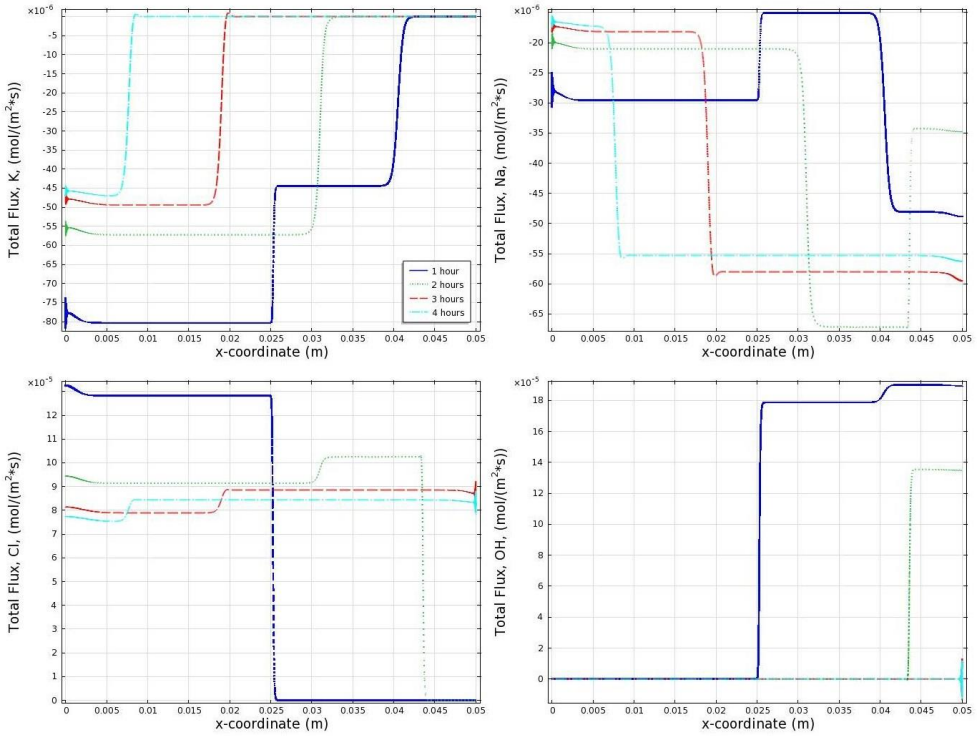

Figure 3.17. Distribution profiles of total fluxes of four ionic species.

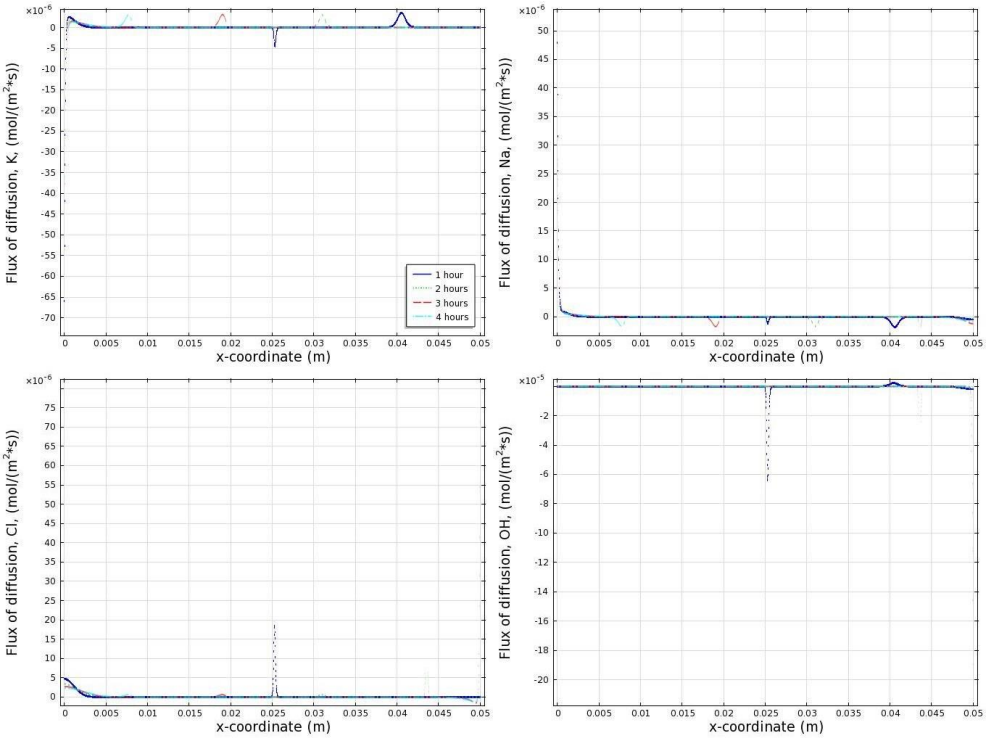

Figure 3.18. Distribution profiles of diffusion fluxes of four ionic species.

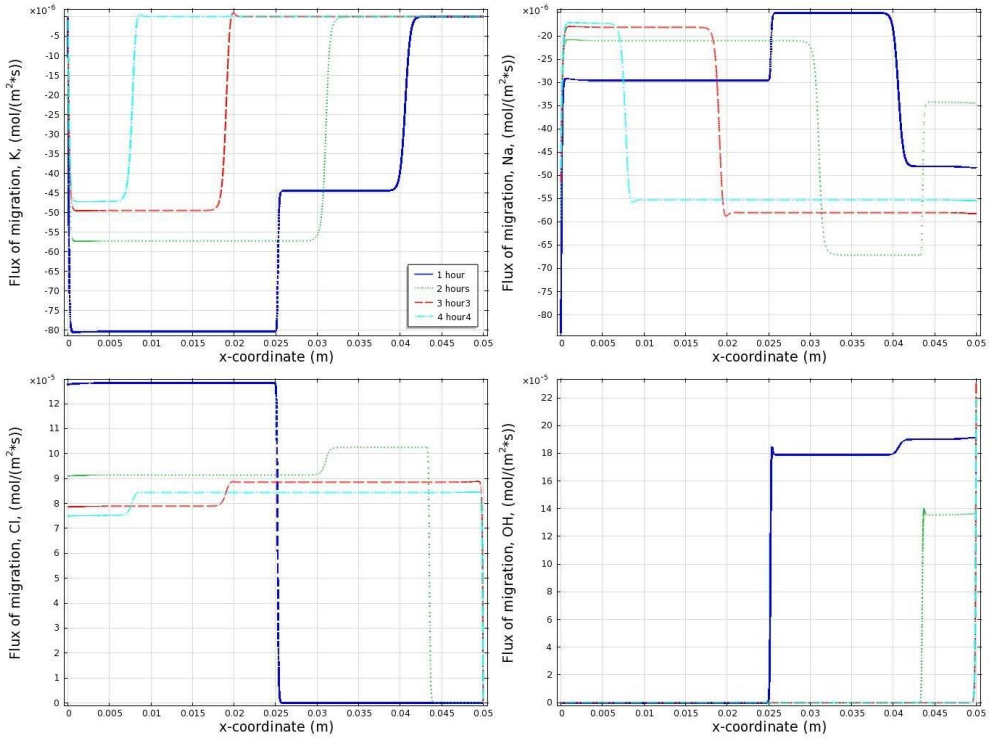

Figure 3.19. Distribution profiles of migration fluxes of four ionic species.

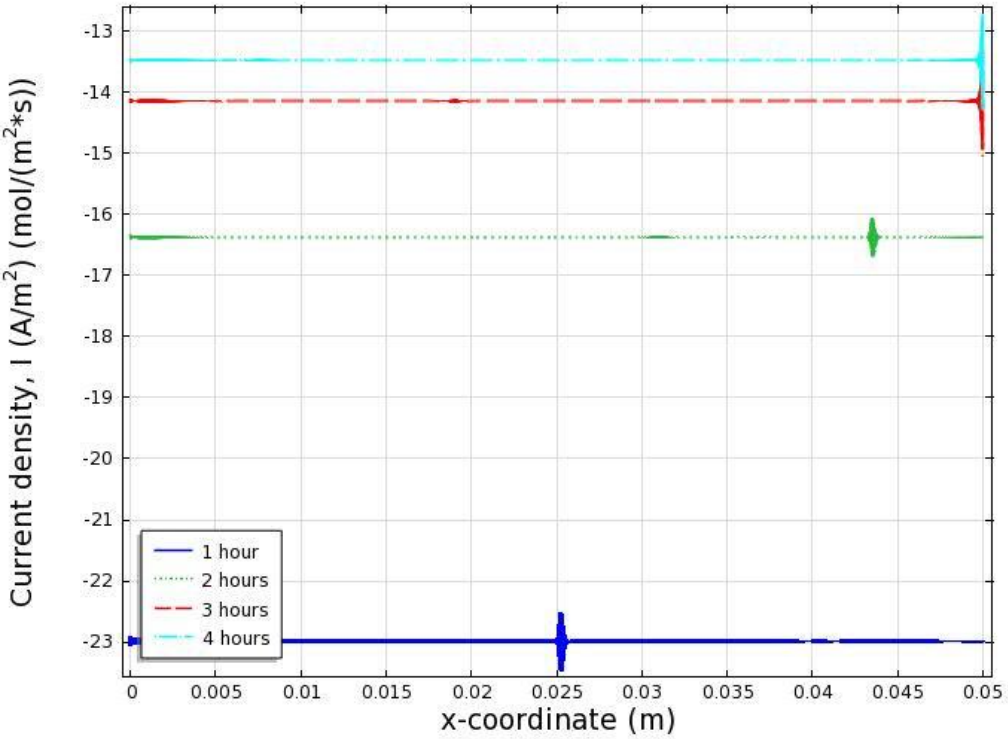

Figure 3.20. Current density distribution profiles.

The distribution profiles of current density are also quite different from those obtained from the preceding model. As depicted in Fig. 3.20, the current density becomes constant at a given time. It also shows that the current density decreases versus the time period especially during the first three hours. This is due to the decrease of the total amount of ions during the process time period as is mentioned above.

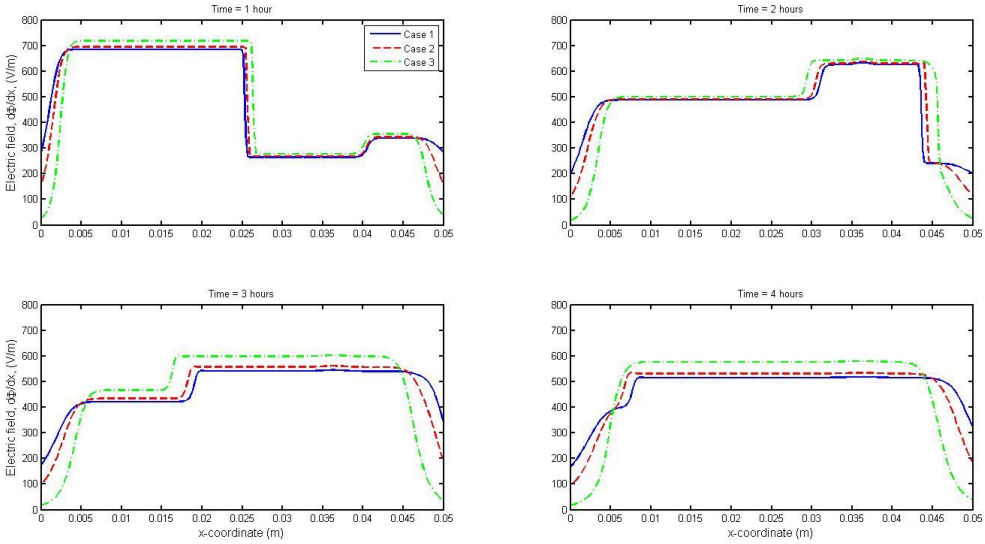

Figure 3.21. Comparison of electric field distribution profiles.

To examine the influence of initial concentrations, two more initial concentrations for potassium, sodium and hydroxyl ions (Cases 2 and 3 listed in Table 3.2) have been utilised. Since the transport of ions in specimen is dominated by migration, the results of electrostatic potential term should be illustrated first. For easier observation, Fig. 3.21 directly plots a comparison of electrostatic potential gradients between the three cases with different initial concentrations. It can be seen from the electric field values that, initial concentrations make an apparent quantitative effect on the electrostatic potential. Nonetheless, qualitatively speaking, this kind of effect is limited. This feature is further validated by Figs 3.22 and 3.23, which show the concentration profiles of four ionic

species; most features (especially the wave speeds of ionic species) are found to be similar to those of Case 1 shown in Figs. 3.13-3.16.

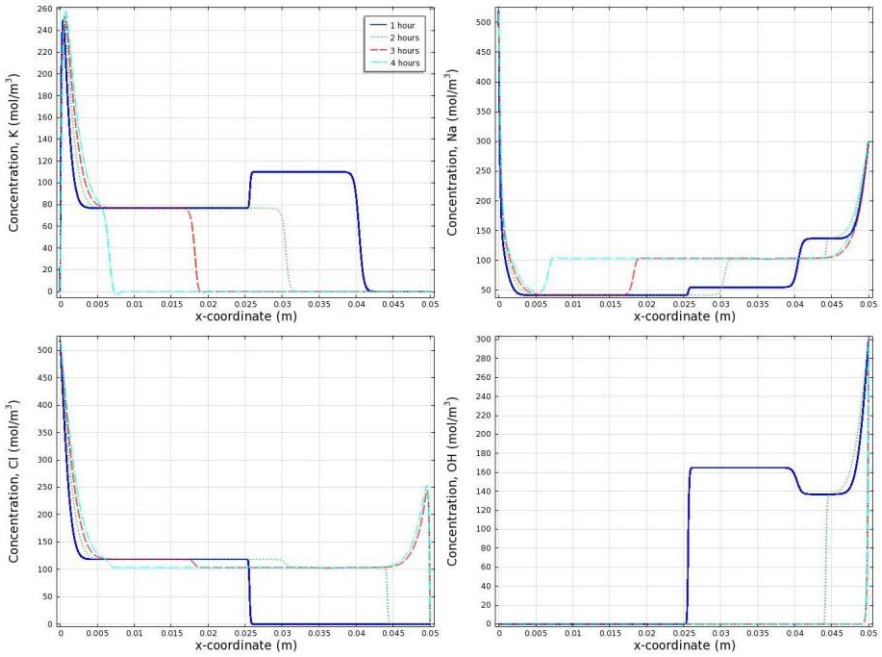

Figure 3.22. 4-hour concentration distribution profiles of Case 2.

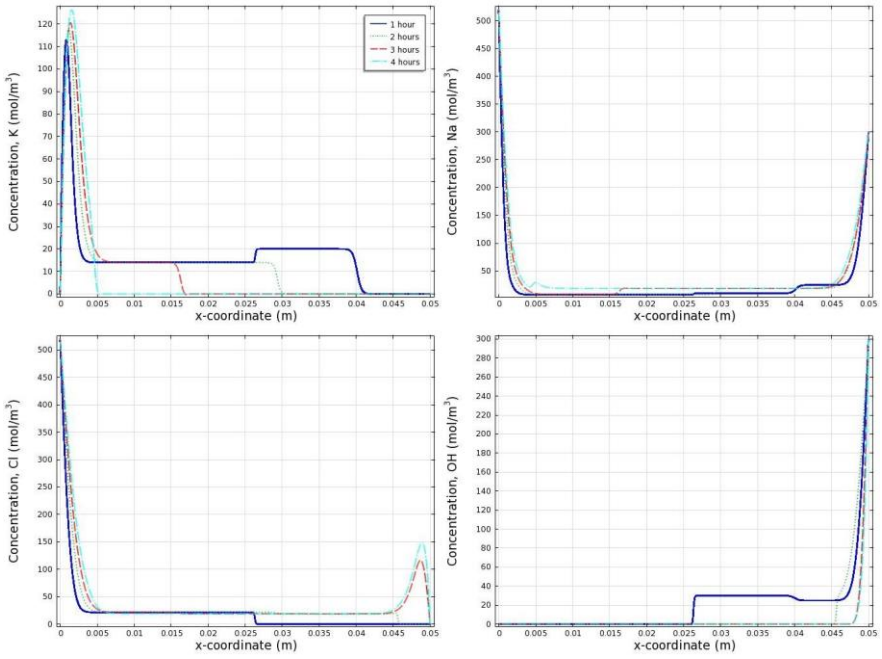

Figure 3.23. 4-hour concentration distribution profiles of Case 3.

However, if one examines the magnitude of concentrations of ionic species in the specimen, a key difference can be found. A comparison of results obtained from the three

cases show that, for the same boundary conditions and an identical applied voltage, if the initial concentrations of the specimen are proportionally lower for potassium, sodium and hydroxyl ions, the obtained ionic concentrations not only of these three species but also of the chlorides are proportionally lower. This feature is not found in the models governed by linear electrostatic potential.

Accompanied by the lower concentrations in Cases 2 and 3, the fluxes of the ions are also proportionally lower, which is reflected in the results of current density plotted together in Fig. 3.24. As it was expected, the current density curves of the three cases all decrease versus process time and these downward trends become gentle after the fourth hour. Between the three cases themselves, Case 1 has the highest current density and Case 3 has the lowest, which is proportionally in accord with the input initial concentrations.

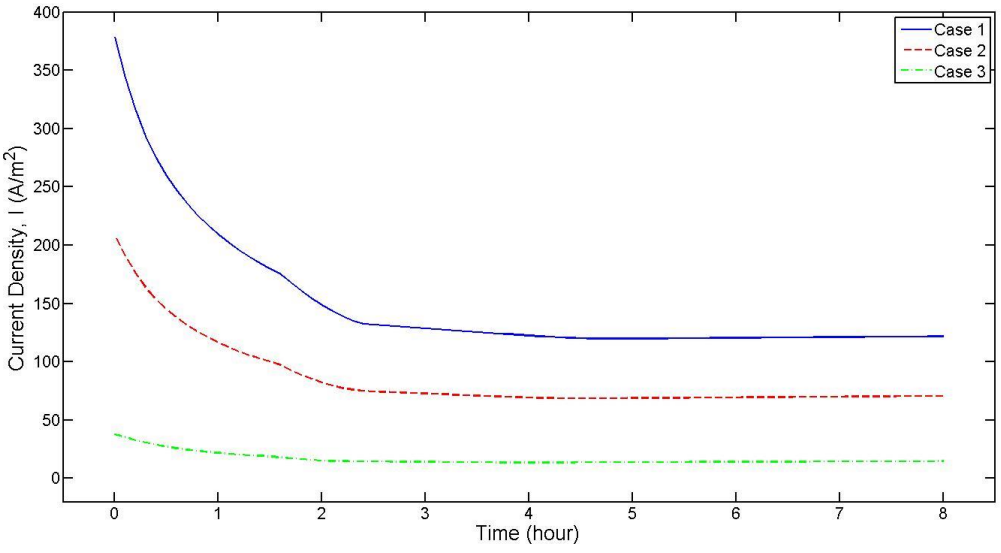

Figure 3.24. Comparison of current density distribution profiles versus time.

To give an overall view of the 1-D models, Fig. 3.25 combines the results obtained from the models based on electro-neutrality and those with different initial concentrations using Poisson's equation. As the most attention is being paid on the chloride penetration,

only the concentration profiles of chlorides are displayed there. The figure shows that among the three different cases with Poisson's equation, the transport behaviours are very close (i.e. the shape of concentration curves and the speeds of migration wave front) except for the peak values at the wave fronts. From the comparison between the models with electro-neutrality and Poisson's equation, however, both wave speeds and the peak values at the wave fronts are quite different. This clearly shows that, when the electro-neutrality condition was used, there would be no electro-static potential coupling and therefore the transport of individual ionic species would be independent of each other.

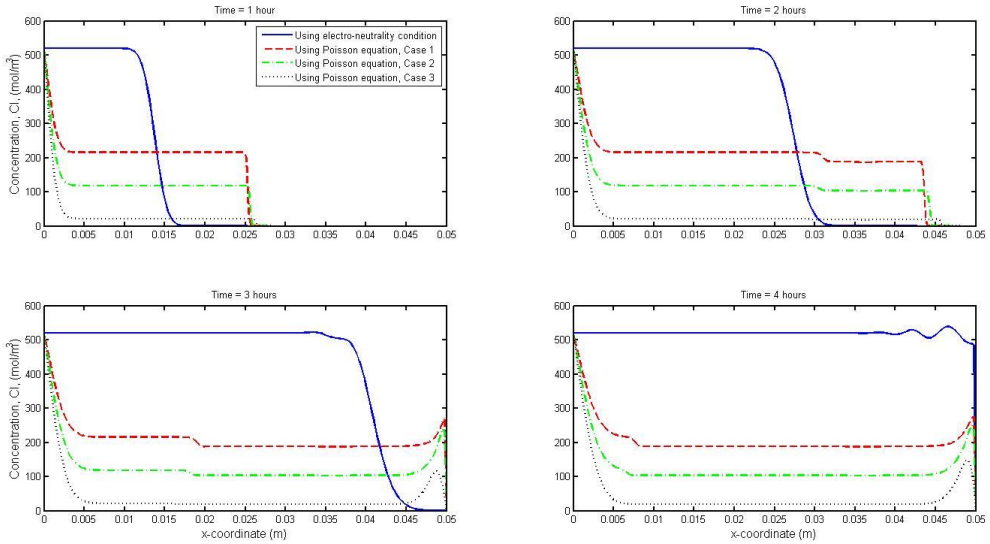

Figure 3.25. Comparisons of chloride concentration distribution profiles.

3.5 Summary

This Chapter has proposed two 1-D numerical models to investigate the transport of ions in a saturated cement paste specimen considering porosity. The first determines the electrostatic potential based on the assumption of electro-neutrality while the other applies the rigorous Poisson's equation. From the present numerical investigation the following conclusions can be drawn:

1) The profile results obtained from the two distinct models are significantly different. If the electro-neutrality condition is employed, the electrostatic potential gradient within the cement paste would be constant, which makes the multi-species transport act like a one-component system. When the electro-neutrality assumption is replaced by the rigorous Poisson's equation, the ionic electro-coupling can be realised.

2) Electro-migration is the dominant transport process in both models due to the influence of an externally applied electric field. However, local diffusion behaviour occurs more frequently in the model using Poisson's equation, which may have significant influence on the development of migration speed.

3) Under the influence of electro-neutrality condition and constant electrostatic potential gradient, the migration velocity of each ionic species is also constant, which entirely depends on its diffusion coefficient and the electro-static potential.

4) Under the influence of Poisson's equation, the migration speed of each ionic species varies with time and also with space. The migration speeds of positively (or negatively) charged ions are almost the same but are significantly different from

those of their opposite charged ions. This evidently shows interactions between different ionic species.

5) Under the influence of Poisson's equation, the distribution of electrostatic potential between the cathode and anode shows the results are likely to form a curve that varies from a convex shape at the first hour to a concave shape at the fourth hour, rather than a straight line in the model adopting electro-neutrality condition.

6) The change of initial concentrations of potassium, sodium and hydroxyl ions will affect not only their own concentration profiles, but also the chloride concentration profiles in the specimen during the process.

7) For the models with constant electrostatic potential gradient, the current density generated by ionic fluxes varies with both time and position, whereas for the models with Poisson's equation, it only varies with time and remains constant with spatial variation. Furthermore, current density is proportionally in accord with the input initial concentrations.

4 CHAPTER FOUR– 2-D TWO PHASE MIGRATION MODEL

In the fourth chapter of this thesis, a series of 2-D models with two-phase composite are developed to simulate the chloride migration test. By exploring models with different shapes and volume fractions of aggregates, some important interaction transport features between ionic species have been found, which have not been seen before in the 1-D model of single phase. The influence of various forms of ionic binding between solid and liquid phases is also examined.

4.1 Introduction

In the recent decades, great efforts have been made on the assessment of ionic transport by using experimental and numerical techniques. Due to the new regulation on the limitation of carbon dioxide emission, cement industry has used additives in reducing the cement content in concrete. Different types of concrete are produced by using different additives. Obviously, properties of concrete will be different when using different additives. To deal with this, from the mechanics point of view, if the properties of each individual material involved in the concrete are known then the properties of the concrete mixture should be predictable. In view of this, experimental data obtained from new types of concrete (involving various kinds of additives) and multi-phase models for simulation are needed.

Note that most experimental data existing in the literature were mostly obtained from traditional concrete. Few experimental data have been published for the new type concrete. Also, most existing numerical models investigating the chloride transport under externally applied electric field are one-dimensional and considering only one phase. For concrete, it is believed that the models involving multi-phase composite material would be more rational and accurate, particularly for the influence of tortuosity caused by aggregates.

In this chapter, a series of numerical models are developed for concrete, which treat the concrete as a composite material with mortar and aggregates two phases for simulating the ionic transport process. Since the Poisson's equation is more appropriate and accurate when taking the multi-component ionic transport into account, the present study uti-

lises this rigorous equation to govern the electrostatic potential in the pore electrolyte solution.

By solving both mass conservation and Poisson's equations, the distribution profiles of four involved ionic species (potassium, sodium, chloride, and hydroxide) and some other valuable variables (i.e. electrostatic potential and fluxes) at any required time are successfully obtained. Through the use of two-dimensional and two-phase numerical model, we have found some important interaction transport features between ionic species which have not been seen before in the 1-D model of single phase. A further investigation about packed inclusions is discussed based on the contribution of the models with different shapes and volume fractions of aggregates. Additionally, in the latter part of this chapter, the influence of various forms of ionic binding is also examined.

4.2 Basic equations

The concrete specimen simulated here is treated as a two-phase composite material. The aggregate is one phase and the cement paste is the other. Note that in meso-scale multi-phase model, one can let (1-ϕ_c) be the volume fraction of the aggregate phase. Since the aggregates are assumed to be impermeable the transport equation is established only in the cement phase. Thus, the common form of mass conservation and Nernst-Planck equation is adopted as follows,

$$\frac{\partial(\varepsilon C_k)}{\partial t} = -\varepsilon \nabla \cdot \mathbf{J}_k \qquad k = 1, \ldots, \mathrm{N} \tag{4.1}$$

$$\mathbf{J}_k = -D_k \nabla C_k - D_k C_k \frac{z_k F}{RT} \nabla \Phi \qquad k = 1, \ldots, \mathrm{N} \tag{4.2}$$

where ε is the porosity of two-phase concrete, C_k is the concentration of the k-th ionic species in the pore solution, t is the time, $\mathbf{J}_k$ is the flux of the k-th ionic species (in 2-D problem, J_k is a vector), and N is the total number of the ionic species contained in the pore solution, D_k and z_k are the diffusion coefficient and the charge number of the k-th ionic species, respectively, $F = 9.648 \times 10^{-4}$ C mol^{-1} is the Faraday constant, R = 8.314 J mol^{-1} K^{-1} is the ideal gas constant, T = 298 K is the absolute temperature, Φ is the electrostatic potential. Substituting Eq. (4.2) into (4.1), yields,

$$\frac{\partial C_k}{\partial t} = \nabla(D_k \nabla C_k) + \frac{z_k D_k F}{RT} \nabla\left(C_k \nabla \Phi\right) \qquad k = 1, \ldots, \mathrm{N} \tag{4.3}$$

Eq. (4.3) plus the Poisson's equation (3.7) can be used to determine the concentrations C_k and electrostatic potential Φ if the initial and boundary conditions are properly defined.

4.3 The simulation of migration tests by using two-phase model with circular aggregates

4.3.1 *Geometry*

Fig. 4.1 shows one of the 2-D concrete numerical models developed to simulate the migration tests of ionic species in concrete specimens. The volume fraction of aggregates is $(1\text{-}\phi_c) = 0.5$. In the figure all circular areas represent the coarse aggregates (the radii of aggregates vary from 1.5 to 10 mm randomly in this geometry) and the rest is the cement or mortar. The size of the plain concrete is 50×50 mm. The location of the aggregates was randomly generated using a MATLAB program. It should be mentioned that, the shape of aggregates may not be perfectly circular in reality, so that in the subsequent studies, the influence of particle shapes on the transport properties of concrete will be examined.

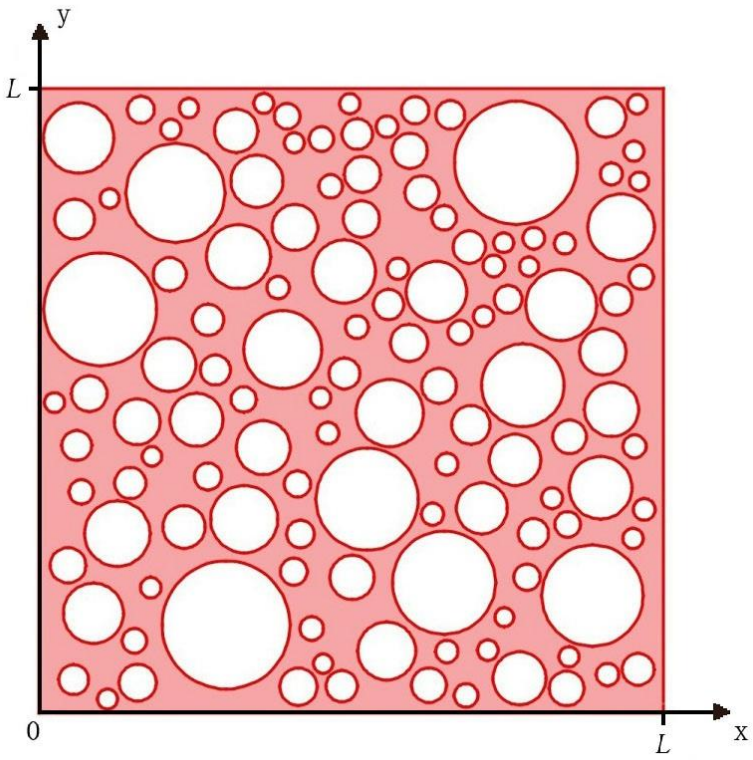

Figure 4.1. Two-dimensional model: section of concrete, $(1\text{-}\phi_c) = 0.5$.

4.3.2 *Numerical simulation*

Similar to the model presented in the previous Chapter, the numerical model is used to simulate an eight-hour migration test, in which the plain concrete specimen of 50×50 mm is located between two compartments, one of which has a 0.52 mole/L NaCl solution, the other of which has a 0.30 mole/L NaOH solution (both of sodium solutions are treated as individual ions in the simulation). Externally, there is a 24 V DC voltage applied between two electrodes inserted into the two compartment solutions. The concrete specimen is saturated with a solution of four ionic species (K, Na, Cl and OH) at the initial time. Since the external compartments here act like two reservoirs as shown in the set-up schematic (Fig. 4.2), during the present simulation, it is assumed that the concentration of each ionic species in the two compartments remains constant. The diffusion coefficients of individual ionic species, and the initial and boundary conditions of variables used in the model are given in Table 4.1, in which the diffusion coefficients of ionic species within pore solution are given by Xia and Li (2013).

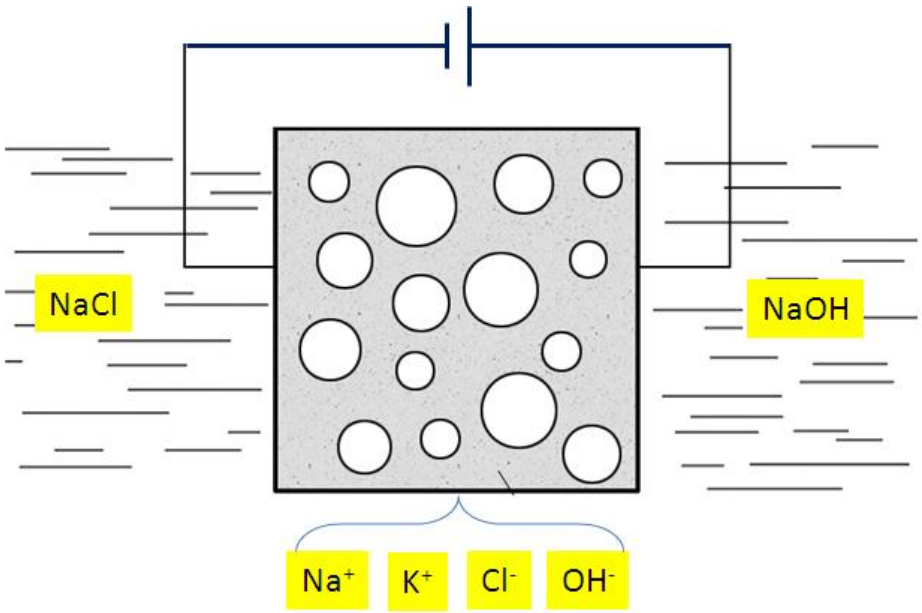

Figure 4.2. Schematic representation of a migration test (section of a concrete speciemen).

Table 4.1. Boundary conditions, initial conditions and diffusion coefficients.

Field variables		Potassium (mole/m^3)	Sodium (mole/m^3)	Chloride (mole/m^3)	Hydroxide (mole/m^3)	Electrostatic potential (V)
Boundary conditions	x = 0	0	520	520	0	$\Phi = 0$
	x = L	0	300	0	300	$\Phi = 24$
	y = 0	$J = 0$	$J = 0$	$J = 0$	$J = 0$	$\partial\Phi/\partial y=0$
	y = L	$J = 0$	$J = 0$	$J = 0$	$J = 0$	$\partial\Phi/\partial y=0$
Initial conditions		200	100	0	300	0
Charge number		1	1	-1	-1	N/A
Diffusion coefficient, $\times 10^{-10}$ m^2/s		1.957	1.334	2.032	5.260	N/A

4.3.3 *Finite element meshing*

Figure 4.3 shows the finite element mesh employed in the model. The mesh is applied only to the cement or mortar since the aggregates are impermeable and therefore they are not included in the model. As it was mentioned earlier, the larger the migration velocity, the smaller the element size required. Since there is 24 V potential difference applied in this case, the element size must be very small. Otherwise, the numerical solution will be oscillatory. Due to the nature of the geometry, the generation of the mesh was controlled by the size of the largest element, which is calculated based on an average value of electrostatic potential gradient (i.e. $\nabla\Phi = \Delta\Phi / L = 480\,\mathrm{V/m}$).

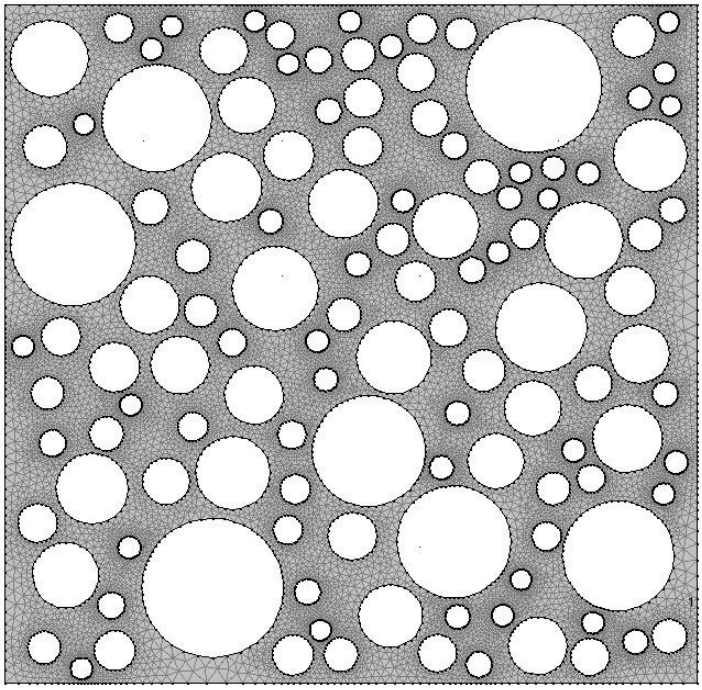

Figure 4.3. Finite element mesh (white circles represent aggregates with a volume fraction (1-ϕ_c) = 0.5).

4.3.4 *Simulation results*

For given initial and boundary conditions, Eqs. (3.7) and (4.3) can be solved numerically. Figs. 4.4-4.8 show the distribution profiles of five field variables (the concentrations of four ionic species and the electrostatic potential) obtained at four different times, in which the two plane coordinates represent the position of the variable in the 2-D concrete model and the vertical coordinate is the value of the variable (concentration or electrostatic potential). Each frame of individual variable represents one instantaneous moment from the first hour to the fourth hour. Note that there are small raises of concentration front due to the boundary derivation of FEA in the low right figure of Fig. 4.6.

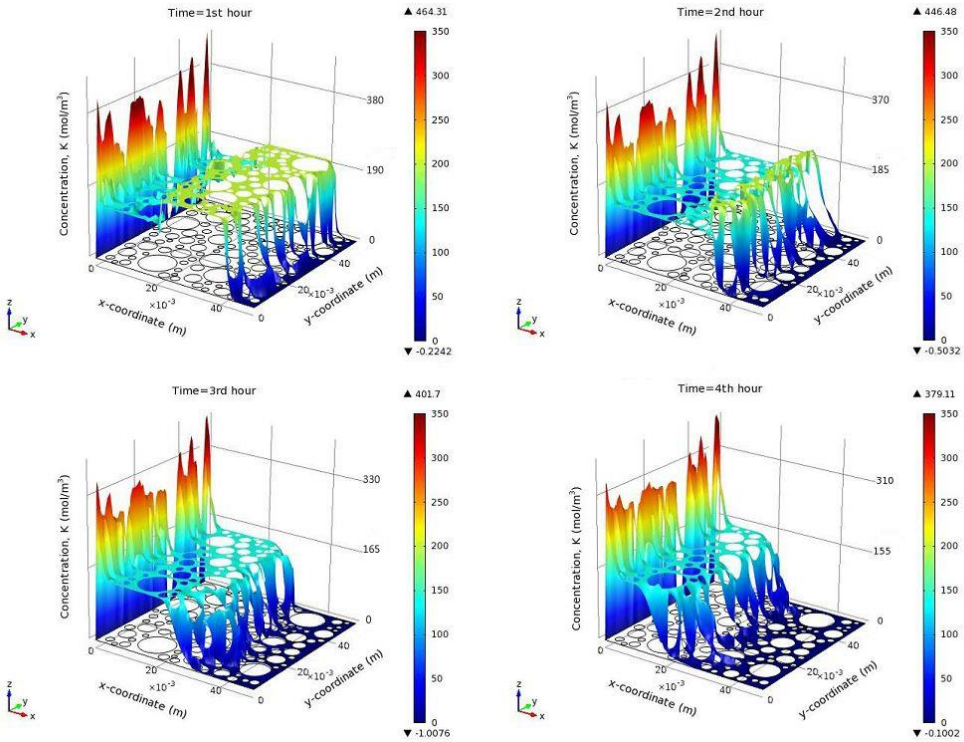

Figure 4.4. Concentration distribution profiles of potassium ions at four different times..

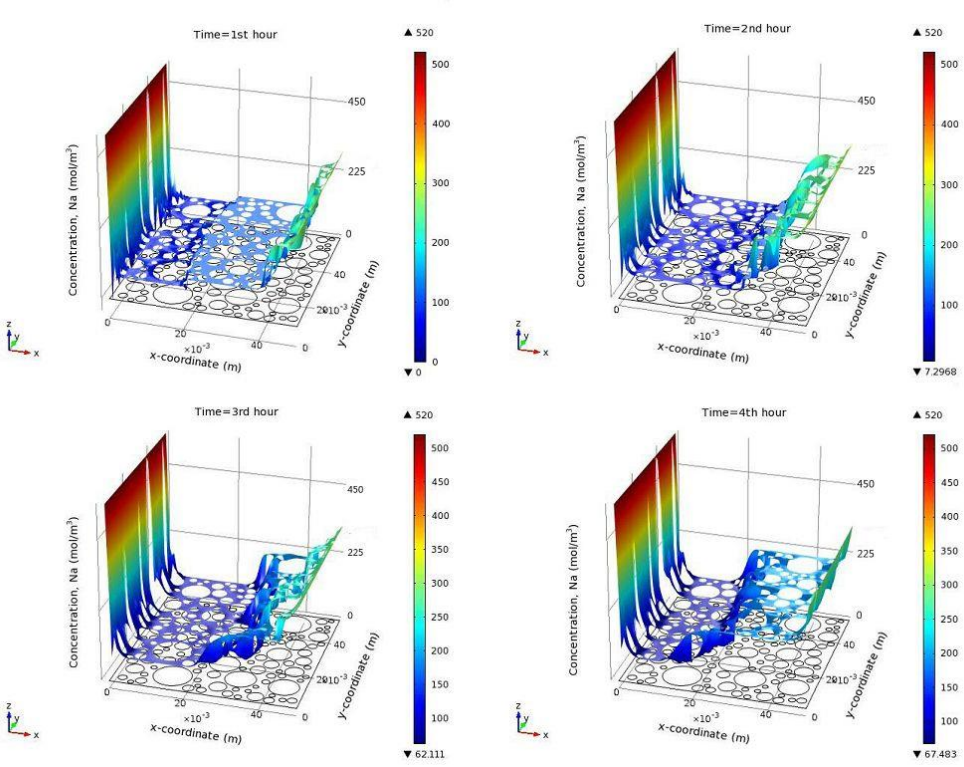

Figure 4.5. Concentration distribution profiles of sodium ions at four different times.

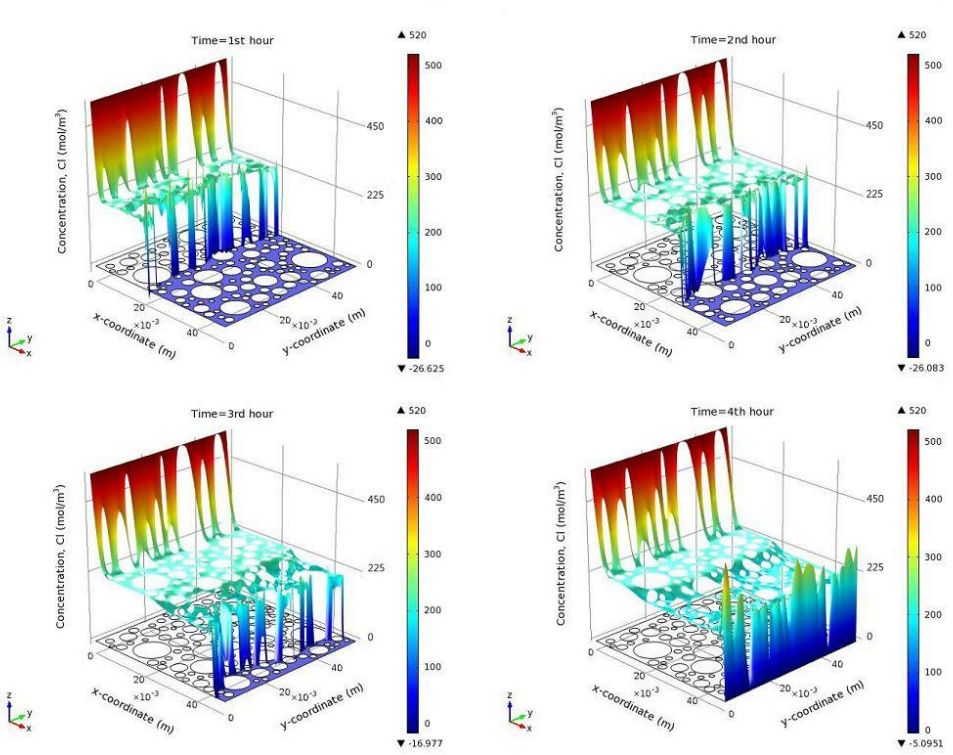

Figure 4.6. Concentration distribution profiles of chloride ions at four different times.

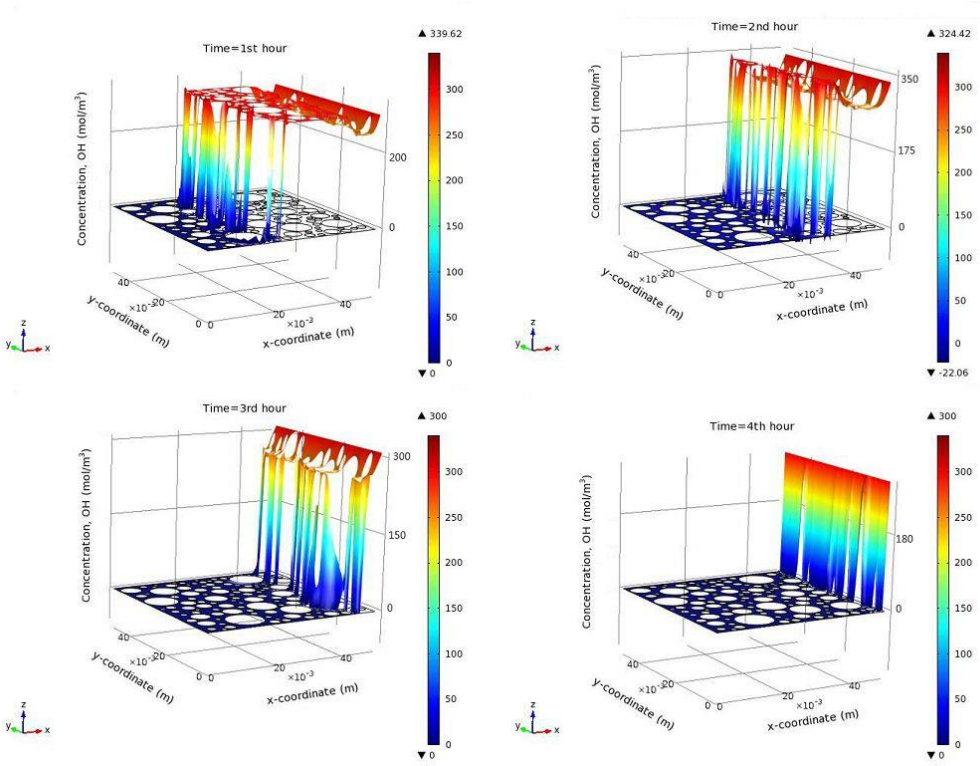

Figure 4.7. Concentration distribution profiles of hydroxide ions at four different times.

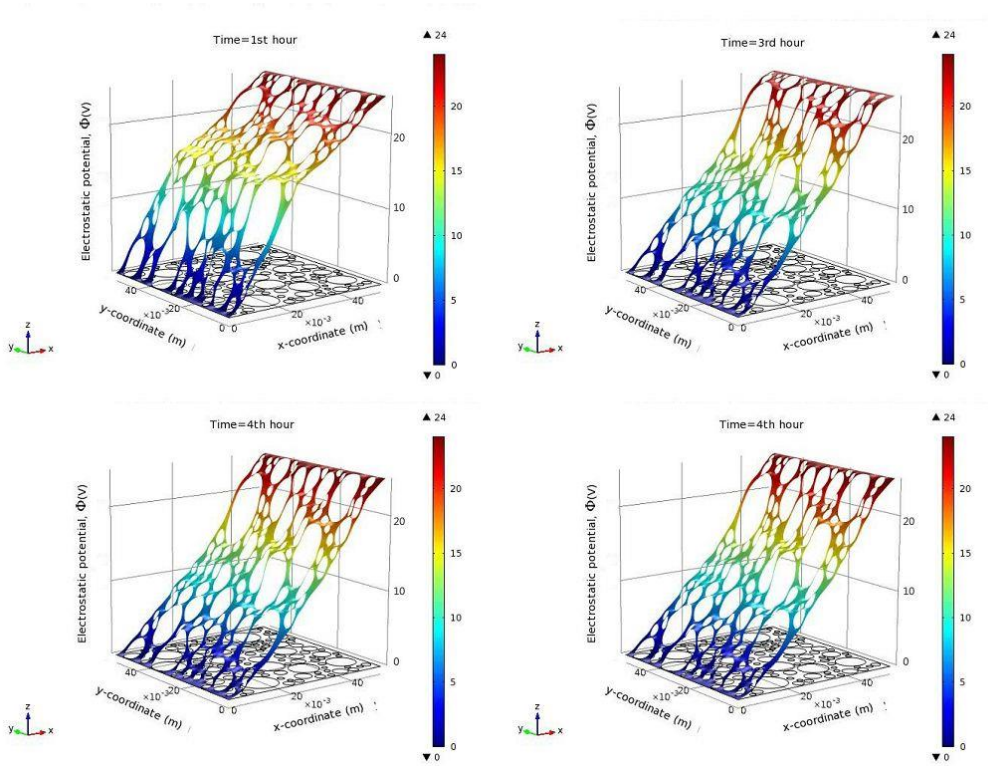

Figure 4.8. Electrostatic potential distribution profiles at four different times.

Qualitatively speaking, the electro-process results obtained from the present model is similar with that from the 1-D model utilised in Section 3.4. This is likely attributed to the identical influence of Poisson's equation. The 3-D plots provide a good overall view on the evolution of transport of four ionic species in the specimen due to the influence of an externally applied electric field. It can be observed from the figures that the ionic transport takes place mainly in the x-axis direction due to the influence of the externally applied electric field. In contrast, the ionic transport in the y-axis direction occurs only locally and it is mainly attributed to the tortuosity influence owing to the existence of aggregates.

In order to make a quantitative plot for each ionic species at a given time, one may still prefer to use the traditional 2-D plot as is usually used in 1-D models. Fig 4.9 shows the variation of chloride concentration distributing along the y-axis in sections with given x values at four different times. Note that due to the existence of aggregates the concentra-

tion is not continuous. Also due to the local influence of the size and position of aggregates the concentration varies irregularly. Nevertheless, in overall, this kind of variation seems not very significant, particularly when compared to its variation along the x-axis, as is shown in Figs. 4.4-4.8. The reason for this is likely due to the 'sealed' boundary conditions employed at $y = 0$ and $y = L$ boundaries as shown in Table 4.1, which make the transport of ions take place almost in one direction. Similar features were found for the other four field variables and thus they are not presented here.

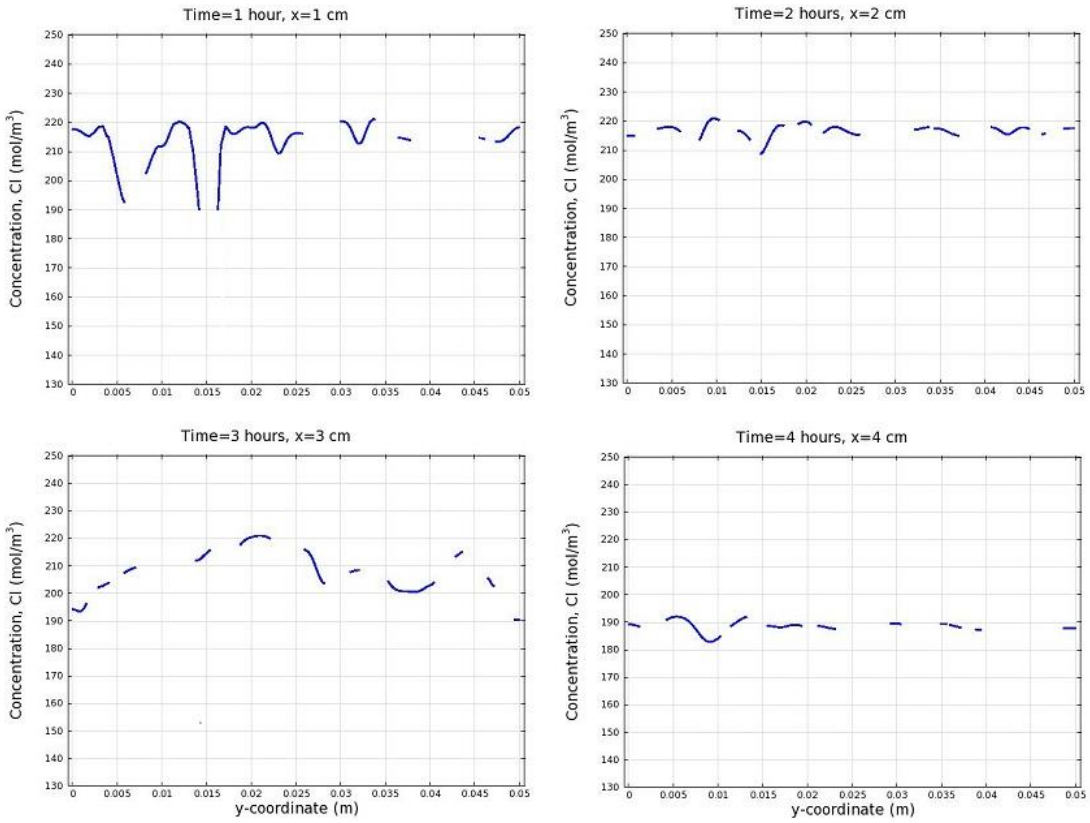

Figure 4.9. Section plot of chloride concentration distribution profiles at four different times.

Since the variations of ionic concentrations and electrostatic potential along the y-axis are very small, one can use their average values in the y-direction, i.e. $\bar{z}(x) = \frac{1}{L}\int_o^L z(x,y)dy$ to represent z(x,y) for each field variable. In this case one can replot Figs. 4.4-4.8 in a 2-D format, which are shown in Figs. 4.10-4.14.

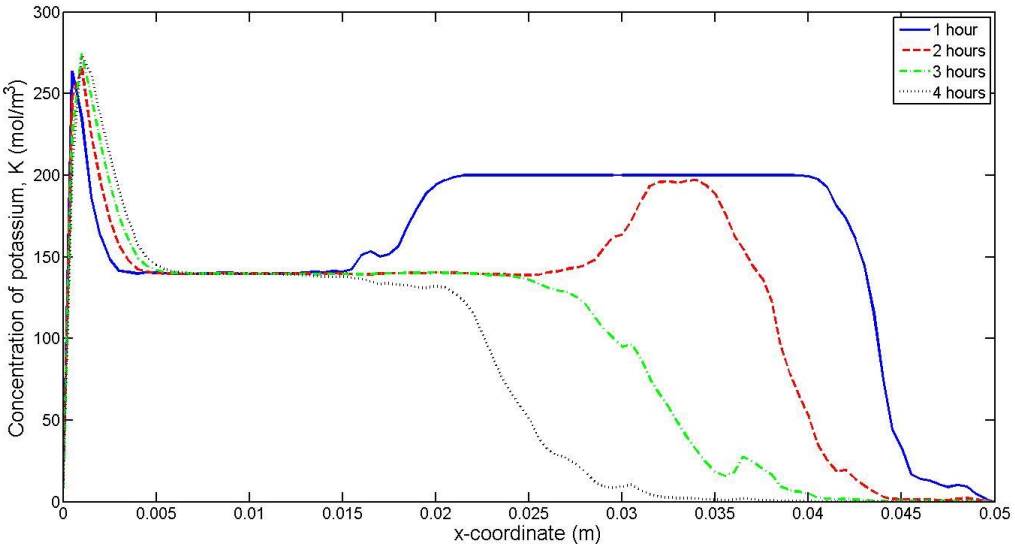

Figure 4.10. 4-hour concentration distribution profiles of potassium ions.

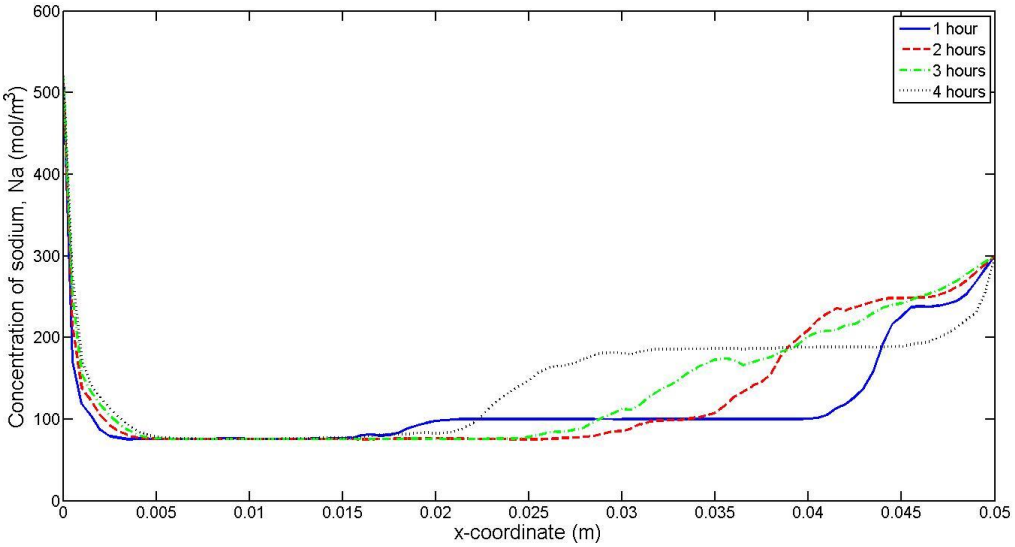

Figure 4.11. 4-hour concentration distribution profiles of sodium ions.

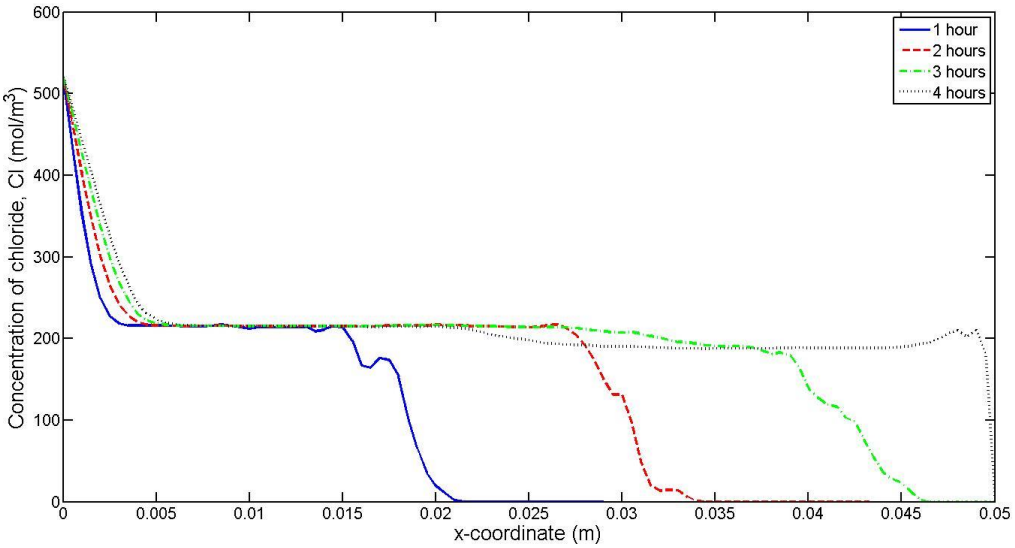

Figure 4.12. 4-hour concentration distribution profiles of chloride ions.

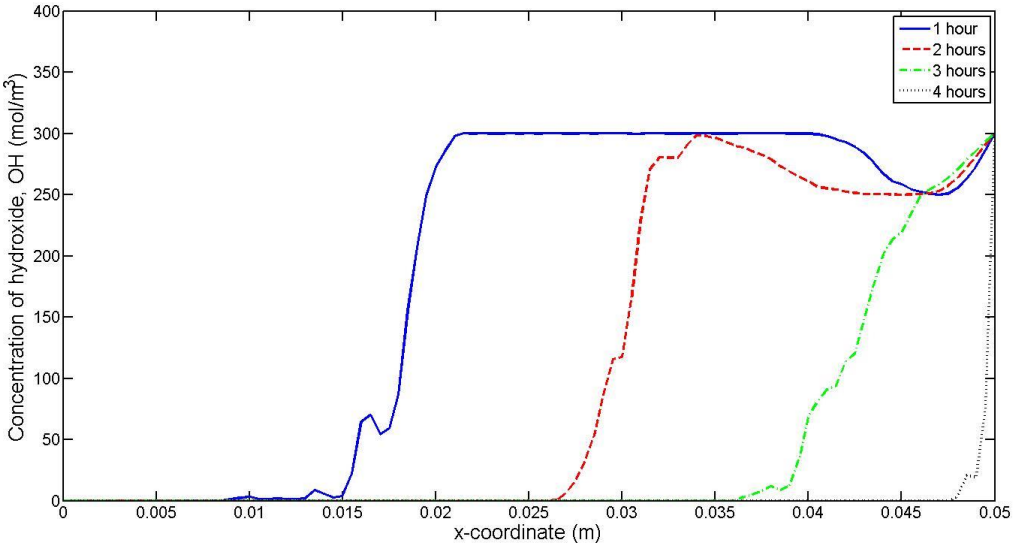

Figure 4.13. 4-hour concentration distribution profiles of hydroxide ions.

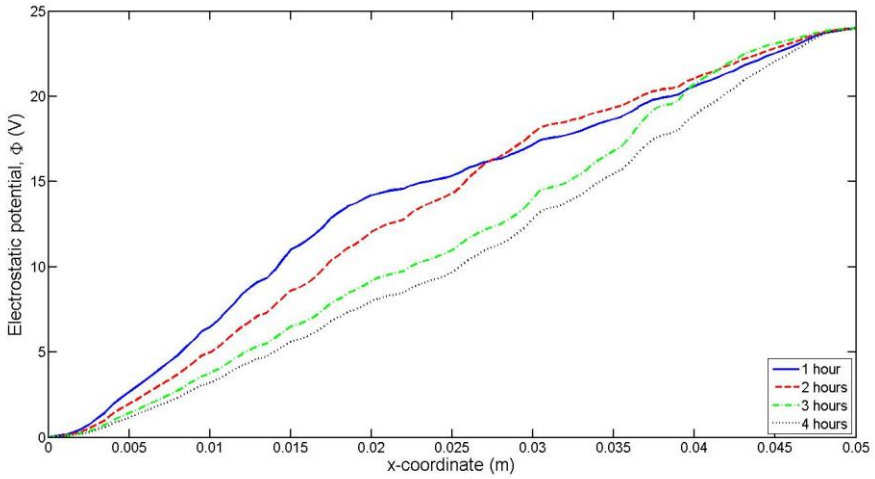

Figure 4.14. 4-hour electrostatic potential distribution profiles.

As is to be expected, due to the effect of aggregates, the distribution curve of ionic concentration or electrostatic potential in the 2-D plot shown in Figs. 4.10-4.14 is not very smooth in some places. Also, it can be seen from Figs.4.10-4.13 that, the transport behaviour of potassium, sodium and chloride ions is quite different from that of hydroxyl ions. The former has a clear diffusion layer in the region near the cathode and a clear migration wave front. The latter has only the migration wave front. For hydroxyl ions, migration is dominant for most of the time. For the other three ionic species, however, diffusion is also very important. This is demonstrated by the migration wave front line that is not very steep (particularly after two hours). The steepness of the migration wave front is found to be different for different ionic species, and also for different times. The hydroxyl ions are found to have the steepest wave front, whereas the sodium ions have the gentlest wave front. The decrease of steepness with time in the concentration profiles reflects the combined influence of diffusion and local tortuosity. This feature of steep degree was not found in the single phase model and it is likely due to the inclusion of aggregates in the two-phase model, which provides a direct influence of tortuosity on ionic diffusion and migration.

In terms of the migration wave speeds of ionic species, the status illustrated in Figs. 4.10-13 is in accordance with that of Figs. 3.12-3.15. The wave speeds of positively (or negatively) charged ions are almost the same but are significantly different from those of their opposite charged ions. This demonstrates that the electrostatic potential gradient here is also not constant but regionally dependent. It can be seen from Figs. 4.10-4.13 that, as time goes on, the amount of sodium and chloride ions rises, whereas the amount of potassium and hydroxyl ions reduces in the concrete specimen. The former is due to the boundary conditions, which supply sodium ions and chloride ions from the anode and cathode, respectively. The latter is due to that, in contrast, the supply of potassium ions from the cathode and hydroxyl ions from the anode does not affect the internal transport of these ions. It is also observed from Figs. 4.10-4.13 that, the rate of the increase of sodium and chloride ions in the specimen is lower than that of the decrease of potassium and hydroxyl ions. The reason for this is probably due to the lower diffusion coefficients of the sodium and chloride ions than those of potassium and hydroxyl ions. Table 4.2 shows a quantitative comparison of the total mole numbers of each ionic species remaining in the specimen at different times. It is evident from the table that, while the sum of negatively charged ions is balanced by that of positively charged ions, the total quantity of all ions in the specimen is indeed decreasing with time.

Table 4.2. Total amount of ions in the specimen (unit thickness).

Time of the test	Initial (mole/m)	1st hour (mole/m)	2nd hour (mole/m)	3rd hour (mole/m)	4th hour (mole/m)
Potassium	0.500	0.385	0.301	0.233	0.181
Sodium	0.250	0.294	0.323	0.342	0.366
Chloride	0	0.215	0.345	0.468	0.537
Hydroxide	0.750	0.463	0.275	0.106	0.010
Total Amount	1.500	1.358	1.247	1.150	1.094

The feature of convex and concave shape existing in the electrostatic potential distribution is more obviously in Figs. 4.8 and 4.14 than in Fig. 3.10. Regardless of the local fluctuation along y-axis caused by the tortuosity of aggregates, these figures further demonstrate that migration speed is not constant but varies with time and region in the 2-D model.

To further demonstrate the variation of migration speed, Fig.4.15 shows the migration fluxes of each ionic species at various different times. It is evident from the figure that the migration fluxes of ionic species vary not only with space but also with time, and most importantly they do not follow a single pattern. A comparison between Figs. 4.15 and 3.18 indicates that, for the two-phase model, the curves of migration fluxes fluctuate more dramatically versus space whereas spread more gentle verses time. The former is due to the local heterogeneous distribution of aggregates. The latter is due to the tortuosity effect, which is also caused by the aggregate phase.

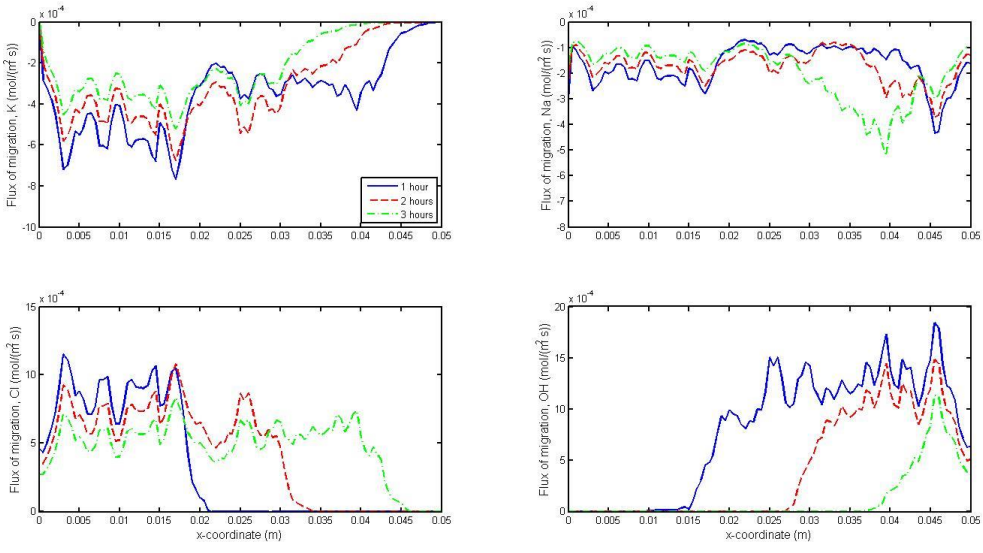

Figure 4.15. Distribution profiles of migration fluxes of four ionic species.

Of particular interest is the migration of chloride ions, as the diffusion coefficient in migration tests is calculated based on the migration profile. Fig. 4.16 shows an overall

comparison of chloride concentration profiles at four different times obtained from the present 2-D, two-phase, multi-component model, the 1-D, single-phase, multi-component model (with ionic interactions obtained from Section 3.4) , and the 1-D, single-phase, one-component model (without ionic interactions obtained from Section 3.3). Interestingly, the two multi-component transport models provide very similar concentrations, but have significantly different travel speeds; the 1-D model produces higher travel speed than the 2-D model does. In contrast, the one-component model provides higher concentration than the two multi-component models do. However, in terms of the travel speed, the one-component model which employs electro-neutrality assumption and the two-phase model which employs Poisson's equation are closer. This implies that the relevance of multi-phases and of electrical interaction between ionic species are equally important.

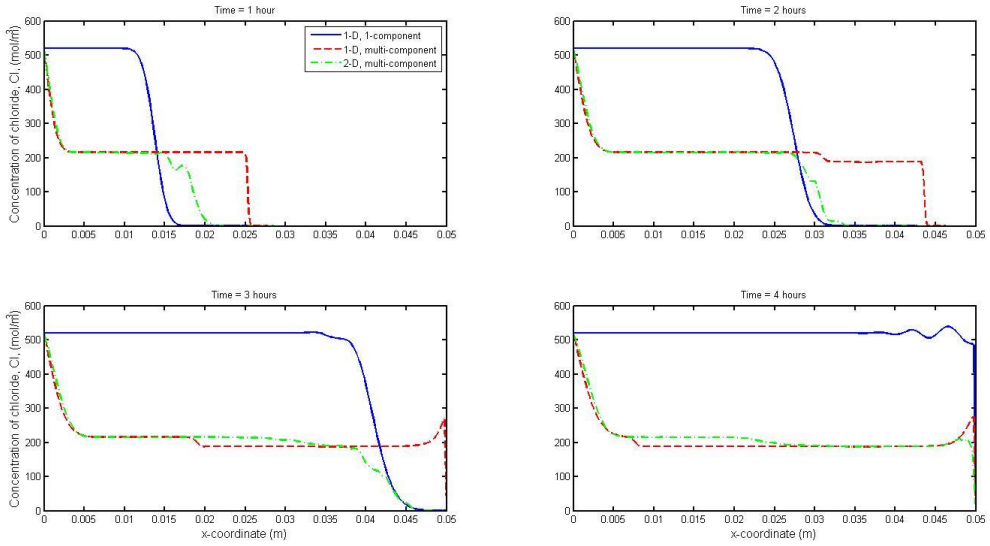

Figure 4.16. Comparisons of chloride concentration profiles between three cases.

To demonstrate the importance of using Poisson's equation in the present two-phase geometry, Fig. 4.17 shows a comparison of concentration profiles of chloride ions, ob-

tained with and without using Poisson's equation. It can be seen from the figure that, the concentration profiles obtained by using an electro-neutrality condition are quite different from those using the Poisson's equation. This again proves that, when the electro-neutrality condition was used, there would be no electro-static potential coupling and therefore the transport of individual ionic species would be independent of each other, which is obviously less reasonable.

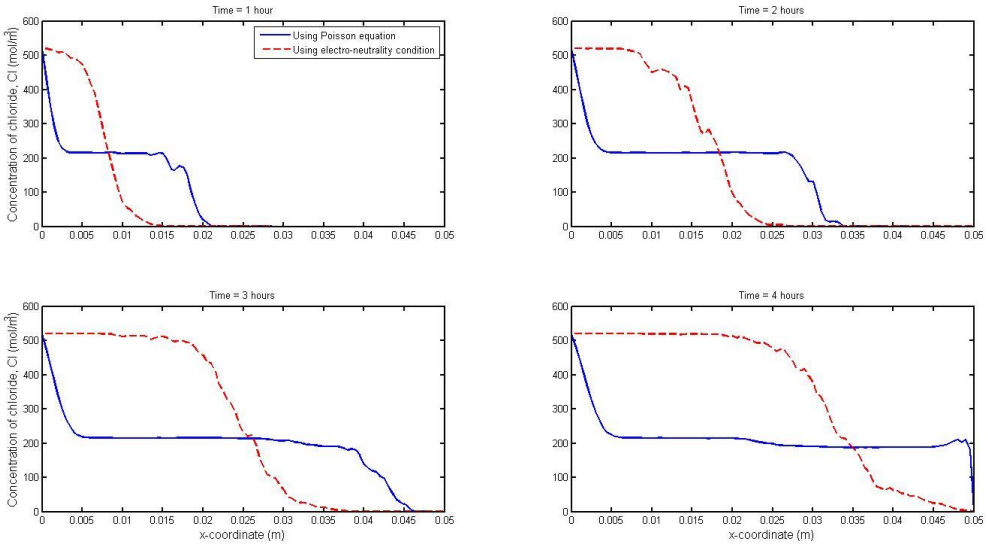

Figure 4.17. Comparison of chloride concentration distribution profiles obtained with and without using Poisson's equation in the two-phase model.

4.4 The simulation of migration tests with different shapes and volume fractions of aggregates

4.4.1 *Geometry and finite element meshing*

In order to further investigate the effect caused by aggregate shapes and volume fractions, a set of 2-D concrete numerical models with various shapes and volume fractions of coarse aggregates were developed. Figs. 4.18-4.21 show the meshed models with the same aggregates volume fraction of $(1-\phi_c) = 0.5$. but different aggregates shapes: ellipse, triangle, rectangle, and mixed shapes. The coordinate detail is exactly same as Fig. 4.1. Just like the models with circular inclusions (Fig. 4.3), only the mortar or cement phase is meshed since the aggregates are assumed to be impermeable. It is noticeable that, the distributions of aggregates in the Figs. 4.18-4.20 are almost uniform whereas only that in Fig. 4.21 is less uniform. A careful examination of the geometry including mixed shape shows that, the smaller sized particles gather more in the region near the cathode (from x=0 to x=0.025 m), whereas the larger ones gather more in the region near the anode (from x=0.025 to x=0.05 m). This setting is deliberately arranged for legible exploration of the influence of tortuosity, which will be explained later in discussions.

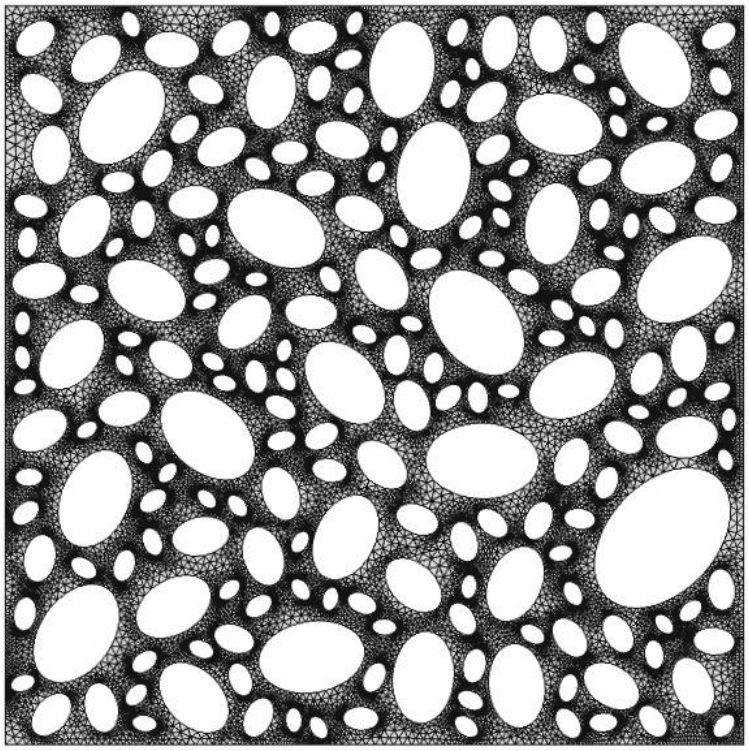

Figure 4.18. Finite element mesh (white ellipses represent aggregates with a volume fraction $(1-\phi_c) = 0.5$).

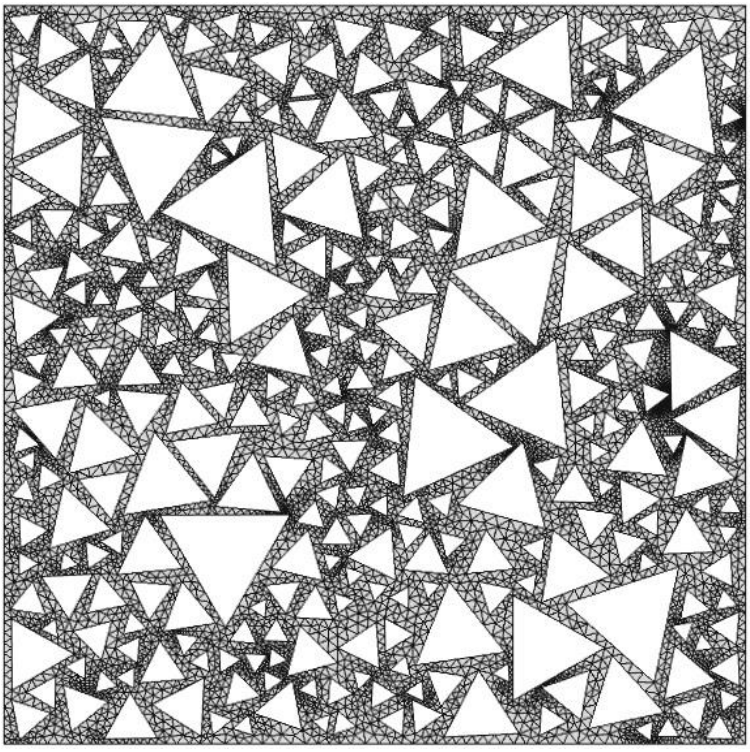

Figure 4.19. Finite element mesh (white triangles represent aggregates with a volume fraction $(1-\phi_c) = 0.5$).

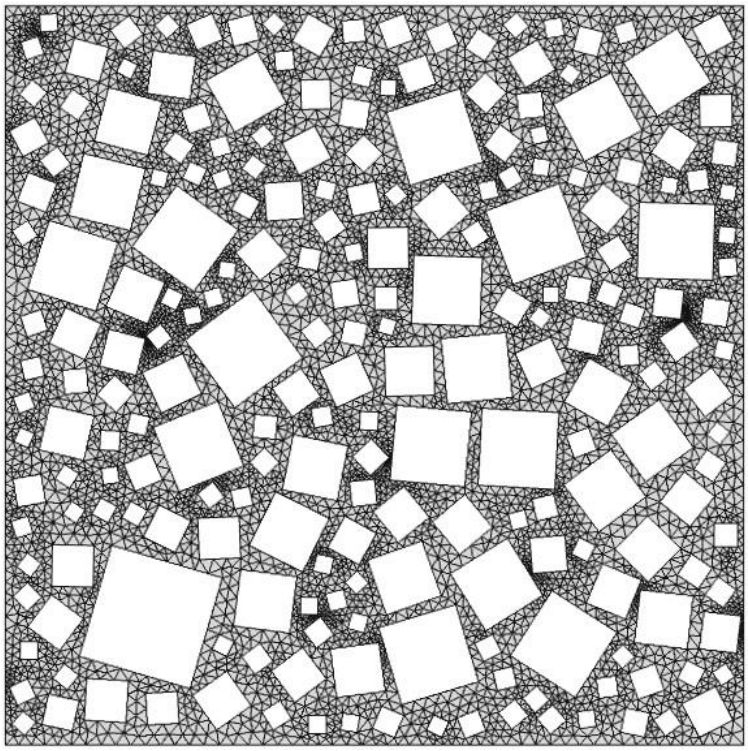

Figure 4.20. Finite element mesh (white rectangles represent aggregates with a volume fraction ($1-\phi_c$) = 0.5).

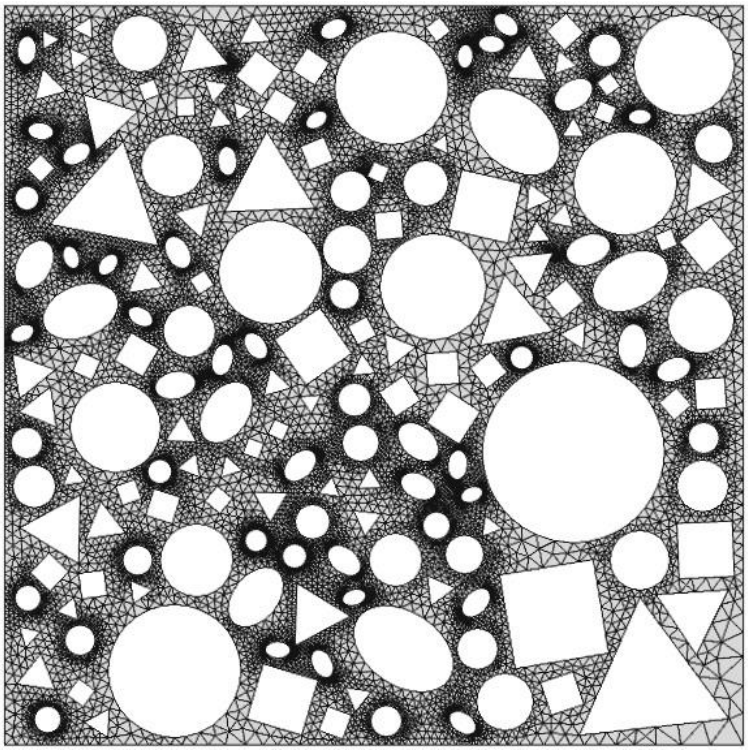

Figure 4.21. Finite element mesh (white holes represent aggregates with a volume fraction ($1-\phi_c$) = 0.5).

4.4.2 *Simulation results*

For given initial and boundary conditions (Table 4.1), the ionic transport in the simulated concrete specimens can be numerically calculated by solving the mass conservation equation and Poisson's equation. As particular interest is of the penetration of chloride ions, here, only the chloride distribution profiles are displayed in the form of the 3-D plot, which are shown in Figs. 4.22-4.25. Generally speaking, with the same aggregates volume fraction, the evolutions of ionic transports in the models filled by ellipse, triangle, rectangle, and mixed shaped aggregates closely resemble that in the circular shaped model. The negatively charged chlorides steadily move from the cathode towards the anode by electro-migration process, which takes place mainly along the x-axis direction. It also can be seen from the figures that, the aggregates split the migration wave fronts into a number of pieces which makes the wave front act like a 'waterfall'. Generally, the pieces of 'waterfall' move at a synchronous velocity throughout the most 3-D figures. However, in the triangle shaped aggregate model (Figs. 4.23), it is noticeable that the speeds of the 'waterfall' pieces are not parallel and ordered. This phenomenon can be explained by the effect of tortuosity. The sharp angle of triangle shape will markedly increasing the length of the flow paths as well as generates many areas with larger tortuosity in the electrolyte solution to decrease the transport of ions in corresponding regions.

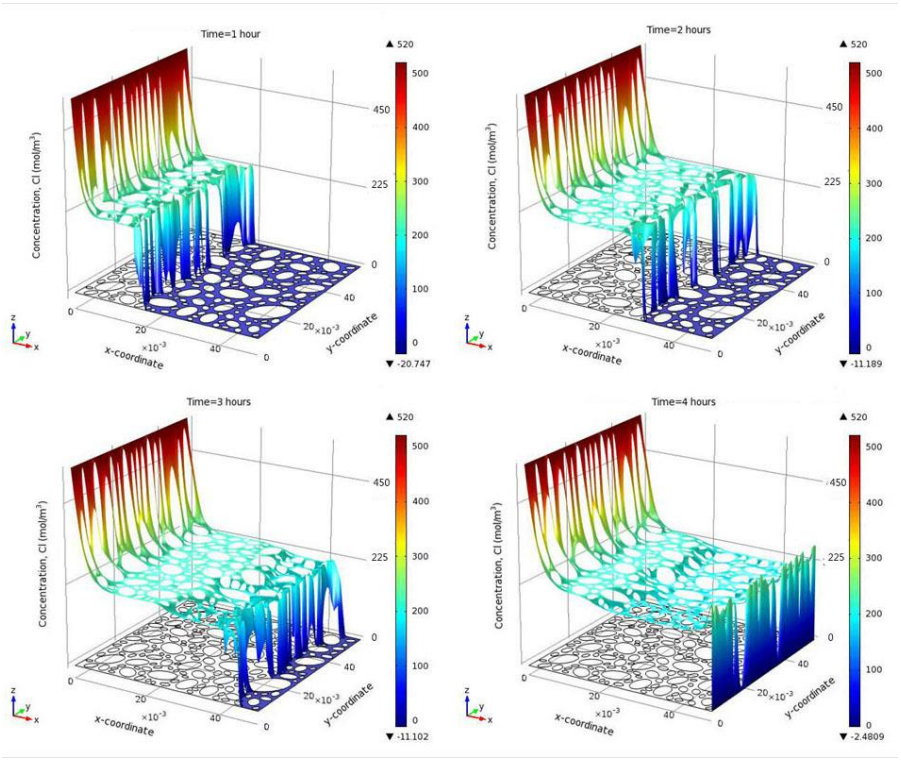

Figure 4.22. Concentration distribution profiles of chloride ions (for aggregates with an ellipse shape).

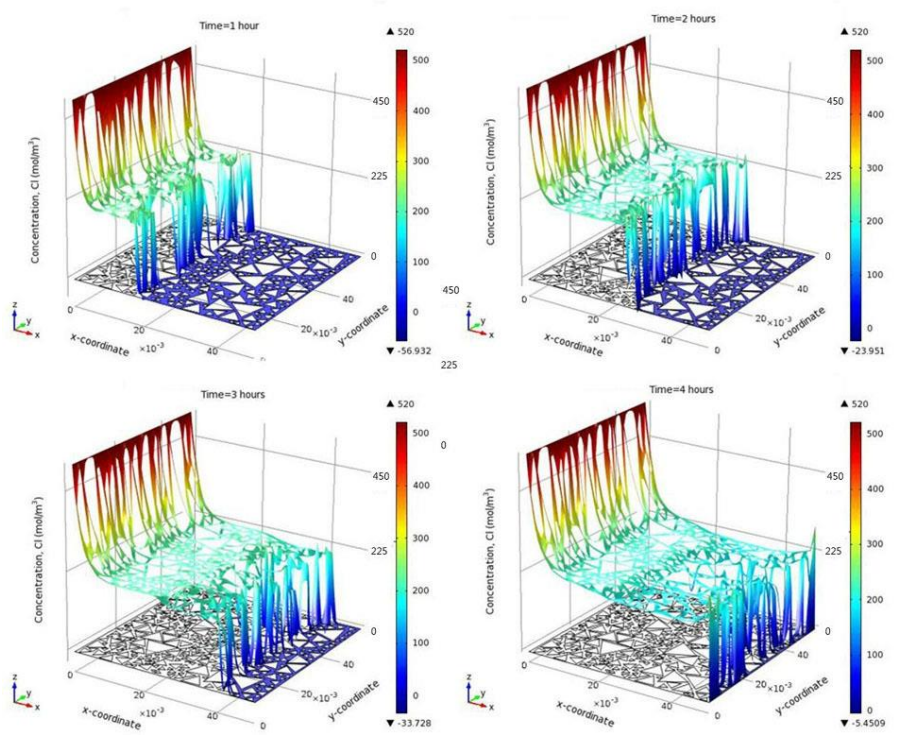

Figure 4.23. Concentration distribution profiles of chloride ions (for aggregates with a triangle shape).

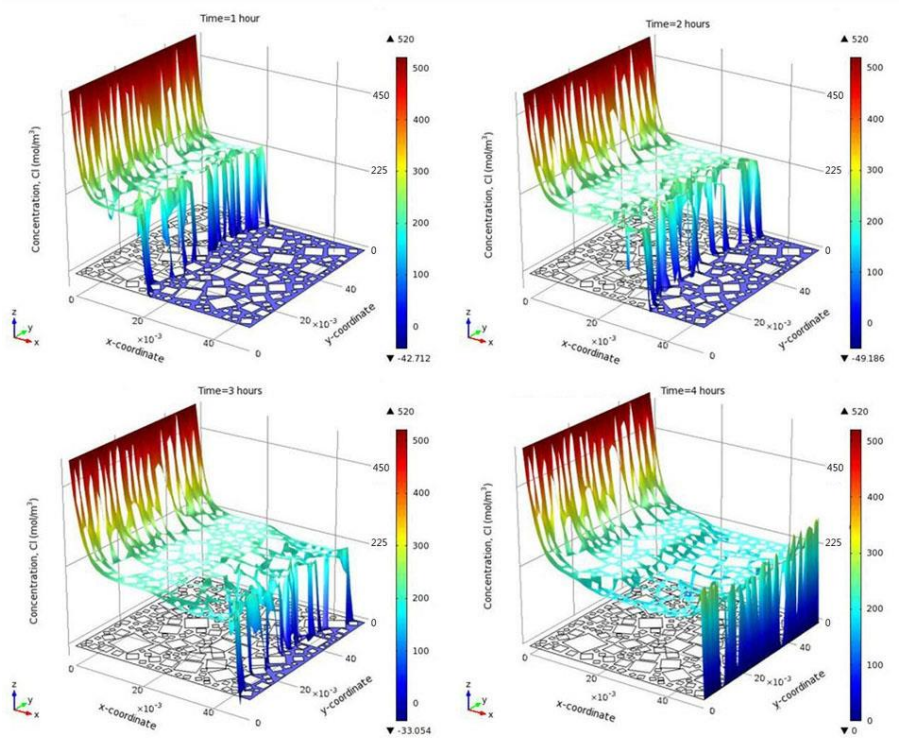

Figure 4.24. Concentration distribution profiles of chloride ions (for aggregates with a rectangle shape).

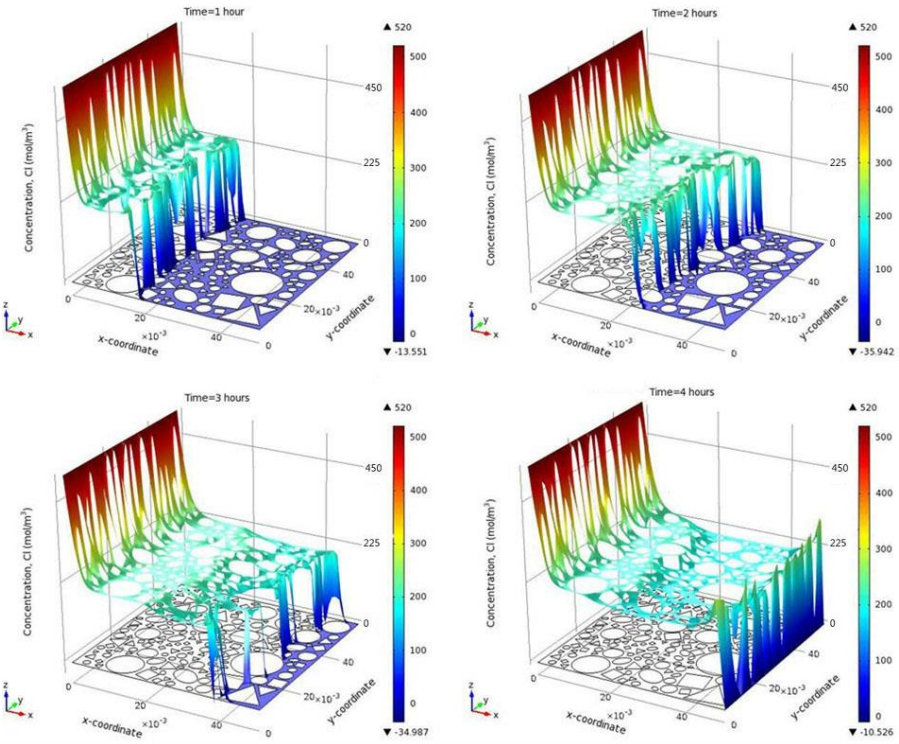

Figure 4.25. Concentration distribution profiles of chloride ions (for aggregates with mixed shapes).

For a more quantitative study, Figs. 4.26-4.29 give comparisons of concentration profiles of four ionic species between five different shapes when they have the same vol-

ume fraction of aggregates. It is clearly shown that, there is only a tiny difference in the migration velocities between the models with the shapes of circular, ellipse and rectangle, which implies a similar tortuosity between the models with these shapes of inclusion. In contrast, from the overall points of view, the triangle shaped aggregates bring a slower velocity than other shaped aggregates due to its largest tortuosity.

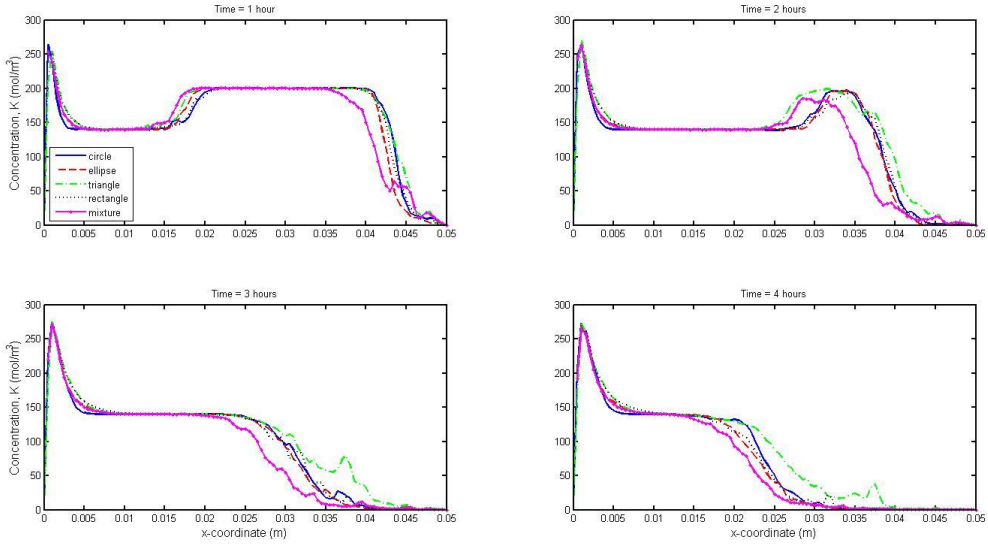

Figure 4.26. Comparisons of potassium concentration profiles between different aggregate shapes, (1-ϕ_c) = 0.5.

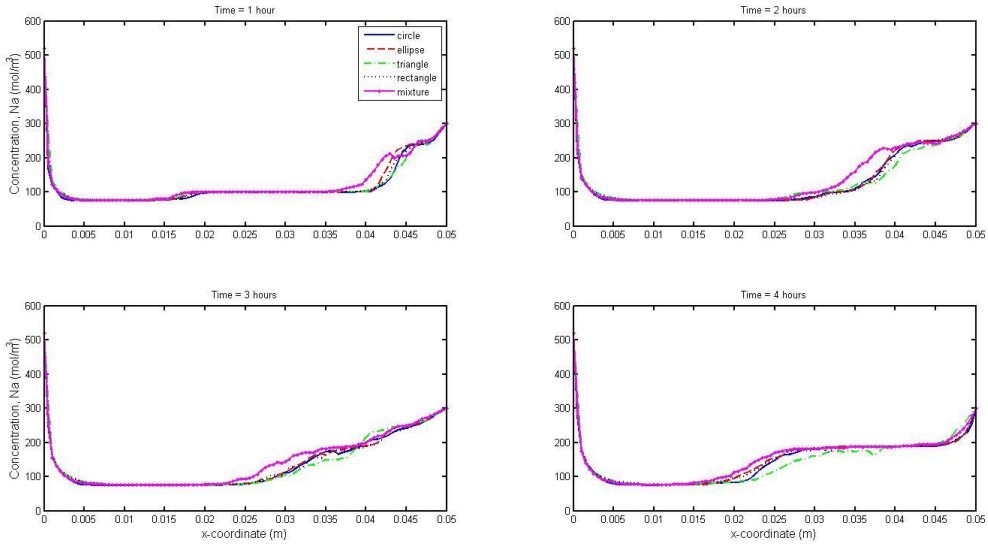

Figure 4.27. Comparisons of sodium concentration profiles between different aggregate shapes, (1-ϕ_c) = 0.5

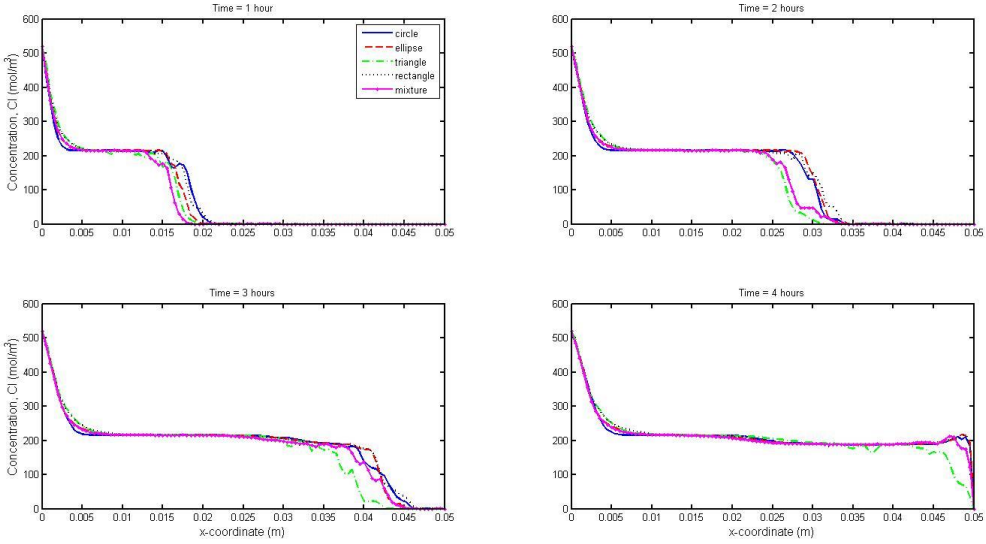

Figure 4.28. Comparisons of chloride concentration profiles between different aggregate shapes, (1-ϕ_c) = 0.5.

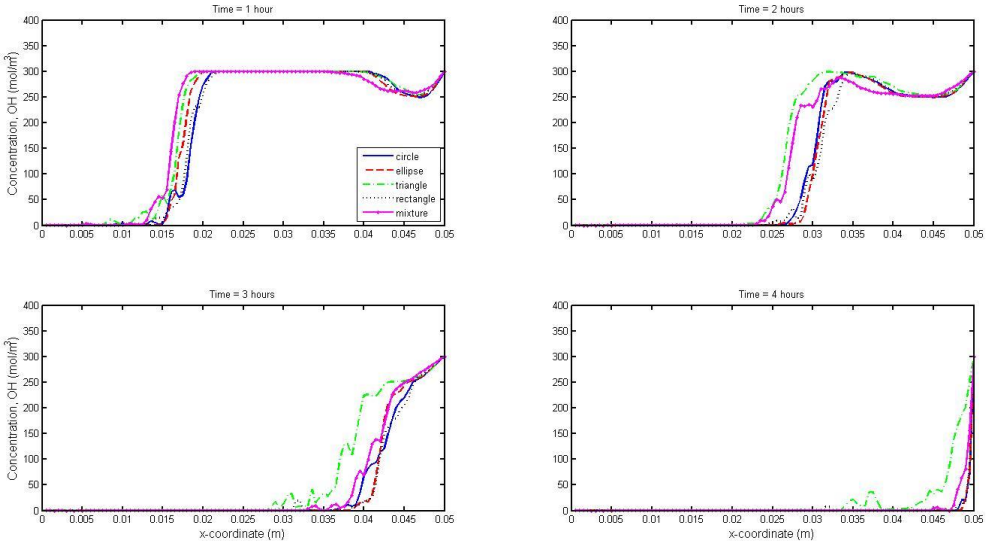

Figure 4.29. Comparisons of hydroxide concentration profiles between different aggregate shapes, (1-ϕ_c) = 0.5.

More interesting features are found in the mixed shaped aggregates. As it was mentioned above that the distribution of the different sized aggregates are deliberately arranged to be less uniform (the smaller ones more gathers in the left side of the concrete specimen and the larger ones do the opposite), the tortuosity of the model including

mixed shaped aggregates is correspondingly less uniform (larger tortuosity in region near the cathode and smaller tortuosity in region near the anode). As a consequence, when the migration waves of the negatively charged ions (both chloride and hydroxide) of the mixed shaped aggregates travel from the section of x=0 to the section of x= 0.025 m, its speed is slower than the others, even including the triangle ones; when they travel from the section of x=0.025 m to the section of x= 0.05 m, the migration waves of the mixed shaped aggregates speed up, overtaking the triangle one and finally almost equalling the evolution of other three shaped aggregates at the region near the anode. This procedure exactly reverses when it happens to the positively charged ions (both potassium and sodium). The phenomenon described above evidently depicts how the tortuosity caused by the aggregate phase affects the ionic transport in concrete.

The above findings seem to indicate that, under the condition of identical volume fraction and similar tortuosity, the shape of aggregate has little impact on the penetrations of ions. To further prove this opinion, more examples are provided here of different shapes with different volume fractions. Figs. 4.30 and 4.31 respectively show the comparisons of different shapes under the aggregate volume fractions of $(1-\phi_c)$ = 0.4 and 0.3. As it was expected, both figures again show that the migration velocities of chlorides are approximately a constant between various shapes, except for the triangle aggregates which has significantly larger tortuosity. Note that the aggregates of mixed shapes in this example are randomly distributed. Therefore, the special behaviour which occurs in Figs. 4.26-4.29 disappears in Figs. 4.30 and 4.31, in terms of the special results of triangle shaped aggregates. Note that triangle shaped aggregates are the extreme case which is very rare in reality. Therefore, it can be concluded that the influence of particle shapes on the permeability of concrete is not very significant.

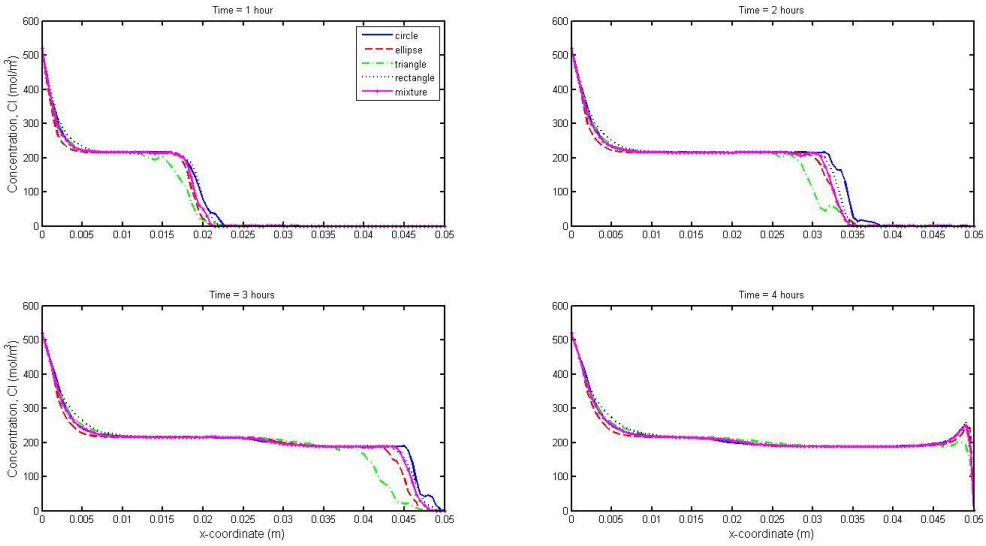

Figure 4.30. Comparisons of chloride concentration profiles between different aggregate shapes, (1-ϕ_c) = 0.4.

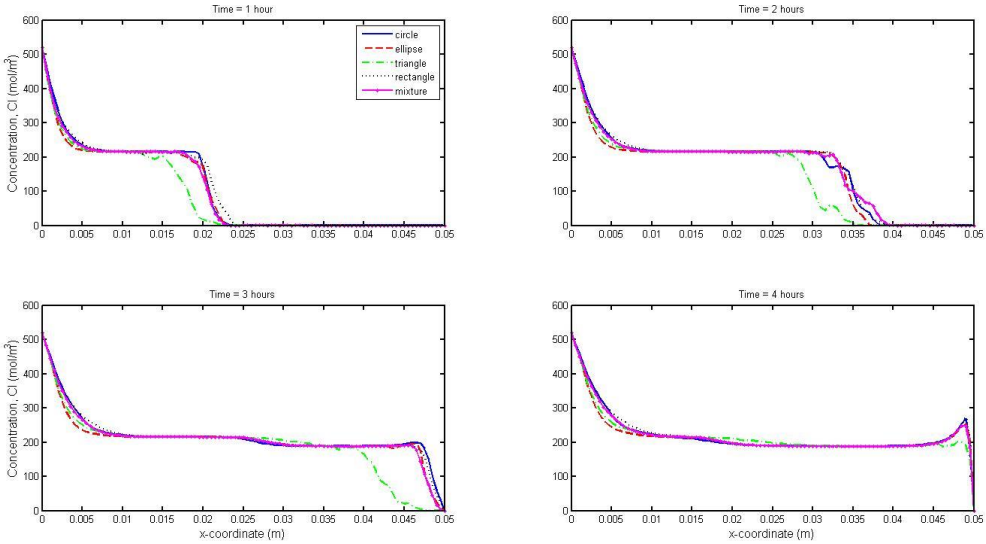

Figure 4.31. Comparisons of chloride concentration profiles between different aggregate shapes, (1-ϕ_c) = 0.3.

In order to examine the influence of the volume fraction of aggregates on the ionic transport, particularly that of chloride ions, Fig. 4.32 shows the concentration distribution profiles of chloride ions at four different times for three different aggregate volume fractions. It can be seen from the figure that, the influence caused by various volume fractions is much more remarkable than that caused by various shapes. Specifically, the

smaller the aggregate volume fraction, the quicker the chloride ions can travel. The reason for this is still likely due to the effect of tortuosity, as the higher the aggregate volume fraction, the larger the tortuosity; therefore, the slower the ionic transport. This is also consistent with what was shown in Fig. 4.16. Here it should be pointed out that, the increase in quantity of aggregates will also increase the volume of interfacial transition zone (ITZ) in the mortar, which can increase the diffusivity of the concrete. However, since the present model does not include the ITZ this kind of effect was not reflected in the results.

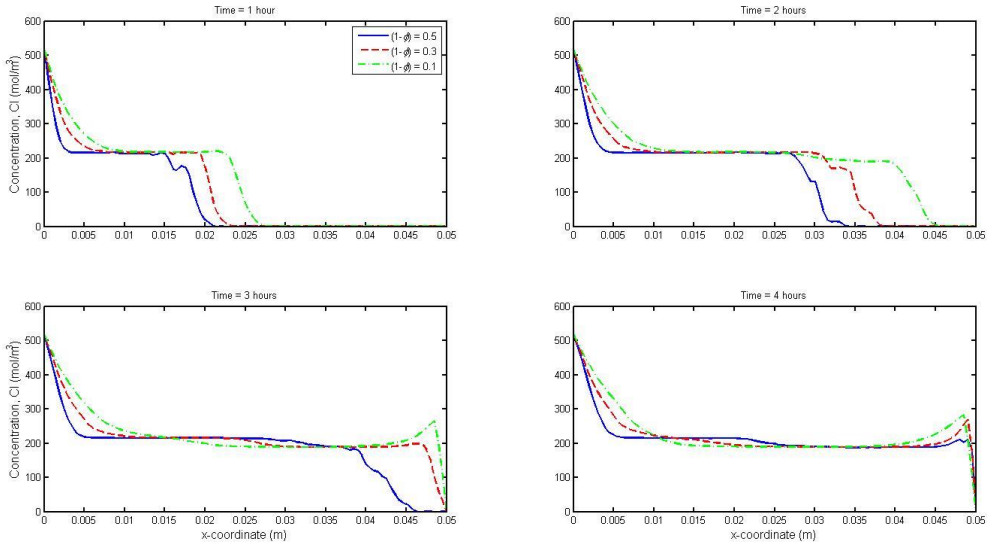

Figure 4.32. Comparisons of chloride concentration profiles between different volume fractions (circular aggregates)

4.5 The simulation of migration tests considering the binding effect

As it was mentioned in Section 2.2.2, ionic binding, both physically and chemically may take place at the pore surfaces, which allows part of free ions in pore solution to be adsorbed by the cementing material of concrete and thus has a great impact on the ionic transport process. The aim of this section is to further add the binding effect into our model and to examine the influence of ionic binding on the transport of ionic species.

It has been demonstrated in the preceding section that the influence of particle shapes on the permeability of concrete is not very significant. Therefore, for simplicity, only the concrete model with circular aggregate inclusion is examined during the following simulation.

4.5.1 *Numerical simulation*

Due to binding, the total concentration of ionic species contained in concrete is divided into two forms – free ions existing in concrete pore solution and the bound ions adsorbed by solid cement matrix. The latter do not participate in the ionic transport process but will affect the concentration distribution results. Hence, Eq. (4.3) needs to be modified as follows:

$$\frac{\partial C_k}{\partial t} + \frac{\partial S_k}{\partial t} = -\nabla J_{\mathrm{k}} = D_k \nabla^2 C_k + \nabla\left[z_k D_k \left(\frac{F}{RT} \nabla \Phi \right) \right] \qquad k = 1, \ldots, \mathrm{N} \qquad (4.4)$$

where S_k is the concentration of bound ions or the adsorption due to chemical reactions of species *k*.

Considering the equilibrium between free and bound concentrations, the binding process is not irreversible since the chlorides will be released again if the concentration in the

electrolyte becomes lower. Experimental data (Li and Page, 1998) suggests that the relationship between the bound and free chloride concentrations is almost independent of the transport rates and approximately satisfy the Langmuir isotherm as follows:

$$S_{\mathrm{Cl}} = \frac{\alpha C_{\mathrm{Cl}}}{w(1+\beta C_{\mathrm{Cl}})} \tag{4.5}$$

where S_{Cl} and C_{Cl} respectively stand for the concentrations of bound and free chlorides, w is the content of the water in which diffusion occurs, expressed per unit weight of cement, $\alpha = 0.42$ and $\beta = 0.8\,\mathrm{mol^{-1}l}$ are the constants which were determined based on the experimental data for the cement of $w = 0.3$. Hence, it is convenient to use a parameter $\lambda = \frac{\alpha}{w(1+\beta C_{\mathrm{cl}})^2}$ to express the proportionality between the concentration rates of free and bound ions, so that Eq. (4.4) for chlorides can be re-expressed as:

$$(1+\lambda)\frac{\partial C_{\mathrm{Cl}}}{\partial t} = -\nabla J_{\mathrm{Cl}} = \nabla(D_{\mathrm{Cl}}\nabla C_{\mathrm{Cl}}) + \frac{z_{\mathrm{Cl}} D_{\mathrm{Cl}} F}{RT}\nabla\left(C_{\mathrm{Cl}}\nabla\Phi\right) \tag{4.6}$$

If only the chloride binding is considered, the other three ionic species (i.e. potassium, sodium and hydroxide) obey the normal form of mass conservation equation.

$$\frac{\partial C_k}{\partial t} = \nabla(D_k\nabla C_k) + \frac{z_k D_k F}{RT}\nabla\left(C_k\nabla\Phi\right) \qquad k \neq \mathrm{Cl} \tag{4.7}$$

By combining the mass conservation equation (Eqs. (4.6) , (4.7)) and the Poisson's equation (Eq. (3.7)), the electro-transport process considering the chloride binding can be described.

The above describes the case most often used in considering binding effect numerically reported in the literature. In terms of the bindings of other ionic species, there is no experimental data available in the literature. Furthermore, in the existing numerical models exploring the multi-species transport, they only used the electro-neutrality condition to couple the binding of other ionic-species, which is demonstrated as a defective condition in the preceding chapter. Note that in the present study, since the more reasonable Poisson's equation is utilised, the governing equations of Eqs. (4.6), (4.7), (3.7) should be sufficient for modelling multi-species transport with binding effect. But for further studies, we again use the charge balance in binding term of other three ionic species, i.e. K, Na and OH, even though Poisson's equation has been coupled between all of these and chloride.

In order to maintain the charge balance between both free and bound ions, the adsorption of the chlorides is assumed to be equilibrated by the adsorption/desorption of the other three ionic species in the pore solution. In view of this, the binding form of mass conservation of four species considering in the present study can be expressed as follows,

$$(1+\frac{\lambda}{3})\frac{\partial C_{\mathrm{K}}}{\partial t} = -\nabla J_{\mathrm{K}} \tag{4.8}$$

$$(1+\frac{\lambda}{3})\frac{\partial C_{\mathrm{Na}}}{\partial t} = -\nabla J_{\mathrm{Na}} \tag{4.9}$$

$$(1+\lambda)\frac{\partial C_{\mathrm{Cl}}}{\partial t} = -\nabla J_{\mathrm{Cl}} \tag{4.10}$$

$$(1-\frac{\lambda}{3})\frac{\partial C_{\mathrm{OH}}}{\partial t} = -\nabla J_{\mathrm{OH}} \tag{4.11}$$

It should be mentioned that, from the Eqs. (4.8)-(4.11), K, Na and Cl get the term of $(1+\lambda/3)$ or $(1+\lambda)$, whereas OH gets the term of $(1-\lambda/3)$. The former three may amount to 'adsorption' while the latter one implies 'desorption'. The Fluxes are also described by Nernst-Planck equation as follows,

$$-\nabla J_{\mathrm{k}} = D_k \nabla^2 C_k + \nabla\left[z_k D_k \left(\frac{F}{RT} \nabla \Phi \right) \right] \tag{4.12}$$

If one combines the mass conservation equation (Eqs. (4.8)-(4.12)) and the Poisson's equation (Eq. (3.7)), the simulation of the electro-transport process considering the adsorption/desorption of all four ionic species can be performed.

The geometry, meshing method, boundary conditions and initial conditions are completely consistent with those used in Section 4.3.

4.5.2 *Simulation results*

By solving the equations of mass conservation of individual ionic species with both binding term and electrostatic coupling of ions in the concrete specimen, two categories of binding results can be obtained. One considers only the chloride binding, whereas the other considers the bindings of all ionic species. Since the binding effect has no impact on electrostatic potential, only the distribution profiles of concentrations during an eight hour electro-process are demonstrated and shown in Figs 4.33-4.36.

The first concern to be examined from the figures is the migration velocity. It can be seen that the electro-coupling features found in the previous models also exist in the results obtained from two sets of binding effect. For each series of curves with the same legend, the migration velocities of positively (or negatively) charged ions are almost the same but are significantly different from those of their opposite charged ions. However,

the wave speeds are significantly different between various examples. The migration velocity obtained from the models without binding effect is much faster than that from other two models throughout Figs. 4.33-4.36, which implies that the binding effect of ions will greatly decelerate the speed of migration.

The two migration velocities considering binding effect, more specifically, for the profiles of negatively charged ions (shown in Figs. 4.35 and 4.36) are generally close. Note that the curve only considering chloride binding has relatively slower migration rate, which means the adsorption of positively charged ions will slightly speed up the migration of chloride and hydroxide. For the profiles of positively charged ions (shown in Figs. 4.33 and 4.34), the gap between two migration velocities becomes much larger whereas this time the curve considering the binding of entire four species obtains far slower migration rate due to the adsorption of more species. This again shows the retardation effect caused by ionic binding during the electro-migration process.

The second concern to be examined from the figures is the concentration value near the migration front. It is apparent from Figs 4.33-4.36 that, except for the hydroxides, the other three ionic species which performance ‘adsorption’ in the governing equations, the concentrations obtained from the models with binding effect become much lower than that from the binding free model. The reason is likely because, a part of ions are adsorbed by solid cement matrix and therefore they do not participate during the migration.

To sum up, the adsorption of ions will decelerate the migration speed of this species and reduce its concentration during the electro-migration process. This phenomenon is in

agreement with the conclusion in Chapter Three that - the higher the concentrations of the electrolyte pore solution, the more the ions can be transported.

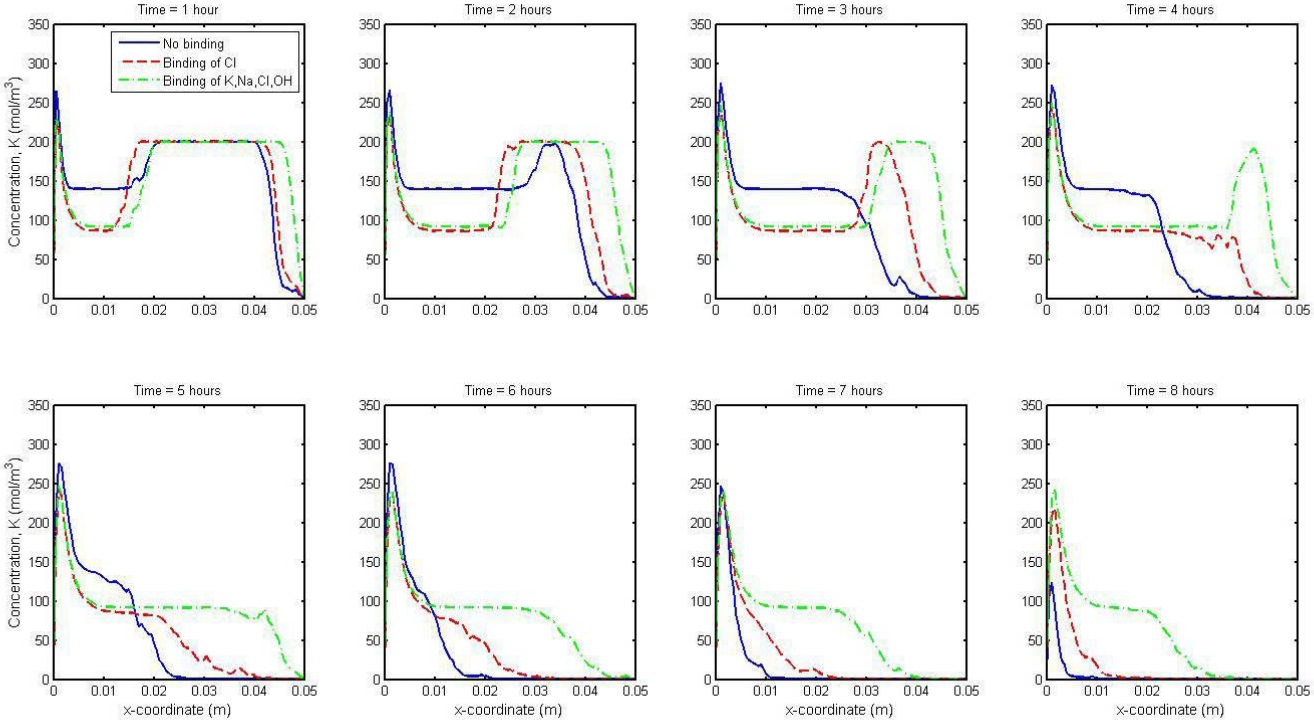

Figure 4.33. Comparison of potassium concentration distribution profiles obtained with and without binding effect.

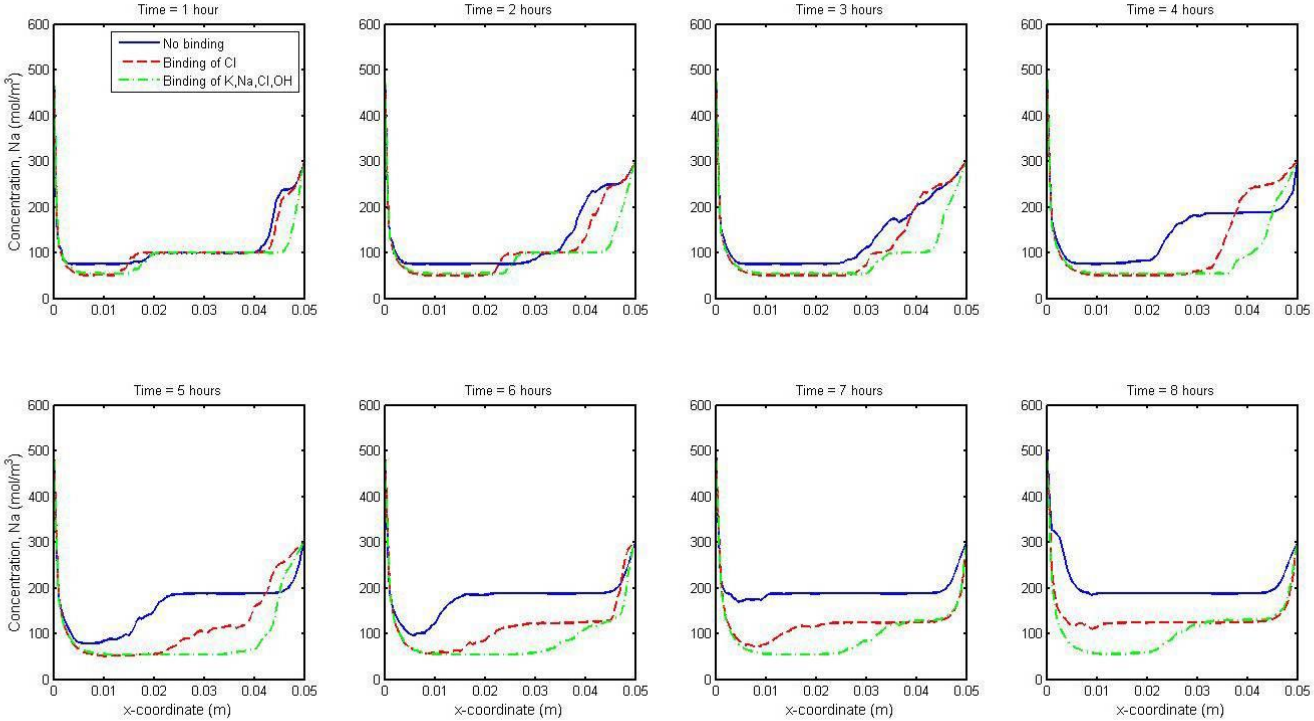

Figure 4.34. Comparison of sodium concentration distribution profiles obtained with and without binding effect.

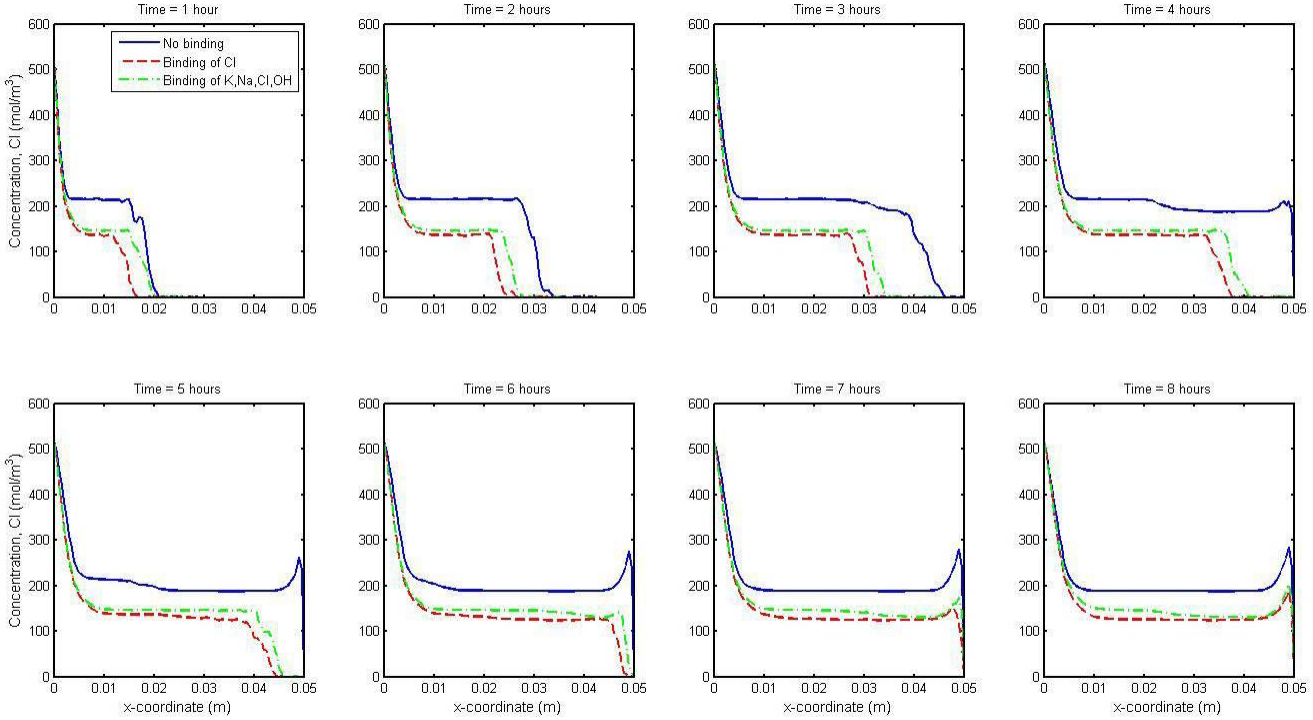

Figure 4.35. Comparison of chloride concentration distribution profiles obtained with and without binding effect.

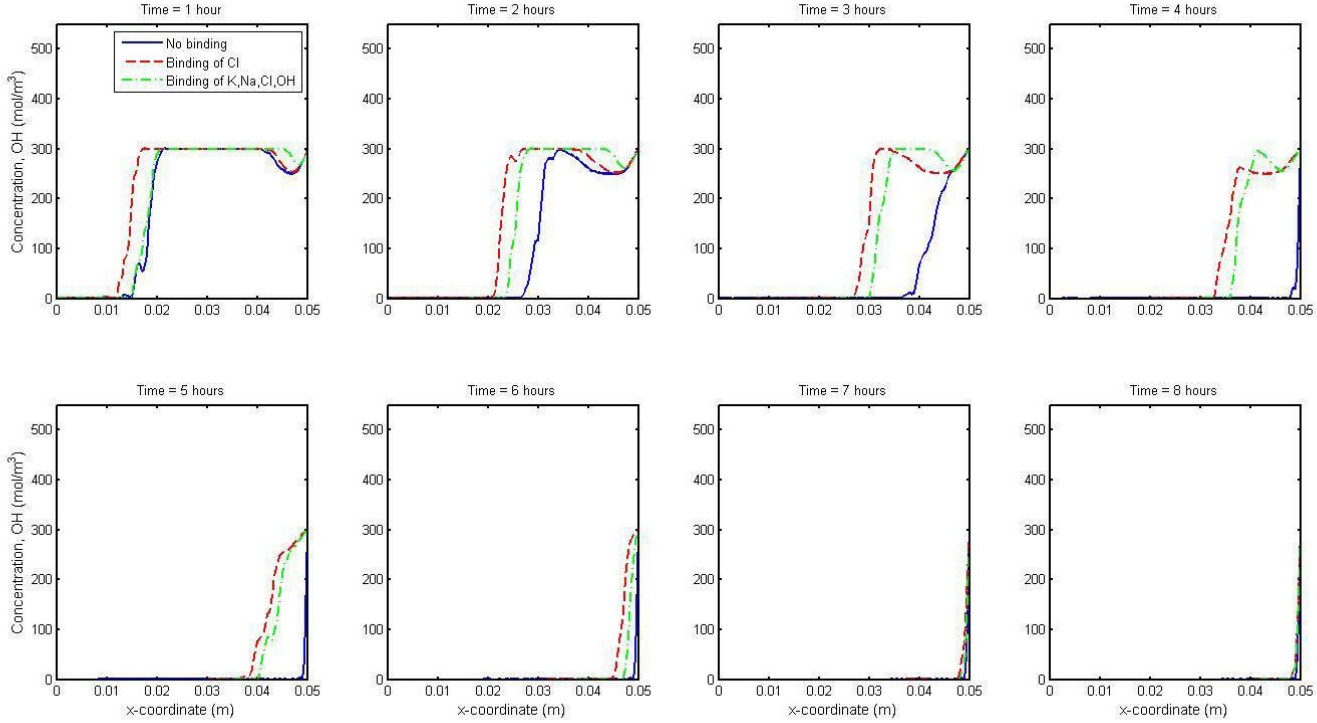

Figure 4.36. Comparison of hydroxide concentration distribution profiles obtained with and without binding effect.

4.6 Summary

This chapter has presented a set of numerical investigations on the transport of ionic species based on 2-D models with two phases. The two-phase numerical model has been used to simulate an eight-hour ionic migration test as well as to examine the interaction transport features, the influences of aggregate phase and the impacts of binding effect. From the present study the following conclusions can be drawn.

1) The variation of the ionic distribution profiles and the electrostatic potential profiles along the y-axis are insignificant. The concentration distribution profiles obtained from the present two-phase multi-component transport model are qualitatively similar to those obtained from the single-phase multi-component transport model, although quantitative difference in results may exist between these two kinds of models, particularly in the travel speed.

2) The hydroxyl ions are found to have the steepest migration wave front, whereas the sodium ions have the gentlest migration wave front. The steepness of each species decreases with time. This feature of steep degree reflects the combined influence of diffusion and local tortuosity, which cannot be found in the single phase model.

3) During the electro-process, the total amount of ions within the specimen will vary with time. For the migration test case employed in the present studies the amount of ions in the specimen is found to decrease with time.

4) Under the condition of identical volume fraction and similar tortuosity, the influence of particle shapes on the migration of concrete is fairly insignificant. Rela-

tively, the influence of volume fraction is much more significant than that of aggregate morphology, due to the more notable influence on tortuosity.

5) The inclusion of aggregates in the model can provide a more accurate influence of tortuosity on both the diffusion and migration of ions.

6) The adsorption of ion will significantly decelerate the migration speed of this species and meanwhile reduce its concentration during the electro-migration process. Because of the ionic interactions caused by Poisson's equation, the binding effect of one species also has impact on the penetrations of other ionic species.

5 CHAPTER FIVE– 2-D THREE PHASE MIGRATION MODEL AND CRACKED CONCRETE MODEL

This chapter includes two parts. In the first part, a series of 2-D concrete models with three-phased composite considering the ITZ phase are developed in order to simulate the chloride migration test and explore the impacts of ITZs on migration rate. Some important factors such as the thicknesses of ITZ, diffusion coefficients in ITZ phase and the volume fractions of aggregates are discussed in detail. In the second part, a group of 2-D cracked concrete models are proposed to examine the effect of cracks on the transport of chlorides. The study involves the investigation of the influence of geometric properties of cracks (i.e. width, depth, volume fraction, pattern and angle of arrangement etc.) on the transport of chlorides.

5.1 2-D three-phased modelling of migration tests

5.1.1 *Introduction*

It is generally believed in concrete technology that a phase of interfacial transition zone (ITZ) exists around sand and coarse aggregates in concrete. Generally speaking, ITZ is a $30-50\,\mu m$ thickness (depending upon the water to cement ratio) interface between the aggregate and bulk mortar phases and compounded by anhydrous and hydrated cement with certain porosity and volume fractions gradients (Aitcin and Mehta, 1990). The ITZ is a region extending $30-50\,\mu m$ from the aggregate, which is deficient in content of cement particles due to the wall effect. Therefore, it has a substantially higher porosity than the bulk mortar (Escadeillas and Maso, 1991), which results in a significant influence on the transport of ions within concrete.

The 2-D numerical models demonstrated in Chapter Four treated the concrete as a composite material with two phases. One is the aggregate which is assumed to be impermeable. The other is the bulk composite of cement or mortar and ITZ. The diffusion coefficients of ionic species adopted are neither for the mortar matrix nor for ITZ but for the composite. This treatment does not give the specific effects associated with ITZ. Obviously, there would be greater accuracy if ITZ was considered separately. However, in the past, due to the limitation of computers and corresponding computations, it was difficult for researches to consider a separate ITZ phase in the numerical simulation of chloride migration tests.

In this section, the concrete is simulated using a series of 2-D models with three phases: the aggregate, the cement and the ITZ. The ITZs here are assumed as uniform aureole shells wrapping the coarse aggregate particles. These models are used to simulate the

migration test described in the previous two chapters. It was proven by Chapter Four that, ionic binding plays a significant role in the transport process and the binding equations considering the charge balance of ionic species in solid phase lead more rational results. Hence, in the present three-phase models this kind of binding isotherms is continuously employed.

As indicated in the previous chapters, by solving both mass conservation and Poisson's equations, the distribution profiles of ionic concentrations at any required time are obtained. Through the three-phased numerical model, we have found some important features about ITZ, which would not been seen in the one- or two-phase models.

5.1.2 *Modelling*

Figures 5.1-5.3 show the 2-D, three-phase concrete models with three different aggregate volume fractions (i.e. $(1\text{-}\phi_c)$ = 0.5, 0.35 and 0.2). The specimen modelled is in the size of 50×50 mm. It can be seen clearly from the zoomed-in Fig. 5.4 that, between the aggregate and bulk mortar phases, there is an aureole shell wrapping each coarse aggregate particle. These regions extending from the aggregates consist of the third phase in concrete – the ITZ phase. For simplification, the porosity gradients distributed within ITZ are ignored and the structure of ITZ phase itself is assumed to be uniform. Therefore, each ionic species in the concrete mixture has two distinct diffusion coefficients, one is the diffusion coefficient in bulk mortar paste and the other is that in ITZ. This is significantly different from the 2-D two-phase model which assuming a unique diffusion coefficient for the composite of bulk mortar matrix and ITZ.

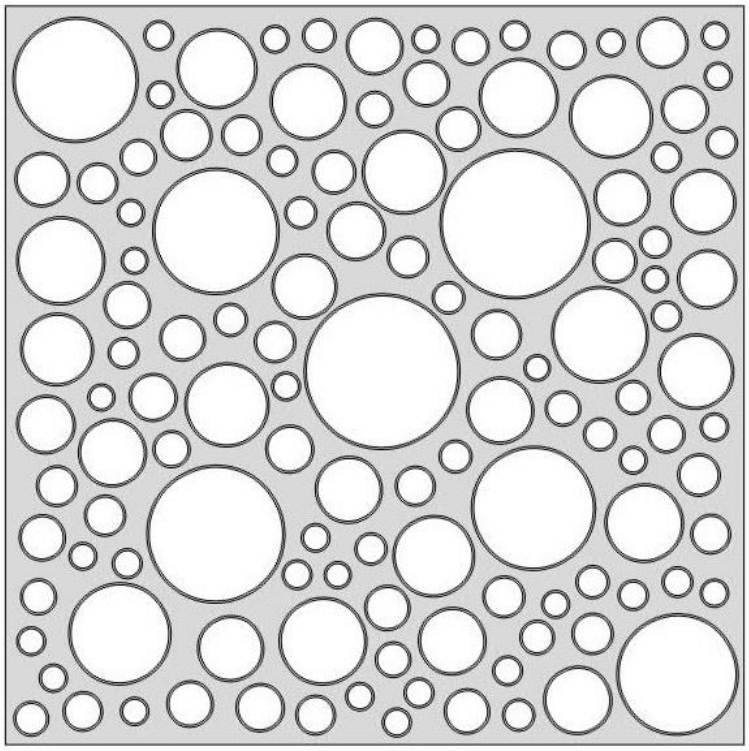

Figure 5.1. Three-phased concrete model: geometry ((1-ϕ_c) = 0.5, 150 μm thick ITZ).

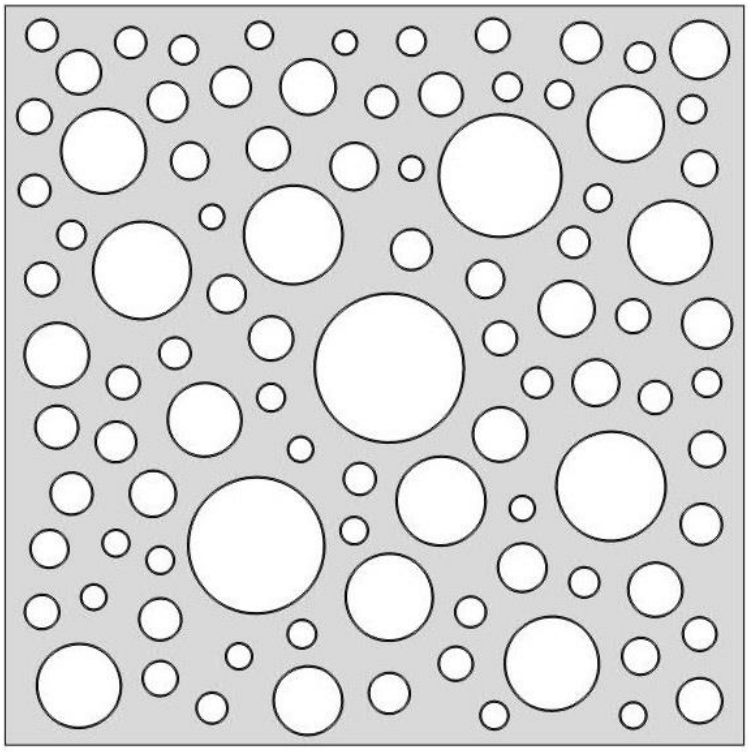

Figure 5.2. Three-phased concrete model: geometry ((1-ϕ_c) = 0.35, 100 μm thick ITZ).

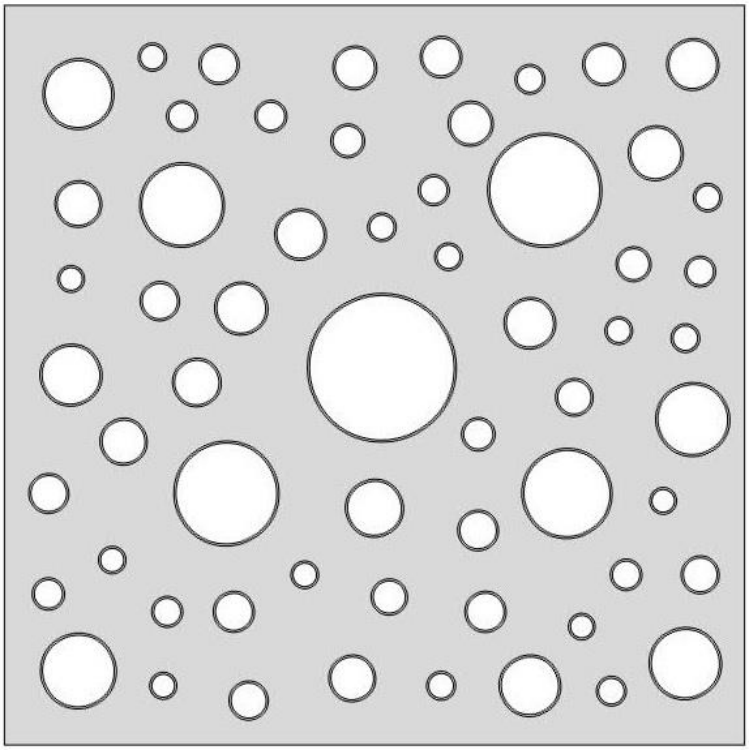

Figure 5.3. Three-phased concrete model: geometry ((1-ϕ_c) = 0.2, 150 μm thick ITZ).

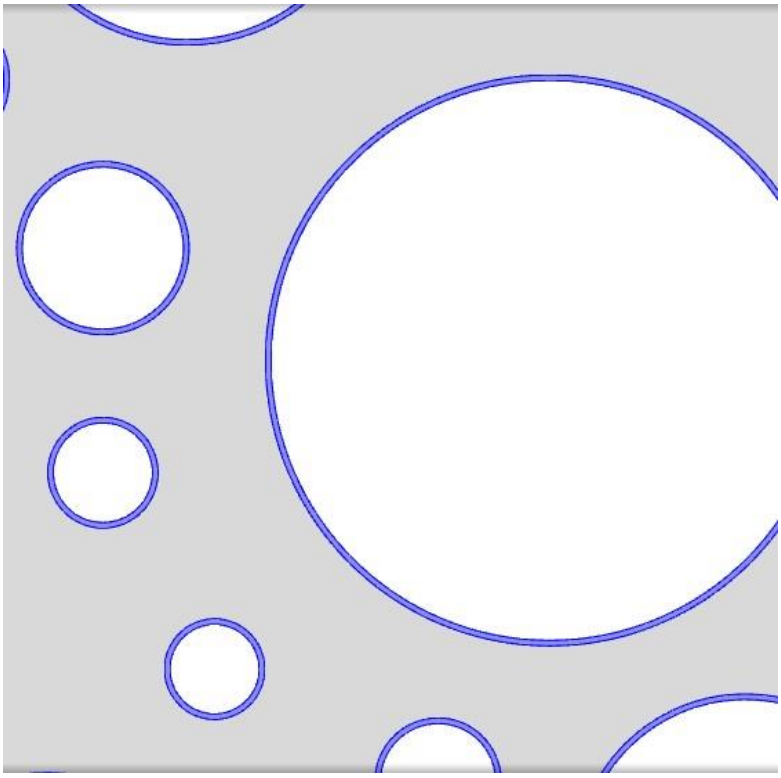

Figure 5.4. Zoomed-in schematic for ITZ phase (the region of deep blue).

It should be mentioned that, the real thickness of ITZ is believed to be about $30-50\,\mu m$. This size however is too small for mesoscale modelling. To overcome this

problem, artificial, thicker thickness ITZs are used herein. In the present numerical models, we use three thicknesses of ITZ, which are $100, 150$ and $200\,\mu m$, respectively. Fig. 5.5 shows the mesh of one of the models used. Alike to Chapter 4, aggregates are assumed to be impermeable. Therefore, ionic transport takes place only in the mortar and ITZ phases although the diffusion coefficients are different in these two phases. The continuous conditions are assumed for both concentration and flux at the interface between mortar and ITZ phases.

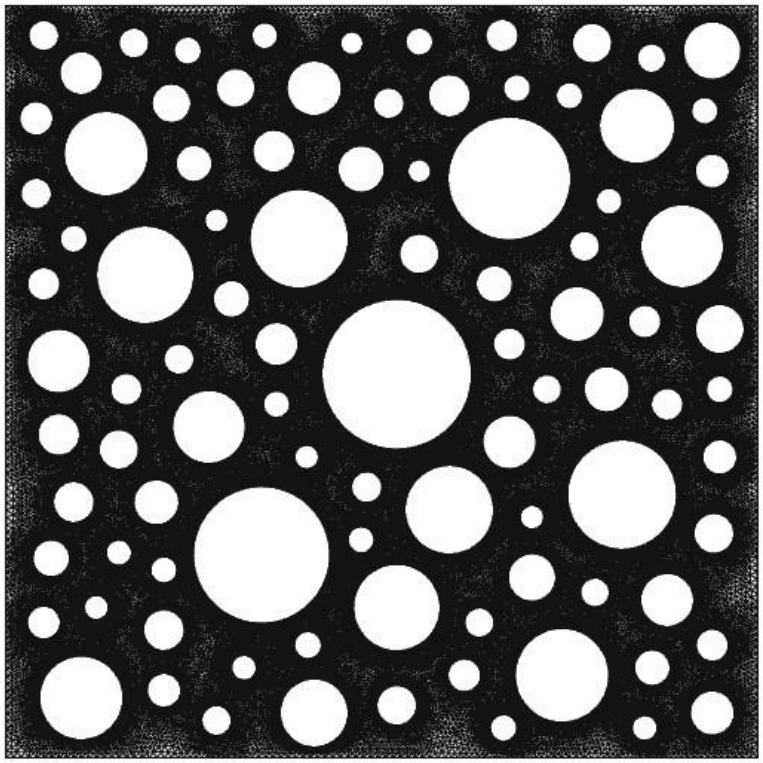

Figure 5.5 Finite element meshed model ($(1-\phi_c) = 0.35$, 100 μm thick ITZ).

The boundary and initial conditions of the five variables (i.e. concentrations of K, Na Cl, and OH and electrostatic potential) are similar to those used in the preceding models. It is believed that the ITZ phase has higher porosity and therefore a larger diffusion coefficient than bulk mortar (Escadeillas and Maso, 1991). Previous studies show that the ratio of diffusion coefficient of ITZ (D_{ITZ}) to that of bulk mortar (D_B) is approximately 4-18 times (Care and Herve, 2004; Zheng and Zhou, 2007; Jiang et al., 2012),

depending on the porosity and w/c ratio of individual specimens. In the present model, three cases of D_{ITZ}/D_B, which are $D_{ITZ}/D_B=5$, $D_{ITZ}/D_B=10$ and $D_{ITZ}/D_B=15$ (Table 5.1) are used.

Table 5.1. Boundary conditions, initial conditions and diffusion coefficients.

Field variables		Potassium (mole/m^3)	Sodium (mole/m^3)	Chloride (mole/m^3)	Hydroxide (mole/m^3)	Electrostatic potential (V)
Boundary conditions	x = 0	0	520	520	0	0
	x = L	0	300	0	300	24
	y = 0	J = 0	J = 0	J = 0	J = 0	$\partial\Phi/\partial y$=0
	y = L	J = 0	J = 0	J = 0	J = 0	$\partial\Phi/\partial y$=0
Initial conditions		200	100	0	300	0
Charge number		1	1	-1	-1	N/A
Diffusion coefficient of bulk mortar (D_B), ×10-10 m2/s		1.957	1.334	2.032	5.260	N/A
Diffusion coefficient of ITZ (D_0), ×10^{-9} m^2/s	Case 1	0.979	0.667	1.016	2.630	
	Case 2	1.957	1.334	2.032	5.260	N/A
	Case 3	2.936	2.001	3.048	7.890	

5.1.3 *Simulation results*

Similar to the previous chapters, by solving both Poisson's equation and the mass conservation equations attached adsorption/desorption term (Eqs (4.6) and (4.8)-(4.10)), the distribution profiles of three-phased concrete models subject to given initial and boundary conditions (Table 5.1) are obtained. Figs. 5.6-5.10 display the distribution profiles of the four ionic species concentrations and the electrostatic potential at four different times (from the first hour until the fourth hour) calculated from one example ($(1-\phi)=0.5$, $D_{ITZ}/D_B=10$, 150 μm thick ITZ). When compared to the 3-D plots obtained from the two-phased concrete model (i.e. Figs. 4.4-4.8), it is found that a series of basic features of the two categories of results are similar. The migration speed between like charged ions, the approximate 1-D flow of ions, the tortuosity effect caused

by aggregates and the steep behaviour of migration wave fronts are found to be qualitatively similar. The only differences seem to be the concentration values at migration wave fronts and their travel speed. The difference of the peak values of wave fronts is due to the ionic binding considered in the present model. In terms of the migration travel speed, it can be seen that, the ionic species within the model including the ITZ phase still has a much faster penetration rate even though the ionic binding is enclosed.

Additional results, calculated from three examples with the same thickness ($150\,\mu m$) and diffusion coefficient ($D_{ITZ} / D_B = 10$) of ITZ but different aggregate volume fractions (i.e. ($1\text{-}\phi_c$) = 0.5., ($1\text{-}\phi_c$) = 0.35. and ($1\text{-}\phi_c$) = 0.2.), are presented for further discussion. For the convenience of comparison, endeavours are made to equally distribute the aggregates in the examples as shown in Figs. 5.1-5.3. The "equal distribution" of aggregates affects not only the location, but also the size gradients.

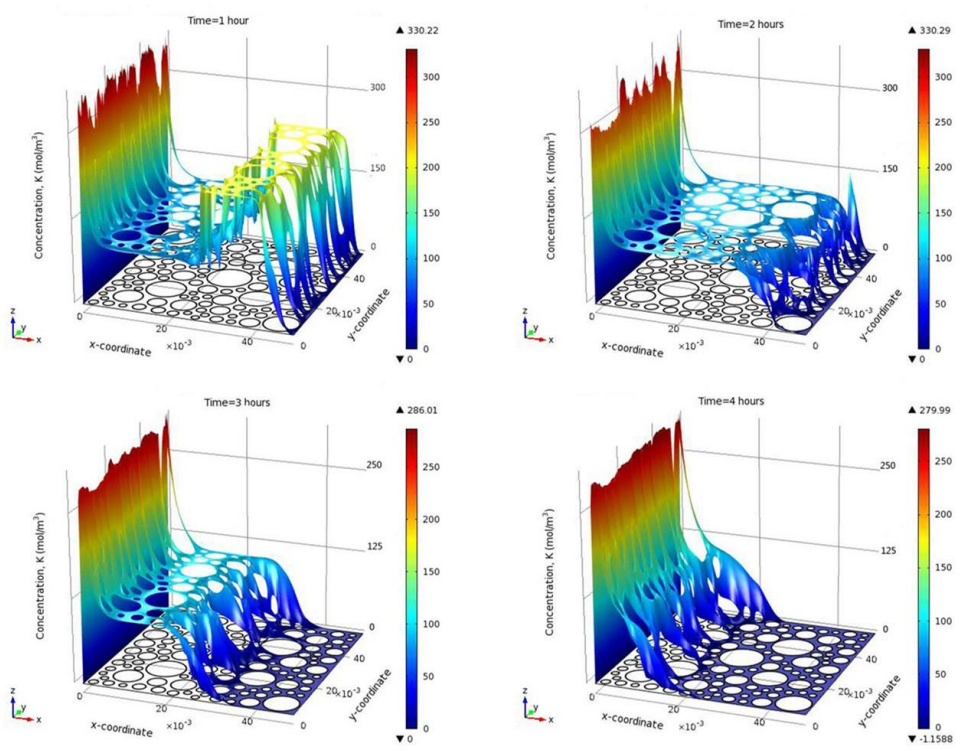

Figure 5.6. Concentration distribution profiles of potassium ions.

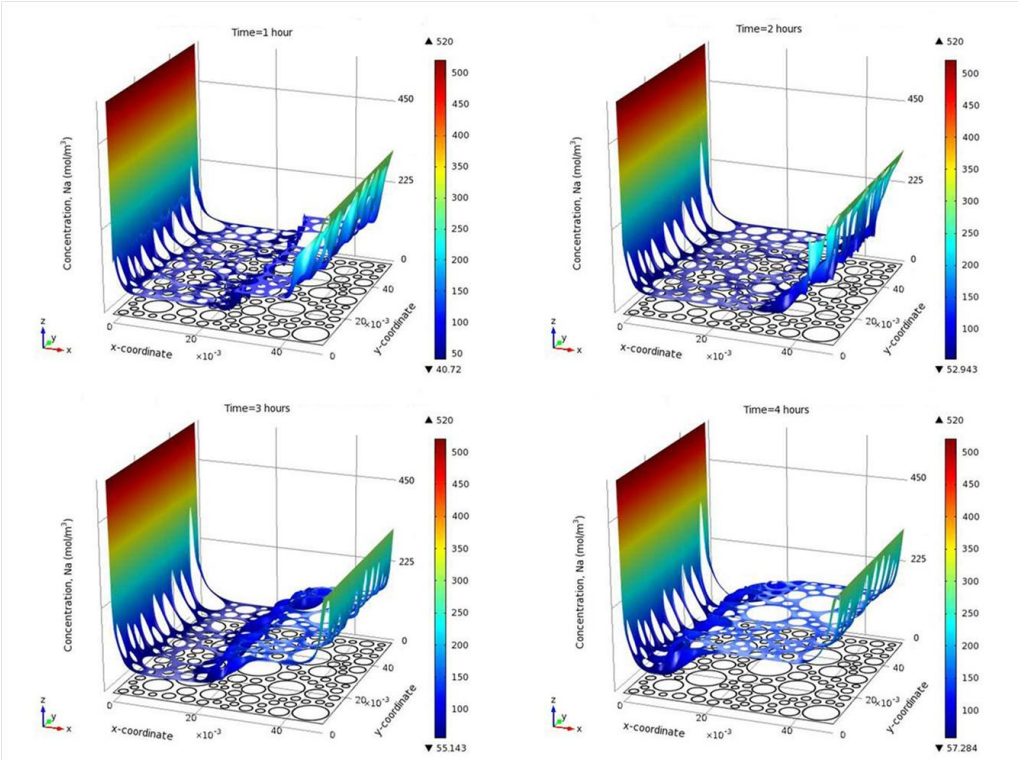

Figure 5.7. Concentration distribution profiles of sodium ions.

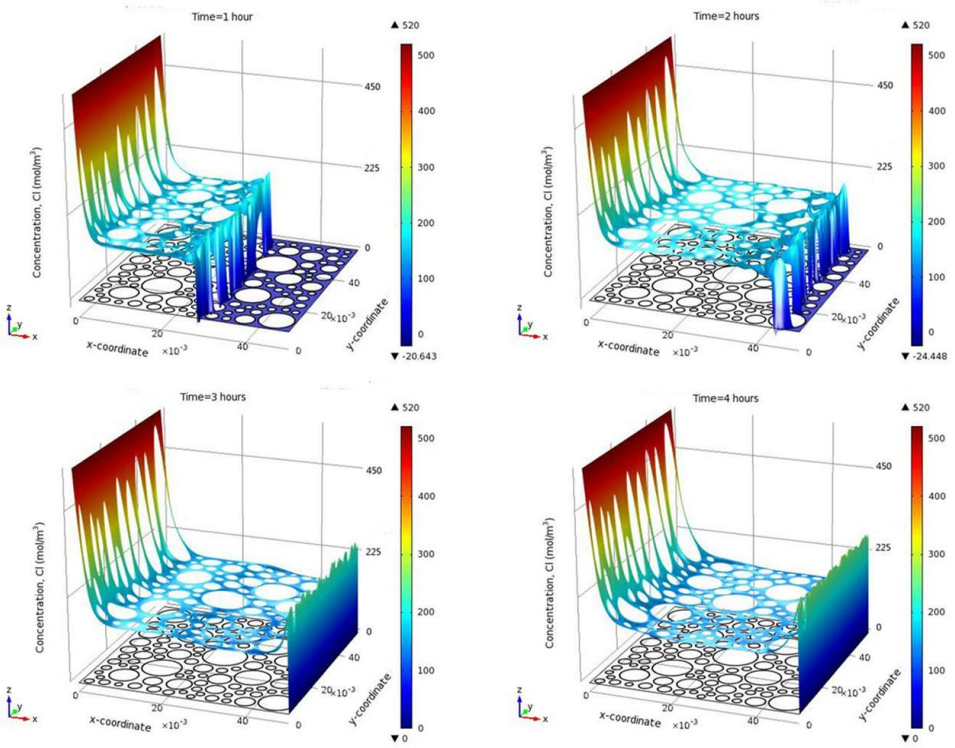

Figure 5.8. Concentration distribution profiles of chloride ions.

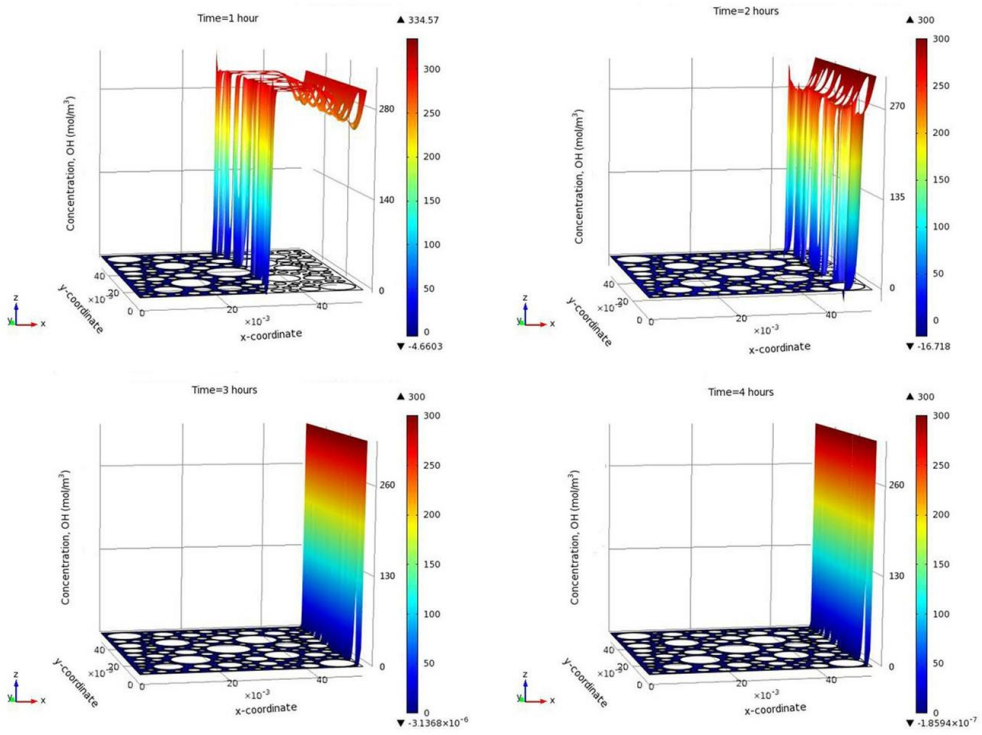

Figure 5.9. Concentration distribution profiles of hydroxide ions.

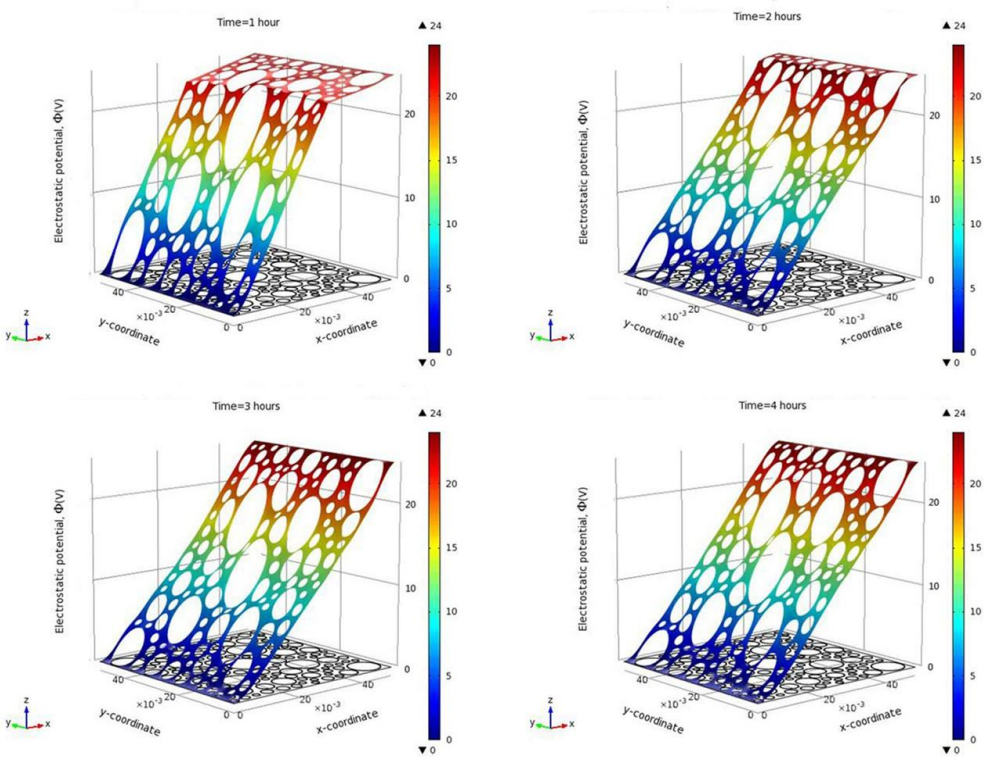

Figure 5.10. Electrostatic potential distribution profiles.

As the variation of ionic concentrations along the y-axis is less significant, the 3-D figures are re-plotted in 2-D form by using their average values. By comparing the curves

of chloride concentrations obtained from three-phased models with three different aggregate volume fractions (Fig. 5.11), it is observed, unexpectedly, that the existence of ITZ phase reverses the pattern of the influence of the aggregates volume fraction during the two-phased model. The largest aggregate volume fraction, $(1-\phi_c) = 0.5.$, has the quickest travel speed; whereas the smallest aggregate volume fraction, $(1-\phi_c) = 0.2.$, has the slowest travel speed. Fig. 5.12 plots the chloride concentration distributions obtained from the corresponding models, which hold exactly the same aggregate distribution but no ITZs. Comparing Figs. 5.11 and 5.12, it is evident that the two groups of results are completely opposed. This is because in the two-phased models, the impact on travel speed of chlorides is dominated by tortuosity under the same electrical voltage. However, in the three-phased models, the chlorides penetrates much more quickly in ITZ phases and the volume fraction of ITZ is non-ignorable (i.e. the volume fraction of ITZ comes to 0.056 in the model with the aggregate volume fraction of 0.35 shown as Fig. 5.2). Thus the dominant effect of the volume fraction of ITZ takes over that of the tortuosity in the three-phased models and the volume fraction of ITZ becomes the key factor in controlling the chloride migration rate. The increase in quantity of aggregates will also increase the ITZ volume, which finally increases the chloride diffusivity of the concrete. Similar features are found for the other three ionic species and thus they are not presented here.

It should be pointed out that the ITZ thickness adopted in this study is considerably large ($100-200\,\mu m$), whereas in reality, it would be much smaller. Therefore, caution should be taken when applying the results obtained here to any real cases.

A more simple and direct way to explore the influence on migration velocity of chloride ions caused by ITZ phase is to perform a sensitivity analysis on ITZ thickness. For this a

series of three-phased models with various thicknesses of ITZs from $100-200\,\mu m$ were generated, while the diffusion coefficient of ITZ and the distribution of aggregates remain unchanged ($D_{ITZ}/D_B = 10$, (1-ϕ_c) = 0.35). The results of chloride distribution are shown in Fig. 5.13. By examining the migration wave fronts from the chloride distribution curves with three different ITZ thicknesses, it is indicated that the migration velocity can approximately scale as the volume of ITZ increases. This view also agrees with Fig. 5.11.

As it was mentioned above, ITZ phase has larger diffusion coefficient than bulk mortar and the ratio of D_{ITZ}/D_B depends on different types of concrete specimen. This opinion is only experimental observations. It is at this stage insufficient to measure the exact diffusion coefficient in ITZ during the tests, which however can be quantified from our three-phased model. Fig. 5.14 shows how the evolution of chloride transport varies with D_{ITZ}/D_B ratio. Note that each curve is obtained from the same geometry, including aggregates ((1-ϕ_c) = 0.35) and ITZs ($150\,\mu m$ thick). It is observed that the migration process is markedly affected by the diffusion coefficient of ITZ. The larger D_{ITZ}/D_B ratio, the faster chloride moves. By comparing Fig. 5.13-14, one can also find that, at this level of ITZ volume fraction, the definitions of ITZ thickness and D_{ITZ}/D_B ratio are equally significant during the simulation of chloride migration process.

By considering the real potential gradient distributions, separate aggregate and ITZ phases, and taking into account the ionic binding, a more rational numerical model can be achieved to simulate both steady and non-steady state migration tests.

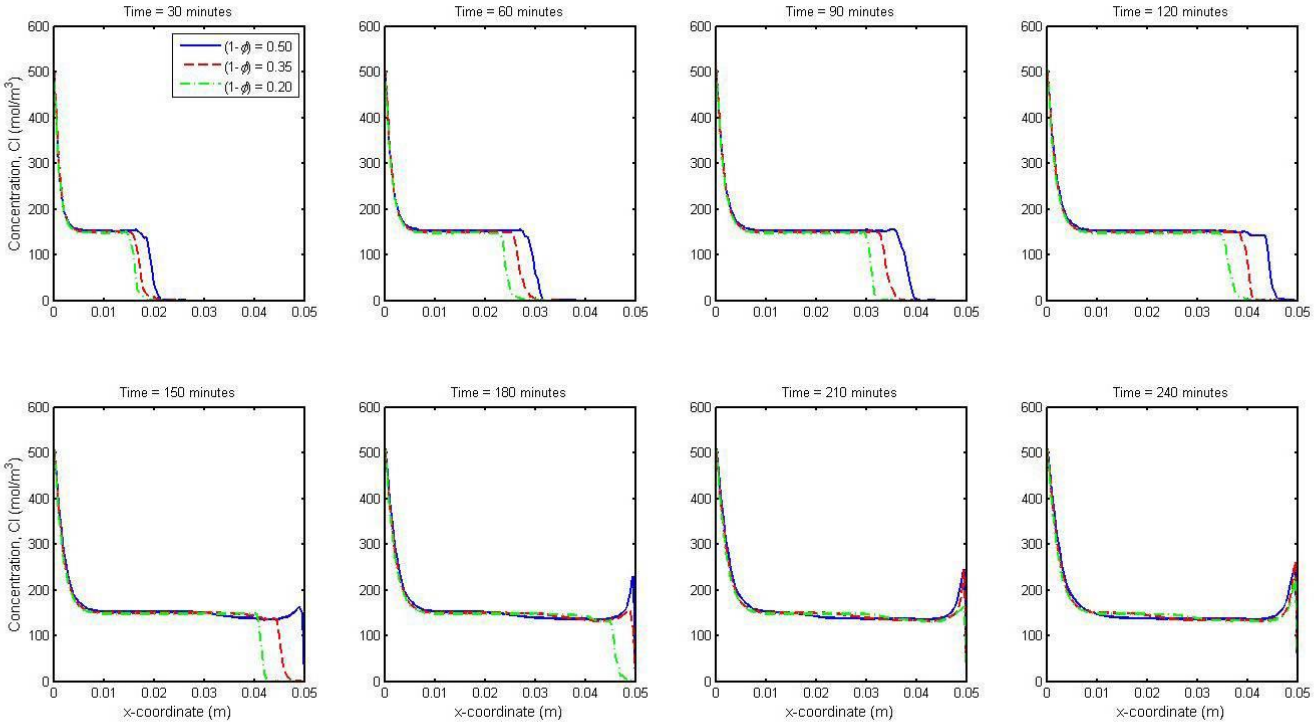

Figure 5.11. Comparison of chloride concentration distribution profiles between different volume fractions.

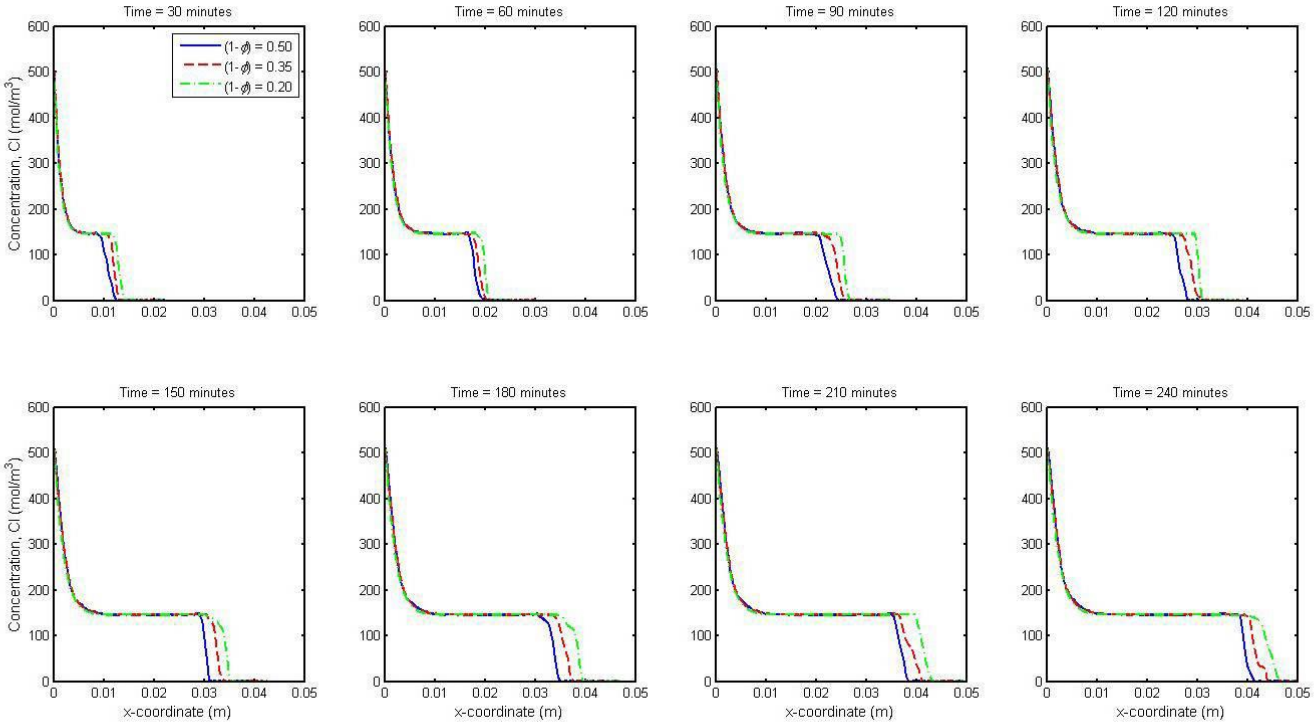

Figure 5.12. Comparison of chloride concentration distribution profiles between different volume fractions (without ITZ phase).

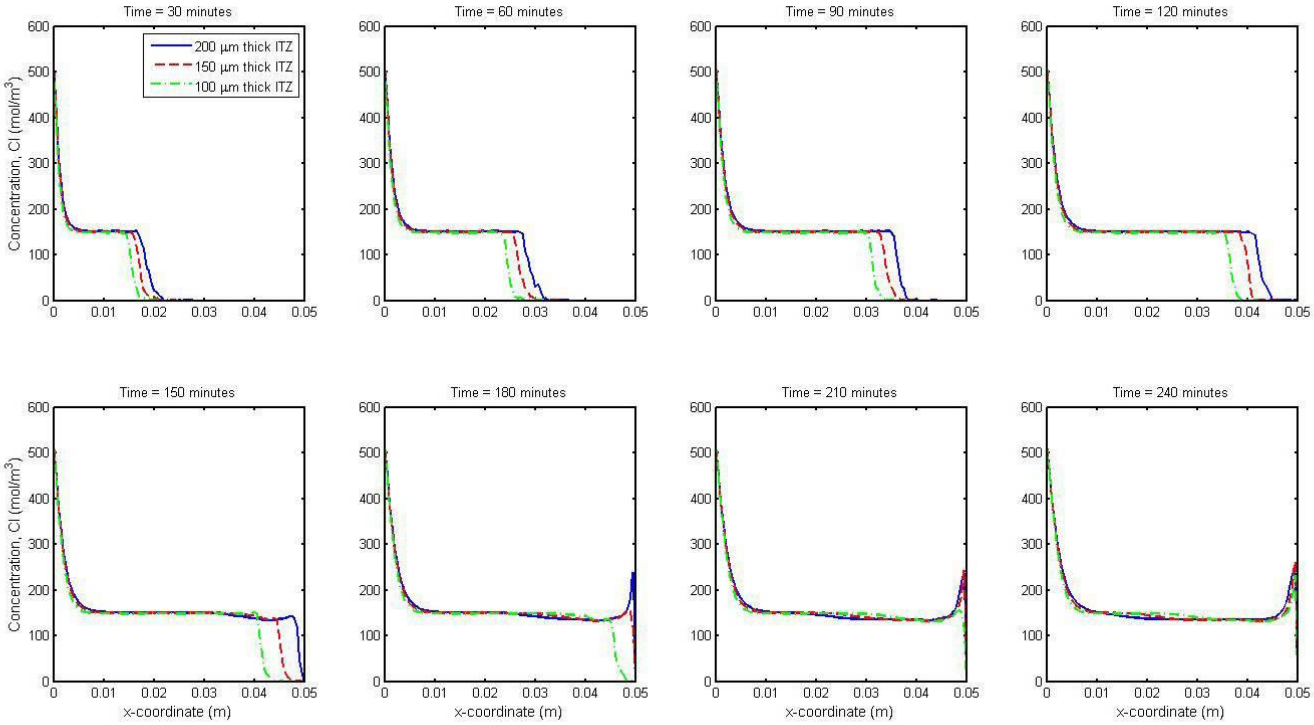

Figure 5.13. Comparison of chloride concentration distribution profiles between different thicknesses of ITZ.

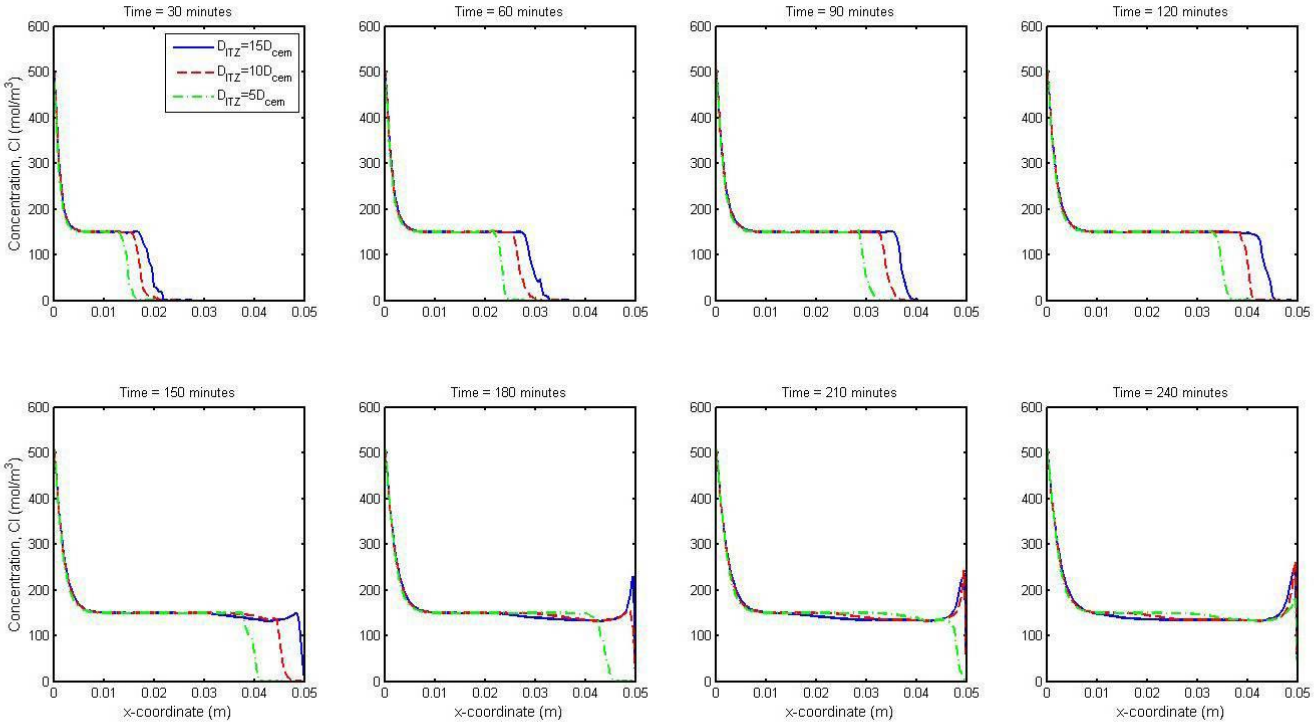

Figure 5.14. Comparison of chloride concentration distribution profiles between different diffusion coefficients of ITZ

5.2 2-D modelling of chloride migration in cracked concrete

5.2.1 *Introduction*

Geometrically speaking, besides the three phases (aggregates, bulk mortar and ITZ) in concrete structures discussed above, the deterioration caused by chloride-induced corrosion is also greatly influenced by the presence of cracks. In recent decades, the effect of concrete cracking has been taken into account by a number of studies (Djerbi et al., 2008; Gérard and Marchand, 2000; Ismail et al., 2008; Jacobsen et al., 1996; Jang et al., 2011; Şahmaran, 2007; Win et al., 2004). A few of numerical models were developed to include cracks to simulate chloride penetration in cracked concrete. For example, Marsavina et al. (2009) developed a 3-D model to investigate the influence of cracks on chloride transport by means of non-steady state migration tests (NT Build 492, 1999). More recently, Bentz et al. (2013) explored a variety of 2-D models for estimating the local concentration as a function of crack width and depth. However, both of the above studies utilised Fick's second law to estimate the concentration of chloride ions, and their numerical models did not take the multi-species coupling and migration process into account.

Cracks can be generated due to various reasons (e.g. plastic and restrained shrinkage, thermal and mechanical loading, expansive degradation reactions, improper design) and have a complicated pore structure at the microscopic scale in real concrete (Park et al., 2012). The micro pore prosperities such as constrictivity, tortuosity and connectivity make the cracks display a complex 3-D geometry. However, in general, one can still simplify the problem from a 3-D to a 2-D case with suitable definitions on crack width and depth. Due to the geometric difficulty in modelling micro-cracks, Bentz et al.

(2013) proposed an imaginary zone consisting of ‘damaged mortar’, which surrounds each crack. This kind of zone is about 1-4 mm width, in which the diffusion coefficient value is smaller than that in cracks but larger than that in bulk mortar. The width of a ‘damaged zone’ depends on the widths of the central crack itself.

In this section, a series of 2-D models to monitor the effect of concrete cracking on the chloride migration was developed. The concrete specimen used in this study is treated as a two-phase composite: one phase is the bulk mortar and the other phase represents the ‘damaged zone’. Each ionic species has distinct diffusion coefficients in these two phases. For simplicity of calculations, no aggregate is involved and ionic binding is ignored in the models. By solving both mass conservation and Poisson’s equations, the distribution profiles of ionic concentrations in cracked concrete can be obtained.

5.2.2 *Modelling*

In order to model the cracked concrete, two hypotheses are made here. Firstly, due to the small width of central crack, the multi-phase structure of damage zone in the present model is ignored. That is the damage zone including the central crack is simplified as a single phase and assumed to be uniform. The ionic diffusion coefficient in the damaged zone, D_{D}, is twenty times higher than that in the bulk mortar (D_{B}). The larger value of D_{D} is probably because, in microscope scale, the cracks increase the connectivity between capillary pores and ITZs within the damaged zone. Secondly, all damage zones in 2-D geometry are assumed to be rectangular in shape and can be characterized by their individual width and depth, which is similar to the treatment of the study of Bentz et al. (2013).

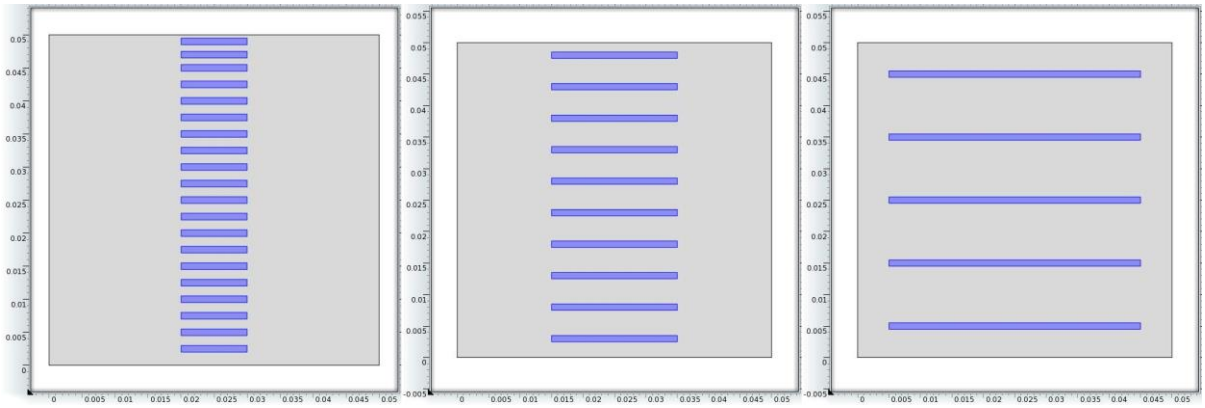

Figure 5.15. Geometry of cracked concrete model with the same width (1 mm) and volume fraction (A_D = 0.08) but different depths of damage zone ((a) 10 mm. (b) 20 mm. (c) 40 mm).

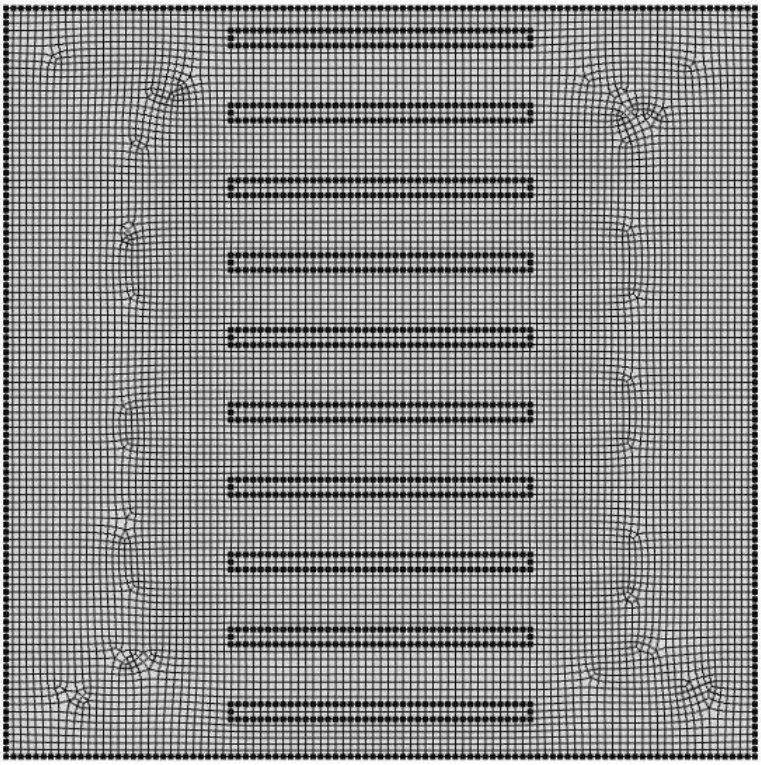

Figure 5.16. Finite element mesh (20 mm depth, 1 mm width, A_D = 0.08).

Figure 5.15 shows the three cracked concrete models used, which have the same width (1 mm) and volume fraction ($A_D = 0.08$) but different depths of damage zone. All of damaged zones are located in a single column. For the convenience of examination and observation, the rectangular shaped damage zones are deliberately arranged in the middle of the concrete as well as to be parallel with the direction of ionic penetration. One may claim that the cracks normally start on the surface and their shape is more like a tri-

angle shape (wider at surface and narrower inside of concrete). For the statement of shape, due to the assumption and treatment of damage zones mentioned above, the particular shape effect of central cracks can be ignored. In term of the location problem, to suit the realistic situation, we can geometrically treat the current cracked concrete model as a crack-repaired concrete: the damages close to the surfaces have been removed, leaving the damage zones in the middle of concrete. In fact, neither the location nor the shape effect of damage zones has qualitative influence on the migration result, which is shown in the following section. Fig. 5.16 shows the FEM mesh for one of three models generated by COMSOL (Svante Littmarck and Saeidi, 1986). The boundary conditions and initial conditions for the three cases studied are given in Table 5.2.

Table 5.2. Boundary conditions, initial conditions and diffusion coefficients

Field variables		Potassium (mole/m^3)	Sodium (mole/m^3)	Chloride (mole/m^3)	Hydroxide (mole/m^3)	Electrostatic potential (V)
Boundary conditions	$x = 0$	0	520	520	0	0
	$x = L$	0	300	0	300	24
	$y = 0$	$J = 0$	$J = 0$	$J = 0$	$J = 0$	$\partial\Phi/\partial y=0$
	$y = L$	$J = 0$	$J = 0$	$J = 0$	$J = 0$	$\partial\Phi/\partial y=0$
Initial conditions		200	100	0	300	0
Charge number		1	1	-1	-1	N/A
Diffusion coefficient of bulk mortar (D_B), $\times 10^{-10}$ m^2/s		1.957	1.334	2.032	5.260	N/A
Diffusion coefficient of damaged zone (D_D), $\times 10^{-9}$ m^2/s		3.914	2.668	4.064	10.520	N/A

5.2.3 *Simulation results*

For given initial and boundary conditions (Table 5.2), the simulated migration test in the cracked concrete specimen can be again calculated by solving the mass conservation equations and Poisson's equation. The distribution profiles of five variables (four ionic species concentrations and the electrostatic potential) at four different times during the

first two hours obtained from one of the models are displayed in Figs. 5.17-5.21. The specimen modelled is 50×50 mm, in which there are ten damaged zones with 1 mm width and 20 mm depth ($A_D = 0.08$). Compared with the previous results (Figs. 4.4-4.8), it is clear that the present profiles are significantly different from those obtained from the former models that have no cracks. As is to be expected, the migration wave fronts travel at two distinct rates. One occurs in the part with no cracks and its speed is similar with that observed from the former model; the other occurs in the damage zones with a much larger speed than that in the non-damaged bulk mortar, acting like a kind of 'pioneers' which take a shortcut through the damage zones. This phenomenon is in agreement with the observation of a greater penetration depth of chlorides spreading from the crack than that observed spreading from the uncracked portion of specimens (Win et al., 2004).

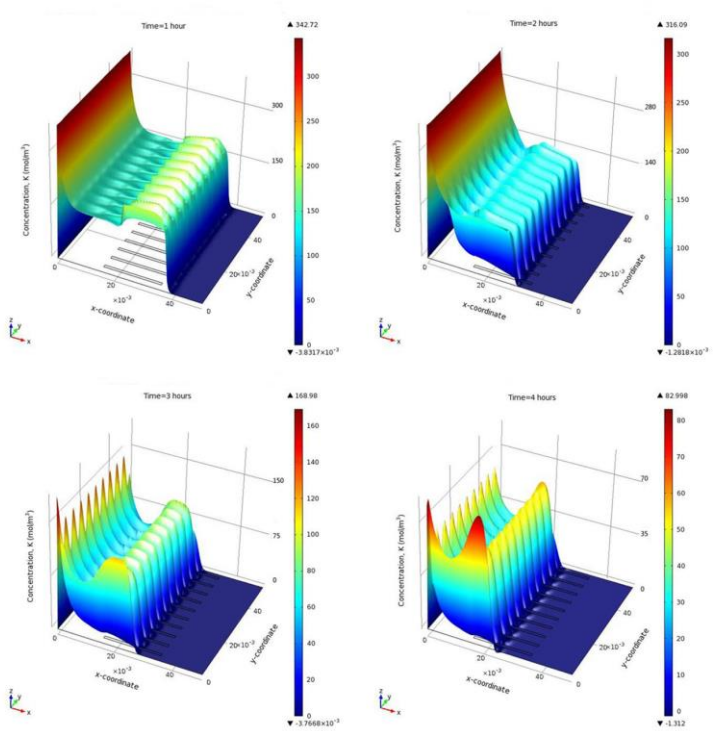

Figure 5.17. Concentration distribution profiles of potassium ions.

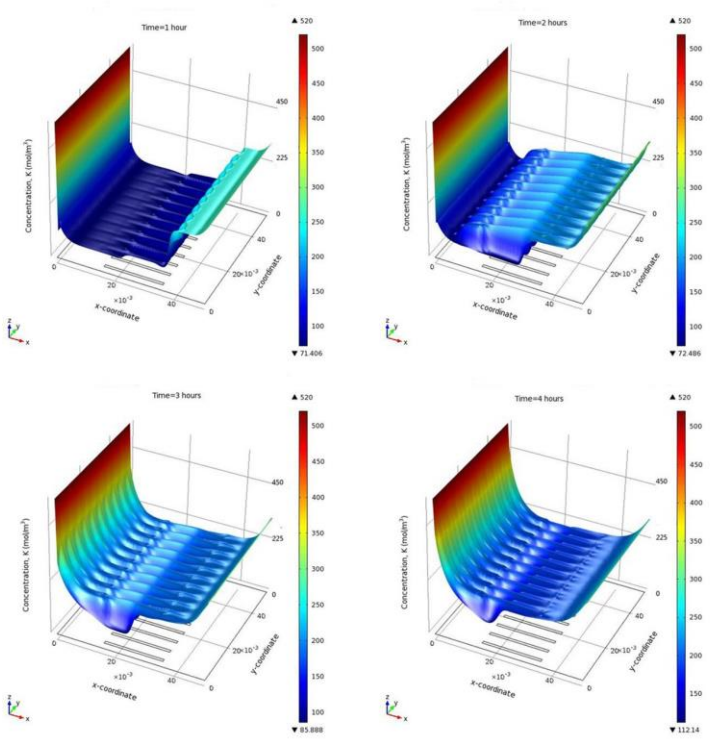

Figure 5.18. Concentration distribution profiles of sodium ions.

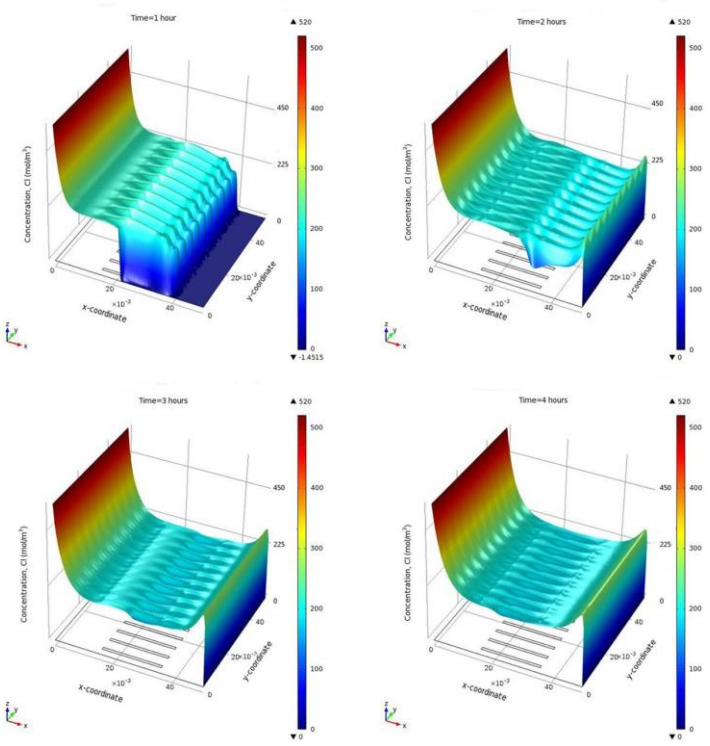

Figure 5.19. Concentration distribution profiles of chloride ions.

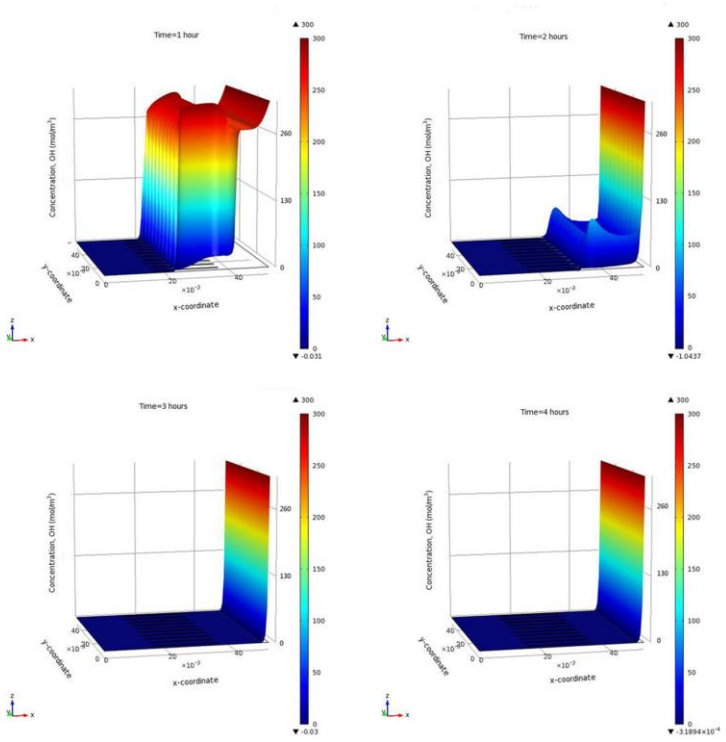

Figure 5.20. Concentration distribution profiles of hydroxide ions.

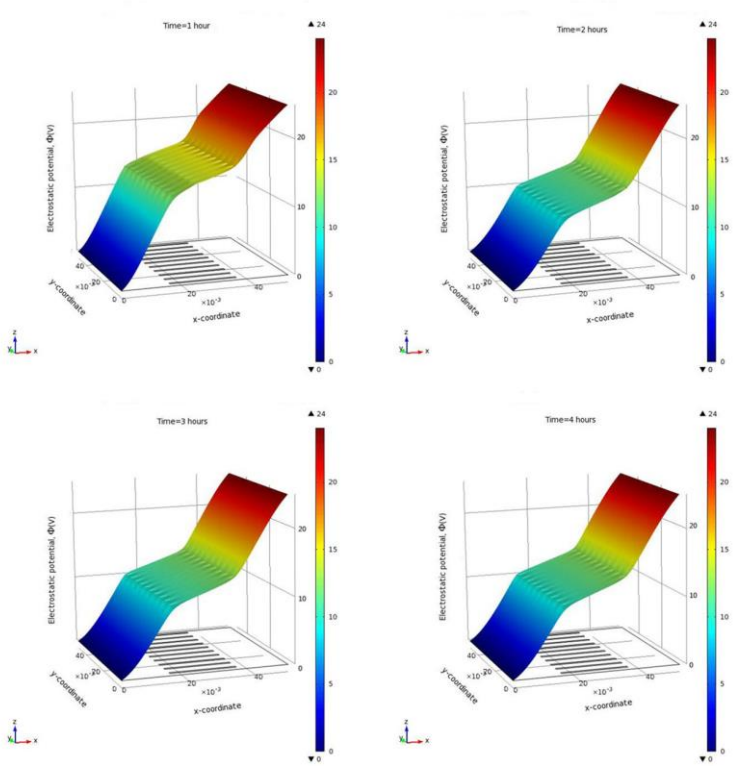

Figure 5.21. Electrostatic potential distribution profiles.

Some interesting characteristics can be found about the ‘pioneer wave fronts’ and Fig. 5.22 shows a typical one. From this zoom-in picture, there is an elliptical aggregation of

ions around each ‘pioneer wave fronts’ and the size of the short axes of an ellipse aggregation is approximately as 2-4 times long as the width of a damage zone. More figuratively speaking, the concentration distribution along the damage zone presents a ‘dumbbell shape’, which is vividly demonstrated in Fig. 5.22. The formation of this kind of ‘dumbbell shaped distribution’ is likely due to the diffusion coefficient gradient. The ion gives priority to travel in the direction which has larger diffusion coefficient: around the middle part of a damage zone, since the neighbouring region is still damaged, the ions tend to only migrate along the x-axis (along the damage zone), acting like a laser beam; whereas around the end of a damage zone, since it has the same diffusion coefficient (all bulk mortar) in each adjacent direction, the ions are thus dispersed. Therefore, the average y-axis concentration in the sections of the end of cracks (e.g. the section of x = 0.045 m of the solid line in the upper left figure of Fig. 5.23) becomes larger than those in the sections of middle part of cracks (e.g. the section of x = 0.025 m of the solid line in the upper left figure of Fig. 5.23) to some extent.

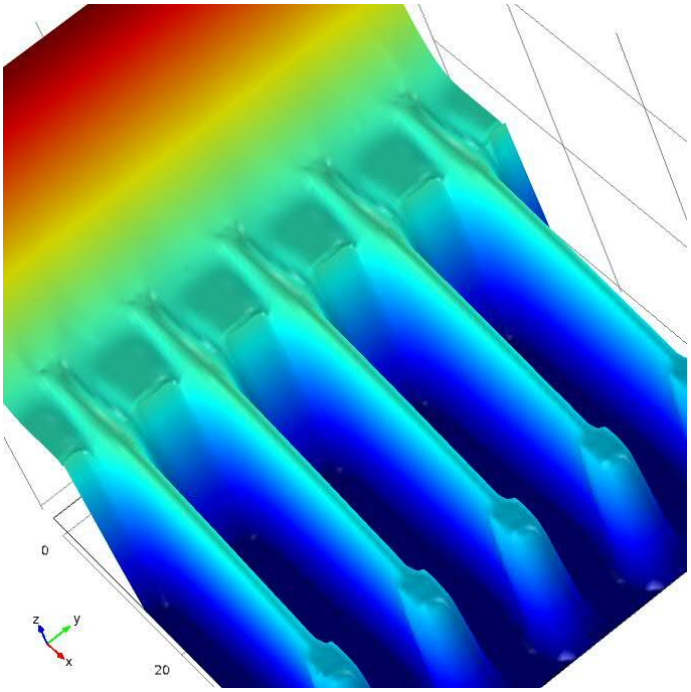

Figure 5.22. Zoomed-in schematic for ‘pioneer wave fronts’.

To understand the influence of crack width and depth on chloride migration, a series of models with variety widths and depths of damage zones are also carried out. In Figs. 5.23-5.25, the average y-axis concentration distributions during the first two hours process are clarified by three categories: the models reported in Fig. 5.23 have the same damage width (1 mm) and fraction ($A_D = 0.08$), but different damage depths (e.g. 10mm, 20mm and 40 mm); the models reported in Fig. 5.24 share the same damage depth (20 mm) and fraction ($A_D = 0.08$), but different damage widths (e.g. 2mm, 1mm and 0.5 mm); the results shown in Fig. 5.25 calculated from three models which contains the distinct numbers of cracks ($A_D = 0.04, 0.08$ and 0.16) but the same size of an individual damage zone (1 mm width and 20 mm depth). By checking the locations of migration waves and the peak values of concentration of migration process, it is safe to draw a general conclusion that, the damage depth dominates the migration rate whereas the damage width has very little impact on the chloride migration. Additionally, in terms of the models with the same depth of damage zones, the chlorides will also achieve more rapid migration rate in the model which has larger damage fraction, however even this effect is not as evident as that of damage depth.

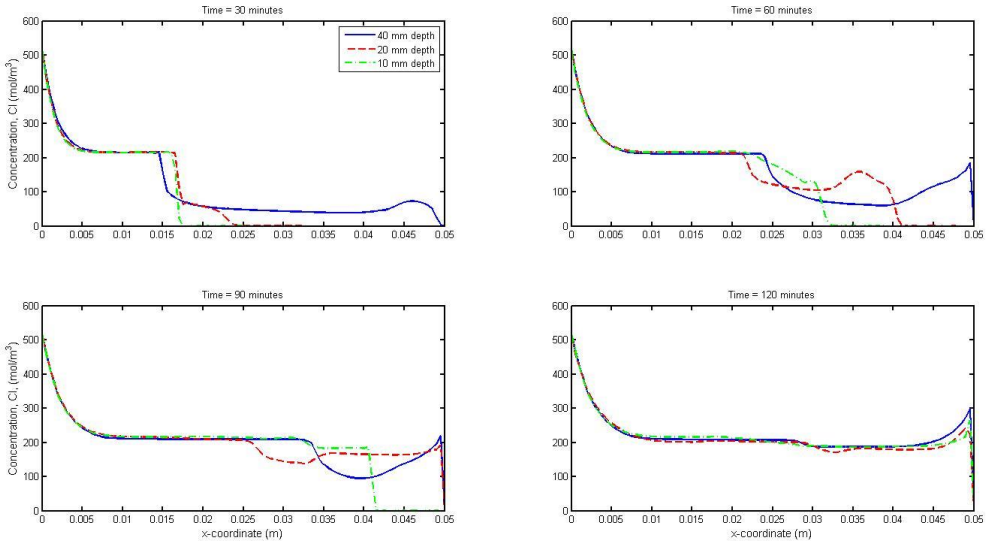

Figure 5.23. Comparisons of average y-axis concentration distributions between three models (different depths).

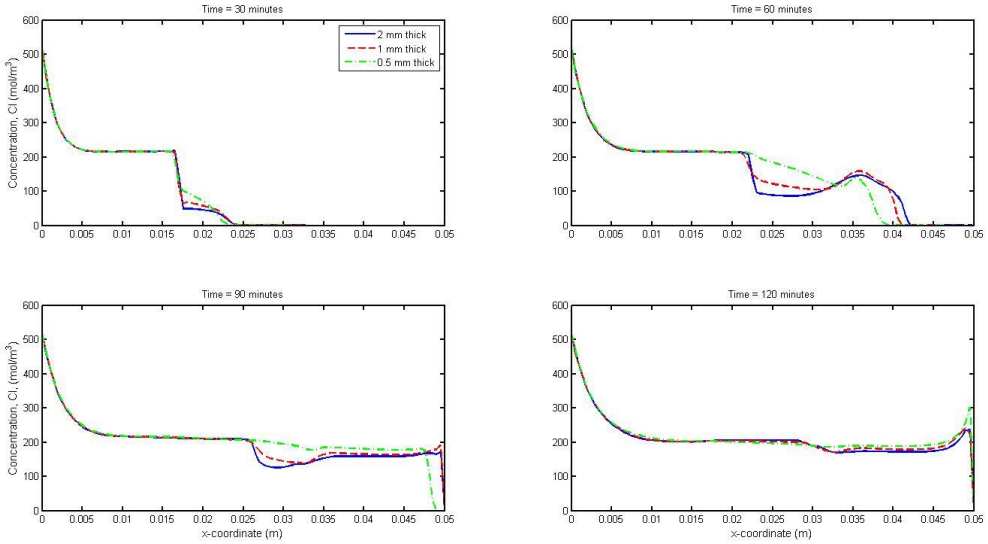

Figure 5.24. Comparisons of average y-axis concentration distributions between three models (different widths).

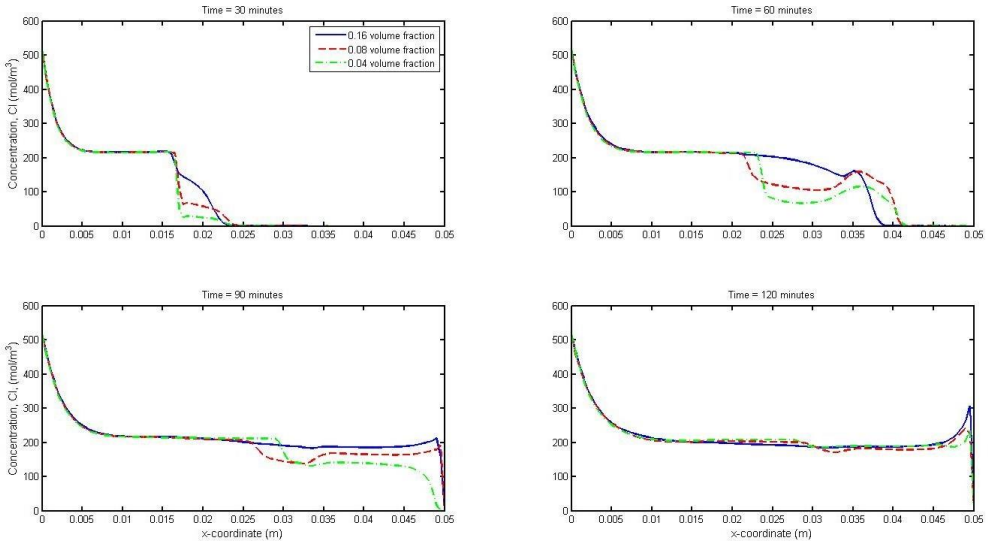

Figure 5.25. Comparisons of average y-axis concentration distributions between three models (different damage fractions).

One may claim that the average y-axis concentration profiles are hard to monitor the quantitative distribution distinction between the areas of the damage zones and the bulk concrete. To deal with this, three categories of cross sections traversing the simulated specimen were selected. As shown in Fig. 5.26, the first section is the centre line of one damage zone. The second section represents the cut line near the damage zones, intersecting the elliptical aggregation of ions at the 'pioneer wave fronts'. The last section is located evenly between two damage zones, where is the farthest section from any damage zones.

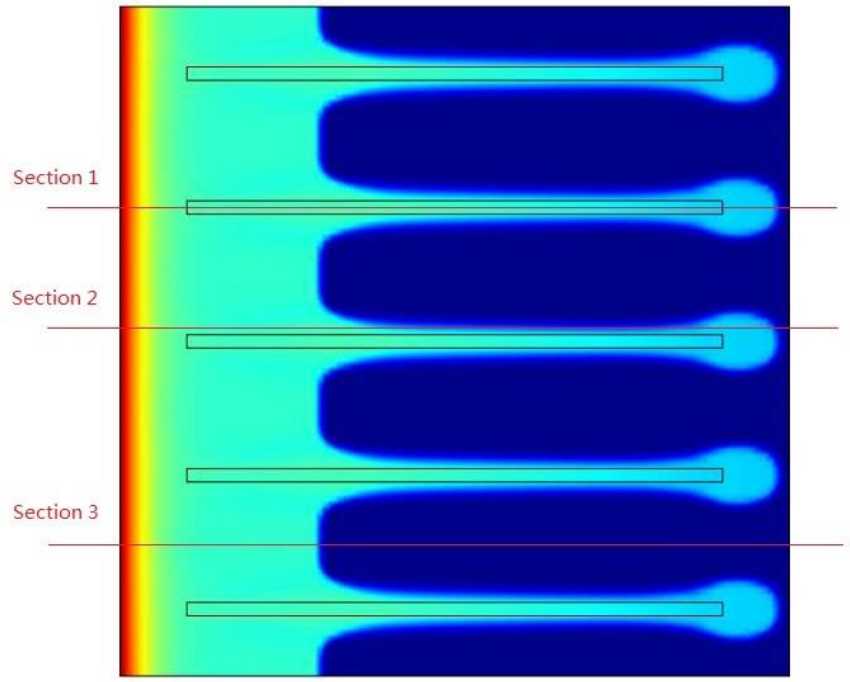

Figure 5.26. Schematic view for three cross sections traversing the simulated specimen.

Looking at the three specified sections mentioned above, one can re-plot and obtain a more visualized view of the sensitivity analysis on the properties of cracked concrete than shown in Figs. 5.23-5.25. Figs. 5.27-5.29 show the comparison of chloride concentration distributions during the first two hours process along the three different sections in the models with the different damage depths as noted previously. Fig. 5.27 clearly demonstrates how the damage depth dramatically accelerates the migration rate: the concrete specimen including 40 mm depth damage zone is much more quickly permeated by the chloride ions. It is apparent from the Fig. 5.28 that the chloride migration rate is also markedly influenced by damage depth in the region near the damage zones, due to the intersection between the cut line of section 2 and the elliptical aggregation of ions around ‘pioneer wave front’. However, when it comes to the third section (non-damaged area of concrete), the situation changes greatly: the concentration profiles seem to be ir-

regular, especially those in the model with 20 mm and 10 mm depth damage zones. With regards to this phenomenon, since in this case the three models have the same damage width and fraction, the model with 20 mm and 10 mm depth damage zones have the larger amount of cracks, which leads the space between two adjacent damage zones to be more narrow. As Fig. 5.22 shows, during the migration process, the chloride concentrations in the damage zones are higher than that in the neighbouring bulk mortar and thus the diffusion behaviour of chlorides occurs. Generally speaking, this kind of 'pollution' caused by local diffusion could produce the disordered concentration distributions profiles, which is illustrated in Fig. 5.29.

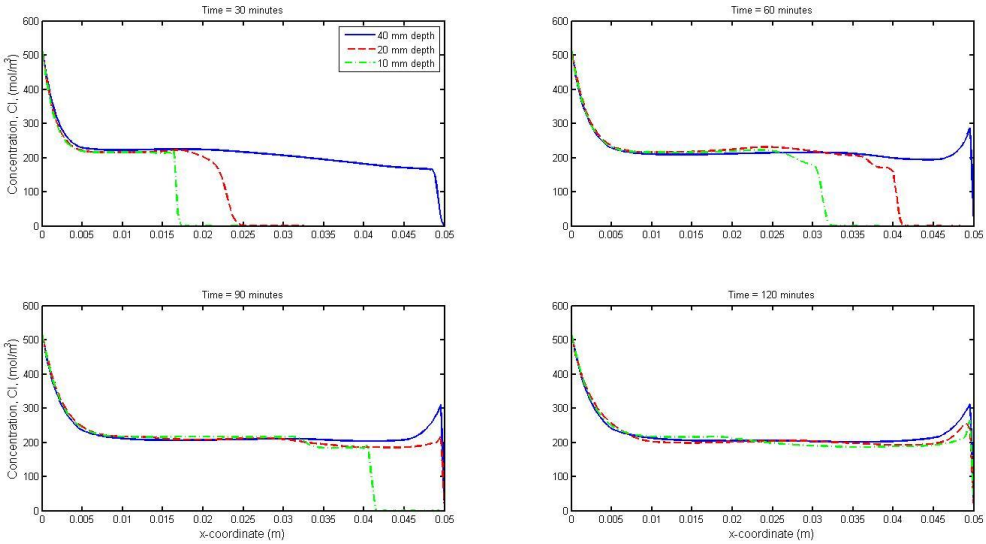

Figure 5.27. Comparisons of concentration distributions in Section 1 between three models (different depths).

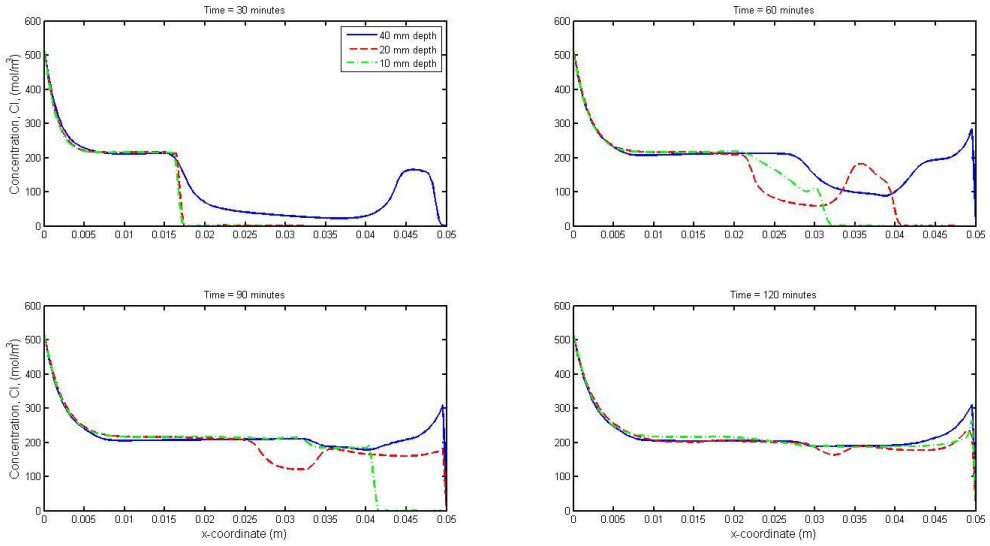

Figure 5.28. Comparisons of concentration distributions in Section 2 between three models (different depths).

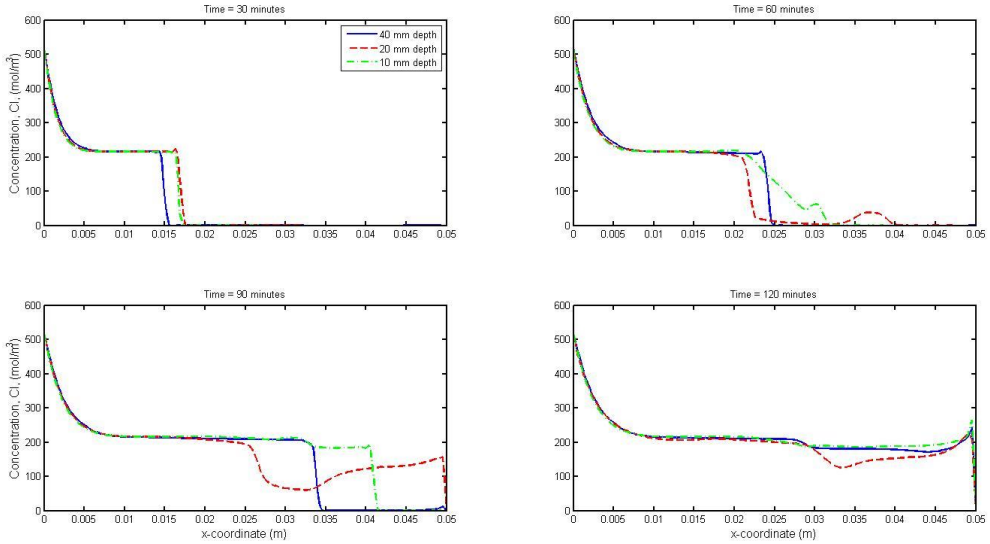

Figure 5.29. Comparisons of concentration distributions in Section 3 between three models (different depths).

Likewise, the chloride concentration distributions focusing on the effect of different damage widths are re-plotted in Figs. 5.30-5.32 based on the three sections of interest. Comparing Figs. 5.27 and 5.30, it is evident that under the same changing multiplier, the influence of damage width is much smaller than that of damage depth. When the damage width is doubled, it only leads to a tiny increase in progress to the chloride penetra-

tion. This feature is reflected in the profiles in the second section (Fig. 5.31). Approximately, one may find that both the migration wave fronts taken place in bulk mortar and the 'pioneer wave fronts' around the end of damage zones have the same travel speed. Similarly with the phenomenon displayed in Fig. 5.29, the 'pollution' behaviour due to local diffusion again disrupts the discipline of concentration distributions profiles along the non-damaged area of concrete: the number of damage zones instead of damage width dominants the chloride migration in Fig. 5.32.

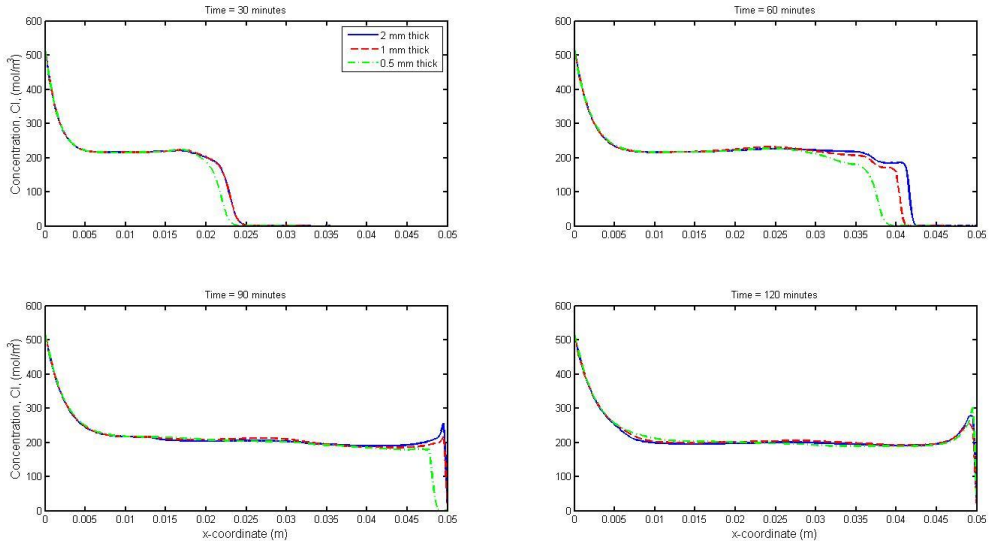

Figure 5.30. Comparisons of concentration distributions in Section 1 between three models (different widths).

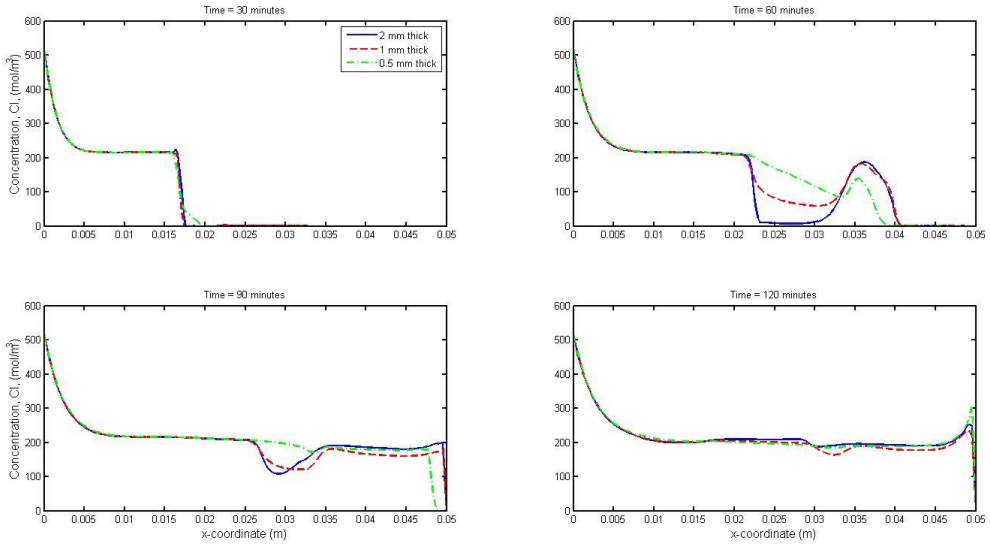

Figure 5.31. Comparisons of concentration distributions in Section 2 between three models (different widths).

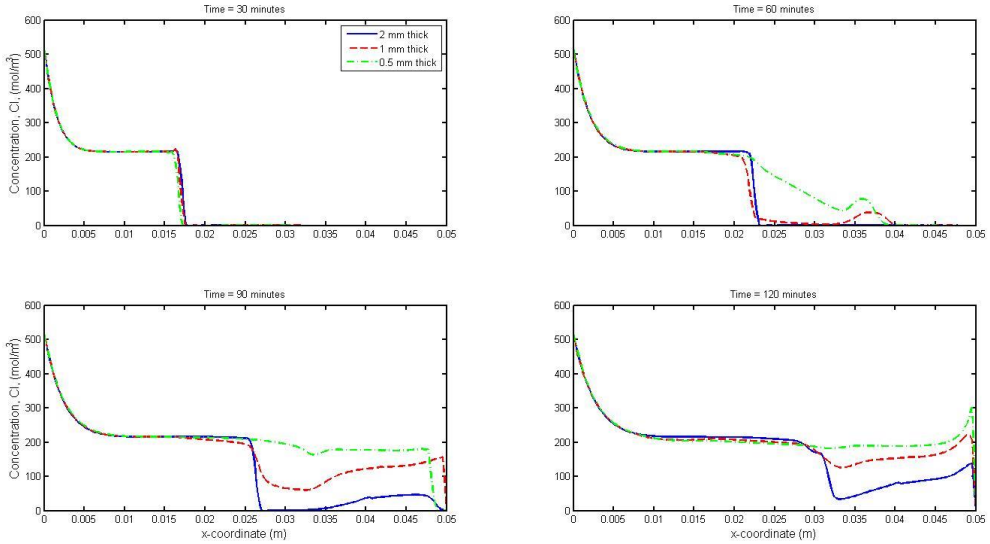

Figure 5.32. Comparisons of concentration distributions in Section 3 between three models (different widths).

Figures 5.33-5.35 show the comparison of concentration distribution profiles focusing on the effect of different damage fractions (the sizes of individual damage zones in the models are uniform). In general, the obtained results in this set of numerical tests are extremely similar to what is showed in Figs. 5.30-5.33. If the damage depth is fixed, the changing of damage fraction does little impact on the chloride migration (Figs. 5.33-

5.34). In addition, the more damage zones contain, the more chlorides travel (Fig. 5.35). Since the damage zones are all centrally located in one column in the simulated concrete specimen, the increase of crack number is only along the y-axis which is orthogonal to the direction of electric field. Therefore, the effects resulted by damage width and fraction on the chloride migration are close.

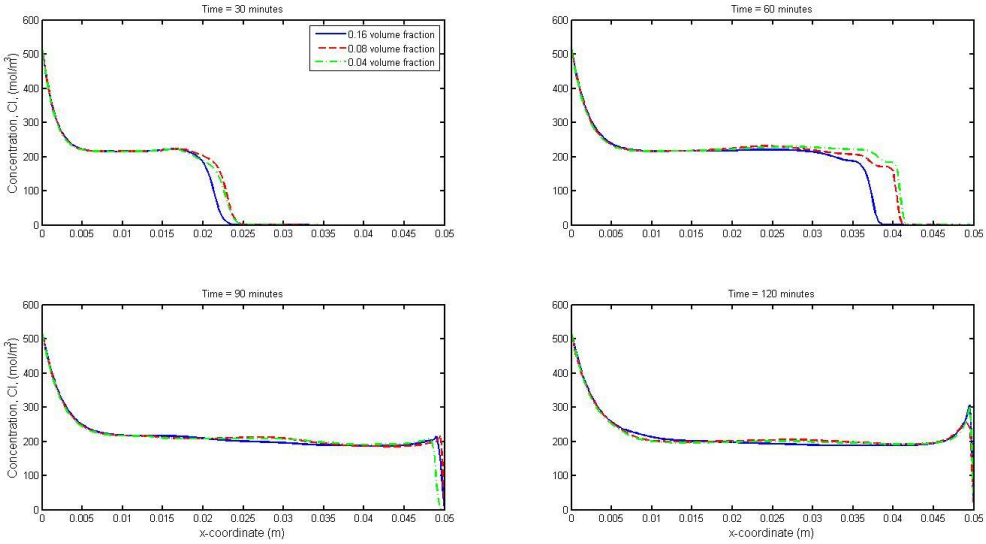

Figure 5.33. Comparisons of concentration distributions in Section 1 between three models (different damage fractions).

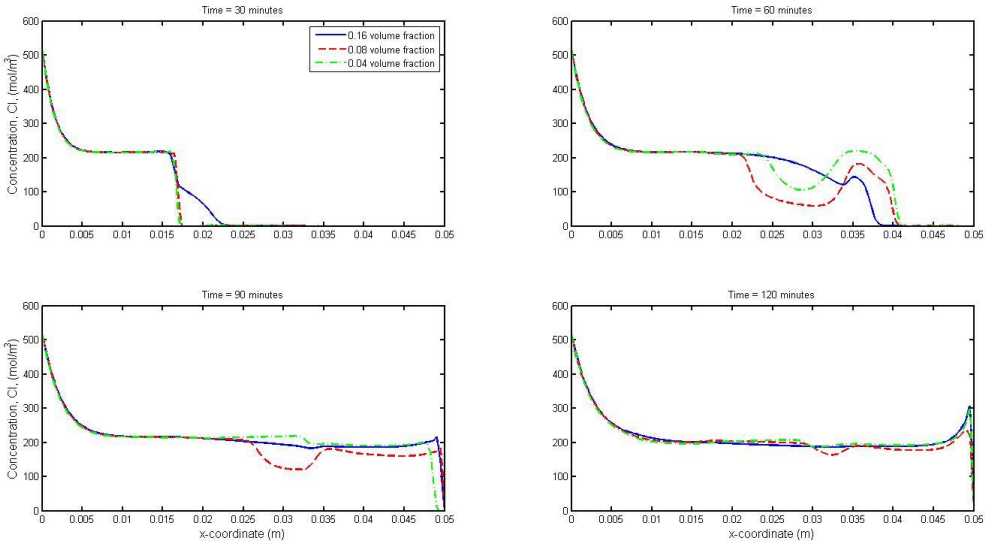

Figure 5.34. Comparisons of concentration distributions in Section 2 between three models (different damage fractions).

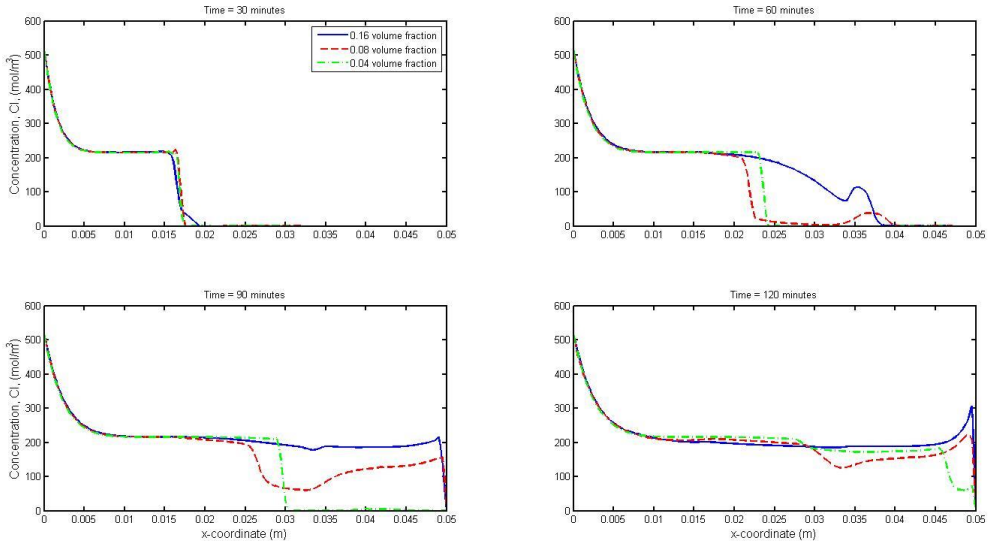

Figure 5.35. Comparisons of concentration distributions in Section 3 between three models (different damage fractions).

As only one column of damage zone is used in the above models, it may hide some significant characteristics during the migration process in cracked concrete. Hence, another category of the sensitivity analysis has been set up. As shown in Fig. 5.36, three models to be analysed are 10 mm depth and double columns of damage zones, 20 mm depth and single column of damage zones, and 10 mm depth and single column of damage zones.

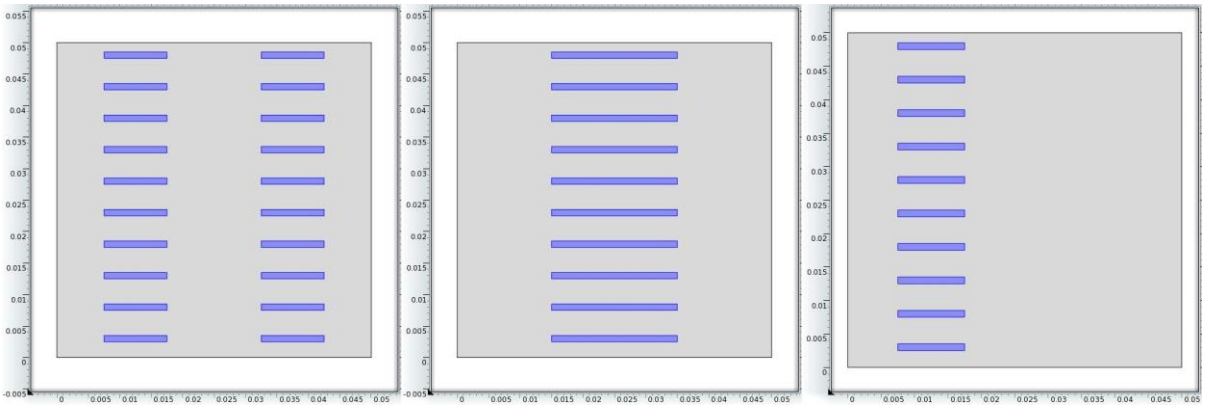

Figure 5. 36. Cracked concrete models with different distributions of damage zones. (a) 10 mm depth, double columns. (b) 20 mm depth, single column. (c) 10 mm depth, single column.

As expected, in the section within a damage zone (Fig. 5.37), the model with the shortest total depth along x-axis (10 mm depth, single column) has the slowest migration

rate, while the other two models have closer migration wave fronts. In the upper left of Fig. 5.37, it may be noticed that, there is an obvious distinction on the locations of wave fronts between solid curve and dot dash curve. However, geometrically speaking, both of these two models have the same distribution of damage zone in the region from x = 0 to x = 0.025 (according to Figs. 5.36 (a) and (c)) thus at least within the left half of the simulated specimen, the solid and dot dash curves should be almost coincident. This distinction would probably be attributed to the ionic interactions. Since the migration of positive charged ions (i.e. potassium and sodium) are speeded up by the column of damage zones in the right half of simulated specimen (the region from x = 0.025 to x = 0.05), the chlorides in the model with 10 mm depth and double columns of damage zones (solid curve) would be drawn a little more than that in the models with single columns of damage zones (dot dash curve) due to the charge balance. This phenomenon can also be found in the concentration profiles in the section near the damage zones (upper left of Fig. 5.38). The above clearly reveals the importance of considering the multi-species ionic transport. Fig. 5.39 gives details of the comparison of concentration distributions in the section crossing the non-damaged mortar between the models shown in Fig. 5.36. It can be seen that, the profiles become even more irregular when subjected to the influences of both the ‘pollution’ behaviour and ionic interactions.

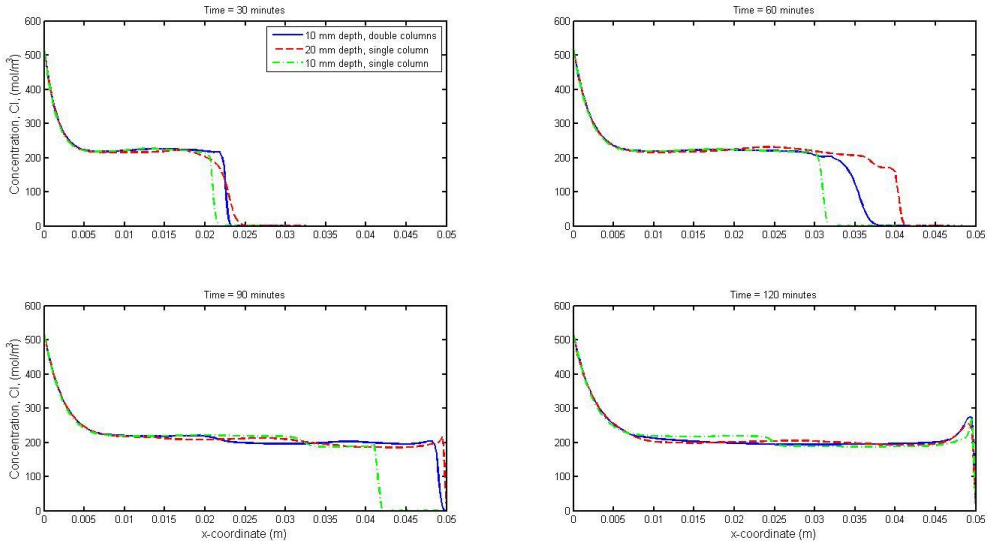

Figure 5.37. Comparisons of concentration distributions in Section 1 between three models (different damage distributions).

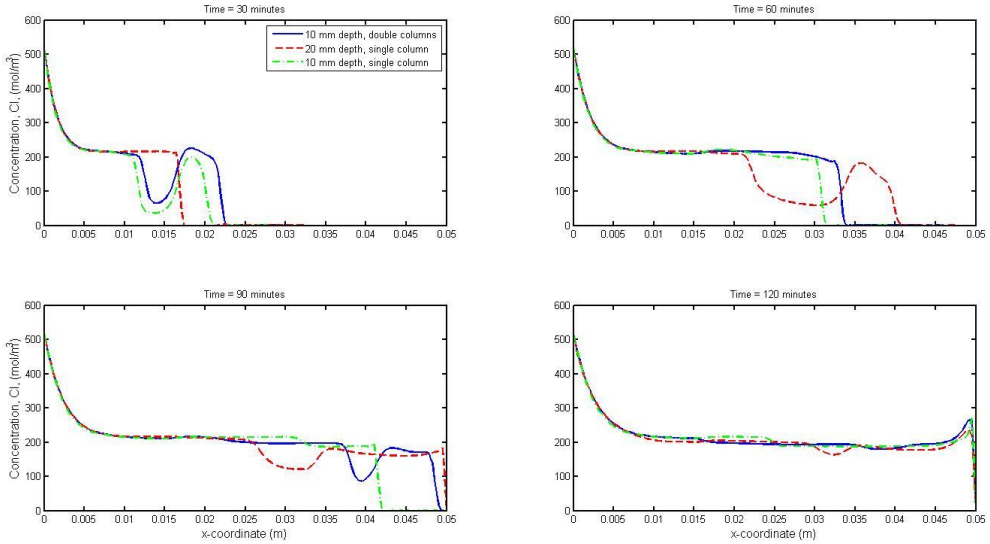

Figure 5.38. Comparisons of concentration distributions in Section 2 between three models (different damage distributions).

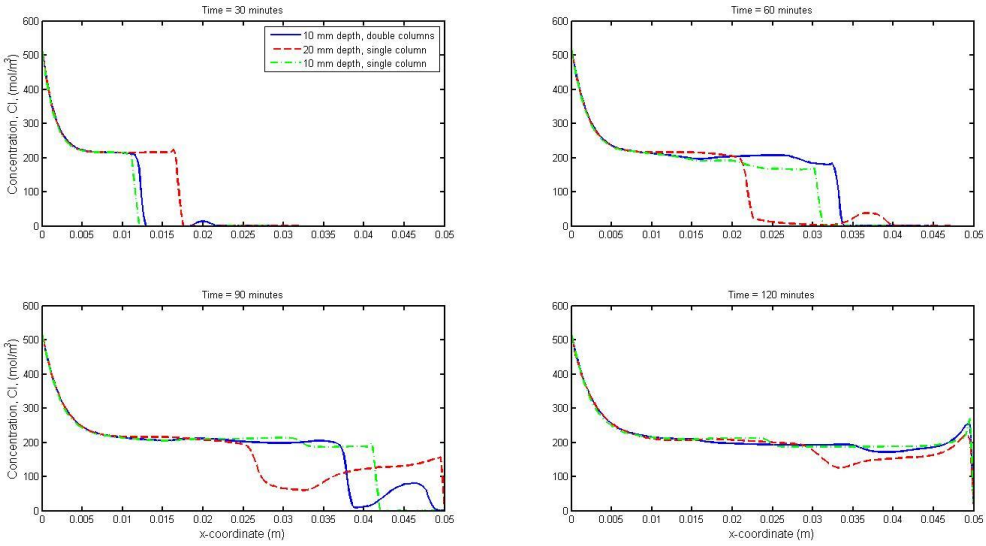

Figure 5.39. Comparisons of concentration distributions in Section 3 between three models (different damage distributions).

To give an overall view of the influence of geometry properties of cracks (i.e. width, depth, volume fraction, pattern and angle of arrangement) on chloride migration, a model which includes a variety of damage zones was rebuilt. The geometry of the model and obtained result are shown in Fig. 5.40. By comparing the result of undamaged one-phase concrete (Fig. 5.41), the concentration distribution profiles in Fig. 5.40 efficiently summarise the result discussed above, i.e., the domination of the damage depth, the pollution caused by local diffusion, the influence of multi-phase ionic interactions, etc.

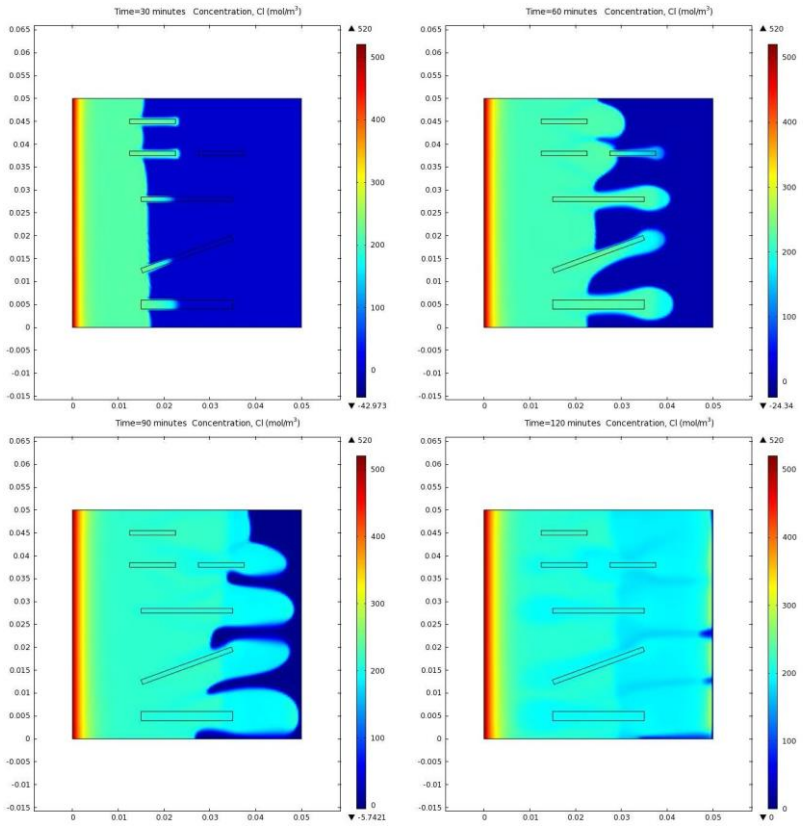

Figure 5.40. Overall view about the influence of cracking zones on chloride migration.

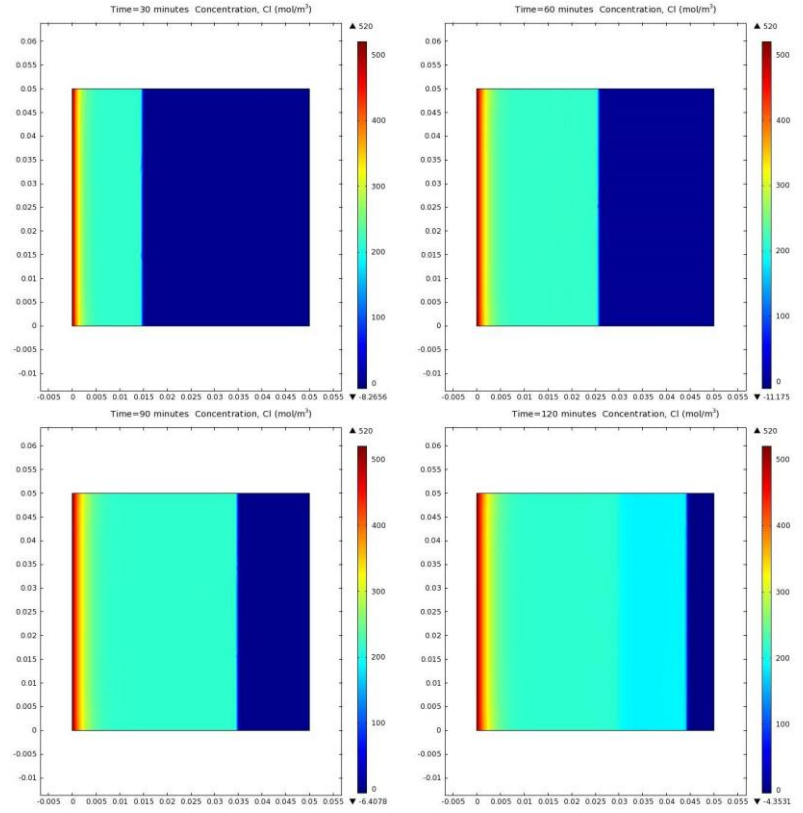

Figure 5.41. Chloride distribution profiles of one-phase uncracked concrete.

Due to the location and shape effect of cracks mentioned before as well as the above cracked models are assumed as a crack-repaired concrete, the normal unrepaired geometry has been built and its chloride distribution profile is shown in Fig. 5.42. From the comparison of Fig. 5.40-42, qualitatively speaking, it is evident that neither the location nor the shape effect of damage zones has much influence on the migration result.

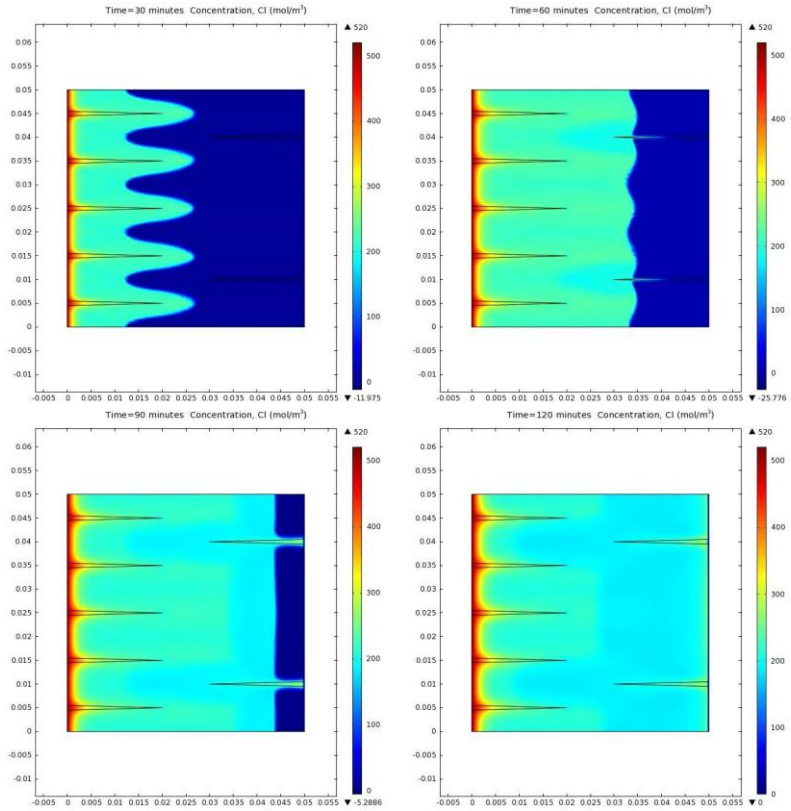

Figure 5.42. Chloride distribution profiles of unrepaired cracked concrete.

5.3 Summary

This chapter has presented a set of numerical investigations on the chloride migration in concrete with ITZs or cracked damage zones, in which each ionic species has two distinct diffusion coefficients, one defined in ITZs or cracked damage zones, the other defined in mortar or no-damaged zone). From the results obtained the following conclusions can be drawn.

1) Comparing the result obtained from the models with and without ITZ phase, a series of basic features such as the migration speed between like charged ions, the approximate 1-D flow of ions, the tortuosity effect caused by aggregates and the steep behaviour of migration wave fronts are qualitatively similar.

2) In the present three-phased models, as the chlorides penetrates much more quickly in ITZ phases as well as the volume fraction of ITZ is non-ignorable, the volume fraction of ITZ plays a significant role in determining the chloride migration rate. This is in disagreement with results shown in two-phased models studied in Chapter Four: only the tortuosity dominates the impact on the migration rate of chlorides. The increase in quantity of aggregates will also increase the ITZ volume, which increases the chloride diffusivity of the concrete to some extent.

3) At the present level of ITZ volume fraction, the definitions of ITZ thickness and $D_{\mathrm{ITZ}} / D_{\mathrm{B}}$ ratio are equally significant during the simulation of chloride migration process.

In the second part of this chapter, 2-D cracked concrete models are proposed to examine the effect of cracks on the migration of chlorides. From the results obtained the following conclusions can be drawn.

1) Unlike the former models, the migration wave front in the cracked concrete travels at two distinct rates. One occurs in the uncracked part of concrete and its speed is similar to that performed in the former models; the other one occurs only in the damage zones and gets much larger speed than that in the non-damaged bulk mortar, acting like a kind of ‘pioneers’ which take a shortcut through the damage zones.

2) Under the action of an externally applied DC voltage, the damage depth, which is exactly parallel to the electric field, dominates the migration rate, whereas the damage width, the damage fraction and the angle between the damage depth and the electrical field has little impact on the chloride migration. Additionally, according to the results of sensitive analysis, the effects of different damage width and fraction on the chloride migration are very close.

3) The results of the chloride migration will be disrupted by the influences of the ‘pollution’ behaviour caused by local diffusion.

4) Ionic interactions of multi-species transport are significant for the study of chloride migration in cracked concrete.

5) Neither the location nor the shape effect of damage zones has qualitative influence on the migration result

6 CHAPTER SIX – PREDICTING CHLORIDE DIFFUSION COEFFICIENT DURING MIGRATION PROCESSES

This chapter presents the findings of a quantitative study to check the validity of models featured in the preceding chapters. The diffusion coefficient of chloride in concrete is evaluated during both diffusion and migration processes. The normalized concrete diffusion coefficients are firstly calculated by using the traditional stationary diffusion models (both in 2-D and 3-D models), then also calculated by using the migration models (with and without binding effect), which are under the actions of externally applied electric field. All of the obtained results are compared with three proven analytical models, i.e., Maxwell's model (Dormieux and Lemarchand, 2000), Bruggeman's equation (Bruggeman's, 1935) and the lower bound of the effective diffusion coefficient proposed by Li et al. (2012) as well as validated against experimental data of an accelerated chloride migration test (ACMT) brought by Yang and Su (2002).

6.1 Introduction

The preceding chapters have proposed a series of numerical studies (one, two or three phase models with different shape and volume fraction of aggregates) to simulate the rapid chloride migration test and presented qualitative analysis of the outputs. A quantitative study which can be used to predict diffusion coefficient of concrete is more attractive to researchers. During recent decades, considerable efforts have been made to investigate chloride diffusion coefficient in heterogeneous concrete materials of multiple phases at both microscopic and mesoscopic levels.

The methods of this research field can be generally classified as analytical and numerical work. The former is based on bringing some empirical models to describe the diffusion coefficient of cement or concrete as reviewed in Chapter two (Section 2.3.1). The latter is of more concern to our studies; however, due to its later start in research history, the number of examples in the literature is much smaller than analytical studies. Recently, with the aim of more accurately predicting the diffusion coefficient of chlorides and studying the influence of various phases of inner concrete structure, some researchers have attempted to establish 2-D and/or 3-D multi-phase concrete models, usually including bulk mortar, aggregate particles and ITZ.

For example, Zeng (2007) established a 2-D hetero-structure model and used FEM to simulate the chloride diffusion behaviour in a heterogeneous concrete composed of two phases (aggregates and cement paste matrix) with distinct chloride diffusivities. It was found that in a heterogeneous concrete, the chloride diffusion lags behind equivalent homogeneous concrete chloride diffusions predicted using the effective diffusion coefficient. Zheng and Zhou (2007) proposed a three-phase composite sphere model to repre-

sent the heterogeneous nature of concrete and derived a closed form expression for chloride diffusion in concrete. Later, Zheng et al. (2009) further investigated the influence of ITZ on the steady-state chloride diffusion in mortars and concretes. More recently, Zheng et al. (2012) represented a 2-D lattice model which contains the diffusivity of aggregate and aggregate shape effect. They obtained an expression which includes the ratio of major and minor axes of the elliptical aggregate particles. Li et al. (2012) used two-phase models in both 2-D and 3-D to predict effective diffusion coefficient of chloride in concrete. They found that the shape of aggregates has a small influence during the diffusion process and also gave a lower bounds of the effective diffusion coefficient of chlorides in concrete as a function of porosity. Dehghanpoor Abyaneh et al. (2013) represented a 3-D numerical model with three phases to investigate the diffusion coefficient of chloride in concrete. The effects of the shape and orientation of ellipse particles have been discussed in this 3-D model.

However, all above-mentioned models only considered the diffusion process of ions and mostly of focused on a stationary problem. It is evident from the differences between Fick's laws and Nernst-Planck equations that, the migration process, which is under the action of an externally applied electric field, results in a much more complex transport behaviour than the diffusion process. Additionally, these numerical diffusion models only take a single-species of ions (i.e. the chlorides) into account during the transport, neglecting the effects of ionic interactions. In this chapter, a quantitative study which is generally based on the multi-phase migration models demonstrated in the previous part of thesis has been conducted. In view of the fact that at present migration tests are more popular in experimental study of chloride diffusivity than the diffusion tests, herein the diffusion coefficient of chloride in concrete has been numerically calculated during not

only diffusion but also migration process. The normalized concrete diffusion coefficients were firstly calculated by using the traditional stationary diffusion models (both 2-D and 3-D), as well as being calculated by using the migration models (with and without binding effect). All of the obtained results were compared with three proven analytical models, i.e., Maxwell's model (Dormieux and Lemarchand, 2000), Bruggeman's equation (Bruggeman's, 1935) and the lower bound of the effective diffusion coefficient proposed by Li et al. (2012) as well as validated against experimental data sets of an accelerated chloride migration test (ACMT) brought by Yang and Su (2002).

6.2 Modelling

6.2.1 *2-D diffusion model*

In order to quantitatively evaluate the diffusion coefficient of chlorides in concrete, the traditional approach is to obtain the normalized diffusion coefficient against with the increase of aggregate volume fraction $(1-\phi)$ from a diffusion model performed by Fick's laws. The normalized chloride diffusion coefficient is calculated from the ratio of chloride diffusion coefficient in concrete (D_c) to that in the cement paste matrix (D_0). Among the most popular numerical models existing in literature, the volume fraction was usually considered only 50% of maximum due to the limitation of random distributing of aggregates. In the present study, it was managed to extend the range of aggregate volume fraction to 70% in the 2-D model which is utilised in Chapters 4 and 5. Fig 6.1 shows the schematic of the geometry with 70% volume fraction of aggregates. The size of the concrete specimen is still 50×50 mm. The finite element mesh used here is similar with that used in the preceding chapters and the aggregate phase are assumed to be impermeable. As it has been proven in Chapter 4, the effect of aggregate shapes on the chloride diffusion in concrete can be ignored. Therefore, only the circular shaped aggregates are used in the model.

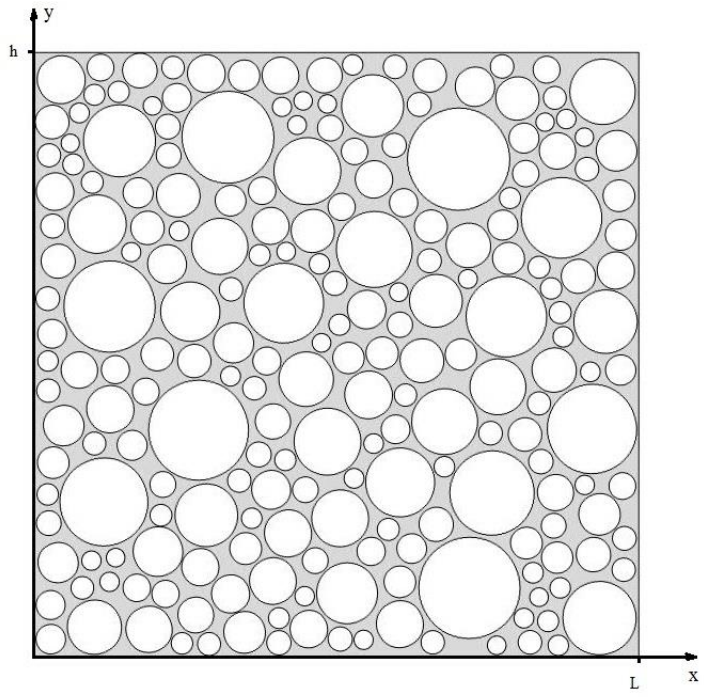

Figure 6.1. Schematic of the geometry: 2-D two phase model.

In the numerical study considered only the diffusion, the process can be simplified to a single-component transport with only chlorides. Chloride diffusion taking place in the cement paste matrix with a given water-to-cement ratio can be described by the Fick's second law as follows,

$$\frac{\partial C}{\partial t} = D_0 \nabla^2 C \tag{6.1}$$

where C is the concentration of chlorides in the cement paste matrix (moles per unit volume of cement paste), t is the time, and ∇ is the Laplace differential operator. For simplicity, the initial condition and boundary conditions are assumed as follows,

$$C(0, x, y) = 0 \tag{6.2}$$

$$C(t,0, y) = C_1, \quad C(t, l, y) = 0 \tag{6.3}$$

$$\frac{\partial C(t, x,0)}{\partial y} = 0, \quad \frac{\partial C(t, x, h)}{\partial y} = 0 \tag{6.4}$$

where C_1 is the chloride concentration at the line x = 0, l = 50 mm and h = 50 mm are the length and height of the plain concrete used in the numerical model, respectively. For given values of D_0 and C_1 one can solve Eq.(6.1) to obtain the chloride concentration distribution profile at any time.

Of particular interest is the x-component of the chloride diffusion flux at the steady state. The total chloride flux, J_t, along the right boundary $x = l$ at the steady state is given by,

$$J_t = \int_o^h J_x(\infty, l, y)dy = -D_0 \int_o^h \frac{\partial C(\infty, l, y)}{\partial x} dy \tag{6.5}$$

The average flux at the right boundary $x = l$ thus is given by,

$$J_{x=l} = \frac{J_t}{h} \tag{6.6}$$

By taking the plain concrete as a representative elementary volume in a macroscopic structure model, the average flux, $J_{x=l}$, thus can be also expressed as,

$$J_{x=l} = -D_{eff} \frac{\partial C}{\partial x} = \frac{D_{eff} C_1}{l} \tag{6.7}$$

Substituting Eqs. (6.5) and (6.7) into (6.6), it yields,

$$D_{eff} = -\frac{D_0 l}{C_1 h} \int_o^h \frac{\partial C(\infty, l, y)}{\partial x} dy \tag{6.8}$$

D_{eff} is the effective diffusion coefficient of chlorides. Note that the average flux at the right boundary $x = l$ has the following relationship with the average flux of the liquid phase of concrete, J_c, due to the porosity existing at the boundary,

$$J_c = J_{x=l} / \phi \tag{6.9}$$

Since the relationship between J_c and D_c also obeys the Fick's first law at the steady state, it can be expressed as,

$$J_c = -D_c \frac{\partial C}{\partial x} \tag{6.10}$$

Substituting Eqs. (6.9) and (6.10) into (6.7), it yields,

$$D_c = D_{eff} / \phi = -\frac{D_0 l}{\phi C_1 h} \int_o^h \frac{\partial C(\infty, l, y)}{\partial x} dy \tag{6.11}$$

Eq. (6.11) indicates that if the chloride flux in the cement paste matrix is computed from the present model shown in Fig 6.1, the average chloride diffusion coefficient in concrete, D_c, will be obtained. The normalized chloride diffusion coefficient can be finally evaluated by the ratio of D_c / D_0.

6.2.2 *3-D diffusion model*

For a more accurate simulation, a 3-D finite element analysis model is developed to follow the deviation used in the 2-D simplification. The concrete cube of $50 \times 50 \times 50$ mm with 55% volume fraction of spherical aggregates is sketched in Fig. 6.2. The geometries with other value of volume fraction of aggregates are not presented here. With respect to the concentration boundary conditions, the front (x = 0) and rear (x = l) surfaces are assumed to have specified concentration boundary conditions (similar with Eq. (6.3)) and all other four surfaces are assumed to have zero flux boundary conditions. Referring to derivation process of Eq. (6.11), the chloride diffusion coefficient in the 3-D model concrete can be computed by the following equation,

$$D_c = -\frac{D_0 l}{\phi C_1 h^2} \int_o^h \int_o^h \frac{\partial C(\infty, l, y, z)}{\partial x} dydz \tag{6.12}$$

where $h = l = 50$ mm are the cross-section size and length of the cube, respectively.

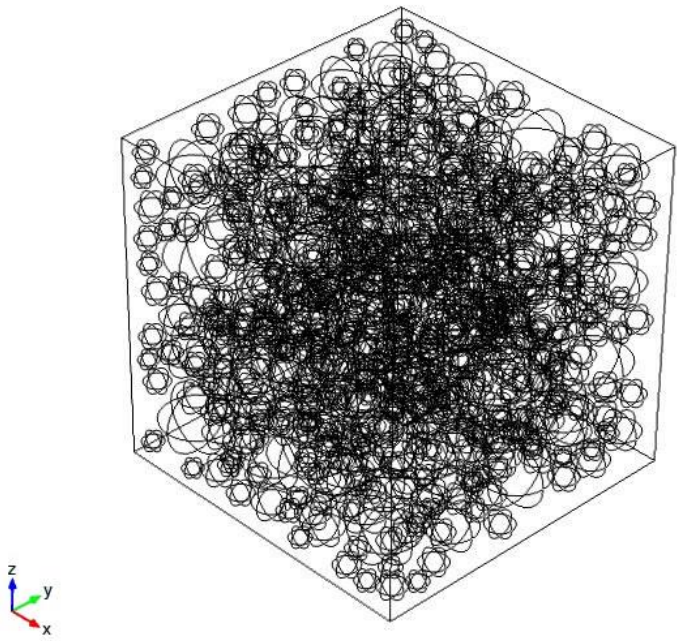

Figure 6.2. Schematic of the geometry: 3-D two phase model..

6.2.3 *2-D migration model*

In recent decades, migration tests become more commonly used in experimental studies of chloride diffusivity than diffusion tests. Therefore from numerical points of view, it is more reasonable to predict diffusion coefficient of chlorides from simulated migration process rather than diffusion process. Comparing the diffusion model performed by Fick's laws, the present migration model has a series of advantages. For instance, it can deal with the more complicated non-linear and time-dependent ionic transport behaviour

as well as consider the ionic interactions caused by multi-species components, which makes the obtained result more rational and reliable against the experiment studies.

A set of 2-D models including different volume fractions of aggregates (with the variation from 0% to 70%) have been used to investigate the normalized chloride diffusion coefficient. The geometry and boundary settings are similar with those used in the preceding chapters. Both the two-phased and three-phased models proposed previously are examined here. As reviewed in Chapter 2, the diffusion coefficient of chlorides can be directly calculated from both the steady and non-steady state migration tests by using two empirical equations (Eqs. (2.47) and (2.48)). However, Xia and Li (2013) argued that Eq.(2.47) based on the flux of chloride ions, which is utilised in steady state migration tests (RCPT) would be less reliable in the multi-species transport simulations under variable initial concentration conditions. Hence, in this chapter Eq. (2.48) based on penetration depth to predict the chloride diffusion coefficient in concrete (D_c) was adopted as follows,

$$D_c = \frac{RTL}{FU} \times \frac{x_d - 2\sqrt{\frac{RTLx_d}{FU}}\,\mathrm{erf}^{-1}(1-\frac{2C_d}{C_1})}{t_d} \tag{6.13}$$

where x_d is the penetration depth of chloride ions at a test duration t_d, C_d is the chloride concentration at x_d, erf^{-1} is the inverse of error function, C_1 is the concentration of chloride at upstream boundary. F= 96487 C/mol, $R = 8.314\mathrm{J}\cdot\mathrm{mol}^{-1}\cdot\mathrm{K}^{-1}$ and T=298K (273+25K) are the Faraday's constant, the universal gas constant and the absolute temperature, respectively.

6.3 Results and discussions

6.3.1 *Analytical models and experimental data*

With the aim of comparison, three proved analytical models and a set of experiment results have been quoted. In terms of the theoretical predictions, Maxwell's model (Dormieux and Lemarchand, 2000), Bruggeman's equation (Bruggeman's, 1935) and the lower bound of the effective diffusion coefficient proposed by Li et al. (2012) are respectively divided by the porosity (ϕ) at first due to the relationship between D_c and D_{eff} (Eq. (6.11)). Then the three adjusted models are plotted in Fig. 6.3. According to Li et al. (2012), the physical meaning of the differences among the three models is the tortuosity, which are equal to $2/(3-\phi)$, $\phi^{0.5}$, and $(1+\phi)/(3-\phi)$ in the Maxwell's model, Bruggeman's equation and the lower bound, respectively. It can be seen from the figure that all the three analytical models decrease with the increase of the aggregate volume fraction ($(1-\phi)$). For the most cases, Maxwell's model has the highest value, whereas the lower bound has the lowest, as well as the gap between them increases with the aggregate volume fraction. More interesting characteristic is found at Bruggeman's equation: initially its value is very close to Maxwell's model but as the increase of aggregate volume fraction it becomes closer to the lower bound. For $(1-\phi) \geq 82.8\%$, Bruggeman's equation owns the lowest value among the three analytical models.

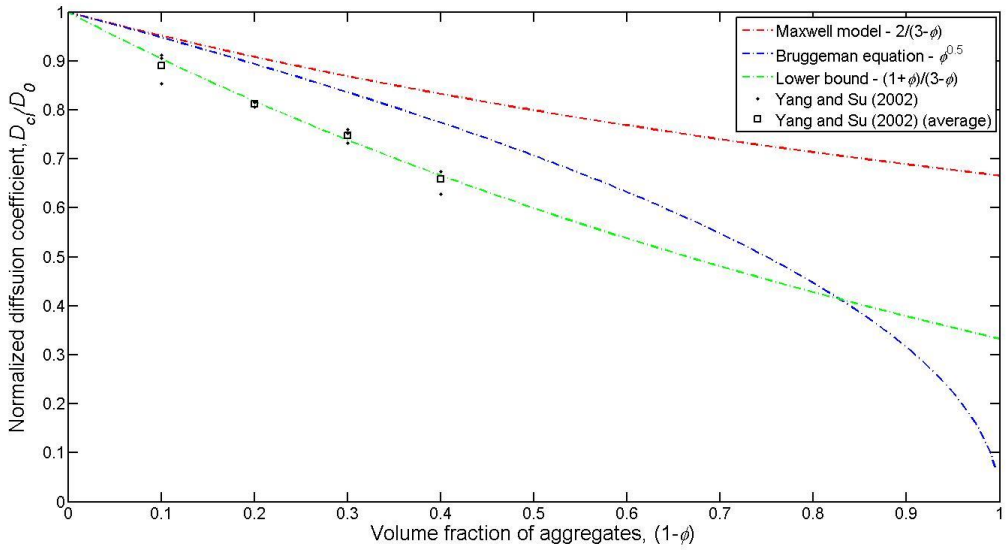

Figure 6.3. Comparisons of three analytical prediction models and experimental data.

In terms of the experimental data, an accelerated chloride migration test (ACMT) brought by Yang and Su (2002) is employed as a reference. The experiment consists of mortars made with ASTM Type I Portland cement at 0.4 w/c ratio and fine aggregates selected at 0%, 10%, 20%, 30% and 40% volume fractions. 50 mm thick samples were cast and cured in water (23 °C) for 12 months and prepared following the specification in ASTM C1202-97. The upstream cell was filled with 0.3 % NaCl solution and the downstream cell was filled with 0.3 N NaOH solution. The chloride concentration in the downstream compartment was monitored and the migration coefficient was obtained at steady-state according to the Nernst–Plank equation. The experiment results of the normalized diffusion coefficient (D_c / D_0) are superimposed Fig. 6.3. It is observed that the average values of experimental data perfectly agree with the lower bound proposed by Li et al. (2012).

6.3.2 *Diffusion models*

For given initial and boundary conditions, the partial differential equation defined by Eq. (6.1) can be solved numerically. Using Eqs. (6.11) and (6.12), two categories of results respectively are obtained from 2-D and 3-D numerical diffusion models. Fig. 6.4 compares the normalized diffusion coefficient (D_c / D_0) calculated with the analytical models and the experimental results mentioned in Section 6.3.1. Note that the 3-D results are only offered up to 55% due to the limitation of random distribution of aggregates. It can be found from the figure that, the normalized diffusion coefficient (D_c / D_0) computed from the 3-D model agrees well with the prediction given by Maxwell's model. Meanwhile, D_c / D_0 computed from the 2-D model is very close to the lower bound from 0% to 50% of $(1-\phi)$, whereas becomes closer to Bruggeman's equation when $(1-\phi)$ fall within the range of 50%-70%.

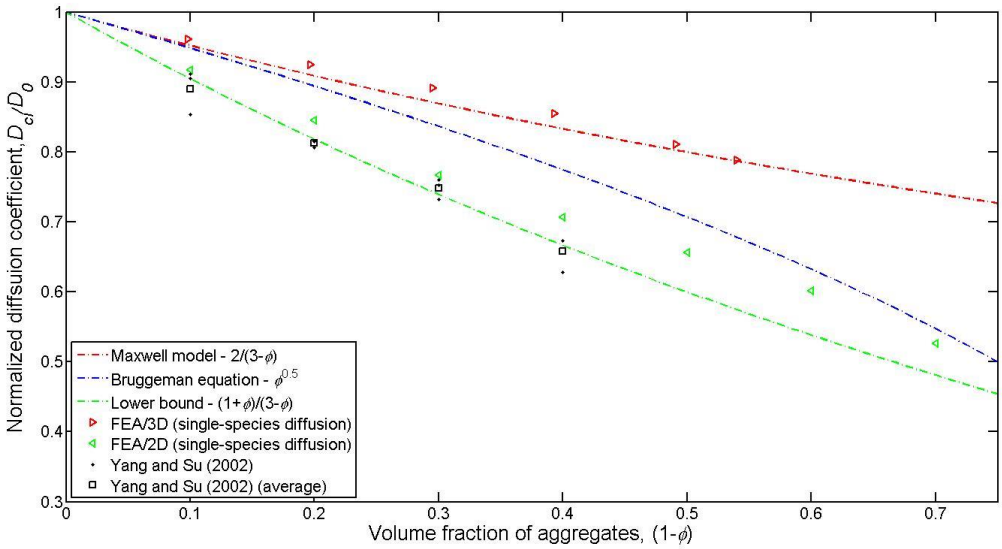

Figure 6.4. Comparison among the analytical models, the experimental data and the numerical diffusion models.

Compared with the experimental results, the experiment data unexpectedly agrees more with the result calculated from the 2-D model rather than with the more realistic 3-D model. Obviously, the 2-D model has one dimension short for the ionic transport and its result should be underestimate and less realistic. The reason of this unexpected phenomenon is probably because that, the aggregates are separate from each other in this numerical model and all of the pores (equivalent to bulk cement paste phase in this case) are connective. In reality, there should be a lot of aggregates locating closely between each other and therefore increasing the penetration length of ions greatly in concrete. In other words, the geometries of models containing randomly generated aggregates reduce the tortuosity of the real concrete to some extent. But interestingly, from the tiny deviation between the results of 2-D model and experiment data (less than 7%), it is revealed that the effect caused by the reduction of tortuosity almost offsets that caused by lack of movement dimension during the ionic transport process. Therefore, it is safe to say that the presented 2-D model is able to simulate the penetration of chlorides in concrete effectively. In view of this, in the following sections, one can also safely continue utilising 2-D migration models to quantitatively monitor the simulated migration tests. This point is very significant since at the moment, it is too difficult for us to present a 3-D migration model to simulate the migration process subjected to an externally applied electric field.

6.3.3 *Two-phase migration model*

The details of solving 2-D two phase migration model have been specifically described in Chapter 4. For the migration models, the normalized diffusion coefficient (D_c / D_0) is calculated by Eq. (6.13) in this study. Apparently, the key variable in this equation is the

penetration depth of chloride ions (x_d) at a selected test duration. Fig. 6.5 shows the distribution profiles of chloride concentration at the first hour in the models with different volume fractions of aggregates. The position of migration wave front is the penetration depth of chlorides which is needed. Note that the migration wave fronts in most of the cases in Fig. 6.5 are not as steep as in the model with the aggregate volume fraction of 0%, which brings difficulties to identify the migration depth of each model. To determine a unified standard, one trace the lines of the migration fronts in parallel, meeting up with the horizontal line of peak value of concentration during migration in the model with 0% volume fraction. As Fig. 6.6 shows, the x-axis and y-axis coordinate values of each intersection point are chosen to be x_d and C_d, respectively. By using Eq. (6.13), the normalized diffusion coefficient can be finally calculated. The results are listed in Table 6.1 and plotted in Fig. 6.7.

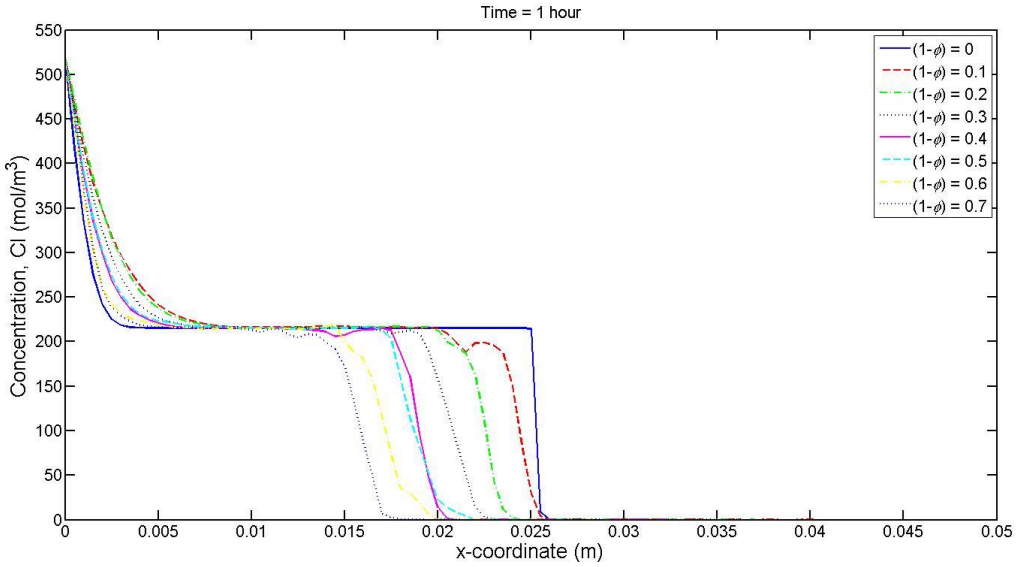

Figure 6.5. Comparisons of chloride concentration distribution profiles between different aggregate volume fractions.

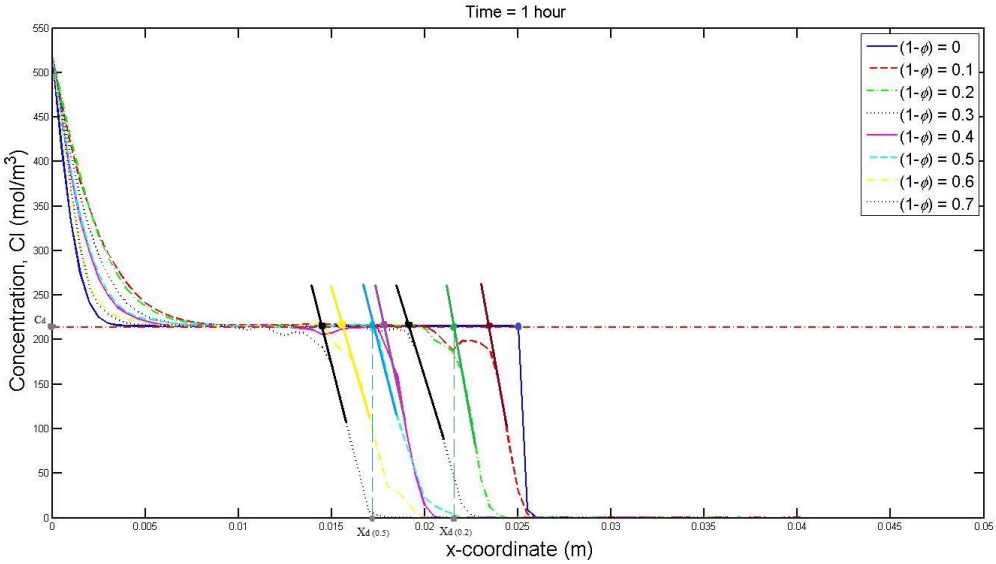

Figure 6.6. Schematic of the migration depth of migration models.

Table 6.1. Normalized diffusion coefficients for the two-phase migration models.

Aggregate volume fraction, (1-ϕ)	0%	10%	20%	30%	40%	50%	60%	70%
Time of the test, t_d, s	3600	3600	3600	3600	3600	3600	3600	3600
Depth of penetration, x_d, m	0.0250	0.0232	0.0211	0.0190	0.0180	0.0173	0.0155	0.0145
Chloride concentration, C_d, mol/m^3	214.4	214.4	214.4	214.4	214.4	214.4	214.4	214.4
Diffusion coefficient in concrete, D_c, ×10^{-10} m^2/s	3.6624	3.3968	3.0871	2.7774	2.6300	2.5269	2.2617	2.1144
Normalized diffusion coefficient, D_c/D_0	1.0000	0.9275	0.8429	0.7584	0.7181	0.6900	0.6175	0.5773

For the purpose of comparison, the curves of analytical predictions, the points of experimental data and the result of 2-D diffusion models in Fig. 6.7 are kept. A good agreement between the present results and those obtained from 2-D diffusion models is observed, especially at the volume fractions of 0%-40%. As the volume fraction increases, the gaps between the two categories of numerical models become larger. At the volume fraction of 70%, the value of D_c / D_0 in two-phase migration is even above Brug-

geman's equation. It is revealed that, in diffusion models the normalized diffusion coefficient has a steady downward trend against the aggregate volume fraction, whereas in migration models this downward trend becomes gentle at the higher volume fractions. Despite this, the result is generally validated by the known experiment data. The maximum of deviation is only 9.12% when $(1-\phi)=0.4$.

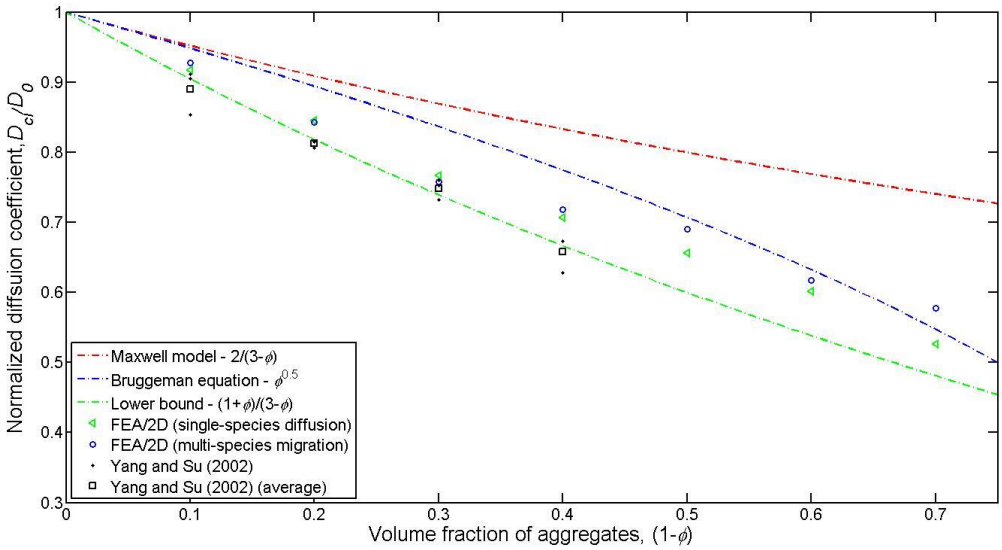

Figure 6.7. Comparison between diffusion models and migration models.

6.3.4 *Three-phase migration models*

As mentioned in Chapter 5, ITZ thickness is $30-50\,\mu m$ in reality however this size level is too small for meshing and beyond our computing ability at present. In the current study, the minimum size of ITZ is $100\,\mu m$ to balance both the calculation efficiency and the reference significance. In order to give a better quantitative examination on the three-phased models, the ratio of diffusion coefficient of ITZ (D_{ITZ}) to that of matrix (D_0) have been correspondingly reduced to about 3 times, which can partly eliminate the effect of larger sized ITZ. Due to the limitation of random distributing of aggregates

wrapped by ITZ, only the models with 0%-50% volume fractions of aggregates are examined here.

Table 6.2. Normalized diffusion coefficients for the three-phase migration models, D_{ITZ}/D_0=2.

Aggregate volume fraction, (1-ϕ)	0%	10%	20%	30%	40%	50%
Time of the test, t_d, s	3600	3600	3600	3600	3600	3600
Depth of penetration, x_d, m	0.0250	0.0235	0.0217	0.0200	0.0190	0.0182
Chloride concentration, C_d, mol/m^3	214.4	214.4	214.4	214.4	214.4	214.4
Diffusion coefficient in concrete, D_c, ×10^{-10} m^2/s	3.6624	3.4411	3.1756	2.9249	2.7774	2.6595
Normalized diffusion coefficient, D_c/D_0	1.0000	0.9396	0.8671	0.7986	0.7584	0.7262

Table 6.3. Normalized diffusion coefficients for the three-phase migration models, D_{ITZ}/D_0=3

Aggregate volume fraction, (1-ϕ)	0%	10%	20%	30%	40%	50%
Time of the test, t_d, s	3600	3600	3600	3600	3600	3600
Depth of penetration, x_d, m	0.0250	0.0238	0.0225	0.0213	0.0200	0.0190
Chloride concentration, C_d, mol/m^3	214.4	214.4	214.4	214.4	214.4	214.4
Diffusion coefficient in concrete, D_c, ×10^{-10} m^2/s	3.6624	3.4854	3.2936	3.1166	2.9249	2.7774
Normalized diffusion coefficient, D_c/D_0	1.0000	0.9517	0.8993	0.8510	0.7986	0.7584

The simulations were carried out at D_{ITZ}/D_0 ratios of 1, 2 and 3 times (where $D_{ITZ}/D_0 = 1$ means there is no ITZ in the geometry and the result is equivalent to the two-phase model shown in the preceding section). The results are shown in Tables 6.2-6.3 and compared with the former references in Fig. 6.8. As expected, the normalized diffusion coefficient (D_c/D_0) decreases with an increase in aggregate volume fraction

and a decrease in D_{ITZ}/D_0. The result of $D_{ITZ}/D_0 = 3$ is found between the two analytical predictions of Maxwell's model and Bruggeman's equation. It may be noticed that the presence of ITZ phase further reduces the downward trend of the decrease of D_c/D_0 throughout the entire cases of aggregate volume fraction. It is evident that the increase of aggregate volume fraction causes two opposing effects on ionic transport. On one hand it slows down transport by increasing the tortuosity of concrete structures. On the other hand it speeds up transport by increasing the porous ITZ wrapping the aggregates, which has much larger diffusivity than cement paste. It also can be found in Fig. 6.8 that, the D_c/D_0 results in the model with $D_{ITZ}/D_0 = 2$ mainly located in the middle between the models with D_{ITZ}/D_0 ratios of 1 and 3. This indicates that the rise of chloride diffusivity with the increase of D_{ITZ}/D_0 during the sensitivity analysis is approximately linear.

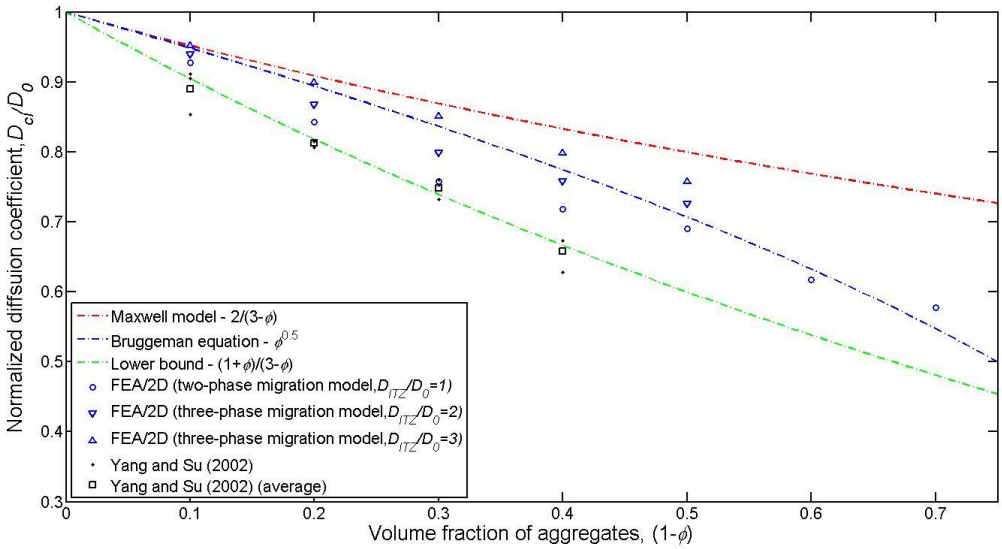

Figure 6.8. Comparison between the migration models with different D_{ITZ}/D_0 values.

6.3.5 *Three-phase migration models with binding effect*

Another point in this chapter is examining the influence of binding effect on the normalized diffusion coefficient (D_c / D_0). However, it should be noted that the modelling of binding effect in this study is dependent on the assumption of Langmuir isotherm. In Eq. (4.5), the two constant, α and β, are also determined based on the experimental data, which brings difficulties to the quantitative study. In this section, for a general qualitative comparison, the same values adopted in Chapter 4 (firstly developed by Li and Page (2000)) are used.

Table 6.4. Normalized diffusion coefficients for the three-phase migration models with binding effect.

Aggregate volume fraction, (1-ϕ)	**0%**	**10%**	**20%**	**30%**	**40%**	**50%**
Time of the test, t_d, s	3600	3600	3600	3600	3600	3600
Depth of penetration, x_d, m	0.0250	0.0219	0.0203	0.0192	0.0182	0.0173
Chloride concentration, C_d, mol/m^3	214.4	146.0	146.0	146.0	146.0	146.0
Diffusion coefficient in concrete, D_c, $\times 10^{-10}$ m^2/s	3.6624	3.1234	2.8904	2.7304	2.5850	2.4543
Normalized diffusion coefficient, D_c/D_0	1.0000	0.8528	0.7892	0.7455	0.7058	0.6701

Table 6.4 gives the calculated D_c / D_0 by using Eq. (6.13). The ITZ phase employed here is $100\,\mu\text{m}$ thick with the diffusivity of $D_{\text{ITZ}} / D_0 = 3$. Comparing the results between the models with and without binding effect shown in Fig. 6.9, it can be seen that the binding effect markedly reduces the value of D_c / D_0. The degree of this reduction is approximately the same as that of the increase caused by ITZ. As a consequence, it brings a good agreement between the two-phase models without binding and the three-phase models with binding. The latter therefore can also be validated by the experiment

work done by Yang and Su (2002). The maximum deviation is only 7.25% when $(1-\phi)=0.4$. That is to say, the full-form numerical model developed in this thesis which includes real potential gradient distributions, separate aggregate and ITZ phases and the binding effect is reliable for simulating the multi-species migration tests.

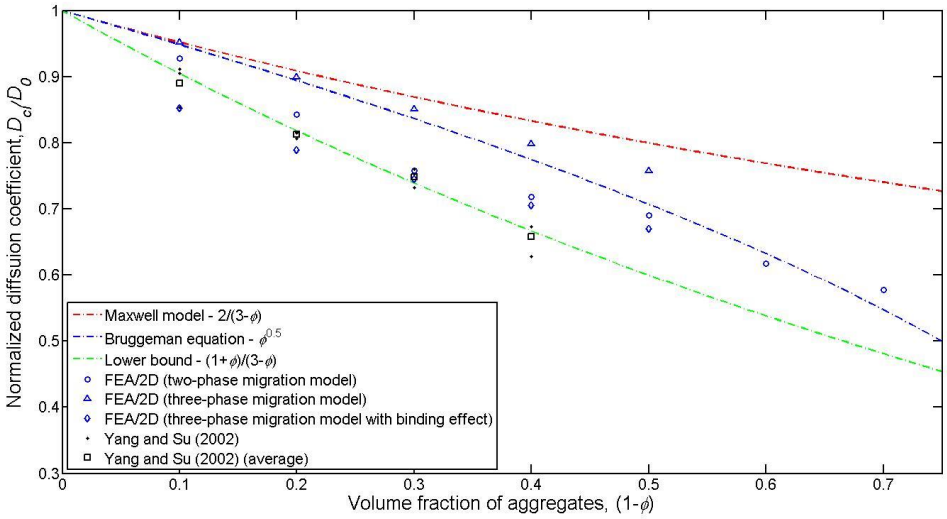

Figure 6.9. Comparison between the migration models with and without binding effect.

6.4 Summary

This chapter has reported on a quantitative study carried out to evaluate and validate the migration models demonstrated in the previous part of the thesis. From the results and discussions of the normalized concrete diffusion coefficients calculated by a series of numerical models, the following conclusions can be drawn.

1) In diffusion models, the results of the normalized diffusion coefficient obtained from 2-D models is closer to the experiment data than that from 3-D models. The effect caused by the reduction of tortuosity almost offsets that caused by lack of movement dimension during the ionic transport process; therefore, the 2-D model is able to simulate the penetration of chlorides in concrete effectively.

2) In two-phase migration models, the results agree well with those obtained from 2-D diffusion models especially at the lower fractions. The difference between them is that, in diffusion models the chloride diffusivity in concrete has a steady downward trend against the aggregates volume fraction, whereas in migration models this downward trend becomes gentle at the higher volume fractions. Despite this, the above result is generally validated by the known experiment data.

3) Three-phase migration models obviously demonstrate two opposing effects on ionic transport caused by aggregate particles. The presence of ITZ phase further reduces the downward trend of the decrease of the chloride diffusivity throughout the entire cases of aggregate volume fractions. Additionally, the rise of chloride diffusivity as the increase of D_{ITZ} / D_0 during the sensitivity analysis is approximately linear.

4) The binding effect will markedly reduce the chloride diffusivity in concrete. The degree of this reduction is approximately the same as that of the increase caused by ITZ. Through comparison with the experiment data, it is concluded that the full-form numerical model developed in this thesis which includes real potential gradient distributions, separate aggregate and ITZ phases and the binding effect is rational and reliable for simulating the multi-species migration tests.

7 CHAPTER SEVEN– CONCLUSIONS AND FUTRUE WORK

This last chapter summarizes the main contributions of this thesis based on the numerical models proposed in the preceding chapters. Findings and the limitations of presented models are listed, and several suggestions are given for possible further studies.

7.1 1-D one phase model

Two sets of 1-D numerical models have been proposed to study the transport of ions in a saturated cement paste specimen subjected to an externally applied electrical field. One determines the electrostatic potential based on the assumption of electro-neutrality, which is used in the majority of the literature. The other applies the rigorous Poisson's equation, which leads a non-linear electrical potential distribution. Through comparison of the two model types, the following conclusions can be drawn:

1) Electro-migration is the dominant transport process in both models due to the influence of an externally applied electric field. However, local diffusion behaviour occurs more frequently in the model using Poisson's equation, which may have significant influence on the development of migration speed.

2) The profile results obtained from the two distinct models are significantly different. If the electro-neutrality condition is employed, the electrostatic potential gradient within the cement paste would be constant, which makes the multi-species transport act like a one-component system. The migration velocity of each ionic species here is also constant, which entirely depends on its diffusion coefficient and the electro-static potential. However, when the electro-neutrality assumption is replaced by the rigorous Poisson's equation, the ionic electro-coupling can be realised. The migration speed of each ionic species varies with time and also with space. Interestingly, the migration speeds of positively (or negatively) charged ions are almost the same but are significantly different from those of their opposite charged ions. This evidently shows interactions between different ionic species achieved in the second set of models.

3) Under the influence of Poisson's equation, the distribution of electrostatic potential between the cathode and anode shows the results are likely to form a curve that varies from a convex shape at the first hour to a concave shape at the fourth hour, rather than a straight line in the model adopting electro-neutrality condition.

4) For the models with constant electrostatic potential gradient, the current density generated by ionic fluxes varies with both time and position, whereas for the models with Poisson's equation, it only varies with time and remains constant with spatial variation. Furthermore, current density is proportionally in accord with the input initial concentrations.

5) A further study on the second set of model shows that the migration amounts of ions in a specimen is heavily dependent on its initial concentrations. The higher the initial concentrations in the specimen, the more the ions can be transported. Moreover, the change of initial concentrations of potassium, sodium and hydroxyl ions will affect not only their own concentration profiles, but also the chloride concentration profiles in the specimen during the process.

7.2 2-D two phase model

To further examine the interaction transport features, the influences of aggregate phase and the impacts of binding effect, a series of 2-D models with two phases (aggregates and bulk mortar) have been developed to simulate the ionic migration tests. A qualitative investigation based on the ionic concentration distribution profiles lead to the following conclusions:

1) The variation of the ionic distribution profiles and the electrostatic potential profiles along the y-axis are insignificant. The concentration distribution profiles obtained from the present two-phase multi-component transport model are qualitatively similar to those obtained from the single-phase multi-component transport model, although quantitative difference in results may exist between these two kinds of models, particularly in the travel speed.

2) The hydroxyl ions are found to have the steepest migration wave front, whereas the sodium ions have the gentlest migration wave front. The steepness of each species decreases with time. This feature of steep degree reflects the combined influence of diffusion and local tortuosity, which cannot be found in the single phase model. The inclusion of aggregates in the model can provide a more accurate influence of tortuosity on both the diffusion and migration of ions.

3) Under the condition of identical volume fraction and similar tortuosity, the influence of particle shapes on the permeability of concrete is fairly insignificant. Relatively, the influence of volume fraction is much more significant than that of aggregate morphology, due to the more notable influence on tortuosity.

4) The adsorption of ions will significantly decelerate the migration speed of this species and meanwhile reduce its concentration during the electro-migration process. Because of the ionic interactions caused by Poisson's equation, the binding effect of one species also has impact on the penetrations of other ionic species.

7.3 2-D three phase model

A series of 2-D concrete models with three-phased composite (aggregate, bulk mortar and ITZ) is presented for study of the impact of the separate ITZ phase. The following conclusions were drawn from the investigation.

1) Comparing the result obtained from the models with and without ITZ phase, a series of basic features such as the migration speed between like charged ions, the approximate 1-D flow of ions, the tortuosity effect caused by aggregates and the steep behaviour of migration wave fronts are qualitatively similar.

2) In the present three-phased models, as the chlorides penetrates much more quickly in ITZ phases as well as the volume fraction of ITZ is non-ignorable, the volume fraction of ITZ plays a significant role in determining the chloride migration rate. This is in disagreement with results shown in two-phased models studied in Chapter Four: only the tortuosity dominates the impact on the migration rate of chlorides. The increase in quantity of aggregates will also increase the ITZ volume, which increases the chloride diffusivity of the concrete to some extent.

3) At present level of ITZ volume fraction, the definitions of ITZ thickness and $D_{\mathrm{ITZ}} / D_{\mathrm{B}}$ ratio are equally significant during the simulation of chloride migration process.

7.4 Cracked concrete models

2-D cracked concrete models are proposed to estimate the effect of cracks during the migration test. From the present investigation of the influence caused by a variety of geometry properties of cracks, the following conclusions were drawn.

1) Unlike the former models, the migration wave front in the cracked concrete travels at two distinct rates. One occurs in the uncracked part of concrete and its speed is similar with that performed in the former models; the other one occurs only in the damage zones and gets much larger speed than that in the non-damaged bulk mortar, acting like a kind of ‘pioneers’ which take a shortcut through the damage zones.

2) Under the action of an externally applied DC voltage, the damage depth, which is exactly parallel to the electric field, dominates the migration rate, whereas the damage width, the damage fraction and the angle between the damage depth and the electrical field has little impact on the chloride migration. Additionally, according to the results of sensitive analysis, the effects of different damage width and fraction on the chloride migration are very close.

3) The results of the chloride migration will be disrupted by the influences of the ‘pollution’ behaviour caused by local diffusion.

4) Ionic interactions of multi-species transport are significant for the study of chloride migration in cracked concrete.

5) Neither the location nor the shape effect of damage zones has qualitative influence on the migration result

7.5 Predicting chloride diffusion coefficient during migration processes

A quantitative study carried out to evaluate and validate the migration models demonstrated in this thesis was reported. From the results and discussions of the normalized concrete diffusion coefficients calculated by a series of numerical models, the following conclusions were drawn.

1) In diffusion models, the results of the normalized diffusion coefficient obtained from 2-D models is closer to the experiment data than that from 3-D models. The effect caused by the reduction of tortuosity almost offsets that caused by lack of movement dimension during the ionic transport process; therefore, the 2-D model is able to simulate the penetration of chlorides in concrete effectively.

2) In two-phase migration models, the results agree well with those obtained from 2-D diffusion models especially at the lower fractions. The difference between them is that, in diffusion models the chloride diffusivity in concrete has a steady downward trend against the aggregates volume fraction, whereas in migration models this downward trend becomes gentle at the higher volume fractions. Despite this, the above result is generally validated by the known experiment data.

3) Three-phase migration models obviously demonstrate two opposing effects on ionic transport caused by aggregate particles. The presence of ITZ phase further reduces the downward trend of the decrease of the chloride diffusivity throughout the entire cases of aggregate volume fractions. Additionally, the rise of chloride diffusivity as the increase of D_{ITZ} / D_0 during the sensitivity analysis is approximately linear.

4) The binding effect will markedly reduce the chloride diffusivity in concrete. The degree of this reduction is approximately the same as that of the increase caused by ITZ. Through comparison with the experiment data, it is concluded that the full-form numerical model developed in this thesis which includes real potential gradient distributions, separate aggregate and ITZ phases and the binding effect is rational and reliable for simulating the multi-species migration tests.

7.6 Suggestions for future work

The work conducted in this thesis has identified several aspects where future investigations may be required.

1) Time-dependent concentrations of external cells

   In the present numerical models, the size of the external cells was assumed to be like a reservoir and thus the concentration of boundary conditions is constant during modelling and calculation. Further study is recommended to monitor the concentration profiles during the simulated test with the limited size of external cells.

2) Real sized ITZs

   The ITZ thickness adopted in Chapter Six had to be $100\,\mu m$ due to the computational limitation, whereas in reality, the thickness is only $30-50\,\mu m$. Though in the present quantitative study the ratio of diffusion coefficient of ITZ to that of matrix have been correspondingly reduced to eliminate the effect of oversized ITZ, real sized ITZs can improve the accuracy of the present model.

3) 3-D model for calculating Nernst-Planck equation

   One significant finding driven by the 3-D diffusion models proposed in Chapter Six was that the relationship between the effects of reduction of tortuosity and the lack of movement dimension. However, this conclusion is only obtained from the diffusion model rather than more interested migration model. To make a more reasonable evaluation on the influences of dimension, 3-D models need to be utilised to solve the ionic migration problem.

4) Convection behaviour

The mortar matrix phase of the present models is assumed to be saturated and thus the convection behaviour would not take place during the ionic transport. Unsaturated mortar matrix may be the objective of future study.

5) Chemical activity

As mentioned in Chapter Two that the full form of Nernst-Planck equation includes not only the diffusion, the convection and the migration term but also the chemical activity term. This term was ignored in the present study due to the assumption of ideal diluted matrix. Therefore, further modelling can be carried out by adding the chemical activity term in Nernst-Planck equation.

6) Experimental work on monitoring other species

The present study focused on not only the chloride ions but also other three popular ionic species in chloride migration tests. However, most existing experimental data is for chlorides (including the accelerated chloride migration test cited for validation of the present numerical results), neglecting the report of other species. Therefore, it is advised that an experimental work which monitors more ionic species should be carried out.

REFERENCE

Aitcin P.C. and Mehta, P.K. (1990): Effect of coarse aggregate characteristics on mechanical properties of high-strength concrete, ACI Materials Journal 87 (2) 103–107.

Andrade, C. (1993): Calculation of chloride diffusion-coefficients in concrete from ionic migration measurements. Cement and Concrete Research 23 (3), 724-742.

ASTM C 1202, (1994): Standard test method for electrical indication of concrete's ability to resist chloride ion penetration, American Society for Testing and Materials, Philadelphia.

ASTM C1543 (2002): 10a Standard Test Method for Determining the Penetration of Chloride Ion into Concrete by Ponding, American Society for Testing and Materials, Philadelphia.

AASHTO T 259 (1980): Standard Method of Test for Resistance of Concrete to Chloride Ion Penetration, (T259-80). American Association of State Highway and Transportation Officials, Washington, D.C., U.S.A.

AASHTO T 277. (1983): Standard method of test for rapid determination of the chloride permeability of concrete, American Association of States Highway and Transportation Officials, Washington. D.C., U.S.A.

AASHTO TP 64-03, (2003): Standard method of test for prediction of chloride penetration in hydraulic cement concrete by the rapid migration procedure, American Association of State Highway and Transportation Officials, Washington.

Atkinson, A. and Nickerson, A. K. (1984): The diffusion of ions through water-saturated cement. Journal of Materials Science 19, 3068–3078.

Bentz, D. P., Garboczi, E. J., Lu, Y., Martys, N., Sakulich, A. R. and Weiss, W. J. (2013): Modeling of the influence of transverse cracking on chloride penetration into concrete. Cement & Concrete Composites 38, 65-74.

Bruggeman, D. A. G. (1935): Berechnung verschiedener physikalischer Konstanten von heterogenen Substanzen: I. Dielektrizitaetskonstanten und Leitfaehigkeiten der Mischkoerper aus isotropen Substanzen. Annalen der Physik 416(7), 636-679.

Caré, S. (2003): Influence of aggregates on chloride diffusion coefficient into mortar. Cement and Concrete Research 33, 1021–1028.

Caré, S. and Hervé, E. (2004): Application of a n-phase model to the diffusion coefficient of chloride in mortar. Transport in Porous Media 56(2), 119-135.

Castellote, M., Andrade, C. and Alonso, C. (2000): Phenomenological Mass-Balance-Based Model of Migration Tests in Stationary Conditions Application to Non-Steady-State Tests. Cement and Concrete Research 30(12), 1885-1893.

Dehghanpoor Abyaneh, S., Wong, H. S. and Buenfeld, N. R. (2013): Modelling the diffusivity of mortar and concrete using a three-dimensional mesostructure with several aggregate shapes. Computational Materials Science 78, 63-73.

Delagrave, A., Marchand, J. and Samson, E. (1996): Prediction of Diffusion Coefficients in Cement-Based Materials on the Basis of Migration Experiments. Cement and Concrete Research 26(12), 1831-1842.

Delagrave, A., Bigas, J. P., Ollivier, J. P., Marchand, J. and Pigeon, M. (1997): Influence of the Interfacial Zone on the Chloride Diffusivity of Mortars. Advanced Cement Based Materials 5(3-4), 86-92.

Demir, F. (2005): A new way of prediction elastic modulus of normal and high strength concrete-fuzzy logic. Cement and Concrete Research 35(8), 1531-1538.

Dormieux, L. and Lemarchand, E. (2000): Mod éisation macroscopique du transport diffusif. Apport des m éthodes de changement d' échelle d'espace. Oil & Gas Science and Technology 55 (1), 15-34.

Djerbi, A., Bonnet, S., Khelidj, A. and Baroghel-bouny, V. (2008): Influence of traversing crack on chloride diffusion into concrete. Cement and Concrete Research 38(6), 877-883.

Escadeillas, G. and Maso, J.C. (1991): In advances in cementitious materials. Mindess, Second Edition.

Elakneswaran, Y., Iwasa, A., Nawa. T., Sato, T. and Kurumisawa, K. (2010): Ion-cement hydrate interactions govern multi-ionic transport model for cementitious materials. Cement and Concrete Research 40 (12), 1756-1765.

Feldman, R. F., Chan, G. W., R. J. and Brousseau, P. J. (1994): Tumidajski, Investigation of the rapid chloride permeability test, ACI Materials Journal, 91(3), 246–255.

Frizon, F., Lorente, S., Ollivier, J. P. and Thouvenot, P. (2003): Transport model for the nuclear decontamination of cementitious materials. Computational Materials Science 27 (4), 507-516.

Friedmann, H., Amiri, O. and Ait-Mokhtar, A. (2008): Shortcomings of geometrical approach in multi-species modelling of chloride migration in cement-based materials. Magazine of Concrete Research 60 (2), 119-124.

Escadeillas, G. and. Maso, J. C. (1991): Approach of the initial state in cement paste, mortar and concrete. In S. Mindess, editor, Advances in cement materials, Ceramic Tansactions 16. American Ceramic Society.

Garboczi, E. J. (1990): Permeability, diffusivity, and microstructural parameters: a critical review. Cement and concrete research 20(4), 591-601.

Garboczi, E. J. and Bentz, D. P. (1992): Computer Simulation of the Diffusivity of Cement-Based Materials. Material Science. 27, 2083-2092.

Garboczi, E. J. and Bentz, D. P. (1997): Analytical formulas for interfacial transition zone properties Original Research Article. Advanced Cement Based Materials 6(3-4), 99-108.

Geyskens, P., Der Kiureghian, A. and Monteiro, P. (1998): Bayesian prediction of elastic modulus of concrete. Journal of Structural Engineering-ASCE 124(1), 89-95.

Garboczi, E. J. and Berryman, J. G. (2001): Elastic moduli of a material containing composite inclusions: Effective medium theory and finite element computations. Mechanics of Materials 33(8), 455-470.

Gérard, B. and Marchand, J. (2000): Influence of cracking on the diffusion properties of cement-based materials– Part I: Influence of continuous cracks on the steady-state regime. Cement and Concrete Research 30(1), 37–43.

Hashin, Z. (2001): Thin interphase/imperfect interface in conduction. Journal of Applied Physics 89 (4), 2261– 2267.

Hashin, Z. and Monteiro, P. J. M. (2002): An inverse method to determine the elastic properties of the interphase between the aggregate and the cement paste. Cement and Concrete Research 32 (8), 1291-1300.

Hobbs, D.W. (1999): Aggregate influence on chloride ion diffusion into concrete. Cement and Concrete Research 29, 1995–1998.

Hooton, R. D., Nagi, M. A. and Ozyidirim, H. C. (2000): The rapid chloride permeability test, HPC Bridge Views 12, 2–4.

Ismail, M., Toumi, A. and Francois, R. (2008): Effect of crack opening on the local diffusion of chloride in cracked mortar samples. Cement and Concrete Research (8-9): 1106-1111.

Jacobsen S., Marchand, J. and Boisvert, L. (1996): Effect of cracking and healing on chloride transport in OPC concrete. Cement and Concrete Research 26 (6), 869-881.

Jang, S. Y., Kim, B. S. and Oh, B. H. (2011): Effect of crack width on chloride diffusion coefficients of concrete by steady-state migration tests. Cement and Concrete Research 41(1), 9-19.

Jiang, J. Y., Sun, G. W. and Wang, C. H. (2012): Numerical calculation on the porosity distribution and diffusion coefficient of interfacial transition zone in cement-based composite materials. Construction and Building Materials 39, 134-138.

Johannesson, B., Yamada, K., Nilsson, L.O. and Hosokawa, Y. (2007): Multi-species ionic diffusion in concrete with account to interaction between ions in the pore solution and the cement hydrates. Materials and Structures 40 (7), 651-665.

Johannesson, B., Hosokawa, Y. and Yamada, K. (2009): Numerical calculations of the effect of moisture content and moisture flow on ionic multi-species diffusion in the pore solution of porous materials. Computers & Structures 87 (1-2), 39-46.

Johannesson, B. (2010a): Development of a generalized version of the poisson–nernst–planck equations using the hybrid mixture theory: presentation of 2D numerical examples. Transport in Porous Media 85 (2), 565-592.

Johannesson, B. (2010b): Comparison between the gauss' law method and the zero current method to calculate multi-species ionic diffusion in saturated uncharged porous materials.Computers and Geotechnics 37 (5), 667-677.

JSCE-G571 (2003): Test Method for Effective Diffusion Coefficient of Chloride Ion in Concrete by Migration. Japan Society of Civil Engineers.

Khitab, A., Lorente, S. and Ollivier, J.P. (2005): Predictive model for chloride penetration through concrete. Magazine of Concrete Research 57 (9), 511-520.

Kubo, J., Sawada, S., Page, C.L. and Page, M.M. (2007): Electrochemical injection of organic corrosion inhibitors into carbonated cementitious materials: part 2. Mathematical modelling. Corrosion Science 49(3), 1205-1227.

Krabbenhoft, K. and Krabbenhoft, J. (2008): Application of the poisson-nernst-planck equations to the migration test. Cement and Concrete Research 38(1), 77-88.

Luping, T. and Nilsson, L.O. (1993): Rapid determination of the chloride diffusivity in concrete by applying an electric field. ACI Materials Journal 89(1), 49-53.

Li, L.Y. and Page, C.L. (1998): Modelling of electrochemical chloride extraction from concrete by using electrochemical method. Computational Materials Science 9, 303–308.

Li, G., Zhao, Y., Pang, S.-S. and Li, Y. (1999): Effective Young's modulus estimation of concrete. Cement and Concrete Research 29, 1455-1462.

Li, L.Y. and Page, C.L. (2000): Finite element modelling of chloride removal from concrete by an electrochemical method. Corrosion Science 42 (12), 2145-2165.

Li, L.Y., Xia, J. and Lin, S. S. (2012): A multi-phase model for predicting the effective diffusion coefficient of chlorides in concrete. Construction and Building Materials, 26 (1), 295-301.

Liu, Q.F., Li, L.Y., Easterbrook, D. and Yang, J. (2012): Multi-phase modelling of ionic transport in concrete when subjected to an externally applied electric field. Engineering Structures 42, 201–213.

Lizarazo-Marriaga, J. and Claisse, P. (2009a): Effect of the non-linear membrane potential on the migration of ionic species in concrete. Electrochimica Acta 54, 2761–2769.

Lizarazo-Marriaga, J. and Claisse, P. (2009b): Determination of the concrete chloride diffusion coefficient based on an electrochemical test and an optimization model. Materials Chemistry and Physics 117,536–543.

Lorente, S., Carcasses, M. and Ollivier, J.P. (2003): Penetration of ionic species into saturated porous media: the case of concrete. International Journal of Energy Research 27 (10), 907-917.

Lorente, S., Voinitchi, D., Bégué-Escaffit, P. and Bourbon, X (2007): The single-valued diffusion coefficient for ionic diffusion through porous media. Journal of Applied Physics 101.

Li, C.Q., Zheng, J.J., Zhou, X.Z. and Mccarthy, M.J. (2003): A numerical method ofor the prediction of elastic modulus of concrete. Magzine of Concrete Research 55(6), 497-505.

Lilliu, G. (2007): 3D analysis of fracture processes in concrete, PhD Thesis, Delft University of Technology, Eburon, Delft.

Liu, Y. and Shi, X. (2012): Stochastic modeling of service life of concrete structures in chloride-laden environments. Journal of Materials in Civil Engineering 24(4), 381-390.

Lee, K.M. and Park, J.H. (2008): A numerical model for elastic modulus of concrete considering interfacial transition zone. Cement Concrete Research 38(3), 396-402.

Lu, X. (1997): Application of the Nernst-Einstein Equation to Concrete. Cement and Concrete Research 27 (2), 293-302.

Marsavina, L., Audenaert, K., Schutter, G. D., Faur, N. and Marsavina, D. (2009): Experimental and numerical determination of the chloride penetration in cracked concrete. Construction and Building Materials 23(1), 264-274.

Martin, P.B., Zibara, H. and Hooton, R.D. (2000): A study of the effect of chloride binding on service life predictions. Cement and Concrete Research 30(8), 1215-1223.

Mcgrath, P. F. and Hooton, R. D. (1996): Influence of Voltage on Chloride Diffusion Coefficients from Chloride Migration Tests. Cement and Concrete Research 26(8), 1239-1244.

Mcgrath, P. F. and Hooton, R. D. (1999): Re-evaluation of the AASHTO T259 90-day salt ponding test. Cement and Concrete Research 29, 1239–1248.

McLachlan, D. S., Blaszkiewicz, M. and Newnham, R.E. (1990): Electrical resistivity of composites. Journal of the American Ceramic Society 73, 2187–2203.

Moore, W. J. (1972): Physical Chemistry, 4th ed., Prentice-Hall Englewood Cliffs, New Jersey.

Nilsen, A.U., Monteiro, P.J.M and Gjorv, O.E. (1995): Estimation of the elastic moduli of lightweight aggregate. Cement Concrete Research 25(2), 276-280.

Nillson, L.O., Massat, M. and Tang, L. (1994): The effect of non-line chloride binding on the predicition of chloride penetration into concrete structures. Malhotra V.M. (Ed.), Durability of Concrete, ACI sp-145, Detroit, 469-486.

Nilsson, L.O., Poulsen, E., Sandberg, P., Sorensen, H. E. and Klinghoffer O.(1996) : Chloride Penetration into Concrete, State of the Art, Transport Processes, Corrosion Initiation, Test Methods and Prediction Models, The Road Directorate Copenhagen.

NT-Build 443 (1995): Concrete, hardened: Accelerated chloride penetration. Concrete Hardened: Accelerated Chloride Penetration. Nordtest, Esbo,Finland

NT-Build 335 (1997): Concrete, Mortar and Cement-Based Repair Materials: Chloride Diffusion Coefficient from Migration Cell Experiments. Nordtest, Esbo, Finland.

NT-Build 492 (1999) : Nordtest Method: Concrete, Mortar and Cement-Based Repair Materials: Chloride Migration Coefficient from Non-Steady-State Migration Experiments.

Nadeau, J.C. (2003): A multiscale model for effective moduli of concrete incorporating ITZ water-cement ratio gradients, aggregate size distributions, and enteapped voids. Cement Concrete Reasearch 33, 103-113.

Newman, J.S. and Thomas-Alyea, K.E. (2004): Electrochemical systems, 3rd edition, John Wiley And Sons Inc., New Jersey,

Narsillo, G. A., Li, R., Pivonka, P. and Smith, D.W. (2007): Comparative study of methods used to estimate ionic diffusion coefficients using migration tests. Cement and Concrete Research 37 (8), 1152-1163.

Oh, B. H. and Jang, S. Y. (2004): Prediction of diffusivity of concrete based on simple analytic equations. Cement and Concrete Research 34, 463–480.

Otsuki, N., Hisada, M., Otani, T. and Maruyama, T. (1999): Theoretical Evaluation of Diffusion Coefficient of Chloride Ion in Mortar from Mobility.' ACI materials journal 96(6), 627-633.

Ouyang, W. Z., Cao, X., and Wang, N. (2009): A mathematical model for electrochemical chloride removal from marine cast iron artifacts, Acta Metallurgica Sinica (English Letters) 22 (2), 91-99.

Park, S. S., Kwon, S. J., Jung, S. H. and Lee, S. W. (2012): Modeling of water permeability in early aged concrete with cracks based on micro pore structure. Construction and Building Materials 27 (1), 597-604.

Pfeifer, D.W., McDonald. D.B. and Krauss, P.D. (1994): The rapid chloride permeability test and its correlation to the 90-day chloride ponding test. Pci Journal 39 (1), 38-47.

Prince, W., Perami, R. and Espagne, M. (1999): Mechanisms Involved in the Accelerated Test of Chloride Permeability.' Cement and Concrete Research 29 (5), 687-694.

Sa'id-Shawqi, Q., Arya, C. and Vassie, P. R. (1998): Numerical modeling of electrochemical chloride removal from concrete, Cement and Concrete Research 28 (3), 391-400.

Sahmaran, M. (2007): Effect of flexure induced transverse crack and self-healing on chloride diffusivity of reinforced mortar. Journal of Materials Science 42(22), 9131-9136.

Sahu, S., Badger, S. and Thaulow, N. (2002): Evidence of thaumasite formation in Southern California concrete. Cement and Concrete Composites, 24, 379-384.

Samson, E. and Marchand, J (1999): Numerical Solution of the Extended Nernst–Planck Model. Journal of Colloid and Interface Science 215,1–8.

Samson, E. and Marchand, J (2007): Modeling the effect of temperature on ionic transport in cementitious materials. Cement and Concrete Research 37, 455–468.

Scanlon, J.M. and Sherman, M.R. (1996): Fly ash concrete: An evaluation of chloride penetration test methods. Concrete International 18 (6), 57–62.

Shane, J. D., Aldea, C.M., Bouxsein, N. F., Mason, T.O., Jenning, H. M. and Shaw, S.P. (1999): Microstructural and pore solution changes induced by rapid chloride permeability test measured by impedance spectroscopy. Concrete Science and Engineering. 1 (2), 110–119.

Shi, C. Stegemann, J. A., Caldwell, R. (1998): Effect of supplementary cementing materials on the rapid chloride permeability test (AASHTO T 277 and ASTM C1202) results. ACI Materials Journal 95 (4), 389–394.

Shi, C. (2004): Effect of mixing proportions of concrete on its electrical conductivity and the rapid chloride permeability test (AASHTO T 277 and ASTM C1202) results, Cement and Concrete Research. 34, 537–545.

Snyder, K.A. and Marchand, J. (2001): Effect of speciation on the apparent diffusion coefficient in nonreactive porous systems. Cement and Concrete Research 31 (12), 1837-1845.

Streicher, P. E. and Alexander, M. G. (1995): A Chloride Conduction Test for Concrete.' Cement and Concrete Research 25(6), 1284-1294.

Sugiyama, T., Ritthichauy, W. and Tsuji, Y. (2003): Simultaneous Transport of Chloride and Calcium Ions in Hydrated Cement Systems.' Journal of Advanced Concrete 1(2), 127-138.

Sugiyama, T., Ritthichauy, W. and Tsuji, Y. (2008): Experimental investigation and numerical modeling of chloride penetration and calcium dissolution in saturated concrete. Cement and Concrete Research 38, 49–67.

Sun, Z., Garboczi, E.J. and Shah, S.P. (2007): Modeling the elastic properties of concrete composites: Experiment, differential effective medium theory, and numerical simulation. Cement Concrete Research 29(1), 22-38.

Svante Littmarck, H.C. and Saeidi, F. (1986): The founders of COMSOL Inc. 1 New England Executive Park, Burlington, MA 01803, USA.

Tang, L. P. and Nilsson, L.O. (1992): Rapid Determination of the Chloride Diffusivity in Concrete by Applying an Electric Field. ACI materials journal 89(1) , 49-53.

Tang, L. P. and Nilsson, L.O. (1993): Chloride Binding Capacity and Binding Isotherms of OPC Pastes and Mortars. Cement and Concrete Research, 23(2),247-253.

Truc, O. (2000): Prediction of Chloride Penetration into Saturated Concrete - Multi - Species - Approach. Unpublished Ph.D. thesis, Chalmers University.

Truc, O., Ollivier, J. P. and Carcasses, M. (2000): A New Way for Determining the Chloride Diffusion Coefficient in Concrete from Steady State Migration Test. Cement and Concrete Research 30(2), 217-226.

Truc, O., Ollivier, J.P. and Nilsson, L.O. (2000a): Numerical simulation of multi-species transport through saturated concrete during a migration test--MSDIFF code. Cement and Concrete Research 30 (10), 1581-1592.

Truc, O., Ollivier, J.P. and Nilsson, L.O. (2000b): Numerical simulation of multi-species diffusion. Materials and Structures 33 (233), 566-573.

Toumi, A., Francois, R. and Alvarado, O. (2007): Experimental and numerical study of electrochemical chloride removal from brick and concrete specimens. Cement and Concrete Research 37 (1), 54-62.

Ukrainczyk, N., Koenders, E. and Breugel, K. (2013): Numerical model for multi-ion diffusion in cmentitious materials-Multidiff Code. International conference on materials, tribology, recycling. Vela Luka, 27-29 June 2013.

Van Brakel, J and Heertjes, P.M. (1974): Analysis of diffusion in macroporous media in terms of porosity, a tortuosity and a constrictivity factor. International Journal of Heat and Mass Transfer 17 (9), 1093-1103.

Walton, J. C. (1990): Mathematical modeling of mass transport and chemical reaction in crevice and pitting corrosion. Corrosion Science 30(8-9), 915–28.

Wang, Y., Li, L.Y. and Page, C.L. (2001): A two-dimensional model of electrochemical chloride removal from concrete. Computational Materials Science 20 (2), 196-212.

Wang, H. and Li, Q. (2007): Prediction of elastic modulus and Possion's ratio for un-saturated concrete. International Journal of Solids Structure 44, (5), 1370-1379.

Whiting, D. (1981): Rapid measurement of the chloride permeability of concrete. Public Roads 45 (3), 101-112.

Win, P. P., Watanabe, M. and Machida, A. (2004): Penetration profile of chloride ion in cracked reinforced concrete. Cement Concrete Research 34, 1073-1079.

Xu, K., Daian J. F. and Quenard, D. (1997): Multiscale structures to describe porous media part II: transport properties and application to test materials. Transport in Porous Media 26 (3), 319-338.

Xi, Y. and Bazant, Z. P. (1999): Modeling chloride penetration in saturated concrete, J. Mater. Civil Eng, 58–65.

Xia, J. and Li, L.Y. (2013): Numerical simulation of ionic transport in cement paste un-der the action of externally applied electric field. Construction and Building Materials 39, 51-59.

Yu, S.W. and Page, C.L. (1996): Computer simulation of ionic migration during electrochemical chloride extraction from hardened concrete. British Corrosion Journal 31 (1), 73-75.

Yang, C.C. (1997): Approximate elastic moduli of light weight aggregate. Cement Concrete Research 27(7), 1021-1030.

Yang, C.C. (1998): Effect of the transition zone on the elastic moduli of mortar. Cement Concrete Research 28(5), 727-736.

Yang, C. C., Cho, S. W. and Huang, R. (2002): The Relationship between Charge Passed and the Chloride-Ion Concentration in Concrete Using Steady-State Chloride Migration Test. Cement and Concrete Research 32(2), 217-222.

Yang, C.C. and Su, J. K. (2002): Approximate migration coefficient of interfacial transition zone and the effect of aggregate content on the migration coefficient of mortar. Cement and Concrete Research 32, 1559–1565.

Yang, C. C. (2003) 'The Relationship between Charge Passed and the Chloride Concentrations in Anode and Cathode Cells Using the Accelerated Chloride Migration Test.' Materials and Structures 36, 678-684

Yang, C. C. and Cho, S. W. (2003): An Electrochemical Method for Accelerated Chloride Migration Test of Diffusion Coefficient in Cement-Based Materials. Materials Chemistry and Physics 81 (1), 116-125.

Yang, C.C. and Cho, S.W. (2004): The relationship between chloride migration rate for concrete and electrical current in steady state using the accelerated chloride migration test. Materials and Structures 37 (271), 456-463.

Yang, C. C. and Wang, L. C. (2004): The Diffusion Characteristic of Concrete with Mineral Admixtures between Salt Ponding Test and Accelerated Chloride Migration Test.' Materials Chemistry and Physics 85(2-3), 266-272.

Yang, C.C. (2005) : Effect of the percolated interfacial transition zone on the chloride migra-tion coefficient of cement-based materials. Materials Chemistry and Physics 91, 538–544.

Yang, C. C. and Cho, S. W. (2005): Approximate migration coefficient of perco-lated interfacial transition zone by using the accelerated chloride migration test. Cement and Concrete Research 35, 344– 350.

Yang, C.C. (2006): On the relationship between pore structure and chloride diffu-sivity from accelerated chloride migration test in cement-based materials. Cement and Concrete Research 36, 1304–1311.

Yang, C. C., Chiang, S. C. and Wang, L. C. (2007): Estimation of the Chloride Diffusion from Migration Test Using Electrical Current. Construction and Build-ing Materials 21(7), 1560-1567.

Yaya, K., Khelfaoui, Y., Malki, B. and Kerkar, M. (2011): Numerical simulations study of the localized corrosion resistance of AISI 316L stainless steel and pure titanium in a simulated body fluid environment. Corrosion Science 53,3309–3314.

Yuan, Q., Shi, C., De Schutter, G., Audenaert, K. and Deng, D. (2009): Chloride Binding of Cement-Based Materials Subjected to External Chloride Environment - a Review. Construction and Building Materials 23(1) , 1-13.

Zeng, Y. W. (2007): Modeling of chloride diffusion in hetero-structured concretes by finite element method. Cement & Concrete Composites 29, 559–565.

Zelinsky, A. G., Pirogov, B. Y. (2006): Numerical simulation of corrosion process with two- step charge transfer mechanism in the Cu/CuSO4 + H2SO4 system. Corrosion Science 48,2867–81.

Zhang, T. C. and Bishop, P. L. (1994): Evaluation of tortuosity factors and diffusivities in biofilms. Water Research 28(2), 2279-2287.

Zhao, X.-H. and Chen, W.F. (1998): Effective elastic moduli of concrete with interface layer. Computers and Structure 66(2-3), 275-288.

Zheng, J. J., Li, C.Q. and Zhou, X.Z. (2006): An analytical method for prediction of the elastic modulus of concrete. Magazine of Concrete Research 58, 665-673.

Zheng, J. J. and Zhou, X.Z. (2007): Prediction of the chloride diffusion coefficient of concrete. Materials and Structures 40, 693–701

Zheng, J. J. Wong, H. S., Buenfeld. N. R. (2009): Assessing the influence of ITZ on the steady-state chloride diffusivity of concrete using a numerical model. Cement and Concrete Research 39, 805–813.

Zheng, J. J., Zhou, X. Z, Wu, Y. W. and Jin, X. Y. (2012): A numerical method for the chloride diffusivity in concrete with aggregate shape effect. Construction and Building Materials 31, 151–156.

PUBLICATIONS

Liu, Q.F., Li, L.Y. and Easterbrook, D. (2012): Multi-phase modeling of ionic transport in concrete under externally applied current density. 3rd International Conference on the Durability of Concrete Structures (ICDCS-2012), Sep.17-19, 2012, Belfast, UK, SLM14/1-8.

Liu, Q.F., Li, L.Y., Easterbrook, D. and Yang, J. (2012): Multi-phase modelling of ionic transport in concrete when subjected to an externally applied electric field. Engineering Structures 42, 201–213.

Liu, Q.F., Li, L.Y. and Yang, J. (2011): Multi-phase modeling of ionic transport in concrete under externally applied electric field. The 19th Annual International Conference on Composites/Nano Engineering (ICCE-19), July.24-31, 2011, Shanghai, China.